

**Oxidized lipids and signaling pathways of G2A receptor involved in
nerve injury induced neuropathic pain**

Dissertation

zur Erlangung des Doktorgrades

der Naturwissenschaften

vorgelegt beim Fachbereich 14

der Johann Wolfgang Goethe - Universität

in Frankfurt am Main

von

Tabea Osthues

aus Starnberg

Frankfurt (2020)

(D30)

Vom Fachbereich 14 der

Johann Wolfgang Goethe - Universität als Dissertation angenommen.

Dekan: Prof. Dr. Clemens Glaubitz

Gutachter: Prof. Dr. Achim Schmidtke

Prof. Dr. Klaus Scholich

Datum der Disputation: 26.03.2021

Declaration

Except where stated otherwise by reference or acknowledgment, the work presented was generated by myself under the supervision of my advisors during my doctoral studies. All contributions from colleagues are explicitly referenced in the thesis.

The figures listed below were obtained in the context of collaborative research:

Fig. 9: Number of immune cells in sciatic nerve 7d after SNI surgery, Andreas Weigert and Praveen Mathoor (Department of Patho Biochemistry, Faculty medicine), they stained the samples, performed the FACS analysis and a pre-evaluation, Béla Zimmer (Clinical Pharmacology, Faculty medicine) performed the sample preparation, the statistical analysis and further evaluation

Fig. 11: Number of immune cells in dorsal root ganglia (DRG) 7d after SNI surgery, Andreas Weigert and Praveen Mathoor (Department of Patho Biochemistry, Faculty medicine), they stained the samples, performed the FACS analysis and a pre-evaluation, Béla Zimmer (Clinical Pharmacology, Faculty medicine) performed the sample preparation, the statistical analysis and further evaluation

Fig. 12: Number of immune cells in spinal cord 7d after SNI surgery, Andreas Weigert and Praveen Mathoor (Department of Patho Biochemistry, Faculty medicine), they stained the samples, performed the FACS analysis and a pre-evaluation, Béla Zimmer (Clinical Pharmacology, Faculty medicine) performed the sample preparation, the statistical analysis and further evaluation

Fig. 14: Number of immune cells in sciatic nerve 1 d after SNI surgery, Andreas Weigert and Praveen Mathoor (Department of Patho Biochemistry, Faculty medicine), they stained the samples, performed the FACS analysis and a pre-evaluation

Fig. 15: Number of immune cells in DRGs 1 d after SNI surgery, Andreas Weigert and Praveen Mathoor (Department of Patho Biochemistry, Faculty medicine), they stained the samples, performed the FACS analysis and a pre-evaluation

Fig. 16: Number of immune cells in spinal cord 1 d after SNI surgery, Andreas Weigert and Praveen Mathoor (Department of Patho Biochemistry, Faculty medicine), they stained the samples, performed the FACS analysis and a pre-evaluation

Fig. 18: Concentrations of various cytokines and chemokines in sciatic nerve, Béla Zimmer performed the Luminex multiplex analysis

Fig. 19: Concentrations of various cytokines and chemokines in ipsilateral L4-L6 DRGs, Béla Zimmer performed the Luminex multiplex analysis

Fig. 21: Concentrations of various cytokines and chemokines in spinal cord, Béla Zimmer performed the Luminex multiplex analysis

Fig. 22: Concentrations of HODEs in sciatic nerve 7d after SNI, Carlo Angioni (Analytics, Faculty medicine) performed the measurement with LC-MS/MS, I performed the sample pre-preparation and the statistical analysis

Fig. 23: Inhibition of 9-HODE production in BMDMs after LPS stimulation, Carlo Angioni (Analytics, Faculty medicine) performed the measurement with LC-MS/MS, I performed the sample pre-preparation and the statistical analysis

Fig. 24: Concentrations of EpOMEs and DiHOMEs in sciatic nerve 7d after SNI, Carlo Angioni (Analytics, Faculty medicine) performed the measurement with LC-MS/MS, I performed the sample pre-preparation and the statistical analysis

Fig. 25: Global proteomic analysis of bone marrow derived macrophages (BMDMs) of wild-type and G2A-deficient mice without stimulation, Kevin Klann (Biochemistry I, Faculty medicine) performed the measurement of proteomics, I performed the sample pre-preparation and the statistical analysis

Fig. 26: Global proteomic analysis of wild-type BMDMs after stimulation with 9-HODE, Kevin Klann (Biochemistry I, Faculty medicine) performed the measurement of proteomics, I performed the sample pre-preparation and the statistical analysis

Fig. 28: Global proteomic analysis of bone marrow derived macrophages of G2A-deficient mice after 9-HODE stimulation, Kevin Klann (Biochemistry I, Faculty medicine) performed the measurement of proteomics, I performed the sample pre-preparation and the statistical analysis

Fig. 29: Global proteomic analysis of bone marrow derived macrophages of wild-type and G2A-deficient mice after 9-HODE stimulation, Kevin Klann (Biochemistry I, Faculty medicine) performed the measurement of proteomics, I performed the sample pre-preparation and the statistical analysis

Table 10. Results of antagonist screening and subsequent cell toxicity assay of the screening hits. Jan Heering (Fraunhofer IME-TMP) performed the high throughput screen and on basis of this together we prepared the cells, and the IP-One measurement, Jan Heering performed statistical analysis

Whenever a figure, table or text is identical to a previous publication, it is stated explicitly in the thesis that copyright permission and / or co-author agreement has been obtained.

The following parts of the thesis have been previously published:

- Chapter “1.3 The GPR132 receptor (G2A)”, Figure 5B, Foster *et al.*, Pharmacol Res Perspect 2019
- Chapter “3.1 Pain perception in G2A-deficient mice after spared-nerve injury”, Figure 8, Osthues *et al.*, Cells 2020
- Chapter “3.2 Neuroimmune modulation in G2A-deficient mice”, Figure 9 – 22 and Figure 24 – 29, Table 8 and 9, Figure 31 – 32 and Figure 33B, Figure 34, Osthues *et al.*, Cells 2020

Frankfurt, 26.10.2020 T. Osthues

Place, Date

Tabea Osthues

Table of Contents

Abstract	I
1. Introduction.....	1
1.1. Pain and Pain Perception	1
1.1.1. Physiological Pain	1
1.1.2. Pathophysiological pain.....	3
1.2. Neuropathic pain	6
1.2.1. Nerve-injury induced neuropathic pain	7
1.3. The Gpr132 receptor (G2A).....	10
1.3.1. Structural features and ligands.....	10
1.3.2. Signaling pathways of G2A	13
1.4. G2A in health and disease	15
1.4.1. G2A and neuropathic pain.....	16
1.5. Aim of this thesis	17
2. Material and Methods	19
2.1. Materials.....	19
2.1.1. Animals	19
2.1.2. Antibodies	19
2.1.3. Buffers and Solutions	22
2.1.4. Cell Culture	25
2.1.5. Cell Culture Medium.....	25
2.1.6. Chemicals	27
2.1.7. Enzymes	30
2.1.8. Equipment and materials.....	30
2.1.9. Kits.....	32
2.1.10. Lipids	33

2.1.11. Marker.....	33
2.1.12. qPCR	33
2.1.13. Software.....	34
2.2. Methods.....	35
2.2.1. Animal models.....	35
2.2.1.1. Animals	35
2.2.1.2. Spared nerve injury (SNI).....	35
2.2.1.3. Assessing mechanical thresholds with the Dynamic plantar test	36
2.2.1.4. Tissue preparation	36
2.2.2. Biochemical methods	36
2.2.2.1. Fluorescence-activated cell sorting (FACS) analysis.....	36
2.2.2.2. Western Blot	37
2.2.2.3. Bradford protein assay	38
2.2.2.4. Enzyme-linked immunosorbent assay (ELISA).....	39
2.2.3. Cell biological methods	41
2.2.3.1. Differentiation and stimulation of Bone marrow derived macrophages (BMDM)	41
2.2.3.2. Transwell migration assay.....	41
2.2.3.3. 9-HODE production assay.....	43
2.2.3.4. Preparation of primary sensory neurons.....	44
2.2.3.5. Agonists and Antagonists of G2A – Screen: IP One Assay with Fluorescence Resonance Energy Transfer (FRET)	45
2.2.4. Molecular biological methods	47
2.2.4.1. RNA Isolation	47
2.2.4.2. cDNA synthesis.....	47
2.2.4.3. Real-time quantitative polymerase chain reaction (qPCR).....	48
2.2.4.4. Calcium-Imaging	48
2.2.5. Immunochemical methods.....	49
2.2.5.1. Cryo-sections	49
2.2.5.2. Immunohistochemistry	50
2.2.6. Analytical methods	50
2.2.6.1. Proteomics.....	50

2.2.6.2. Liquid-chromatography-tandem mass spectrometry for lipid detection (LC-MS/MS)	52
2.2.7. Data analysis and statistics	53
3. Results	54
3.1. Mechanical hypersensitivity in G2A-deficient mice after spared-nerve-injury ..	54
3.2. Neuroimmune modulation in G2A-deficient mice	55
3.2.1. Distribution of immune cells at the site of injury	55
3.2.2. Distribution of immune cells at involved dorsal root ganglia.....	57
3.2.3. Distribution of immune cells at spinal cord level	59
3.2.4. Changes along the pain transmission pathway after SNI surgery: Cytokines, chemokines and growth factors	60
3.2.5. Changes along the pain transmission pathway after SNI surgery: Lipid mediators	65
3.3. Signaling pathways in macrophages	68
3.3.1. General comparison of wild-type and G2A-deficient macrophages.....	68
3.3.2. Signaling pathways after 9-HODE stimulation	69
3.3.3. MMP9 regulation after G2A activation in macrophages	74
3.3.4. Investigation of further signaling pathways involved in migration.....	76
3.4. Inhibition of G2A receptor	80
3.4.1. Screen for G2A inhibitors	80
3.4.2. Inhibitory effect of G2A inhibitors on TRPV1-mediated Ca ²⁺ influx.....	81
3.4.3. Effects of G2A11, G2A13 and G2A19 on the migratory behavior of macrophages	83
4. Discussion	87
4.1. Role of G2A in trauma induced neuropathies and subsequent neuroimmune interaction	87
4.2. G2A in the crosstalk of immune cells and primary sensory neurons during acute phase of trauma induced neuropathies	91

4.3. G2A: A target for the treatment of neuropathic pain?	99
I. Zusammenfassung	102
II. Abbreviations.....	107
III. Table of Figures.....	118
1. Introduction.....	118
2. Material and Methods	118
3. Results	118
4. Discussion	120
Annex.....	120
References	122
Annex	151
Publikationen	190
Danksagung.....	191
Lebenslauf	192

Abstract

Neuropathic pain, a form of chronic pain, is a steadily rising health problem due to health costs and increasing numbers of patients. Neuropathic pain conditions arise upon metabolic disorders, infections, chemotherapeutic treatment, trauma or nerve injury. Especially nerve injury induced neuropathic pain is characterized by spontaneous or ongoing pain due to neuroimmune interactions. Thereby, inflammatory mediators, released by the injured nerve, recruit to and activate immune cells at the site of injury. Those mediators further activate transient receptor potential vanilloid 1 (TRPV1), a known channel involved in pain perception, or bind to G-protein coupled receptors (GPCR) in peripheral nerve endings. The following activated second messenger signaling pathways lead to sensitization of TRPV1. One of those GPCRs is G2A.

The overall aim of this thesis was to investigate the role of G2A in nerve-injury induced neuropathic pain. For this, the common mouse model of nerve-injury induced neuropathic pain, the spared-nerve injury, was used. As measurements with dynamic plantar aesthesiometer showed, G2A-deficiency leads to reduced mechanical hypersensitivity. Upon analysis with FACS, ELISA and Luminex a reduced number of macrophages and neutrophils at the injured nerve, as well as less inflammatory mediators (TNF α , IL-6, VEGF) in G2A-deficient animals was observed. In dorsal root ganglia (DRGs) there was only a reduced number of macrophages and less IL-12 observed in G2A-deficient animals. Additionally, in wild-type mice, G2A agonist 9-HODE was elevated at the injured nerve, as a LC-MS/MS analysis showed.

To investigate the underlying pathways of G2A-9-HODE signaling, a proteom screen was performed. This screen revealed upregulation of multiple proteins involved in migration in wild-type macrophages. Additionally, Ca-Imaging and transwell migration assays showed that the G2A antagonist G2A11, had desensitizing effects on DRG neurons and inhibited macrophage migration.

Overall, the results suggest that loss of G2A has dual effects. On the one hand loss of G2A is antinociceptive. On the other hand, G2A-deficiency leads to reduced inflammation, suggesting G2A as promising target in treatment of neuropathic pain. Here, an antagonist had inhibitory effects on the migration and the sensitization.

1. Introduction

The human body has developed complex and various mechanisms to ensure its wellbeing and survival [1, 2]. However, survival can be threatened by tissue damage caused by injury, toxic molecules, infections or different diseases [1, 3, 4]. The cause of a threat generates diverse stimuli, which are detected by the body through nociception [1, 3]. Nociception is an adaptive tool of the body and is defined as a neural process to encode and process noxious mechanical, thermal and / or chemical stimuli [4, 5]. Thereby, specialized peripheral sensory neurons, namely the nociceptors, transduce the potentially injurious stimuli into neuronal electrical activity [3, 5, 6]. The electrical activity is then transmitted as an all-or-none action potential from the site of stimulus via primary afferent nerve fibers to the spinal cord and central synapses. Into the synaptic cleft the neurotransmitter glutamate is released leading to a postsynaptic reaction of second-order nociceptors, which conduct the signal to the central nervous system (CNS) and finally the brain [4, 5]. In the brain, especially the amygdala, the nociceptive signal is then processed according to its aversive properties [1, 7].

1.1. Pain and Pain Perception

1.1.1. Physiological Pain

Nociception is a highly specialized ability of the body, because the nociceptors must be able to differentiate between non- and noxious stimuli [8]. The subjectively perceived result of the generation of action potentials is a nociceptive pain [2]. Pain is defined by the International Association for the Study of Pain (IASP) as an unpleasant sensory and emotional experience associated with, or resembling that associated with, actual or potential tissue damage. (IASP, as of 20th August 2020, <https://www.iasp-pain.org/Education/Content.aspx?ItemNumber=1698#Pain>) In fact, the body uses pain as a warning mechanism to prevent tissue damage and harm [4, 9–11]. The awareness of such harm or tissue damage is achieved by the stimulus detection system of the body, the nociceptors [9]. The peripheral nerve endings of the nociceptors innervate all tissues in the body, from the skin, the muscles, the internal organs, to the visceral and the deep tissue [3, 11, 12].

When stimuli reach intensities of high threshold values and undeniably unpleasant sensations the high-threshold nociceptors are getting activated and transmit the excitation to the CNS [1, 9]. Such unpleasant sensations are evoked by extreme temperatures, mechanical or chemical stimuli, also called noxious stimuli [4, 8, 9, 13]. The noxious stimuli activate specific membrane

Introduction

ligand-gated and voltage-gated ion channels, which are expressed by nociceptors, such as – among others - transient receptor potential vanilloid 1 (TRPV1) channel [7, 9, 11, 14].

The TRPV1 channel normally has a high activation threshold at a temperature above 40 °C [8, 14, 15]. TRPV1 converts the noxious physical stimulus into electrical activity, which is amplified by sodium channels, to evoke an action potential [6, 13]. Once the action potential is generated, the signal is transmitted over the cell bodies, the dorsal root ganglia (DRG) or trigeminal ganglia (TG) to the spinal cord. From here, the excitation is further transmitted via the thalamus to the cortex of the brain [1, 16]. The brain processes the signal and sends back to the periphery the information about withdrawal from the noxious stimulus [10] (Fig. 1).

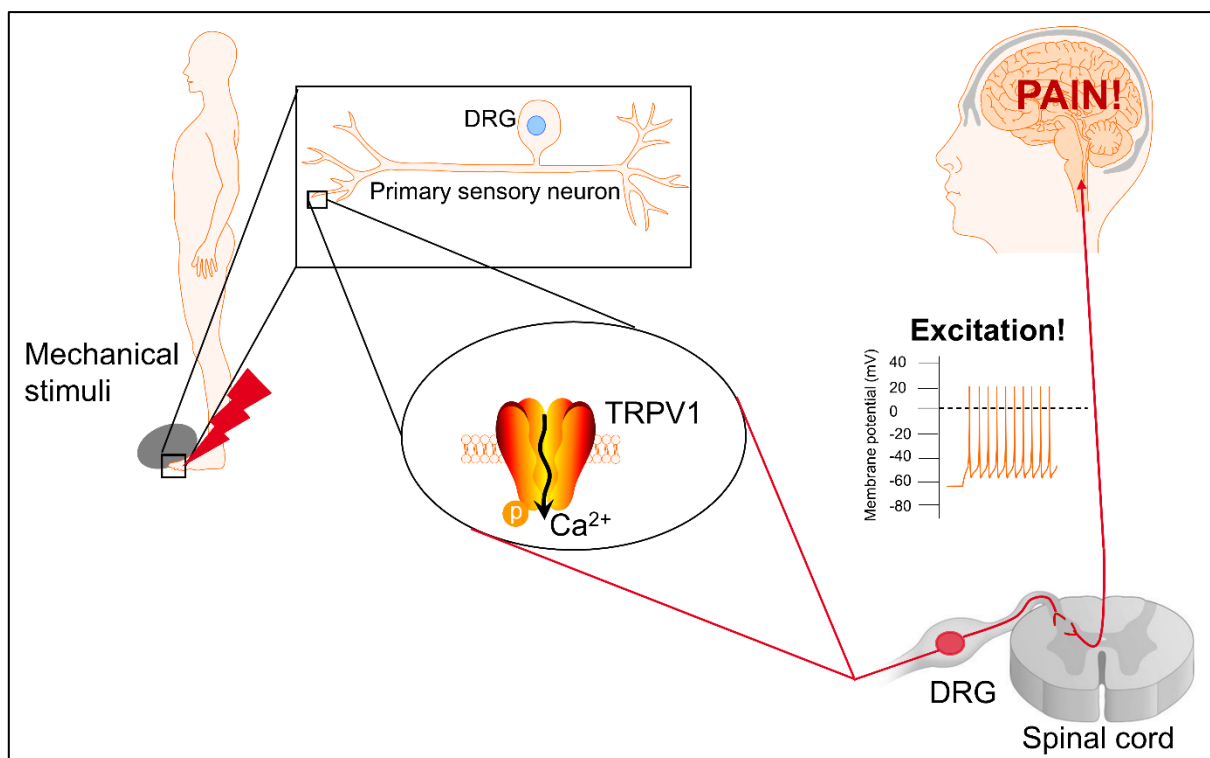


Figure 1. Nociception. After mechanical stimuli channels like TRPV1 in nociceptive primary sensory neurons react by producing an inward current of calcium ions leading to action potentials. They are transmitted through the cell bodies, the DRG into the spinal cord and further to the brain. Here the signal is experienced as painful.

The nociception is processed by different forms of nociceptors. First, A δ fibers are myelinated medium diameter afferents, conducting the stimulus of acute pain to the brain rapidly [1, 9]. A δ fibers are mechanosensitive and do have high mechanical thresholds [3]. Secondly, A β fibers are also myelinated large-diameter afferents, but conduct low-threshold mechanical stimuli and are not activated by nociceptive stimuli [3, 6]. However, the most important afferents for pain perception are the C fibers. They are small unmyelinated afferents and can be divided into

subgroups depending on their reactivity. Thus, there is a subgroup of C fibers that is heat-responsive, but mechanically insensitive. Further subgroups of C fibers are more responsive to chemical stimuli like capsaicin [1]. Apart from their responsiveness, they all conduct slowly and react mainly either on high-intensity mechanical, thermal or chemical stimuli [1, 3, 8]. They conduct so called second pain, which is mainly a long-lasting and burning sensation [17–19].

After the painful stimulus is gone, by healing of tissue injury or withdraw reflexes, the activated state of nociceptors returns back over time to its normal high-threshold activation state and with it the associated pain disappears [9, 20].

1.1.2. Pathophysiological pain

When activated peripheral nociceptors remain in the state of activation long after the initial trigger of acute pain is gone and there is still a pain experience without any obvious trigger, it is called chronic pain [1, 13, 21]. Thus, the pain no longer has the advantage of its protective function [22].

In general, the term chronic pain is generic for various pain types, such as inflammatory pain, cancer pain, spinal cord injury, brain injury, vascular diseases, autoimmune diseases, exposure to neurotoxins, metabolic disorders and neuropathic pain after nerve injury [10, 23]. In the latter one, it seems that the neuropathic component plays an important role concerning the severity of pain and its comorbidities, as well as reduced quality of life and increased health-care costs [24]. In Germany alone, around 17 % of people suffer from chronic, long-lasting pain conditions, as the German Pain Society reports (<https://www.schmerzgesellschaft.de/topnavi/patienteninformationen/schmerz>, as of March 26, 2020). Moreover, the most common symptomatic chronic pain condition, recurrent tension-type headaches, affects 1.9 billion people worldwide [25]. These numbers show that chronic pain is an emerging health burden, associated with negative consequences for the quality of life, treatment costs and employability [24, 26–28]. Thereby, chronic pain often arises from multiple events, including socio-demographic, psychological, clinical and biological factors [25]. In fact, mostly elderly people and women are at a higher risk to develop a chronic pain condition [25, 29, 30].

The link between acute and chronic pain has been extensively studied. So far, researchers concluded that several maladaptive mechanisms play a crucial role in the transition from acute to chronic pain. Thereby, various factors such as repeated environmental exposures to injury, inflammation, diseases, cancer, infections, stress in genetically predisposed individuals and

Introduction

activation of transcription factors with subsequent change in gene expression can lead to long lasting changes in functional properties of sensory neurons [1, 3, 8, 31, 32].

Additionally, the development of chronic pain is associated with an inflammatory reaction through prolonged proinflammatory cytokine release, that causes delay of inflammatory resolution [7, 33, 34]. These changes in the inflammatory reaction can be initiated and maintained either at the periphery or at central sites like spinal cord, trigeminal nucleus, brain stem or cortex [1, 23]. In the periphery the occurring altered neuronal activity, is called peripheral pain sensitization, and at central sites it is called central sensitization [12, 22, 23, 27]. Peripheral sensitization leads to an increased excitability of the peripheral nociceptors endings, due to a reduction of the normally high-threshold of nociceptors [12, 27]. This occurs often after tissue damage and inflammation, during which inflammatory mediators such as cytokines, lipids, histamines and other mediators reduce the activation threshold of nociceptor channel TRPV1, among others, resulting in enhanced heat sensitivity [8, 12, 14, 27, 31]. The occurring sensitization of TRPV1 is due to second messenger signaling cascades activated through those inflammatory cytokines, which bind to and stimulate G-protein coupled receptors (GPCR) in the nociceptors [7, 31, 35]. As a consequence, the sensitized state results in increased and prolonged responses to noxious stimuli, which means the pain experience elevates, also called hyperalgesia [12, 14, 16].

Additionally, action potentials are generated upon stimuli which normally do not activate nociceptors, such as light touch, which is defined allodynia [12, 14, 16] (Fig. 2). Both phenomena are associated with a reduction of the activation threshold of peripheral nociceptors [14].

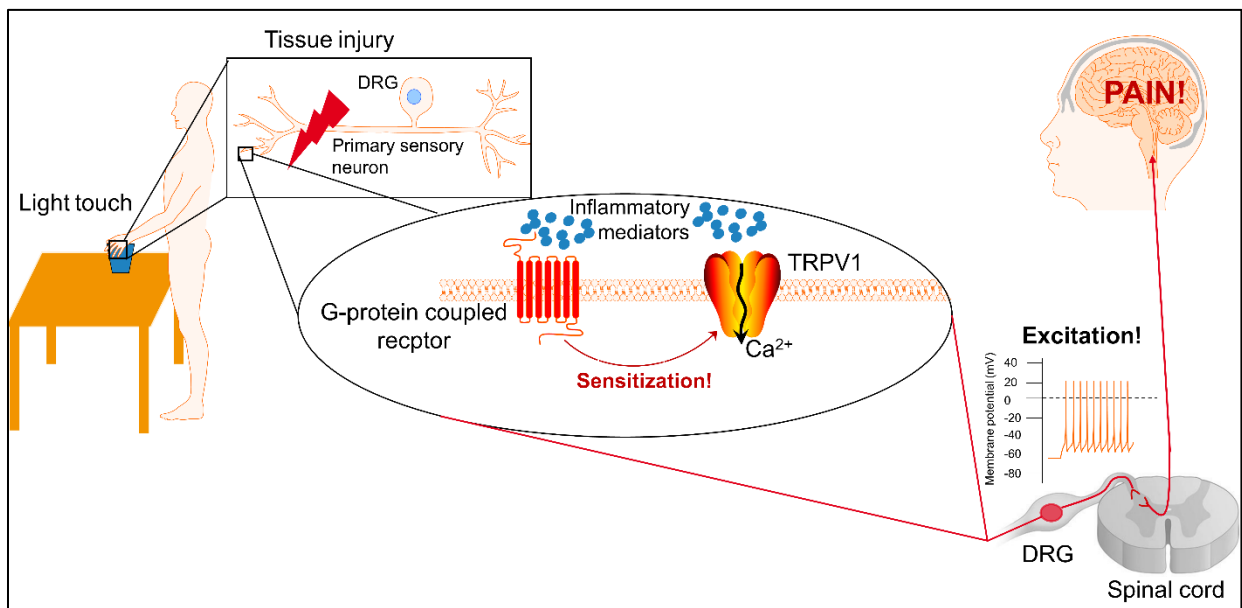


Figure 2. Peripheral sensitization. Tissue injury leads to inflammation, leading to release of inflammatory mediators. They directly bind to TRPV1 or activate GPCRs and by this lower the activation threshold of TRPV1 channels (sensitization) leading to increased action potential generation (excitation) and subsequent pain, even after innocuous light touch (allodynia).

In contrast, central sensitization is often associated with mechanical allodynia [36]. During central sensitization neuronal circuits in the spinal cord representing the injured region undergo structural and functional changes leading to increased synaptic efficacy [12, 36]. Thereby, changes in membrane excitability, synaptic efficacy, receptors and ion channels lead in a first phase to increased or augmented action potential outputs [2, 9, 37]. Additionally, inhibitory neurons, which normally dampen nociceptive signals, fail to decrease the excessive neuronal activity through reduced activity during central sensitization [37]. In a second phase, posttranslational modifications of neurotransmitter receptors and changes in their release result via second messenger signaling, such as ERK, in transcriptional changes within the central neurons, like induction of cyclooxygenase 2 (COX-2) [2, 22, 37]. Additionally, during central sensitization astrocytes and microglia are getting activated through neuropeptides or inflammatory mediators, which enter the CNS through increased permeability of the blood-brain-barrier [31, 33, 37]. Nevertheless, central sensitization is an adaptive mechanism, which often occurs after peripheral nerve-injury, leading to firing of damaged and non-damaged A- and C-fibers [37].

1.2. *Neuropathic pain*

Neuropathic pain is the term for a broad variety of chronic pain conditions, which are caused by postherpetic and trigeminal neuralgia, painful radiculopathy, diabetes, HIV infection, leprosy, amputation, peripheral nerve injury and stroke [33, 38, 39]. Although, autoimmune diseases like multiple sclerosis, bone compression in cancer, bacterial infections, traumatic injury, alcohol abuse or chemotherapeutic treatments can also lead to neuropathic pain [40, 41].

Neuropathic pain is, in contrast to inflammatory pain, defined by the International Association for the Study of Pain (IASP) as a direct consequence of a lesion or disease of the somatosensory nervous system and was found in one third of back pain patients (IASP, <https://www.iasp-pain.org/Education/Content.aspx?ItemNumber=1698#Neuropathicpain>, as of April 1, 2020, [24, 42]. Overall, between 6.9 – 10 % of people worldwide, which is more than 20 million people, suffer from neuropathic pain [40, 43–45]. Interestingly, such conditions depend on the diagnosis criteria in the geographical area of residence of the affected people: In the Middle East and Israel around 50 % of people suffer from neuropathic pain, whereas in Japan and Lybia only 4 % are affected [43, 44].

Characteristic symptoms of neuropathic pain are allodynia, hyperalgesia, spontaneous pain, ongoing pain, burning pain, paresthesia, pricking and abnormal, unpleasant sense of touch or loss of sensation [13, 23, 33, 34]. Interestingly, there is an undeniably high non-response to standard analgesics like nonsteroidal antiinflammatory drugs (NSAIDs) or low pain relief through other treatments [41, 46]. This means, less than 50 % of patients report less pain and / or a lot of side effects they have to deal with, when treated against neuropathic pain [46].

The underlying cause of neuropathic pain has been extensively studied. Overall, researchers agree that especially chronic pain conditions are undeniably connected with inflammation [7, 16, 31, 47]. A local form of inflammation at the site of nerve damage either in the peripheral or central nervous system emerges during neuropathic pain [31, 48]. This neuroinflammation is characterized by neuroimmune interactions between immune cells and neurons, occurring in response to injury, infection, or autoimmune-mediated damage to neurons [14, 48, 49]. Thereby, both, the neuronal and the immune system, can survey and modulate the degree of inflammation and pain sensitization through similar detection receptors [7, 14]. Such receptors may be used for the detection of bacteria, the sensing of acid, hypoxia, neuropeptides or inflammatory cytokines [14]. However, the neuroinflammatory component is a major feature of nerve-injury induced neuropathic pain [10, 21]. In other neuropathic pain conditions, the degree

of neuroinflammation is lower and the neuronal component predominates. For example, in neuropathic pain induced by chemotherapeutic drugs damage of the neurons caused by toxicity of the cytostatic drugs is characteristic [50, 51]. Thus, depending on the cause of neuropathic pain, the underlying mechanisms leading to neuropathic pain can be highly diverse [42, 52, 53]. Nevertheless, in this work the focus will be on the mechanisms underlying nerve-injury induced neuropathic pain.

1.2.1. Nerve injury induced neuropathic pain

There is a substantial body of literature on the mechanisms of neuroimmune interactions. Briefly, after tissue damage, such as nerve-injury, two major mechanisms take place: First, resident macrophages are getting activated and subsequently secrete various inflammatory mediators, such as cytokines, chemokines, bradykinin, histamine, prostanoids, prostaglandins, and further substances [2, 22, 41]. Second, nerve injury leads to alterations in cytokine and chemokine receptors, as well as in TRPV1 expression in neurons [3, 48]. Furthermore, there is an increased release of growth factors or neuropeptides like brain-derived neurotrophic factor (BDNF), calcitonin-gene related peptide (CGRP), substance P or nerve growth factor (NGF), resulting in further activation of immune cells and increase of TRPV1 expression and neuronal activity [14, 23, 33].

Previous research has found that cytokines produced by macrophages and other immune cells, such as tumor necrosis factor α (TNF α), interleukin 6 (IL-6) and IL-1 β , lead to axon damage. But, they are also able to directly or indirectly modulate nociceptor activity and subsequent increase spontaneous firing [1, 21, 47, 48]. The secreted cytokines and signaling molecules recruit circulating leukocytes to the area of damaged tissue [21, 41]. The recruitment occurs due to migration of leukocytes through chemokine and cytokine binding to GPCRs and the activation of underlying signaling pathways [2]. Besides, GPCRs are also found on neurons and get activated on neurons, too. For example, NGF acts on GPCRs or tyrosine kinase receptors leading to activation of phospholipase C (PLC) or protein kinase C (PKC), which in turn phosphorylate ion channels like TRPV1 [6, 13, 16, 31, 54].

Overall, the first infiltrating immune cells to arrive at the injured nerve are neutrophils. They secrete inflammatory mediators, which recruit further macrophages, followed by the activation of lymphocytes such as T cells [23, 41, 55]. According to Cobos and colleagues, genes and transcripts correlated with the onset of tactile allodynia showed a striking immune component and were primarily expressed in T cells and macrophages [56] (Fig. 3). The infiltration of macrophages and T cells to the site of injury together with the increased production of

Introduction

inflammatory mediators is a major feature of neuroinflammation [23]. Normally, the amount of inflammatory mediators is a complex and well controlled mechanism to facilitate healing by removing debris of degenerating axons and dead cells [34, 57]. Although, if the organism is not able to control the inflammation anymore and cannot switch from inflammation to resolution phase, a chronic state of inflammation is reached leading to tissue dysfunction [2, 34].

Previous research has demonstrated that bradykinin, prostaglandins, protons, adenosine triphosphate (ATP), nerve growth factor (NGF), $\text{TNF}\alpha$, IL-6, IL-1 β , chemokines like C-C chemokine receptor type 2 (CCR2), micro RNAs, lipid mediators, serotonin and nucleotides are algogenic substances [8, 23, 27, 31, 32, 41]. Thus, the inflammatory products are detected by the nociceptors through increased expression of the respective receptors, resulting in peripheral sensitization and subsequent pain hypersensitivity [14, 22, 23, 27]. A number of authors have reported that IL-6 and IL-1 β induce prostaglandin production, TRPV1 expression and enhanced TRPV1 excitability [7, 33, 34]. According to Lim *et al.* IL-6 is also able to reduce inhibitory transmission on central level such as the spinal cord [48] (Fig. 3).

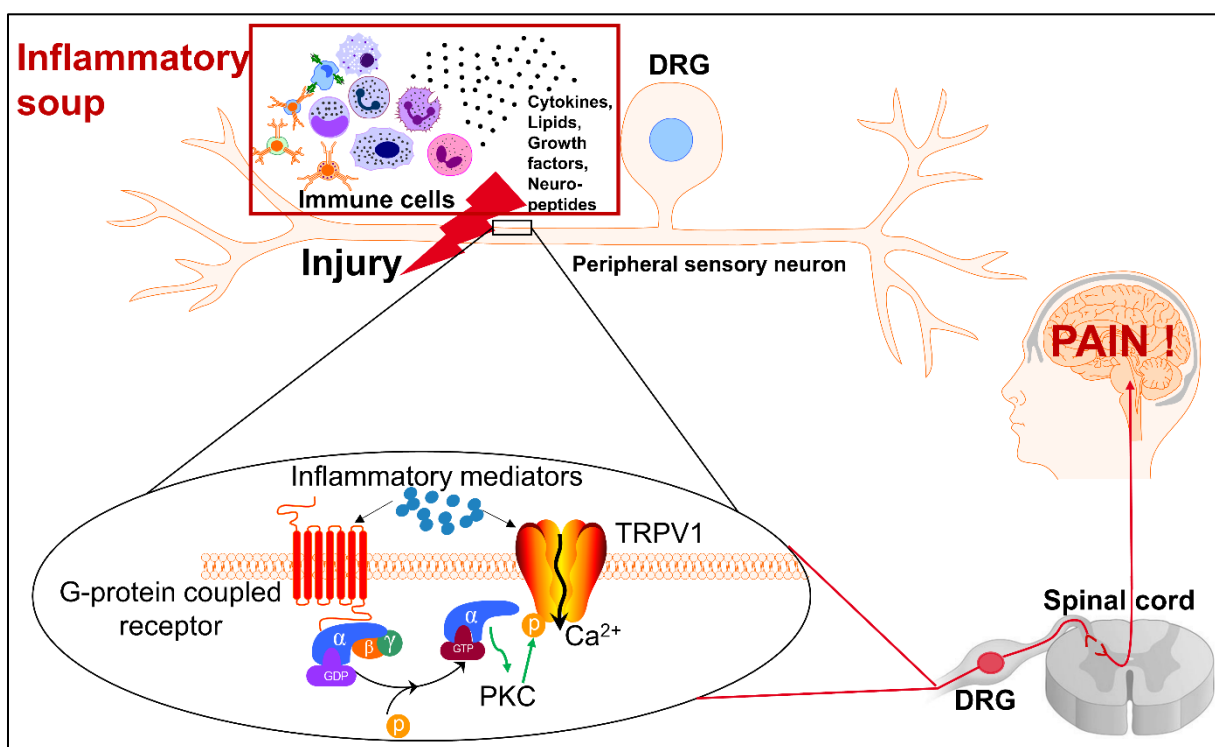


Figure 3. Induction of neuropathic pain. Nerve injury leads to neuroinflammation, associated with increased release of inflammatory mediators and infiltrating immune cells. The inflammatory mediators directly bind to TRPV1 or activate GPCR leading to phosphorylation of TRPV1. The phosphorylation leads to increased opening probability of TRPV1 and subsequent TRPV1 sensitization. The produced signal is then transmitted via the DRGs to the spinal cord and from there to the brain, where the information is translated into pain sensation.

Introduction

In contrast, TNF α leads to enhanced glutamate release of the C-fiber terminals. Thereby, it increases excitation on spinal cord level and induces neuronal sensitization through TRPV1 and the ankyrin type TRP channel TRPA1 [7, 23, 34, 48]. TNF α and IL-6 are able to act at CNS level because they can enter the CNS due to disruption of the blood-brain barrier through matrix metalloproteinase 2 and 9 (MMP2, MMP9), released by neurons [9, 33]. Further cytokines, especially interferon γ (IFN γ) secreted by T cells, activate cells of the CNS, astrocytes and microglia, which is manifesting during neuroinflammation, but not during acute pain [23, 27, 33].

Additionally, there is a large amount of research on further voltage-gated and TRP channels to be involved in the generation of neuropathic pain [9]. Drawing on earlier work by Bennett (2019) TRPA1, the melastatin type TRP channels TRPM8 and TRPM2 play a role in peripheral sensitization in neuropathic pain, too. Whereas, canonical TRP channels TRPC4 and 5 mediate central sensitization during the initiation of persistent pain after nerve injury [3].

In conclusion, it can be noted that the mechanisms underlying neuropathic pain after nerve-injury are complex and difficult, due to remarkable crosstalk of immune cells and neurons. This interaction might be a reason for the difficulties in treatment of neuropathic pain.

In general, only 30 % of patients respond to the gold standard treatments leading to a high number needed to treat (NNT) to reach a satisfactory pain relief [27, 58]. Thus, 7 to 8 patients have to be treated with the first-line treatments, such as the calcium channel blockers pregabalin and gabapentin, to get at least 50 % of pain reduction in 1 patient [58]. This poor outcome might be, because these drugs act only on a subunit of voltage-gated calcium channel Cav_{2.2} [9]. Hence, other mechanisms concerning TRPV1 or voltage-gated sodium-channels still are active and not addressed by these substances. Further treatments like serotonin-noradrenaline reuptake inhibitors, tricyclic antidepressants or opioids all have a NNT of 4 to 6 and act only on CNS level leading to side effects like respiratory depression, dizziness, nausea and concerning opioids risk of addiction [23, 48, 58]. Interestingly, Finnerup *et al.* reported about studies where treatment of neuropathic pain resulted even in an increase of pain experience [58]. However, there are only few positive studies about different treatment options of neuropathic pain, Finnerup and colleagues recommend the following drugs as first-line treatments, regardless of their moderate balance between desired and undesired effects: gabapentin, pregabalin, serotonin-noradrenaline reuptake inhibitors duloxetine or venlafaxine, tricyclic antidepressants. For second-line treatment capsaicin 8 % and lidocaine patches, as well as tramadol are recommended. However, the patches are only recommended for

peripheral neuropathic pain conditions. Strong opioids and botulinum toxin A are listed as third-line treatment recommendations [58]. Unfortunately, acquainted inflammatory drugs including NSAIDs like diclofenac or acetaminophen lead to no response concerning the pain relief in neuropathic pain patients [38, 40]. Next to this, there are various new treatment approaches like inhibition of cytokines, MMPs or TRPV1. However, there is a lack of a sufficient amount of studies and the few studies showed no satisfactory results so far [59]. Furthermore, due to their physiological functions cytokine, MMP or TRPV1 inhibitors could have extremely undesirable side effects [23, 35, 60, 61]. At this point it is important to consider the targets of the presented drugs. All of them are targeting only one component of the complexity of neuropathic pain, namely either the immune system (mainly cytokine inhibitors or NSAIDs) or the neuronal system (pregabalin, tricyclic antidepressants, TRPV1 inhibitors) [48]. Hence, it seems to be inevitable to target both, the neuronal and the immune component. Therefore, receptors expressed on both, neurons and immune cells, could be promising targets, such as cytokine and chemokine receptors or GPCRs [2, 3, 6, 13, 16, 31, 48, 54].

1.3. The Gpr132 receptor (G2A)

1.3.1. Structural features and ligands

During the last years there has been growing interest in the G-protein coupled receptor Gpr132, also named G2A [62]. The name G2A emerged of the observed cell cycle arrest in the G2/M phase and subsequent blockage of the accomplishment of mitosis [62]. A number of studies have been demonstrated that G2A is mainly expressed in hematopoietic tissues, macrophages, dendritic cells, mast cells, T and pro-B cells, as well as in tumor cell lines [62–65]. These findings strongly support the view of G2A playing an important role in hematopoiesis and immunity, which could affect among other physiologic states, tumor development and tumor growth [66]. Findings of Le and Lahvic *et al.* also point in this direction: The group of Le observed that mice with G2A-deficiency develop an autoimmune syndrome at age of one year, with enlarged secondary lymphoid organs, increased T and B cell numbers, increased responses of B and T cells and lymphocytic infiltration into various organs [67]. These features seem to be associated with the human autoimmune syndrome systemic lupus erythematosus [67]. Additionally, Lahvic and colleagues reported that marrow of G2A-deficient animals showed a functional defect in competitive long-term engraftment and a reduced number of functional long-term hematopoietic stem cells. The group concluded that G2A plays a crucial role in regenerative processes [68].

Introduction

G2A belongs to the largest superfamily of membrane proteins, which are encoded in over 800 genes [69–71]. The gene of G2A is encoded in a human genome region on chromosome 14q32.3, which is associated with ovarian cancer predisposition and progression [62]. The gene consists of four exons and three introns [72]. So far, there is no mutation associated with a clinical human diseases. However, a single nucleotide polymorphism in the human gene of G2A may lead to internal intimal media thickness of the carotid artery [73]. G2A, among most other GPCRs, is classified into class A of the six GPCR classes, the rhodopsin-like class [74, 75]. Furthermore, G2A belongs to the subclass of proton-sensing GPCRs, since it shares strong homologies with the family members T cell death associate gene 8 (TDAG8), ovarian cancer GPCR 1 (OGR1) and GPR4 [62, 66, 76]. Although, G2A has shown to have only weak proton-sensing properties, compared with its family members, due to loss of histidine residues, which are essential for the proton-sensing activity of OGR1 and GPR4 [77]. However, a recent study showed that lactate produced by tumors leads to activation of G2A resulting in a M2 like phenotype of macrophages and metastasis, as well as a poor outcome in patients with breast cancer [78]. Interestingly, it was also found in two independent studies that a more acidic pH leads to G2A localization on the cell surface, which differs from the other family members [79, 80].

Human G2A shares around 70 % identity with mouse and is highly conserved around the species like chimpanzee, rhesus macaque, wolf, cattle, rat, frog and zebrafish (https://www.ncbi.nlm.nih.gov/homologene?cmd=Retrieve&dopt=MultipleAlignment&list_uids=8350, as of April 6, 2020) [62, 81]. An exemplary alignment is shown in figure 4 of human, wolf and mouse (Fig. 4). As figure 4 shows, there is a high amount of amino acids being fully conserved in mouse, human and wolf (*), such as R203 [81](Fig. 4, black rectangle). Interestingly, the histidine residues important for the proton-sensing properties are not conserved, in neither mouse, human or wolf [82]. Nevertheless, there are a lot of conserved sites where amino acids of groups with strong similar properties are replaced, which is mostly indicated by the same color of the amino acids (Fig. 4). The high amount of conserved sites was confirmed by Murakami and colleagues, who observed that in human and mouse G2A was expressed in the same tissues and cells [79].

In general, all of the so far known GPCRs share a common core structure consisting of an extracellular N-terminal domain, seven membrane-spanning α -helices, interleaved with three intra- and three extracellular loops and an intracellular C-terminal domain. The extracellular domain is important for ligand binding. The ligands can be light, peptides, odor molecules,

Introduction

neurotransmitters, hormones, lipids, ions, extracellular protease activity, calcium and chemokines, and are subsequent involved in every physiological system [69, 71, 75].

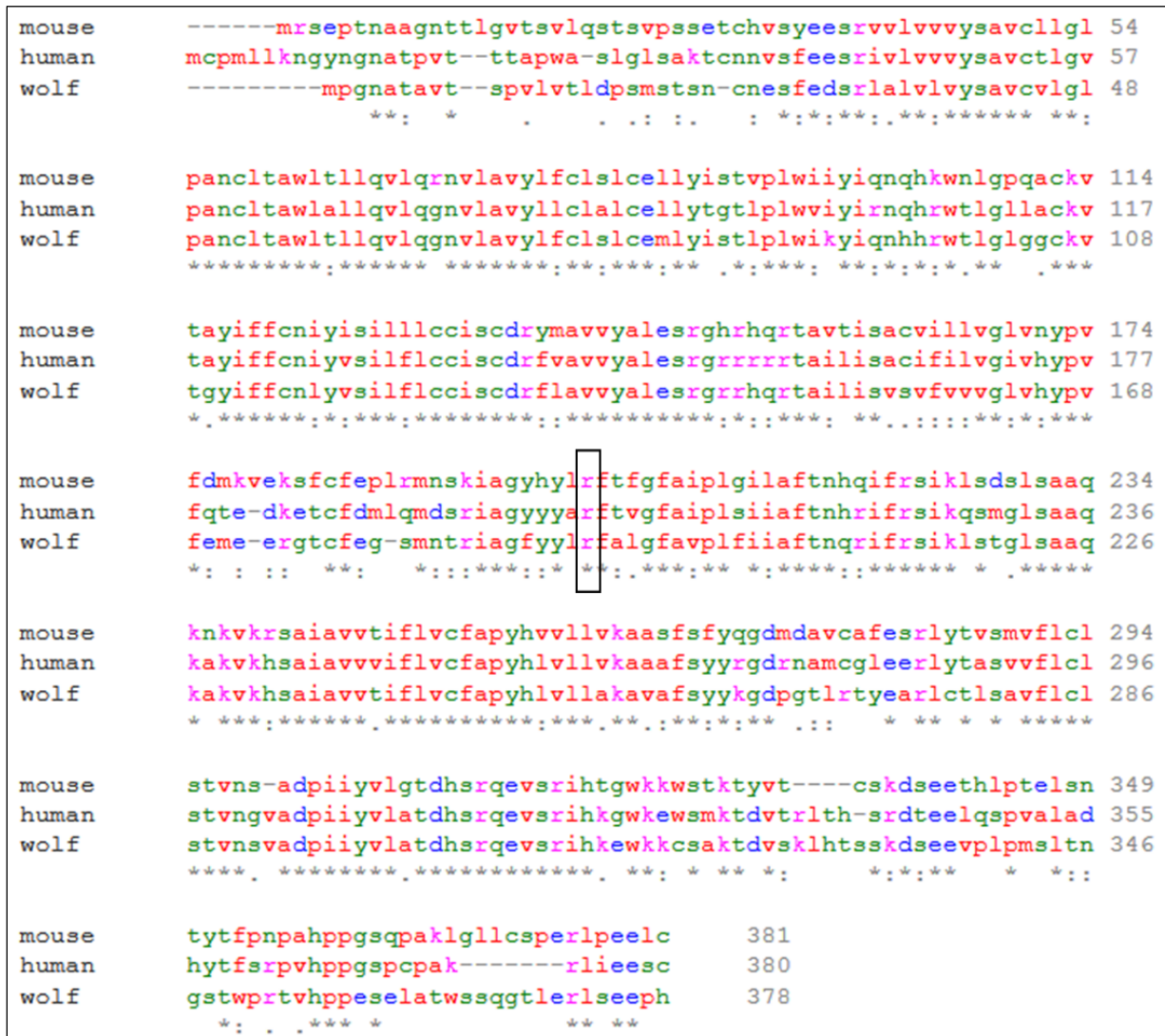


Figure 4. Alignment of G2A protein in different species. Protein sequences were used from NCBI database and a multiple sequence alignment with Clustal W was performed (Clustal Omega, <https://www.ebi.ac.uk/Tools/services/web/toolresult.ebi?jobId=clustalo-l20200527-101539-0541-41117307-p2m&showColors=true&tool=clustalo>). Red indicates small hydrophobic, blue acidic, magenta basic –H amino acids, green depicts hydroxyl plus sulfhydryl plus amine and G, grey indicates the rest of amino acids. The (*) asterisk indicates single, fully conserved residue, the colon (:) indicates conservation between the groups with strong similar properties and the point (.) indicates conservation between the groups of weak similar properties. The black rectangle depicts a fully conserved residual at position 203.

1.3.2. Signaling pathways of G2A

After its discovery, a lot of effort was taken into account to decipher the role of G2A and the underlying signaling pathways in a physiologic context. It was observed that G2A expression was upregulated in lymphocytes upon oxidative stress, DNA damage or upon bacterial infections [62, 83–86]. The upregulation was due to binding of transcription factors Runx1, c/EBP and Pu.1, all acting synergistically, at the promoter of human G2A [68, 87]. However, one has to keep in mind, that the promoter sequences of mouse and human are somewhat different and therefore, this expression activation mechanism does not apply for mouse G2A [88]. Interestingly, in mice there was found a link between peroxisome proliferator-activated receptor γ (PPAR γ) activation and reduced G2A expression through binding of PPAR γ to the G2A promoter region [65]. Another report showed that G2A was activated through binding of Foxp1 in pre-B cells leading to G2 arrest, which was also confirmed in patient samples [89].

Now, it should be turned to the meta discourse of the possible ligands of G2A. There is an undeniable evidence for G2A being a lipid binding GPCR [69, 90–92]. Nevertheless, the one and only specific ligand of G2A seems to remain elusive so far, since there have been several ligands postulated for G2A. Reports about lysophosphatidylcholine (LPC) as agonist of G2A were retracted and could not be reproduced in later studies [68, 81, 91, 93]. However, a recent study used soluble LPC, which seem to inhibit the actions of G2A. Normally, to transduce the signal from the extracellular domain to the inside of the cell, the bound ligand evokes a conformational change of the GPCR [69, 71]. This conformational change forms a cavity inside the cell and leads to transduction of the signal into the cytoplasm of the cell [75]. Thereby, the characteristically coupled heterotrimeric guanine-nucleotide-binding signal transducing protein (G protein) is activated and guanosine diphosphate (GDP) is replaced by guanosine triphosphate (GTP) [71, 75]. Then the GTP-liganded G α or G $\beta\gamma$ subunits are released from the receptor to bind to their downstream effector targets, such as cyclic adenosine monophosphate (cAMP), phospholipase C (PLC) and calcium, inositol monophosphate (IP), PKC, PKA or mitogen-activated protein kinases (MAPK) [71, 75, 91]. Regarding the actions of soluble LPC, it inhibited Ca²⁺ mobilization, AMPK phosphorylation and secretion of high mobility group box 1 (HMGB1), which plays an important role in DNA repair [94]. Next to this, LPC signaling seems to result in migration and more M1 like phenotype of macrophages [95, 96].

Furthermore, some researchers used lysophosphatidylserine as ligand for G2A. They, observed that it leads to clearance of neutrophils through macrophages by increasing cAMP levels and subsequent cAMP-dependent PKA activation followed by enhanced Ras-related C3 botulinum toxin substrate 1 (Rac1) activation [97, 98]. The clearance of neutrophils through

Introduction

G2A signaling could be confirmed in an acute zymosan-induced inflammatory mouse model. However, in inflammatory lung injury, no effect through G2A signaling was observed [99]. Additionally, 11,12-epoxyeicosatrienoic acid (11,12-EET) was found to be a ligand of G2A, which seems to be required for embryonic hematopoiesis [68].

Next, a further lipid was found to be a ligand of G2A. The oxidative metabolite of linoleic acid 9-hydroxyoctadecadienoic acid (9-HODE) was first found to be a ligand of human G2A, but later it was also confirmed for mouse G2A [81, 84, 90, 100]. The structure of 9-HODE is shown in figure 5, as well as the proposed binding of 9-HODE to G2A (Fig. 5). As the group of Foster postulated in an earlier study, lipids like 9-HODE seem to enter G2A via the transmembrane domain 4 and 5 [81].

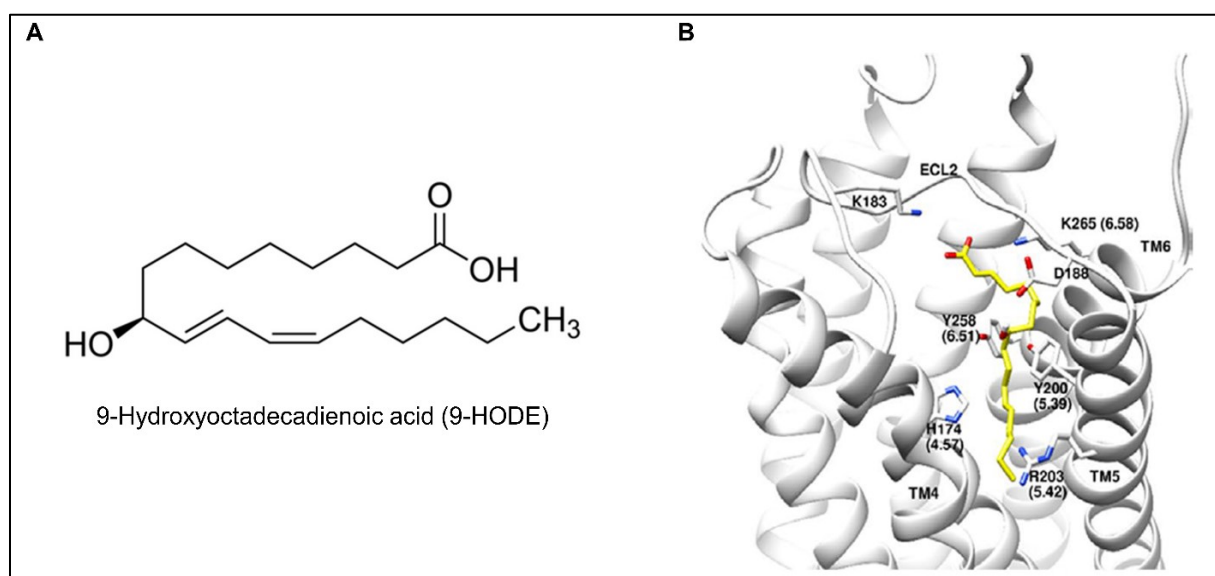


Figure 5. Binding of 9-HODE to G2A. (A) Structure of the oxidative linoleic acid metabolite 9-HODE. (B) 3D modulation of agonist binding of 9-HODE (yellow) to its receptor G2A. Proposed by Foster *et al.* in *Pharmacology Research & Perspectives*, 2019, Fig. 6B [81].

Through binding of agonists the actions of G2A are modulated, depending on its coupled G-protein (Fig. 6). Mostly $G\alpha$ proteins are coupled to G2A, which can be divided into $G\alpha_s$, $G\alpha_{12/13}$, $G\alpha_{i/o}$, and $G\alpha_{q/11}$ [71]. Each of the different $G\alpha$ -proteins result into different signaling pathways. Thus, it was demonstrated that G2A is mainly coupled to $G\alpha_{13}$, which leads to Rho activation and by this resulting in contact inhibition, survival, proliferation of cells and tumor initiation [90, 101–103]. However, it seems possible for G2A to interact synergistically with $G\alpha_s$ and $G\alpha_{13}$ leading to caspase-dependent apoptosis [63, 102]. Several studies have suggested a coupling of G2A only to $G\alpha_s$, leading to increased PLC activation and subsequent IP accumulation followed by elevated Ca^{2+} levels in either, HEK, HeLa or Cos-7 transfected cells (Fig. 6) [79,

90, 102]. Interestingly, increased Ca^{2+} levels and cAMP levels were observed when G2A heteromerizes with its family member OGR1 [104].

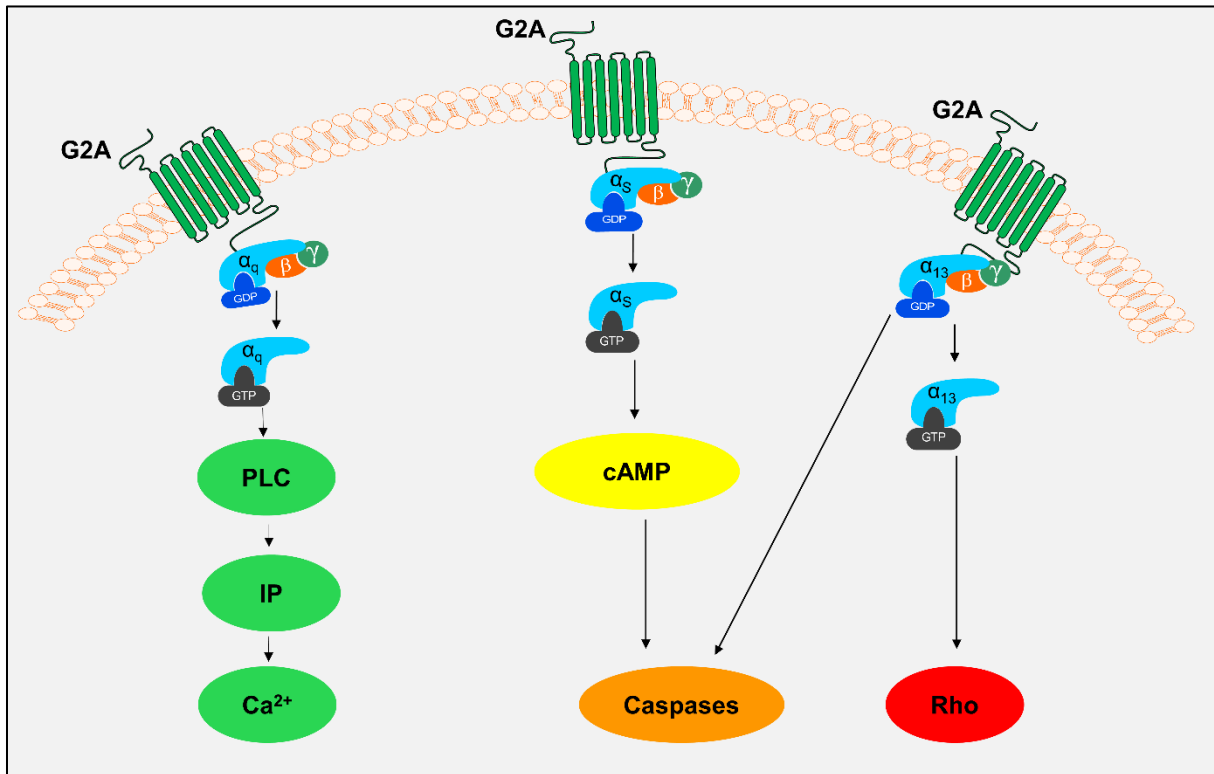


Figure 6. G2A signaling through different G-protein coupled pathways. G2A can couple to different G-proteins, like $\text{G}\alpha_q$, $\text{G}\alpha_s$ or $\text{G}\alpha_{13}$. Each coupling leads to different underlying signaling pathways.

1.4. G2A in health and disease

At this point it is appropriate to raise the issue of the concrete physiological functions of G2A, which are the consequence of the signaling pathways discussed. However, the results are inconclusive. Thus, there are studies claiming an antiinflammatory role for G2A in atherosclerosis, colitis or *Propionibacterium acnes* infections [63, 73, 86, 98, 103]. Those studies demonstrated, that knockdown or loss of G2A resulted in enhanced activation of ERK, phosphorylated Akt and nuclear factor kappa-light-chain-enhancer (NF- κ B), leading to increased secretion of inflammatory mediators such as IL-6, IL-8 and IL-1 β , survival gene expression and reduced monocyte-endothelial interactions [73, 86, 103]. In mice deficient for ApoE and G2A, there was further observed a reduced engulfment of apoptotic cells and increased atherosclerosis development [73].

In contrast, further studies concluded a proinflammatory role for G2A with inflammatory mediator secretion like IL-1 β , PGE2, IL-6 and IL-8, as well as proinflammatory M1 like phenotype of macrophages [65, 84, 90, 100]. The IL-1 β release was due to G2A activation through 9-HODE leading to JNK activation [90]. Interestingly, in a tumor context, G2A expression is associated with a poor outcome, due to the aggressiveness of cancer, high metastasis, more relapse and higher number of M2 like macrophages [64, 65, 78]. A quite clear function of G2A seems to be its involvement in migration and chemotaxis of macrophages and T cells [77, 95, 100]. On this basis, it can be concluded that G2A plays a crucial role in inflammation and tumor progression. However, it seems to be context-dependent whether it has anti- or proinflammatory function.

1.4.1. G2A and neuropathic pain

In the context of neuropathic pain, the role of G2A is so far only poorly understood since there are only a few studies on this subject. First, it was demonstrated, that G2A is mainly expressed in the brain and mostly in nociceptors with light or no myelination. Furthermore, its expression was strikingly co-localized with TRPV1 channels indicating a role in pain perception [105]. Interestingly, the heteromerization of G2A with OGR1 was reported to partially activate L-type Ca²⁺ channels, which are reported to be involved in pain after peripheral nerve injury [9, 104, 106]. As Huang and colleagues reported earlier, G2A-positive neurons co-expressed OGR1 at an amount of 70 %, indicating a role for G2A and OGR1 during pain and pain initiation through L-type Ca²⁺ channels [105].

Unfortunately, only few insights were gained so far and are inconclusive regarding the role of G2A in neuropathic pain. There has been reported an antinociceptive effect of G2A in chronic inflammation induced by CFA. When G2A was silenced a prolonged hyperalgesia due to increased granulocyte and macrophage numbers, as well as impaired clearance of neutrophils through macrophages was observed. Therefore, the group of Su suggested G2A being a threshold regulator in the control of chronic inflammation, especially in the beginning of inflammation through PKA signaling [107].

The recently found agonists of G2A of the N-acylglycines group might indicate an antinociceptive effect, too, since N-acylglycines are known for their antiinflammatory and antinociceptive functions [81]. In contrast, in an acute zymosan-induced inflammatory model, loss of G2A resulted in reduced hyperalgesia due to a reduced number of proinflammatory macrophages and reduced number of engulfed neutrophils at the site of inflammation [100].

There is only one study so far, which examined the role of G2A in neuropathic pain after chemotherapy. In this study, the researchers demonstrated that loss of G2A resulted in reduced mechanical hypersensitivity from day 2 onwards after oxaliplatin treatment. They further showed that 9-HODE was increased in wild-type paw, sciatic nerve and DRGs after oxaliplatin treatment, together with upregulated G2A expression in DRGs, which seems to be important for its pronociceptive effect. The decreased mechanical hypersensitivity was due to PKC activation leading to TRPV1 sensitization [85]. TRPV1 sensitization was further reported to be mediated by $G\alpha_q$ and $G\alpha_s$ coupled receptors, such as G2A [108] (see 1.3 The Gpr132 receptor (G2A)).

Few studies on G2A effects on pain were also performed in patients. Thus, patients with neck pain or chronic widespread pain showed increased plasma levels of 9-HODE were found and in diabetes patients G2A was upregulated in activated monocytes [109, 110]. Similar results were observed in patients with primary Sjögren's syndrome, who suffered from widespread pain [111]. These results indicate a role of 9-HODE and G2A in neuropathic pain in humans and mice. However, in a mouse model of multiple sclerosis, which is a disease associated with neuropathic pain, G2A seems to have no significant effect on the severity of the disease or the number of T cells *in vivo* [112].

In conclusion, there are contradictory studies concerning the role of G2A during inflammation and inflammatory pain [65, 98, 100, 103, 107]. Research is now slowly beginning to focus on the impact of G2A in neuropathic pain induced by diabetes, chemotherapy and nerve-injury. So far, only one study could show a pro-nociceptive effect of G2A after chemotherapeutic treatment. Thus, the question remains of the role of G2A in further neuropathic pain conditions.

1.5. Aim of this thesis

In this thesis the role of G2A in nerve-injury induced neuropathic pain should be examined. So far, only very little is known about the role of G2A in neuropathic pain conditions. Although, a reduced mechanical hypersensitivity was observed after oxaliplatin treatment in G2A-deficient mice, indicating a pronociceptive role of G2A in neuropathic pain [85]. However, in chemotherapy-induced neuropathic pain, the inflammatory component only plays a minor role concerning the mechanical hypersensitivity [31, 113, 114]. Although, G2A is mainly expressed on immune cells and its commonly known ligand 9-HODE was demonstrated to be increased in various pain models and was shown to increase TRPV1 activation [85, 109, 111, 115, 116]. Additionally, G2A can have various roles on inflammation (see 1.3. The Gpr132 receptor (G2A)) [62, 73, 98, 100]. However, the distinct roles of G2A and its underlying signaling

pathways are elusive so far. Therefore, the central hypothesis of this thesis is that G2A modulates mechanical hypersensitivity and neurogenic inflammation in nerve-injury induced neuropathic pain.

Studies on current treatments revealed large placebo-effects, severe side effects or no pain relief at all and a high number needed to treat of 4 to 10, treatment of neuropathic pain is still a challenge [38, 40, 58, 61, 117]. Therefore, it is of utmost importance to find new approaches to treat neuropathic pain. Here, G2A could be a promising new target, as it is expressed on immune cells, but also sensitizes TRPV1 in neurons [62, 85]. Therefore, through targeting G2A a modulation of the immune response together with the neuronal response could be possible when it comes to medication of neuropathic pain [31, 47].

Thus, an additional aim of this thesis was to find possible antagonists of G2A and to determine their effect on TRPV1 sensitization, as well as their effect on inflammation in the context of nerve-injury induced neuropathic pain (Fig. 7).

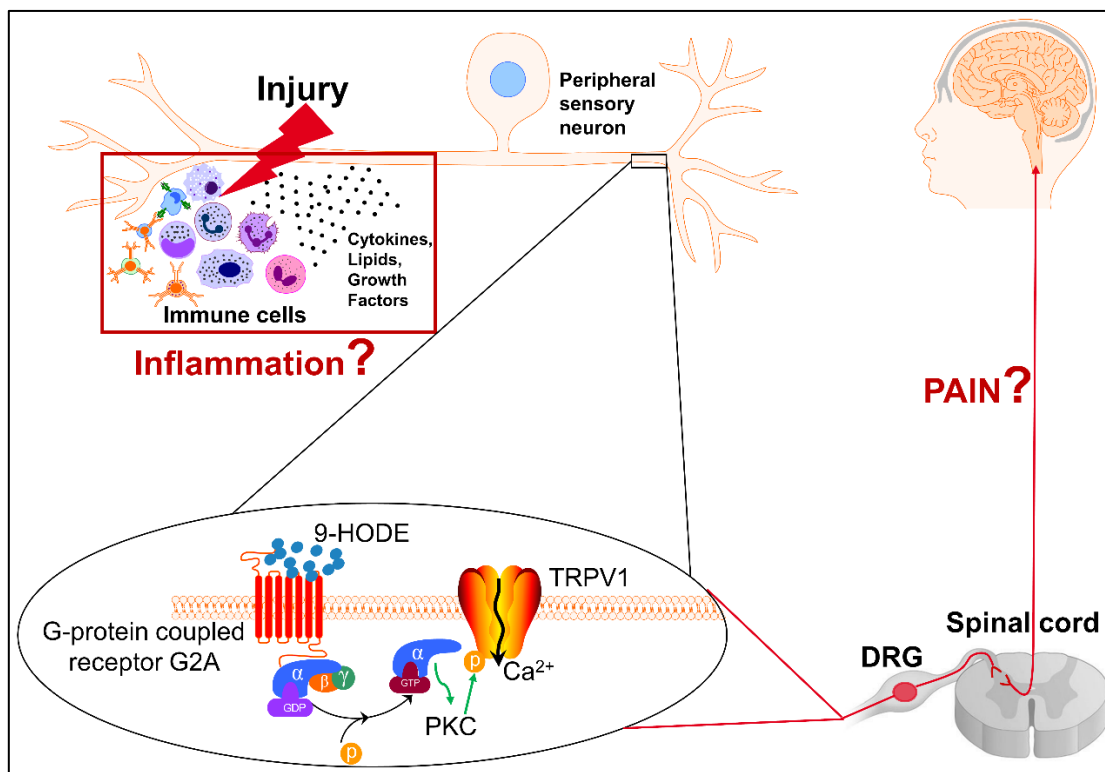


Figure 7. Scheme of open questions in nerve injury induced neuropathic pain. Nerve injury leads to neuroinflammation, associated with increased release of inflammatory mediators and infiltrating immune cells. The inflammatory mediators directly bind to TRPV1 or activate G2A, which then sensitizes TRPV1 response, by phosphorylating the channel. The produced signal is then transmitted via the DRGs to the spinal cord and from there to the brain, where the information is translated into pain sensation. The questions remain, whether G2A has an effect on inflammation and on pain sensitization in nerve-injury induced neuropathic pain.

2. Material and Methods

2.1. *Materials*

2.1.1. Animals

<u>Animals</u>	<u>Supplier</u>
C57BL/6NRj	Janvier Labs, LaRochelle, France
B6.129X1(C)-GPR132 ^{tm1Whit/J} (G2A KO) [67]	mfd diagnostics, Wendelsheim

2.1.2. Antibodies

<u>Antibody</u>	<u>Dilution</u>			<u>Supplier</u>
	<i>IHC</i>	<i>WB</i>	<i>FACS</i>	
Anti-Cluster of differentiation 11b (CD11b)	1:500			Abcam, Cambridge, UK
Anti-CD11b			1:200	Biolegend, San Diego, California, USA
Anti-CD11c			1:200	BD Biosciences, Franklin Lakes, New Jersey, USA
Anti-CD19			1:100	BD Biosciences, Franklin Lakes, New Jersey, USA
Anti-CD3e			1:100	BD Biosciences, Franklin Lakes, New Jersey, USA
Anti-CD4			1:50	Biolegend, San Diego, California, USA
Anti-CD45			1:50	Miltenyi Biotec, Bergisch Gladbach
Anti-CD8a			1:100	Biolegend, San Diego, California, USA
Anti-F4-80			1:200	Biolegend, San Diego, California, USA
Anti-Glyceraldehyde 3-phosphate dehydrogenase (GAPDH) antibody - loading control		1:1000		Abcam, Cambridge, UK

Material and Methods

Anti-Glucocorticoid-induced tumor necrosis factor receptor (GITR) (CD357)		1:100	Biolegend, San Diego, California, USA
Anti-goat horse radish peroxidase (HRP) conjugate		1:5000	Abcam, Cambridge, UK
Anti-HLA-DR (MHCII)		1:100	Miltenyi Biotec, Bergisch Gladbach
Anti-lymphocyte antigen 6 complex locus C (Ly6C)		1:200	BD Biosciences, Franklin Lakes, New Jersey, USA
Anti-Ly6G		1:100	Biolegend, San Diego, California, USA
Anti-mouse HRP conjugate		1:5000	Sigma Aldrich, Deisenhofen
Anti-Neurokinin receptor 1.1 (NK1.1)		1:100	BD Biosciences, Franklin Lakes, New Jersey, USA
Anti-rabbit HRP conjugate		1:5000	Sigma-Aldrich, Deisenhofen
4',6-Diamidin-2phenylindol (DAPI)	1:1000000		Carl Roth, Karlsruhe
goat anti-Engulfment and cell motility protein 1 (ELMO1)	1:1000		abcam, Cambridge, UK
Goat anti-Glial fibrillary acidic protein (GFAP)	1:1000		Abcam, Cambridge, UK
goat anti-Matrix metalloproteinase 9 (MMP9)		1:500	Novusbio, Centennial, Colorado, USA
Goat anti-Protein tyrosine kinase 7 (PTK7)		1:1000	R&D Systems, Minneapolis, Minnesota, USA
goat anti-rabbit Alexa fluor 488 (AF488)	1:1000		abcam, Cambridge, UK
goat anti-rat Cyanine fluorescent dye 488 (CF488)	1:400		Biotium, Fremont, California

Material and Methods

Goat anti-Transgelin (Tgln)	1:1000	Novusbio, Centennial, Colorado, USA
Mouse anti- Extracellular signal regulated kinase 2 (ERK2)	1:1000	Santa Cruz Biotechnology, Dallas, Texas, USA
Mouse anti-Heat shock protein 90 α/β (Hsp90 α/β)	1:1000	Santa Cruz Biotechnology, Dallas, Texas, USA
Mouse anti- Phosphoinositide 3-kinase (PI3K)	1:1000	Enzo life sciences, Farmingdale, US
Rabbit anti-CD11b	1:100	abcam, Cambridge, UK
Rabbit anti-Chemokine- like receptor 1 (CMKLR1)	1:1000	Origene, Rockville, USA
Rabbit anti-C-X-C chemokine ligand 7 (CXCL7)	1:500	NSJ Bioreagents, San Diego, USA
Rabbit anti-C-X-C chemokine receptor type 4 (CXCR4)	1:1000	Biossantibodies, Woburn, Massachusetts, USA
Rabbit anti-GFAP	1:1000	Novusbio, Centennial, Colorado, USA
Rabbit anti-Ionized calcium binding adapter molecule-1 (Iba1)	1:100	Wako Chemicals, Neuss
Rabbit anti-Integrin alpha- IIb precursor (Itga2b)	1:1000	Biorbyt, Cambridge, UK
Rabbit anti-Low density lipoprotein receptor (LDLR)	1:500	abcam, Cambridge, UK
Rabbit anti-MMP9	1:1000	Proteintech, Rosemont, Illinois, USA
Rabbit anti-MMP9	1:800	Novusbio, Centennial, Colorado, USA

Material and Methods

Rabbit anti-p38 Mitogen-activated protein kinase (MAPK)	1:1000	Cell Signaling, Frankfurt am Main
Rabbit anti-phospho-p38 MAPK	1:1000	Cell Signaling, Frankfurt am Main
Rabbit anti-phosphor-p44/42 MAPK (ERK1/2)	1:1000	Cell Signaling, Frankfurt am Main
Rabbit anti-Ras-related C3 botulinum toxin substrate 1 (Rac1)	1:1000	abcam, Cambridge, UK
Rabbit anti-Rat sarcoma (Ras)	1:1000	Cell Signaling, Frankfurt am Main
Rabbit anti-Rho-associated protein kinase 1 (ROCK-1)	1:500	Abcam, Cambridge, UK
Rabbit anti-ROCK-2	1:500	Abcam, Cambridge, UK
Rat anti-F4-80	1:500	abcam, Cambridge, UK
Sheep anti-rabbit Cyanine 3 (Cy3)	1:1000	Sigma-Aldrich, Deisenhofen

2.1.3. Buffers and Solutions

<u>Buffer/Solution</u>	<u>Ingredients</u>
10x sodium dodecyl sulfate (SDS) running buffer	0.25 M Tris/HCl pH 8.3 1.92 M Glycin 1 % (w/v) Sodium dodecyl sulfate (SDS)
4x Laemmli buffer	100 mM Tris(hydroxymethyl)aminomethane (Tris) (pH 7.4) 8 % (w/v) SDS 10 % (w/v) 2-Mercaptoethanol 40 % (w/v) Glycerol 0.1 % (w/w) Bromphenolblue
Antibody solution Immunohistochemistry 1 (IHC1)	1 % Bovine serum albumin (BSA) (w/v) in Phosphate buffered saline with tritone (PBST)
Antibody solution IHC2	1 % (w/v) BSA in Phosphate buffered saline (PBS)

Material and Methods

Antibody solution western blot (WB)	1 % (w/v) BSA in Tris-HCl, NaCl with Tween (TNT)
Blocking buffer WB	5 % (w/v) milk powder in Tris-HCl, NaCl (TN)
Blocking IHC 1	3 % (w/v) BSA in PBST
Blocking IHC 2	3 % (w/v) BSA in PBS
Blotting buffer - Western Blot	20 % (v/v) Trans-Blot Turbo Buffer 20 % (v/v) Ethanol 60 % (v/v) H ₂ O
Borat buffer - coating cover slips	50 mM boric acid 23.6 mM sodium borate Add 100 ml aqua dest. Adjust pH 8.5
Dehydration buffer	20 % (w/v) sucrose in water
Fluorescence-activated cell sorting (FACS) Solution 1	Dulbecco's Modified Eagle's Medium (DMEM) 3 mg/ml Collagenase 1 µl/ml DNase
FACS Solution 2	DMEM 10 % (v/v) Fetal calf serum (FCS)
FACS Solution 3	0.5 % (w/v) BSA in PBS
Fixation IHC	2 % (w/v) Paraformaldehyde (PFA) in PBS, pH 7.4
Inositol monophosphate (IP)-One Agonist buffer	IP-One Buffer 1.5 % (v/v) Dimethyl sulfoxide (DMSO)
IP-One Antagonist buffer	IP-One Buffer 1.5% (v/v) DMSO 12.5 µM 9-Hydroxyoctadecadienoic acid (HODE)
IP-One buffer	10 mM 4-(2-Hydroxyethyl)piperazine-1-ethanesulfonic acid (HEPES) 146 mM NaCl 4,2 mM KCl 1 mM CaCl ₂ 0.5 mM MgCl ₂ 6H ₂ O 50 mM LiCl ₂ 5.5 mM D-Glucose, free H ₂ O

Material and Methods

	0.1% (w/v) fatty acid free BSA
	pH 7.4
Lysis buffer	50% Phosphosafe
	50% cOmplete ULTRA
Phosphate buffered saline with triton (PBST)	0.1% (v/v) triton-x in PBS
Phosphate buffer IHC	23 mM NaH ₂ PO ₄
	126 mM Na ₂ HPO ₄
	add 1 L water
Ponceau solution - Western Blot	2.62mM Ponceau
	0.5% (v/v) acetic acid
Ringer solution	145 mM NaCl
	1,25 mM CaCl ₂ * 2H ₂ O
	1 mM MgCl ₂ * 6H ₂ O
	5 mM KCl
	10 mM Glucose
	10 mM HEPES
	pH 7,3
Running Gel 12 % - SDS polyacrylamide gel electrophoresis (SDS PAGE)	8 ml Rotiphorese® Gel 30
	5 ml running gel buffer
	100 µl 10% (w/v) Ammonium peroxydisulfate (APS)
	20 µl N,N,N',N'-Tetramethylethylene-1,2- diamine (TEMED)
	6,8 ml H ₂ O
Running gel buffer - SDS PAGE	1.5 M Tris/HCl pH 8.8
	0.4% (w/v) SDS
Stacking gel 4 % - SDS-PAGE	1,3 ml Rotiphorese® Gel 30
	2,5 ml stacking gel buffer
	50 µl 10% (w/v) APS
	10 µl TEMED
	6,1 ml H ₂ O
Stacking gel buffer - SDS PAGE	0.5 M Tris/HCl pH 6.8
	0.4% (w/v) SDS
Standard dilution solution – LUMINEX	50% Assay Diluent

Material and Methods

Trimethyltryptamine (TMT) labeling buffer – Proteomics	50% Lysis buffer 0.2 M 4-(2-Hydroxyethyl)-1-piperazinepropanesulfonic acid (EPPS) pH 8.2 10% (v/v) Acetonitrile
TN buffer - Western Blot	10 mM Tris/HCl pH 7.4 100 mM NaCl
TNT buffer – Western Blot	10 mM Tris/HCl pH 7.4 100 mM NaCl 0.1% (v/v) Tween
Zamboni Fixative	20 g PFA in 150 ml picric acid (heated to 60 °C) 2.52% NaOH (dropwise till clear solution) filtrated and cooled down add to 1 L phosphate buffer IHC

2.1.4. Cell Culture

Cell Culture Device / Medium

B27 Supplement
F12 Nutrient Mix + GlutaMax™
Fetal calf serum (FCS)
Fura-acetoxymethylester (Fura-AM)
Gentamycin
Glutamin
Hanks' balanced salt solution (HBSS) (+Ca, +Mg)
Macrophage- colony stimulating factor (M-CSF)
Neurobasalmedium
Penicillin /Streptomycin
PhosphoSafe
Poly-L-Lysin
Roswell Park Memorial Institute (RPMI) Medium 1640 – GlutaMAX-I
Trypan blue

Supplier

Gibco, Waltham, Massachusetts, USA
Gibco, Waltham, Massachusetts, USA
Sigma-Aldrich, Deisenhofen
Biotium, Fremont, California, USA
Biozym Scientific GmbH, Hessisch Oldendorf
Sigma-Aldrich, Deisenhofen
Gibco, Waltham, Massachusetts, USA
Peprotech, Hamburg
Gibco, Waltham, USA
Gibco, Waltham, Massachusetts, USA
Merck, Darmstadt
Sigma-Aldrich, Deisenhofen
Gibco, Waltham, USA
Sigma-Aldrich, Deisenhofen

2.1.5. Cell Culture Medium

Medium name

Ingredients

Material and Methods

Bone marrow derived macrophages (BMDM) medium	RPMI medium 1640 - GlutaMAX™-I 1 % (v/v) Penicillin/Streptomycin 10 % (v/v) FCS 0.2 µl/ml M-CSF
Chinese hamster ovary cells (CHO) K1 – medium	F12 Nutrient Mix - GlutaMax™ 10 % (v/v) FCS 1 % (v/v) Penicillin/Streptomycin
Dorsal root ganglia (DRG) medium – DRG culture	Neurobasal medium 1 % (v/v) Pen/Strep 1 % (v/v) Glutamine 1x (v/v) B27 50 µg/ml gentamicin
Transwell stop solution	1 % (w/v) BSA PBS sterile filtrated
Transwell – Solution 1	RPMI medium 1640 - GlutaMAX™-I 1 % (v/v) Penicillin/Streptomycin RPMI 10 % (v/v) FCS
Transwell – Solution 2	RPMI medium 1640 - GlutaMAX™-I 1 % (v/v) Penicillin/Streptomycin RPMI 1 µM 9-HODE
Transwell – Solution 3	RPMI medium 1640 - GlutaMAX™-I 1 % (v/v) Penicillin/Streptomycin RPMI 1 µM 9-HODE 0.1 µM G2A Antagonist (G2A11, G2A13 or G2A19)
Transwell – Solution 4	RPMI medium 1640 - GlutaMAX™-I 1 % (v/v) Penicillin/Streptomycin RPMI 1 µM 9-HODE 1 µM G2A Antagonist (G2A11, G2A13 or G2A19)
Transwell – Solution 5	RPMI medium 1640 - GlutaMAX™-I 1 % (v/v) Penicillin/Streptomycin RPMI 1 µM 9-HODE

Material and Methods

	10 μ M G2A Antagonist (G2A11, G2A13 or G2A19)
Transwell – Solution 6	RPMI medium 1640 - GlutaMAX™-I 1 % (v/v) Penicillin/Streptomycin 1 μ M 9-HODE DMSO same amount as 10 μ M G2A Antagonist
Transwell medium	RPMI medium 1640 - GlutaMAX™-I 1 % (v/v) Penicillin/Streptomycin
Trypan blue solution	4 % (w/v) trypan blue 0.9 % (w/v) NaCl
Wash medium - DRG culture	Neurobasal medium 10 % (v/v) FCS 1 % (v/v) Pen/Strep 1 % (v/v) Glutamine

2.1.6. Chemicals

<u>Chemical</u>	<u>Supplier</u>
0.9 % NaCl	B. Braun, Melsungen
4-(2-Hydroxyethyl)-1-piperazinepropanesulfonic acid (EPPS)	Sigma-Aldrich-Deisenhofen
Acetic acid	Sigma-Aldrich, Deisenhofen
Acetonitrile (ACN)	Sigma-Aldrich, Deisenhofen
Ammonia	Thermo Fisher, Scientific, Waltham, USA
Ammonium persulfate (APS)	Sigma-Aldrich, Deisenhofen
Ammonium-bicarbonate (ABC)	Sigma-Aldrich, Deisenhofen
Baicalein (Bai)	Sigma-Aldrich, Deisenhofen
Boric acid	Merck, Darmstadt
Bovine serum albumin (BSA)	Carl Roth, Karlsruhe
Bradford Reagent	Sigma-Aldrich, Deisenhofen
Bradykinin acetate	Sigma-Aldrich, Deisenhofen
Bromphenolblue	Bio-Rad, Hercules, California, USA
Butylated hydroxytoluene (BHT)	Sigma-Aldrich, St. Louis, USA
Calcium-(II)-chloride-Dihydrate	Sigma-Aldrich, St. Louis, USA

Material and Methods

Capsaicin (E-N-(4-Hydroxy-3-methoxybenzyl)-8-methyl-6-nonen acid amid)	Merck, Darmstadt
Chloroform	Sigma-Aldrich, St. Louis, USA
cOmplete ULTRA tablets	Roche Holding AG, Basel, Switzerland
Copper-(IV)-sulfate pentahydrate	Sigma-Aldrich, Deisenhofen
D+ Sucrose	Carl Roth, Karlsruhe
Diclofenac	Tocris, Bristol, UK
Dimethyl sulfoxide (DMSO)	Honeywell, Bucharest, Romania
Distilled water	Gibco, Waltham, Massachusetts, USA
DPX Mountant for histology	Sigma-Aldrich, Deisenhofen
Dulbecco's Phosphate buffered saline (DPBS)	Gibco, Waltham, Massachusetts, USA
Ethanol 70 %	Carl Roth, Karlsruhe
Ethanol p.a.	Honeywell, Bucharest, Romania
Ethyl acetate	Merck, Darmstadt
Fatty acid free BSA	Sigma-Aldrich, Deisenhofen
Formic acid	Sigma-Aldrich, Deisenhofen
Frema milk powder	Reformhaus
Glucose	Sigma-Aldrich, Deisenhofen
Glycerol	Appli-Chem, Darmstadt
Glycin	Carl Roth, Karlsruhe
2-(4-(2-Hydroxyethyl)-1-piperazinyl)-ethanesulfonic acid (HEPES)	AppliChem, Darmstadt
Isoflurane	Abbvie Inc., Chicago, USA
Isopropanol (2-Propanol) 100 % (v/v)	Sigma-Aldrich, Deisenhofen
Ketoconazole	Tocris, Bristol, UK
Linoleic acid (LA)	Sigma Aldrich, Deisenhofen
Lipopolysaccharide <i>E. coli</i> (LPS)	Sigma-Aldrich, Deisenhofen
Lithium chloride	Sigma-Aldrich, Deisenhofen
Endoproteinase LysC (LysC)	Wako Chemicals, Neuss
Magnesium chloride	Sigma-Aldrich, Deisenhofen
Methanol	Carl Roth, Karlsruhe
Monosodium phosphate	Sigma-Aldrich, Deisenhofen
Nordihydroguaiaretic acid (NDGA)	Cayman Chemical, Ann Arbor, Michigan, USA

Material and Methods

O-[4-(1,1,3,3-tetramethylbutyl)phenoxy]polyethoxyethanol (Triton® X-100)	Sigma-Aldrich, Deisenhofen
Paraformaldehyde (PFA), fluid	Carl Roth, Karlsruhe
PFA, powder	AppliChem, Darmstadt
Phenol	Ambion, Waltham, USA
Picric acid based solution, saturated with water	Morphisto GmbH, Frankfurt am Main
Pierce® enhanced chemiluminescence (ECL) Western Blotting Substrate	Thermo Fisher Scientific, Waltham, USA
Polyoxyethylen(20)-sorbitan-monolaurat) (Tween®-20)	Sigma-Aldrich, Deisenhofen
Ponceau S	Sigma-Aldrich, Deisenhofen
Potassium chloride	Merck, Darmstadt
Potassium iodide	Sigma-Aldrich, Deisenhofen
Potassium sodium tartrate dihydrate	Merck, Darmstadt
Rotiphorese® Gel 30	Carl Roth, Karlsruhe
Sodium borate	Fluka Honeywell, Bucharest, Romania
Sodium chloride	Sigma-Aldrich, Deisenhofen
Sodium dodecyl sulfate (SDS)	Carl Roth, Karlsruhe
Sodium hydroxide	AppliChem, Darmstadt
Sodium phosphate dibasic	VWR Chemicals, Darmstadt
Superfix, Fixation concentrate	Tetenal Europe, BW Plus Röntgen, Kamp-Lintfort
Tetramethylethylenediamine (TEMED)	Carl Roth, Karlsruhe
Tissue tek® O.C.T.™ Compound	Sakura Finetek Europe, Alphen aan den Rijn, Netherlands
Trimethyltryptamine (TMT) reagents	Thermo Fisher Scientific, Waltham, USA
Tracking Beads	BD Biosciences, Franklin Lakes, USA
Trans Blot Turbo Buffer	Bio-Rad, Hercules, USA
Trifluoroacetic acid (TFA)	Sigma-Aldrich, Deisenhofen
Tris(hydroxymethyl-)aminoethane (Tris)/HCl pH 8.3	Sigma-Aldrich, Deisenhofen
Ultrafin B7W negative Developer	Tetenal Europe, BW Plus Röntgen, Kamp-Lintfort

Material and Methods

Urea	Sigma-Aldrich, Deisenhofen
Zileuton (Zileut)	Tocris, Bristol, UK
β -Mercaptoethanol	AppliChem GmbH, Darmstadt

2.1.7. Enzymes

<u>Enzyme</u>	<u>Supplier</u>
Accutase	Sigma-Aldrich, Deisenhofen
Collagenase from Clostridium histolyticum	Sigma-Aldrich, Deisenhofen
Dispase II	Roche, Basel, Switzerland
RNase free DNase	Promega Corporation, Madison, USA
Trypsin-Ethylenediaminetetraacetic acid (EDTA) (0.05 %)	Gibco, Waltham, USA

2.1.8. Equipment and materials

<u>Device</u>	<u>Supplier</u>
22 cm long, 75 μ m ID fused-silica column	ReproSil-Pur, Dr. Maisch
24 well flat bottom plate	Greiner bio-one, Kremsmünster, Austria
384 well TC polystyrol plate, white	Greiner bio-one, Kremsmünster, Austria
5 ml Polystyrene Round-Bottom Tube	Corning Life Sciences, New York, USA
96 well flat bottom plate	Greiner bio-one, Kremsmünster, Austria
Agilent 1200 binary HPLC pump and degasser	Agilent, Waldbronn
Amersham Protran Western Blotting Membranes, Nitrocellulose	Sigma-Aldrich, Deisenhofen
Bio-Plex 200	Bio-Rad, Hercules, USA
C18 column	Phenomenex, Torrance, USA
CEA RP New Film	BW Plus Röntgen, Kamp-Lintfort
Cell culture dish, sterile 35/10mm	Greiner bio-one, Kremsmünster, Austria
Cell culture dish, sterile, 145/20mm	Greiner bio-one, Kremsmünster, Austria
Cell culture plate-IP-One Nunc 384 well microtiter plate	Thermo Fisher, Waltham, USA
Cover slips	Thermo Scientific Menzel, Waltham, USA
Cover slips 12 mm \varnothing	Glaswarenfabrik Karl Hecht GmbH, Sondheim von der Röhn

Material and Methods

Cryotom CM3050S	Leica Camera, Wetzlar
Dionex HPLC	Thermo Fisher Scientific, Waltham, USA
Dumont #7 Forceps	F.S.T, Heidelberg
Dynamic Plantar Aesthesiometer	Ugo Basile, Comerio, Italy
Easy nLC1200	Thermo Fisher Scientific, Waltham, USA
Empore C18 resin material	Thermo Fisher Scientific, Waltham, USA
Fluorescence-activated cell sorting (FACS) aria III cell sorter	BD Biosciences, Franklin Lakes, USA
Feather® Standard Scalpel No. 11	Pfm medical, Cologne
Fine bone scissor	F.S.T, Heidelberg
Fluorescence camera, AxioCam MRm	Carl Zeiss, Oberkochen
Fluorescence microscope, Axio Observer.Z1	Carl Zeiss, Oberkochen
Fusion Lumos mass spectrometer	Thermo Fisher Scientific, Waltham, USA
Gemini NX C18 column and precolumn (150 x 2 mm inner diameter, 5 µm particle size, 110 Å pore size)	Phenomenex, Aschaffenburg
Glass vials	Ziemer GmbH, Langenwehe
HTC Pal autosampler	CTC analytics, Zwingen, Switzerland
Incelligence Cell Reader	Bio-Rad Laboratories, Hercules, California, USA
Kalt Suture Needle	F.S.T, Heidelberg
Leica DMI4000 B microscope, CTR 6500 HS, DFC360 FX-Camera	Leica Microsystems, Wetzlar
LSRII/FOrtessa flow cytometer	BD Biosciences, Franklin Lakes, USA
Mayo-Hegar-Needle-Holder	F.S.T, Heidelberg
Multiplate reader Tecan infinite F200 Pro	Tecan Life Sciences, Männedorf, Switzerland
Neubauer counting chamber	LO Laboroptik Ltd, Lancing, UK
Non-sterile silk suture Thread	F.S.T, Heidelberg
Object slide	Thermos Scientific, Waltham, USA
Oribtrap	Thermo Fisher Scientific, Waltham, USA
Quadrupole tandem mass spectrometer QTRAP 5500	Sciex, Darmstadt

Material and Methods

QuantStudio Real-Time PCR, Quant Studio 5	Thermo Fisher, Waltham, USA
S&T forcep	F.S.T, Heidelberg
SDS gel chamber	Bio-Rad, Hercules, USA
SepPak tC18 column	Waters GmbH, Eschborn
SONOPLUS sonifier	Bandelin, Berlin
Tans Blot Turbo Transfer System	Bio-Rad, Hercules, USA
Tans-Blot® Turbo™ Mini-size transfer stacks	Bio-Rad, Hercules, USA
Tecan multidrop equipped with a standard cassette	Tecan Life Sciences, Männedorf, Switzerland
Thincert cell culture for 24 well plates	Greiner bio-one, Kremsmünster, Austria
Tissue forceps	F.S.T, Heidelberg
Tissue Tek Cryomold	Sakura Finetek Europe, Alphen aan den Rijn, Netherlands
Vannas spring scissor	F.S.T, Heidelberg

2.1.9. Kits

<u>Kit</u>	<u>Supplier</u>
Micro-bicinchoninic acid (μ BCA) assay	Thermo Fisher Scientific, Waltham, USA
Enzyme-linked immunosorbent assay (ELISA) Interleukin 1 β (IL-1 β) mouse Quantikine Kit	R&D Systems, Minneapolis, USA
ELISA IL-6 mouse for lysates	Ray Biotech, Peachtree Corners, USA
ELISA mouse Nerve growth factor (NGF)	DL Develop, Wuxi, China
ELISA Tumor necrosis factor α (TNF α) mouse for lysates	Ray Biotech, Peachtree Corners, USA
First Strand cDNA Synthesis Kit	Thermo Fisher, Waltham, USA
mirVana miRNA Isolation Kit	Applied Biosystems, Foster City, USA
Mouse Cytokine Magnetic 20-Plex Panel	Life technologies, Carlsbad, USA
Mouse total Matrix-metalloproteinase 9 (MMP-9) Quantikine ELISA kit	R&D Systems, Minneapolis, USA

2.1.10. Lipids

<u>Lipids</u>	<u>Supplier</u>
(±)9- Hydroxyoctadecadienoic acid (HODE)	Cayman Chemical, Ann Arbor, Michigan, USA
11,12- Dihydroxy-eicosa-5,8,11,17-Tetraenoic Acid (DiHETE)	Cayman Chemical, Ann Arbor, Michigan, USA
11,12- Epoxyeicosatrienoic acid (EET)	Cayman Chemical, Ann Arbor, Michigan, USA
12(13)- Epoxy octadecenoic acid (EpOME)	Cayman Chemical, Ann Arbor, Michigan, USA
12,13- Dihydrox octadecenoic acid (DiHOME)	Cayman Chemical, Ann Arbor, Michigan, USA
13-HODE	Cayman Chemical, Ann Arbor, Michigan, USA
14,15-DiHETE	Cayman Chemical, Ann Arbor, Michigan, USA
14,15-EET	Cayman Chemical, Ann Arbor, Michigan, USA
17(18)- Epoxyeicosatetraenoic acid (EEQ)	Cayman Chemical, Ann Arbor, Michigan, USA
19(20)- Epoxydocosapentaenoic acid (EpDPA)	Cayman Chemical, Ann Arbor, Michigan, USA
5,6-DiHETE	Cayman Chemical, Ann Arbor, Michigan, USA
5,6-EET	Cayman Chemical, Ann Arbor, Michigan, USA
8,9-DiHETE	Cayman Chemical, Ann Arbor, Michigan, USA
8,9-EET	Cayman Chemical, Ann Arbor, Michigan, USA
9(10)-EpOME	Cayman Chemical, Ann Arbor, Michigan, USA
9,10-DiHOME	Cayman Chemical, Ann Arbor, Michigan, USA

2.1.11. Marker

<u>Marker</u>	<u>Supplier</u>
Prestained protein MW, 1.4 mg/ml peqGOLD Protein-Marker II	Peqlab Biotechnologie GmbH, Erlangen VWR Chemicals, Darmstadt

2.1.12. qPCR

<u>Primer</u>	<u>Supplier</u>
Activating transcription factor 3 (ATF3) TaqMan® Gene Expression Assays (mouse)	Thermo Fisher, Waltham, USA

Material and Methods

Glyceraldehyde 3-phosphate dehydrogenase (GAPDH) TaqMan® Gene Expression Assays (mouse)	Thermo Fisher, Waltham, USA
G-protein coupled receptor 132 (Gpr132) TaqMan® Gene Expression Assays (mouse)	Thermo Fisher, Waltham, USA
Interleukin 12a (IL-12a) TaqMan® Gene Expression Assays (mouse)	Thermo Fisher, Waltham, USA
IL-12b TaqMan® Gene Expression Assays (mouse)	Thermo Fisher, Waltham, USA
Inducible nitric oxide synthase (i-Nos) TaqMan® Gene Expression Assays (mouse)	Thermo Fisher, Waltham, USA
Matrix metalloproteinase 9 (MMP9) TaqMan® Gene Expression Assays (mouse)	Thermo Fisher, Waltham, USA
Nicotinamide adenine dinucleotide phosphate (NADPH) oxidase 2 (Nox-2) TaqMan® Gene Expression Assays (mouse)	Thermo Fisher, Waltham, USA
Nox-4 TaqMan® Gene Expression Assays (mouse)	Thermo Fisher, Waltham, USA
TaqMan® Gene Expression Master Mix	Thermo Fisher, Waltham, USA
TaqMan® RealTime PCR	Applied Biosystem, Foster City, USA
Vascular endothelial growth factor (VEGF) TaqMan® Gene Expression Assays (mouse)	Thermo Fisher, Waltham, USA
Xanthine dehydrogenase (Xdh) TaqMan® Gene Expression Assays (mouse)	Thermo Fisher, Waltham, USA

2.1.13. Software

Software

Analyst software version 1.6.3

Excel 2016

Supplier

Sciex, Darmstadt

Microsoft, Redmond, USA

FlowJo V10	BD, Heidelberg
GelAnalyzer 2010	
Graph Pad Prism 7	Graph Pad Software, San Diego, USA
Multiquant Software version 3.0.2	Sciex, Darmstadt
Proteome Discoverer 2.2	Thermo Fisher, Waltham, USA
QuantStudio Real-Time PCR, Quant Studio 5	Thermo Fisher, Waltham, USA
ZenPro	Carl Zeiss, Oberkochen

2.2. Methods

2.2.1. Animal models

2.2.1.1. *Animals*

For all herein presented experiments animals with a C57BL/6NRj background were used, or G2A-deficient with a BL/6 background. The strain of G2A-deficient mice was generated by the lab of Prof. Owen Witte, University of California (San Francisco) [67] and was bred at MFD diagnostics (Wendelsheim, Germany). Wild-type mice were purchased from a commercial breeding company (Janvier, Le Genest-Saint-Isle, France). All animals were kept under stable temperature conditions (22 ± 0.5 °C) as well as day/night (12 h/12 h) conditions. The animals were fed with dry food and water ad libitum before and during all experiments. For better comparison of the results animals were matched in sex and age in wild-type and G2A-deficient groups (9-61 weeks, male and female).

Preclinical pain experiments were in accordance with the suggestions from the Preclinical Pain Research Consortium for Investigating Safety and Efficacy (PPRECISE) Working Group [118]. Behavioral experiments with the named mice were approved by the local animal ethics commission (Darmstadt) with the permit numbers FK/1046 and FK/1113. During all behavioral experiments the experimenter was blinded.

2.2.1.2. *Spared nerve injury (SNI)*

For preclinical pain experiments the common standard model of nerve injury induced pain in mice, the spared nerve injury (SNI) was used [119, 120]. Therefore, animals were anaesthetized with 2 % isoflurane in an oxygen stream. Then longitudinal to the femoral bone and proximal to the knee joint a small skin incision was performed. The underlying muscle layer was separated with a S&T forceps (F.S.T, Heidelberg) and a vannas spring scissor

(F.S.T, Heidelberg) to expose the sciatic nerve distal to the knee. Afterwards, two branches of the sciatic nerve, the tibial and the common peroneal nerves, were first ligated and then two millimeters of the nerves were cut out at the distal site of ligation, leaving the sural nerve intact. The nerve was placed back under the muscle layer and the wound was closed with 1 or 2 stitches and with a 0.08 mm braided silk suture (F.S.T., Heidelberg). For seven days the mice were used for behavioral experiments. After seven days the mice were euthanized for further preparations.

2.2.1.3. Assessing mechanical thresholds with the Dynamic plantar test

The mechanical pain threshold of mice was determined with a dynamic plantar Aesthesiometer (Ugo Basile, Comerio, Italy). Therefore, mice were placed in test cages onto an elevated grid 1 to 2 hours before the measurement allowing them to accommodate. Then, baseline measurements were performed by pushing a steel rod against the outer plantar side of the right and left hind paw. Thereby, a linear ascending force from 0 to 5 g in 0.5 g/s intervals was applied within 10 s. The time until fast withdraw of the paw, named paw withdraw latency, was documented since it indicates a nociceptive behavior of the mice. The cut-off time was set at 20 s. After baseline measurements, SNI surgery was performed followed by measuring the nociceptive behaviors of mice at days 1, 2, 4 and 7 [121].

2.2.1.4. Tissue preparation

Seven days after SNI surgery the animals were euthanized. Then, the legs were cut open longitudinal to the femoral bone and the sciatic nerve which was exposed to SNI surgery (ipsilateral) and the sciatic nerve without SNI surgery (contralateral) was dissected. Next, the longitudinal to the spinal cord tissue and ribs were cut followed by carefully opening of the vertebral canal. Thereby, special care was taken not to damage the spinal cord. For LUMINEX measurements the spinal cord was cut in the middle to separate the ipsi- and contralateral site from each other. After dissecting the spinal cord L1 to L6, the rest of the spinal cord was removed and the DRGs L4 to L6 of ipsi- and contralateral site were dissected out of their cavities in the vertebral canal. The dissected tissues were frozen immediately in liquid nitrogen and were then kept at -80 °C until further analysis.

2.2.2. Biochemical methods

2.2.2.1. Fluorescence-activated cell sorting (FACS) analysis

Fluorescence-activated cell sorting (FACS) was used to analyze the different cell types in various tissues of mice after SNI surgery. Therefore, treated wild-type mice (C57BL/6NRj, 11

weeks) and G2A-deficient mice (15-18 weeks) were euthanized. Then sciatic nerves (SN), spinal cord (SC) and dorsal root ganglia (DRGs) (L4-6) of ipsi- and contralateral site were dissected. Afterwards 500 μ l of 4 °C cold PBS was added to each sample. The nerves were transferred into 6-well plates to chop them into small pieces. Spinal cord samples were pottered. DRG samples were not further chopped, since they are already small pieces of tissue. Each sample was then mixed with 500 μ l of FACS-Solution 1 (see 2.1.3 Buffers and Solutions) and incubated for 30 min at 37 °C and 5 % CO₂. Every 10 min the samples were inverted. After 30 min, 500 μ l of FACS-Solution 2 (see 2.1.3 Buffers and Solutions) was added to each sample. The samples were mixed well and then transferred through a 70 μ m filter into a 2 ml Eppendorf tube. After washing the filter with FACS-Solution 3 (see 2.1.3 Buffers and Solutions) the samples were centrifuged at 400 g for 5 min. The supernatant was discarded, the cell pellet was resuspended in 500 μ l FACS-Solution 3 (see 2.1.3 Buffers and Solutions) and centrifuged again at 400 g for 5 min. The supernatant was discarded, the pellet was resuspended in 50 μ l FACS-Solution 3 (see 2.1.3 Buffers and Solutions) and transferred into a FACS tube. The Eppendorf tube was washed with 50 μ l FACS-Solution 3 (see 2.1.3 Buffers and Solutions). Then the samples were stained with different fluorochrome-conjugated antibodies: anti-CD3-PE-CF594, anti-CD4-V500, anti-CD8-BV650, anti-CD11b-BV605, anti-CD11c-AlexaFluor700, anti-CD19-APC-H7, anti-Ly6C-Per-CP-Cy5.5, anti-NK1.1 PE, anti-CD45-Vio-Blu, anti-MHC-II-APC, anti-F4/80-PE-Cy7, anti-GITR-FITC, and anti-Ly6G-APC-Cy7. Concentrations of the single antibodies are listed in 2.1.2 Antibodies. All antibodies and secondary reagents were titrated to determine optimal concentrations. The stained samples were analyzed on a LSR II/Fortessa flow cytometer. The obtained data was analyzed using FlowJo V10. Comp-Beads (BD Biosciences, Franklin Lakes) were used for single-color compensation to create multicolor compensation matrices. For gating, fluorescence minus one control was used. The instrument calibration was controlled daily using Cytometer Setup and Tracking beads [122–124].

2.2.2.2. *Western Blot*

For quantification of different proteins in various samples, Western Blot analysis was performed. First, 20-30 μ g protein extracts were mixed with 1x Laemmli-buffer and heated to 95 °C for 5 min. Then the samples were loaded onto a gel consisting of 4% stacking gel and 12 % running gel, which was prepared before according to the recipe under 2.1.3. Buffers and Solutions. In a Mini-PROTEAN electrophoresis chamber (Bio-Rad, Munich) protein extracts were separated on the gels via SDS gel electrophoresis first for 20 min at 80 V, followed by another hour at 140 V. Afterwards four filtering papers were dampened with turbo blot buffer

(Bio-Rad, Munich) and then put on the Trans-Blot®Turbo™ Transfer System (Bio-Rad, Munich). On top of them a dampened nitrocellulose membrane (Amershan Protran, Little Chalfont) was placed followed by the SDS gel and another four dampened filtering papers. The blotting was then carried out for 7 min at 25 V and 1.3 A. To ensure the transfer of the proteins from the gel onto the membrane, the membrane was stained with Ponceau solution followed by washing the membrane with aqua distilled and TN buffer for 15 min. Then the membrane was blocked with blocking buffer WB for 2 h on a rocking shaker. Afterwards the membrane was incubated over night at 4 °C with the desired primary antibody in Antibody solution Western Blot on a rotator. HSP90 or GAPDH was used as loading control depending on the molecular weight of the desired detected protein. The next day, the membrane was washed three times for 5 min with TNT buffer. The respective second antibody was then added to the membrane and incubated for 1 h on the rocking shaker at room temperature. Detection was performed after another five washing steps with TNT buffer via Pierce® ECL Western Blotting substrate. Therefore, the membrane was incubated for 1 min with the 1:1 mixed substrate solution of the Pierce® ECL Western Blotting kit. A CEA RP film (BW Plus Röntgen, Kamp-Lintfort) was then exposed to the membrane for 20 to 30 min followed by development and fixation [122].

The appropriate solutions and buffers are listed in 2.1.2 Antibodies and 2.1.3 Buffers and Solutions.

Quantification of protein amount on the film was performed by measuring the intensity of bands. Therefore, the scanned pictures were loaded into GelAnalyzer 2010 software and the background was subtracted via the baseline mode method [125]. Afterwards intensities of the single bands were determined. The values were used for the calculation of the amount of protein compared to loading control in percentage using Microsoft Excel 2016.

2.2.2.3. *Bradford protein assay*

The protein amount in tissue lysate or bone marrow derived macrophage (BMDM) culture samples was determined with the Bradford protein assay for western blot or Luminex protocol.

A BSA stock (1 mg/ml) was prepared in the lysis buffer of samples (see 2.1.3. Buffers and Solutions). For standard curve calculation the BSA stock was diluted to 5, 4, 3 and 2 µg in 10 µl PBS. As blank only PBS was used. The samples were diluted 1:5 in PBS. Then, 190 µl Bradford reagent was added to all samples, the BSA samples and the tissue lysate or BMDM samples. The absorbance at 595 nm was measured immediately with a multiplate reader Tecan infinite F200 Pro. The obtained data was used for calculation of the standard curve,

which served for the evaluation of protein amount in tissue lysate or BMDM samples [126]. All measurements were performed in technical duplicates.

2.2.2.4. *Enzyme-linked immunosorbent assay (ELISA)*

Another method for quantification of protein is the enzyme-linked immunosorbent assay (ELISA). ELISA experiments were performed with lysates of the sciatic nerve tissue dissected from wild-type and G2A-deficient mice (see 2.2.1.4. Tissue preparation). In all herein described ELISAs, the samples and standards were measured in technical duplicates. If not otherwise depicted the values were calculated by using the equation given by the regression of the standard curve, which was calculated with Graph Pad Prism version 7.1.

IL-1 β and MMP9

First, 500 μ l cell lysis buffer 2 (R&D Systems, Minneapolis, USA) was added to thawed nerve tissue, which was then chopped with the vannas spring scissor (F.S.T., Heidelberg) in small pieces. Afterwards the tissue was incubated for 30 minutes in cell lysis buffer 2 with mixing the solution every 10 min. Then the samples were centrifuged at 10,000 rpm for 10 minutes. The supernatant was used for Bradford protein assay (see 2.2.2.3 Bradford protein assay) and the following ELISA measurements.

Afterwards the reagents and the standard dilution series of the IL-1 β kit were prepared according to the manufacturer's instructions (R&D Systems, Minneapolis, USA). For MMP-9 ELISA the reagents were prepared accordingly. IL-1 β and MMP9 ELISA were performed according to the manufacturer's instructions. The samples were used undiluted and 50 μ l of the samples were added to the each well of the 96-well plate of the respective kit. The optical density was then determined by absorbance at a wavelength of 405 nm and a wavelength correction of 540 nm with a multiplate reader Tecan infinite F200 Pro. For calculation the difference of 450 nm and 540 nm was calculated and the values were used for the equation given by the regression of the standard curve, which was calculated with Graph Pad Prism version 7.1.

TNF α and IL6-ELISA

First, 600 μ l cell lysis buffer of the TNF α -ELISA kit (Ray Biotech, Peachtree Corners, USA) was added to nerve tissue, which was then handled the same way as before in the IL-1 β ELISA. Afterwards the reagents and standard dilution series of the TNF α kit or IL-6 kit were prepared according to the manufacturer's instructions (Ray Biotech, Peachtree Corners, USA). Then 100 μ l of respective standard concentrations or undiluted samples were added to each

well of the 96-well plate of the TNF α kit or the IL-6 kit, respectively. The following steps were performed according to the manufacturer's instructions. The absorbance was measured at 450 nm with a Multiplate reader Tecan infinite F200 Pro.

NGF-ELISA

The samples were prepared by adding 600 μ l of ice-cold PBS. The nerves were chopped in small pieces with a vannas spring scissor (F.S.T, Heidelberg) and sonicated twice for 10 s at 60 %. Afterwards they were centrifuged at 10,000 g for 10 min. The supernatant was used for Bradford Protein Assay (see 2.2.2.3 Bradford protein assay) and the following ELISA measurements.

First, all reagents and plates had to be prepared according to the manufacturer's instructions (DL Develop, Wuxi, China). Then 100 μ l of standard or undiluted sample was added to each well of the 96-well plate of the NGF-ELISA kit. The following procedure was conducted according to the manufacturer's instructions (DL Develop, Wuxi, China). The absorbance at 450 nm was measured with a multiplate reader Tecan infinite F200 Pro.

LUMINEX Multiplex assay

LUMINEX is a technique to detect up to 20 different cytokines and chemokines in one sample at the same time. At the day of measurement the reagents have had to be at room temperature. Standards and reagents were prepared according to the manufacturer's instructions (Life technologies, Carlsbad, USA). Frozen ipsi- and contralateral samples of sciatic nerve, spinal cord and DRGs (L4-6) tissue were thawed. Samples were lysed using 400 μ l lysis buffer for nerve samples, 150 μ l lysis buffer for spinal cord samples and 120 μ l lysis buffer for DRG samples. DRG samples were then sonicated twice at 60 % for 10 s. Nerve samples were first chopped, spinal cord samples were first pottered before they were sonicated twice at 60 % for 10 s. Afterwards all samples were centrifuged for 10 min at 10,000 rpm. The following procedure of LUMINEX multiplex assay were performed according to the manufacturer's instructions using Mouse cytokine magnetic 20-Plex Kit (Life technologies, Carlsbad, USA). The residual supernatants were used for Bradford assay analysis (2.2.2.3 Bradford protein assay). Finally, 20 different cytokines were measured with a Bio-Plex device (Bio-Rad Laboratories, Hercules, USA). For calculation Microsoft Excel 2016 and Graph Pad Prism version 7.1 were used.

2.2.3. Cell biological methods

2.2.3.1. *Differentiation and stimulation of Bone marrow derived macrophages (BMDM)*

Mice (C57BL/6NRj, m, or G2A-deficient (G2A^{-/-}), m, 9-32 weeks) were sacrificed, the hind legs were dissected from the body and transferred into ice-cold PBS. The bones were cleaned from muscle tissue, cut open and put into 0.5 ml Eppendorf tubes with holes at their peak end, sitting in 1.5 ml Eppendorf tubes. In the 1.5 ml Eppendorf tubes 50 µl of BMDM medium was added. Then both tubes with the bones were centrifuged for 1 min at 13,000 rpm to isolate the bone marrow. Afterwards, 12.5 ml BMDM medium was used for resuspension of the bone marrow cell pellet. 2 ml of the suspension was added to each well of a 6-well plate. The cells were incubated over night at 37 °C followed by a change of BMDM medium the next day. After 3 to 4 days of incubation at 37 °C 2 ml of fresh BMDM medium was added to each well. After 7 days the cells were fully differentiated and used for further experiments. [100, 127, 128]

For stimulation experiments, BMDM medium was changed to serum-free BMDM overnight. Then cells were stimulated with 1 µM 9-HODE for 0, 5, 10 and 15 min or 1, 2, 4, 6, 10 and 24 h. The cells were harvested by adding lysis buffer and scrapping the cells of the bottom of the plate. Then the cells were sonicated twice for 10 s at 60 %. Whole protein amount was measured by Bradford protein assay (2.2.2.3 Bradford protein assay) [85, 100, 129]. The protein extracts were used for further analysis either for proteome screen, western blots or MMP-9 ELISA. The appropriate solutions are listed in 2.1.4 Cell culture medium.

2.2.3.2. *Transwell migration assay*

For analysis of the migratory behavior of the macrophages, a transwell migration assay was performed as previously described and according to the manufacturer's instructions with minor adjustments [130] (Greiner bio-one, Kremsmünster, Austria). Briefly, grown and cultivated BMDMs were starved over night at 37 °C with 5 % CO₂ by incubating them with Transwell medium. The next day the cells were washed with PBS and then 400 µl accutase per well was added, to loosen the cell-bottom connections of the BMDMs. After incubation for 5 min at 37 °C the reaction of the accutase was stopped with 800 µl transwell stop solution per well. Afterwards the cells were scraped off with a cell scraper from the bottom of the 6-well plate. After centrifugation at 1,000 rpm for 5 min, the cells were resuspended in 1 ml of Transwell medium. The number of cells per ml was counted by using trypan blue solution in a 1:2 dilution with the cell suspension and a Neubauer counting chamber. The cells were then diluted up to 7.44 x 10⁵ cells/ml. Afterwards, the Thincert inserts with a transparent membrane and a pore

Material and Methods

diameter of 8 μm were placed into each well of a 24-well plate. 300 μl of the cell suspension was added to each insert. The cells were then incubated for 10 min at 37 °C. Then the desired solutions (Transwell – Solution 1-6) for testing the migratory behavior were prepared. 750 μl of the solutions were added to the well below the inserts as table 1 shows. The appropriate solutions are listed in 2.1.4 Cell culture medium. The experiments were performed in technical triplicates of each condition and for each antagonist in general.

After incubation for 4 h at 37 °C and 5 % CO_2 the medium was aspirated of the wells and the inserts. The inserts and wells were washed twice with 1 ml PBS and then 1 ml 4.5 % PFA was added to each well and incubated for 2 min at room temperature. After another washing step with PBS 1 ml methanol was added to each well and incubated for 20 min at room temperature.

Table 1. Conditions of the transwell migration assay for testing migratory behaviour of bone-marrow derived macrophages regarding different substances. Abbreviations: 9 H, 9-HODE; μM , micro molar; FCS: fetal calf serum; DMSO: dimethyl sulfoxide.

	1	2	3	4	5	6
A	without FCS	without FCS	without FCS	with FCS	with FCS	with FCS
B	1 μM 9 H	1 μM 9 H	1 μM 9 H	1 μM 9 H + 0.1 μM G2A Antagonist	1 μM 9 H + 0.1 μM G2A Antagonist	1 μM 9 H + 0.1 μM G2A Antagonist
C	1 μM 9 H + 1 μM G2A Antagonist	1 μM 9 H + 1 μM G2A Antagonist	1 μM 9 H + 1 μM G2A Antagonist	1 μM 9 H + 10 μM G2A Antagonist	1 μM 9 H + 10 μM G2A Antagonist	1 μM 9 H + 10 μM G2A Antagonist
D	1 μM 9H + DMSO	1 μM 9H + DMSO	1 μM 9H + DMSO			

The wells were washed again with PBS. The cells in the inserts were then removed with a cotton bud. The cells on the outside of the inserts were stained with 1 ml of 0.2 $\mu\text{g/ml}$ DAPI solution for 2 min by adding the DAPI solution to each well. Afterwards, the wells were washed again with PBS and the membrane was cut out of the insert. The membrane was placed on an object slide with the downside of the membrane looking upwards. After putting some drops of tissue tek® O.C.T.™ Compound on the slides a cover slip was placed on top of the membranes. Five pictures were taken in the middle of each membrane with the Fluorescence microscope

Axio Observer.Z1 at a 20x magnification. The images were evaluated by counting the cells with image J software and Graph Pad Prism Version 7.1.

2.2.3.3. *9-HODE production assay*

There are three main enzymes, which are thought to be responsible for the 9-HODE production: The cyclooxygenases (COX), the lipoxygenases (LOX) and the cytochrome P450 (Cyp450) [92]. For examination of the 9-HODE production pathway, an assay to analyze the 9-HODE production during inflammation was established. For that, cultivated BMDMs were used and harvested with 400 μ l accutase as for the transwell migration assay. After centrifugation at 1,000 rpm for 5 min the cell pellet was resuspended in 1 ml of BMDM medium. The number of cells per ml was counted by using trypan blue solution in a 1:2 dilution with the cell suspension and a Neubauer counting chamber. The cells were then diluted up to 10^6 cells/ml and seeded into 24 well chambers, with 500 μ l cell suspension per well. The appropriate solutions are listed in 2.1.4 Cell culture medium.

The cells were incubated for 2 h at 37 °C and 5 % CO₂. Afterwards, the cells were treated with either 50 μ M ketoconazole - a known inhibitor of Cyp-epoxygenase [131] - or Nordihydroguaiaretic acid (NDGA) - known for its inhibitory effects on LOX [132]. Furthermore, the cells were treated with 5 μ M Diclofenac - a general COX inhibitor [133] -, Zileuton (Zileut)- a selective 5-LOX inhibitor [134] - or Baicalein – an inhibitor for 12- and 15-LOX [135]. After 30 min incubation at 37 °C and 5 % CO₂, 10 μ M Linoleic acid (LA) or LA together with 100 ng/ml lipopolysaccharide (LPS) was added to the cells as indicated exemplarily in table 2. The experiment was performed in triplicates. After 6 h the medium and the cells were harvested. The harvested medium and cell pellets were frozen in -80 °C until further analysis with LC-MS/MS (see 2.2.6.2 LC-MS/MS).

Material and Methods

Table 2. Exemplary conditions of the 9-HODE production assay in order to see which enzyme is responsible for the 9-HODE production during inflammation. Abbreviations: LA, linoleic acid; KCZ: ketoconazole; NDGA: Nordihydroguaiaretic acid; DMSO: dimethylsulfoxide, LPS: lipopolysaccharide.

	1	2	3	4	5	6
A	cells	cells	cells	cells with LA, KCZ	cells with LA, KCZ	cells with LA, KCZ
B	cells with LPS + LA, KCZ	cells with LPS + LA, KCZ	cells with LPS + LA, KCZ	cells, KCZ	cells, KCZ	cells, KCZ
C	cells with LA, NDGA	cells with LA, NDGA	cells with LA, NDGA	cells with LA + LPS, NDGA	cells with LA + LPS, NDGA	cells with LA + LPS, NDGA
D	cells, NDGA	cells, NDGA	cells, NDGA	cells with LA+LPS, DMSO	cells with LA+LPS, DMSO	cells with LA+LPS, DMSO

2.2.3.4. Preparation of primary sensory neurons

Male mice (8-10 weeks, C57BL/6NRj) were sacrificed and the spine was cut open. For the preparation of DRG the spinal cord was dissected and all DRGs were isolated from the spine. During the preparation nerves were dissected from the DRGs and only the DRGs were transferred into ice cold HBSS with CaCl₂ and MgCl₂ for calcium imaging experiments.

The dissected DRGs were centrifuged at 1,000 rpm for 3 min at room temperature and then treated with collagenase/dispase (500 U/ml collagenase, Sigma, Deisenhofen, Germany and 2.5 U/ml dispase II, Roche, Mannheim, Germany) dissolved in DRG medium for 75 min at 37 °C. Afterwards cells were centrifuged again and washed twice with wash medium – DRG culture. The DRG neurons were incubated with 0.05 % Trypsin-EDTA (Invitrogen, Carlsbad, California, USA) for 10 min at 37 °C. After centrifugation and repetition of the washing steps, the cells were resuspended in DRG medium. The suspension was then plated on poly-L-lysine coated glass coverslips, whereby 30 µl of cell suspension was plated on each cover slip and incubated for 2 h at 37 °C. Then 2 ml of DRG medium was added to the cells and incubated over night at 37 °C [121, 136]. The appropriate media are listed in 2.1.4 Cell Culture Medium.

2.2.3.5. *Agonists and Antagonists of G2A – Screen: IP One Assay with Fluorescence Resonance Energy Transfer (FRET)*

Since there is no known inhibitor of the G2A receptor in mice, it was a stated objective to find specific antagonists for the G2A receptor, as well as new G2A agonists. Therefore, an IP-One assay with CHO K1 cells stably transfected with G2A + GNA11 was performed. First, the medium was aspirated and the transfected cells were washed twice with PBS before 4 ml trypsin was added. After incubation for 2 min at room temperature, 8 ml of CHO K1 medium was added to stop the enzymatic properties of trypsin. The cells were then harvested and centrifuged at 1,200 rpm for 5 min. The supernatant was aspirated and the cells were resuspended in 4 ml CHO K1 medium. Afterwards, the cells were resuspended in fresh medium, and counted by using trypan blue in a 1:20 dilution and an intelligence cell reader (Bio-Rad, Waltham, USA). Cell density was adjusted to 0.3 Mio cells/ml. Using a Tecan multidrop equipped with a standard cassette 50 µl of the cell suspension was added to each well of a white 384-well TC polystyrol plate sparing only those dedicated for standards. Afterwards the plate was centrifuged for 1 min at 250 rpm and was incubated over night at 37 °C and 5 % CO₂.

The next day, an aliquot of 100 µg 9-HODE in ethanol was evaporated under a stream of argon gas and was then diluted in DMSO at a final concentration of 50 mM. Substances to be tested were diluted in DMSO at a final concentration of as well 50 mM, respectively. In a 96 well plate a dilution series of 1:2.5 of the test compounds was prepared as exemplarily indicated in table 3. For the antagonist compounds the Antagonist buffer was used and for the agonist compounds the respective agonist buffer. The appropriate media are listed in 2.1.4 Cell Culture Medium and in 2.1.3 Buffers and Solutions. The dilution series then contained 1.5 % DMSO.

Material and Methods

Table 3. Example of Dilution Series of one test compound in a 96-well plate.

	Compound 1	
A	0.0006	0.3891
B	237.5	0.1556
C	95	0.0623
D	38	0.0249
E	15.2	0.0100
F	6.08	0.0040
G	2.432	0
H	0.9728	0.0016

The next day, the cells in the 384-well plate were washed four times with 60 μ l IP-One buffer per well. Afterwards 10 μ l of IP-One buffer per well was added to the cells. The dilution series of the compounds was then transferred from the 96-well plate onto the cells with 5 μ l per well resulting in 0.5 % DMSO during treatment. For each compound the experiment was conducted in triplicates. The cells with the compounds were then centrifuged at 250 rpm for 1 min. For prevention of evaporation and exposure to light an aluminum cover foil was applied before incubation for 90 min at 37 °C. Afterwards, the plates were chilled for another 10 min at room temperature before they were again centrifuged at 250 rpm for 1 min.

According to the manufacturer's instructions the IP-One detection mixtures containing either FRET donor coupled anti IP1 antibody or D2 FRET-acceptor coupled IP1 were prepared in IP-one lysis buffer (component of the IP-One assay kit; composition not declared). All wells containing treated cells or standards received 3.2 μ l per well of each mixture with additions always intercepted by centrifugation steps (250 rpm for 1 min). On wells for the background control of FRET donor detection in the FRET acceptor channel received no FRET acceptor and the respective volume was replaced with lysis buffer. A cover foil was applied and the plates were then incubated over night at room temperature. The next day, the mixture was centrifuged at 250 rpm for 1 min and then measured in a Tecan F200 plate reader. The fluorescence intensities at 665 nm (FRET acceptor) and at 620 nm (FRET donor) were detected in a filter-based setting with 100 flashed each followed by a delay of 100 μ s before measurement for 400 μ s. The actual homogenous time resolved fluorescence (HTRF) signal was determined by $665 \text{ nm} * 10000 / 620 \text{ nm}$ [137–140].

2.2.4. Molecular biological methods

2.2.4.1. *RNA Isolation*

RNA was isolated from DRG, spinal cord or sciatic nerve with mirVana miRNA Isolation Kit (Applied Biosystems, Foster City, USA). Therefore, the tissue was lysed in 100 μ l Kit lysis buffer and homogenized with sonication two times at 60 % for 10 s. The samples were shortly centrifuged and the supernatant was mixed well with 10 μ l miRNA Homogenate followed by incubation on ice for 10 min. After addition of 100 μ l Acid phenol:chloroform the mixtures were mixed for at least 60 s and centrifuged at 10,000 g for 5 min at room temperature. The aqueous phase at the top of the mixture was aspirated and transferred into a new Eppendorf tube. 1.25 times of the aspirated volume of ethanol was added and the mixture was transferred onto a filter column. After centrifugation for 15 s at 10,000 rpm the flow through was discarded. The filter column was washed with 700 μ l miRNA Wash solution 1 and then twice with 500 μ l miRNA wash solution 2/3. After a last centrifugation of the column at 10,000 rpm for 1 min the RNA on the column was eluted by adding 100 μ l 95 °C hot elution buffer at and centrifuging at maximum speed for 30 s. The amount of RNA was measured with NanoDrop (Thermo Fisher, Waltham, USA) and stored at – 80 °C until cDNA synthesis.

2.2.4.2. *cDNA synthesis*

The First Strand cDNA Synthesis Kit (Thermo Fisher, Waltham, USA) was used for reverse transcription of the isolated RNA [141]. Therefore 400 ng RNA was used and mixed with equal volume of mastermix, which is indicated in table 4.

Table 4. Master mix composition for reverse transcription using First Stand cDNA Synthesis Kit.

Ingredient	Volume for one reaction
dNTPs	2 μ l
Random Hexamer Primer	1 μ l
RNase block	1 μ l
MMLV-RT	2 μ l
Reaction buffer	2 μ l
RNase free water	Fill to the desired volume

The reverse transcription was performed using the following program (table 5):

Table 5. Overview of the reverse transcription PCR program.

Time	Temperature
5 Min.	25 °C
60 Min.	37 °C
5 Min.	70 °C

2.2.4.3. Real-time quantitative polymerase chain reaction (qPCR)

For quantitative qPCR the TaqMan® Gene Expression Assay System was used by adding 8.5 µl TaqMan® gene expression mastermix to 1 µl cDNA and 0.5 µl assay primer for the TaqMan® system (IL-12a, IL-12b, VEGF, Nox-2, Nox-4, Xdh, ATF3, MMP9, TGFβ, G2A) [142]. Afterwards the qPCR program was conducted with the QuantStudio™ Design & Analysis Software v1.4.3 (Thermo Fisher, Waltham) (see table 6).

Table 6. Program for qPCR run conducted with QuantStudio™.

Time	Temperature	Cycles
2 min	60 °C	
15 min	95 °C	
15 s	95 °C	40
1 min	60 °C	

The data was evaluated using the $\Delta\Delta C(T)$ method as described previously [143].

2.2.4.4. Calcium-Imaging

Calcium influx into neuronal cells after stimulation with different compounds was evaluated in real-time with calcium-imaging experiments. Therefore, 24 h after preparation (see 2.2.3.4 Preparation of primary sensory neurons) DRG cultures were stained for 60 min at 37 °C with 5 µM Fura-2-AM-Ester (Biotium, Fremont, California, USA) in the dark. Then the cover slips with the stained DRG neurons were transferred in the perfusion cell of the calcium-imaging system. Here, cells were treated with different solutions by using a digital perfusion system. The program conducted is exemplarily shown in table 7. In a first run cells were rinsed with ringer solution for 3 min at a flow rate of around 1-2 ml/min at 37 °C (Table 7). For TRPV1 sensitizing experiments, cells were then incubated for 2 min with either control vehicle (ethanol), 1 µM 9-HODE (Cayman Chemicals, Ann Arbor, Michigan, USA) or 1 µM 9-HODE

together with different concentrations of G2A antagonists (0.1, 1, 10, 50 μ M G2A11, G2A12, G2A13, G2A19, G2A23, G2A24; SIA Enamine, Riga) dissolved in ringer solution. Afterwards cells were stimulated for 15-30 s with the TRPV1 agonist capsaicin (Merck Millipore, Darmstadt, Germany) at a concentration of 50 – 200 nM dissolved in ringer solution. As positive control 75 mM KCl was applied at the end of each experiment to identify the neurons [121].

Table 7. Overview running program of Ca-Imaging sensitization experiment.

Solution	Time	Channel
Ringer	3 min.	8
Vehicle (ethanol) / 1 μ M 9-HODE / 1 μ M 9-HODE + Antagonist (0,1, 1, 10, 50 μ M)	2 min	5 + 6
200-50 nM capsaicin in Ringer	15-30 s	4
Ringer	5 min	8
75 mM KCl in Ringer	45 s	7
Ringer	1 min	8

For determining the Ca-influx into the cells, the cells were excited at of 340 and 380 nm. Intracellular calcium increase leads to chelating of the Fura-2 with the calcium and results in an increase of the emission at 510 nm and a decrease of the fluorescence intensity at 380 nm. Since the difference in the ratio of F_{340}/F_{380} is proportional to the calcium concentration, after each run the ratio of F_{340}/F_{380} of the control, 9-HODE and 9-HODE together with the respective antagonists was determined and analyzed statistically. For that, every two seconds images of the cells were taken during the whole run, with help of a Leica calcium-imaging setup consisting of a Leica DMI 4000 b inverted microscope equipped with a DFC360 FX (CCD) camera, Fura-2 filters, and an N-Plan 10x/0.25 Ph1 objective (Leica, Wetzlar, Germany). In each experiment an area with a large cell number was chosen and for each condition 20-110 cells were monitored during the whole run. The images taken were processed with the LAS AF-software (Leica, Wetzlar, Germany) [144].

2.2.5. Immunochemical methods

2.2.5.1. *Cryo-sections*

After sacrificing the mice (C57BL/6NRj or G2A-deficient BL/6), the skin was removed from the back and the muscles on the right and left of the spinal cord were dissected. Afterwards the

vertebral canal was cut open on the right and left of the spinal cord without damaging the spinal cord. The spinal cord was carefully prepared out of the vertebral canal. Spinal cord L1-L4 was used and incubated overnight in Dehydration buffer at 4 °C. The next day neurons at both sites of the spinal cord were dissected. Then the spinal cord was embedded vertically in tissue tek® O.C.T.™ Compound cryomold (Sakura, Alphen aan den Rijn, Netherlands) and frozen at -80 °C. For preparing slices of nerve. The contralateral and ipsilateral site of sciatic nerve were dissected after sacrificing the mice. The nerves were directly transferred into tissue tek® O.C.T.™ Compound cryomold (Sakura, Alphen aan den Rijn, Netherlands). For serial sections of 12 µm thickness of both types of tissue a cryostat (Leica CM3050S, Leica Microsystems, Wetzlar) was used. The sections were transferred onto object slides (SuperFrost®, Thermo Fisher, Waltham). The sections were dried at room temperature and then stored at -80 °C until they were used for immunohistochemistry. The appropriate solutions are listed in 2.1.3 Buffers and Solutions.

2.2.5.2. *Immunohistochemistry*

For identification of differences of important proteins regarding neuropathic pain, immunohistochemistry was performed. Therefore, the prepared serial sections were thawed and fixed with Fixation IHC solution for 20 min at room temperature. Afterwards, the tissue samples were washed with PBS for 5 min followed by permeabilization of the tissue with PBST for 15 min at room temperature. Then, unspecific binding sites were blocked with Blocking IHC1 solution for 45 min. The respective first antibodies were incubated over night at 4 °C. After three washing steps with PBS the respective second antibodies with AF488- or Cy3-coupled fluorescence were incubated for 1 h at room temperature in the dark. The tissue sections were stained with DAPI with an end concentration of 0.1 µg/ml for 5 min at room temperature in the dark. Again, the sections were washed three times with PBS followed by three times PBS on the sections for 5 min at room temperature. Then the tissue sections were embedded under a cover slide (Thermo Scientific Menzel, Waltham, USA) with DPX mountant (Sigma-Aldrich, Deisenhofen). Pictures were taken with a Zeiss Axio Observer.Z1 microscope and AxioCam MRm-camera (Carl Zeiss, Oberkochen) [145, 146]. The appropriate solutions are listed in 2.1.3 Buffers and Solutions, the appropriate antibodies are depicted in 2.1.2 Antibodies.

2.2.6. Analytical methods

2.2.6.1. *Proteomics*

Sample preparation for LC-MS²

Material and Methods

The concrete signaling pathways underlying the 9-HODE-G2A signaling mechanisms were of special interest, since they are not known yet. Therefore, a global proteome analysis was performed [147, 148]. As described above, BMDMs were used for this experiment, stimulated with or without 9-HODE for 24 h. As previously described, the lysates of the BMDMs were precipitated using three volumes of ice-cold methanol, one volume Chloroform and two and a half volumes ddH₂O. After centrifugation at 14,000 g for 45 min at 4 °C the upper aqueous phase was aspirated. Three 3 volumes of ice-cold methanol were added and the samples were mixed. The proteins were pelleted by centrifugation at 14,000 g for 5 min at 4 °C. After washing with ice-cold methanol, the protein pellets were dried at room temperature. Then they were resuspended in 8 M Urea, 10 mM EPPS pH 8.2 and 1 mM CaCl₂ followed by determining the protein concentration with a μ BCA assay (ThermoFisher Scientific, 23235). Samples were diluted to 2 M urea using 10 mM EPPS pH 8.2 with 1 mM CaCl₂ and incubated with LysC (Wako Chemicals) at 1:50 (w/w) ratio at 37 °C. The next day the samples were diluted to 1 M Urea using 10 mM EPPS pH 8.2 with 1 mM CaCl₂. After incubating the samples at a 1:100 (w/w) ratio of trypsin (Promega, V5113) for 6 h at 37 °C the samples were acidified to a pH of 2-3 using trifluoroacetic acid (TFA). Peptides were purified with SepPak tC18 columns (Waters, WAT054955) according to the manufacturer's instructions. Eluates were dried and peptides were resuspended in 0.2 M EPPS pH 8.2 and 10 % (v/v) Acetonitrile. Peptide concentration was determined with μ BCA. Peptides were mixed with TMT reagents (ThermoFisher Scientific, 90111, A37724, 90061) at a 1:2 (w/w) ratio with. Reactions were incubated for 1 h at room temperature and subsequently quenched by addition of hydroxylamine to a final concentration of 0.5 % for 15 min at room temperature. Samples were pooled in equimolar ratio, acidified, and dried. Before MS-analysis, peptide samples were purified using Empore C18 (Octadecyl) resin material (3M Empore). Material was activated by incubation with Methanol for 5 min, followed by washing each material with 70 % (v/v) acetonitrile / 0.1 % (v/v) TFA and 5 % (v/v) acetonitrile / 0.1 % (v/v) TFA. Samples were resuspended in 5 % (v/v) acetonitrile / 0.1 % (v/v) TFA and loaded to resin material. Peptides were washed with 5 % (v/v) acetonitrile / 0.1 % (v/v) TFA and eluted with 70 % (v/v) acetonitrile (ACN). Samples were dried and resuspended in 0.1 % (v/v) formic acid (FA) for LC-MS³.

High-pH Reverse Phase Fractionation

For high pH reversed phase fractionation on the Dionex HPLC, 500 μ g of pooled and purified TMT labelled samples were resuspended in 10 mM ammonium-bicarbonate (ABC), 5 % ACN, and separated on a 250 mm long C18 column (Aeris Peptide XB-C18, 4.6mm ID, 2.6 μ m particle size; Phenomenex) using a multistep gradient from 100 % Solvent A (5 % ACN, 10 mM

ABC in water) to 60 % Solvent B (90 % ACN, 10 mM ABC in water) over 70 min. Eluated peptides were collected every 45 s into a total of 96 fractions, which were cross-concatenated into 12 fractions and dried.

LC-MS³

Peptides were resuspended in 0.1 % (v/v) FA and separated on an easy nLC 1200 (ThermoFisher Scientific) and a 22 cm long, 75µm ID fused-silica column, which has been packed in house with 1.9 µm C18 particles (ReproSil-Pur, Dr. Maisch), and kept at 45 °C using an integrated column oven (Sonation). Peptides were eluted by a non-linear gradient from 5-38 % acetonitrile over 120 min and directly sprayed into a Fusion Lumos mass spectrometer equipped with a nanoFlex ion source (ThermoFisher Scientific) at a spray voltage of 2.6 kV. Full scan MS spectra (350-1400 m/z) were acquired at a resolution of 120,000 at m/z 200, a maximum injection time of 100 ms and an AGC target value of 4x 10⁵ charges. MS² scans were performed for up to 10 most intense ions in the IonTrap (Rapid) with an isolation window of 0.7 Th, a maximum injection time of 85 ms and CID fragmented using a collision energy of 35 % for 10 ms. Synchronous precursor selection-based MS (SPS-MS³) was performed on the 10 most intense MS² fragment ions with an isolation window of 0.7 Th (MS1) and 2 m/z (MS2). Ions were fragmented using Higher-energy collisional dissociation (HCD) with a normalized collision energy of 65 and analyzed in the Orbitrap with a resolution setting of 50,000 at m/z 200, scan range of 110-500 m/z, AGC target value of 1x 10⁵ and a maximum injection time of 86 ms. Dynamic exclusion was set to 45 s to minimize repeated sequencing of already acquired precursors.

Finally, the data was analyzed with the software proteome discoverer 2.2 (Thermo Fisher).

2.2.6.2. Liquid-chromatography-tandem mass spectrometry for lipid detection (LC-MS/MS)

After dissecting contralateral and ipsilateral side of sciatic nerve, L4 – L6 dorsal root ganglia and spinal cord from euthanized animals the samples were directly frozen in liquid nitrogen. The tissue weight was determined and lipid identification and quantification were performed as described previously [85, 149]. Briefly, tissue samples were homogenized using a swing mill and analytes were extracted from homogenates using liquid–liquid extraction with ethyl acetate after spiking with a mixture of the deuterated internal standards. After liquid-liquid extraction, combined organic phases were removed at a temperature of 45 °C under a gentle stream of nitrogen. The residues were resuspended in 50 µl of methanol/water/BHT (50:50:10⁻⁴, v/v/v), then centrifuged for 2 min at 10,000 g and transferred to glass vials (Ziemer GmbH,

Langenwehe, Germany). For calibration, PBS samples were spiked with working solutions of the analytes, which were prepared in methanol/BHT (100:0.1 (v/v) and processed as described for the homogenates. The LC-MS/MS system consisted of a triple quadrupole tandem mass spectrometer QTRAP 5500 (Sciex, Darmstadt, Germany) equipped with a Turbo-V source operating in negative electrospray ionization mode, an Agilent 1200 binary HPLC pump and degasser (Agilent, Waldbronn, Germany) and a HTC Pal autosampler (CTC analytics, Zwingen, Switzerland). Chromatographic separation of the lipids was performed using a Gemini NX C18 column and precolumn (150 x 2 mm inner diameter, 5 µm particle size, and 110 Å pore size; Phenomenex, Aschaffenburg, Germany) and a linear gradient using a flow rate of 0.5 ml/min in a total run time of 17.5 min. Thereby, the gradient changed from 85 % mobile phase A (water:ammonia 100:0.05, v/v), to 10 % A and 90 % mobile phase B (acetonitrile:ammonia 100: 0.05, v/v). The conditions were held for 1 minute until the mobile phase shifted back to 85 % A. These conditions were maintained for 4 min to re-equilibrate the column.

Analyst software version 1.6.3 (Sciex, Darmstadt, Germany) was used for data acquisition while further quantification was performed with Multiquant Software version 3.0.2 (Sciex, Darmstadt, Germany) using the internal standard method (isotope-dilution mass spectrometry). Calibration curves were calculated by linear regression with 1/concentration weighting [136].

2.2.7. Data analysis and statistics

In general, analysis of the data was conducted with Microsoft Excel 2016 and Graph Pad Prism 7, regarding Immunohistochemistry and transwell migration assays Image J software was used for evaluation. Therefore, raw data was used to calculate the mean and the standard error of the mean (SEM) as quantification of the variance of triplicate or duplicate measurements of samples. Data with Gaussian distribution was evaluated statistically with an unpaired Student's t-Test with Welch's correction, which assumes no equal standard deviation of the compared groups. Behavioral experiments, Luminex data and FACS data were statistically evaluated with a two-way analysis of variance (ANOVA) followed by *post hoc* Bonferroni test or Holm-Sidak correction. When more than two groups were analyzed, a one-way ANOVA was used with Turkey *post hoc* test. A *p* value of <0.05 was considered statistically significant.

3. Results

3.1. Mechanical hypersensitivity in G2A-deficient mice after spared-nerve-injury

During neuropathic pain the TRPV1 channel in primary sensory neurons is sensitized [3, 54, 150]. However, approaches in treatment of neuropathic pain by targeting the TRPV1 channel resulted in an elevated body temperature in humans and rats, indicating a crucial role for TRPV1 in temperature homeostasis [60, 151, 152]. Thus, pain perception through TRPV1 has to be targeted through indirect mechanisms, such as GPCR activation, e.g. G2A [108, 151–154]. In an earlier study, it was shown that G2A sensitizes TRPV1 and that G2A-deficient mice showed reduction of mechanical hypersensitivity in chemotherapy-induced neuropathic pain, indicating G2A being a promising target for neuropathic pain treatment [85]. Although, mechanisms underlying neuropathic pain are highly variable, even in the various pain modalities itself, and depend on the cause of neuropathic pain [22, 56, 155]. Thus, it is of interest to understand each type of neuropathic pain in its complete unity. Since, chemotherapy-induced neuropathic pain and its underlying mechanisms are well-documented, the focus of this work was on a neuropathic pain model with a major immunological component [10, 21]. Furthermore, it is known that G2A is mainly expressed in immune cells and on TRPV1-positive small diameter neurons, indicating a role at neuronal and immunological level [62, 105]. Therefore, it was of interest to examine the effects of G2A-deficiency in the context of nerve-injury induced neuropathic pain. To do so, the commonly used model for nerve-injury in mice, the spared-nerve injury (SNI) was subjected to G2A-deficient and wild-type mice [119, 120, 156].

After SNI surgery, the paw withdrawal responses of the mice were measured in seconds (s) with a dynamic plantar aesthesiometer. The mechanical responses of hind paws after SNI induction (ipsilateral) showed a steady decrease of the paw withdrawal time in wild-type mice from day 1 after SNI to 4 s (Fig. 8A, light grey triangle). Whereas in G2A-deficient mice the threshold decreased after the first day in an equal manner but remained stable over time at around 6 s (Fig. 8A). Animals, which were subjected to sham surgery showed a stable mechanical threshold during the period of measurement. Similar results were observed in contralateral site, which showed a threshold constantly between 9 and 11 s in wild-type, G2A-deficient and sham-surgery mice (Fig. 8B).

Results

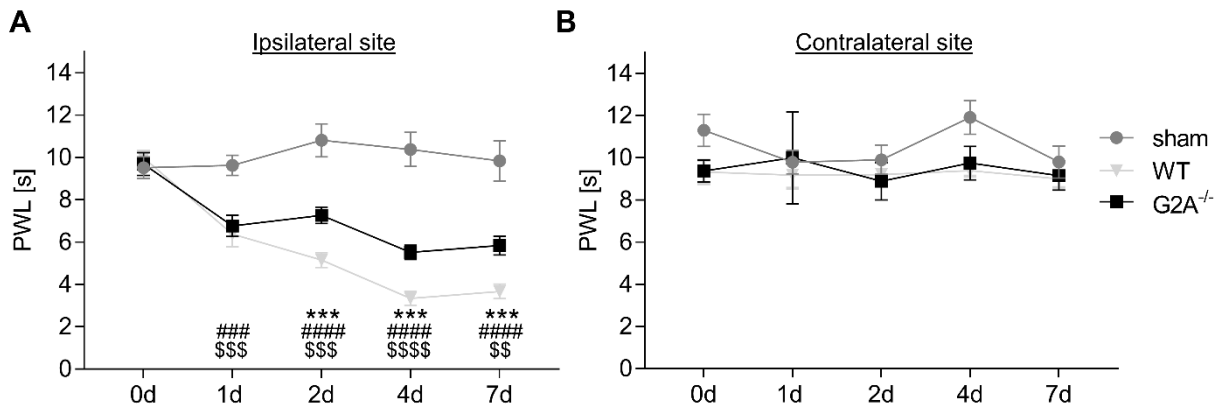


Figure 8. Nociceptive behavior after spared-nerve injury with dynamic plantar. Mechanical pain threshold of (A) ipsilateral site and (B) contralateral site of wild-type (WT, grey, rectangles) and G2A-deficient (G2A^{-/-}, black, squares) mice before (baseline) and after SNI surgery. Animals with sham-surgery are depicted in dark grey circles. Data is presented as mean \pm SEM. $n=10$ animals per group, two-way ANOVA with Bonferroni correction, $*p<0.05$, $**p<0.01$, $***p<0.005$, $****p<0.001$ (wild-type vs. G2A-deficient); $###p<0.005$, $####p<0.0001$ (wild-type vs. sham); $$$$p<0.01$, $$$$$p<0.005$, $$$$$$p<0.0001$ (G2A-deficient vs. sham). Data of day 2, 4, 7 was collected by Marco Sisignano in wild-type and G2A-deficient animals.

On this basis, it can be concluded that G2A-deficiency leads to a reduction of mechanical hypersensitivity after nerve-injury from day two on compared to wild-type mice.

3.2. Neuroimmune modulation in G2A-deficient mice

The findings strongly support the view of nociceptive sensitization through G2A after nerve injury. Peripheral sensitization in terms of nerve injury is often accompanied by inflammation-associated changes at the injured nerve, an environment that is also called inflammatory soup [8, 157]. Thereby, nerve injury leads to infiltration of immune cells and increased production of inflammatory mediators, hallmarks of neuroinflammation, which are crucial in initiation of neuropathic pain [21, 22, 31, 158]. Based on that, experiments were conducted regarding the neuroimmune interaction in wild-type and G2A-deficient mice.

3.2.1. Distribution of immune cells at the site of injury

Nerve damage is known to result in macrophage infiltration, T cell activation and increased expression of proinflammatory cytokines [53]. Therefore, tissues regarding the pain transmission pathway, sciatic nerve (SN) (Fig. 9 and 10), L4-L6 DRGs (Fig. 12 and 13) and spinal cord (Fig. 14 and 15) were dissected 1 and 7 days (7 d) after SNI surgery and prepared for FACS analysis.

Since already one day after SNI surgery a decrease of the paw withdrawal was observed in both genotypes (Fig. 8), the number of immune cells at this early time point was examined. As

Results

the FACS measurements showed there were no differences in the number of all immune cell types in ipsi- and contralateral site of sciatic nerve one day after SNI surgery (Fig. 9).

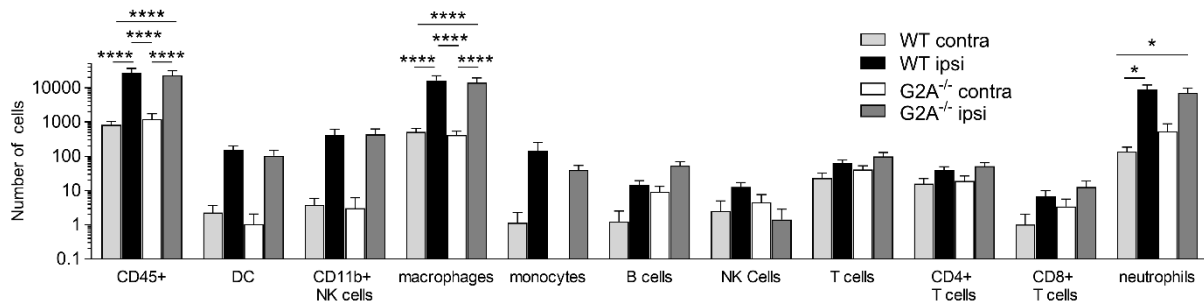


Figure 9. Number of immune cells in sciatic nerve 1 d after SNI surgery. FACS measurements of immune cells at the ipsi- (ipsi) and contralateral (contra) site of sciatic nerve in wild-type (WT, black and light grey) and G2A-deficient (G2A^{-/-}, white and dark grey) mice. Data is presented as mean ± SEM. n=5 animals per group, two-way ANOVA with Holm-Sidak method, *p<0.05, **p<0.01, ***p<0.005. FACS sorting was performed by Praveen Mathoor and preanalysis was done by Andreas Weigert.

However, 7 days after SNI surgery, the amount of each immune cell type was around 10 times higher at the ipsilateral sciatic nerve (SN) (Fig. 10, black and dark grey) than contralateral SN of wild-type and G2A-deficient mice (Fig. 10, light grey and white). Though, only the number of CD45⁺ immune cells and macrophages were significantly reduced in G2A-deficient mice, at the ipsilateral site (Fig. 10, black and dark grey). Next to this, the number of neutrophils was also significantly reduced at the ipsilateral site of G2A-deficient SN (Fig. 10, black and dark grey). Regarding dendritic cells (DC), CD11b⁺ natural killer (NK) cells, monocytes, B cells, T cells, NK cells remarkably all of them revealed a tendency of decreased numbers in both sites of G2A-deficient mice (Fig. 10, white and dark grey).

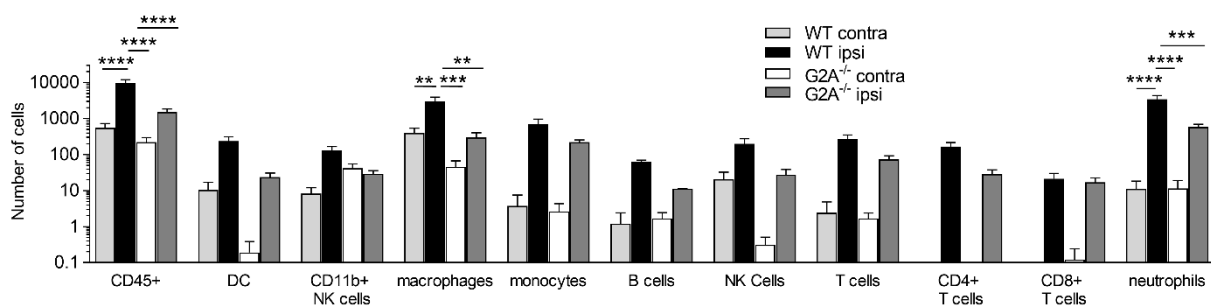


Figure 10. Number of immune cells in sciatic nerves 7 d after SNI surgery. FACS measurement of immune cells at the ipsi- (ipsi) and contralateral (contra) site of sciatic nerve in wild-type (WT) and G2A-deficient (G2A^{-/-}) mice. Data is presented as mean ± SEM. n=5 animals per group, two-way ANOVA with Holm-Sidak method, *p<0.05, **p<0.01, ***p<0.005, ****p<0.001. FACS sorting was performed by Béla Zimmer, Praveen Mathoor and preanalysis was done by Andreas Weigert.

Results

Concerning macrophages, the FACS results could be confirmed by immunohistochemistry (Fig. 11). For that, sciatic nerve tissue was dissected 7 d after SNI, was embedded into tissue tek and sliced into 12 μm slices. The slices were then stained with CD11b, an immune cell surface molecule [159], and F4-80, which is expressed mainly on macrophages [160]. As figure 10 shows, injured nerve of wild-type mice contained a lot of CD11b⁺/F4-80⁺ macrophages, confirming earlier reports about macrophages in sciatic nerve [27] (Fig. 11A). In contrast, less F4-80⁺/CD11b⁺ macrophages were observed in SN of G2A-deficient mice (Fig. 11B).

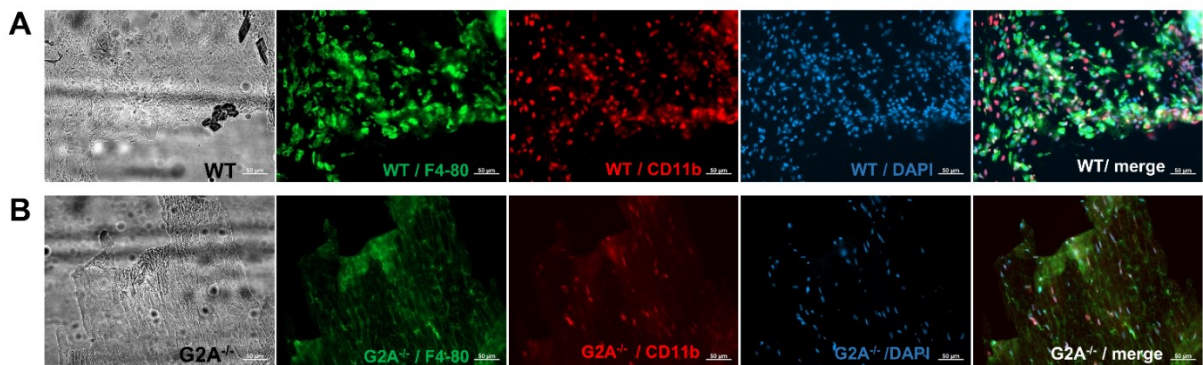


Figure 11. Amount of F4-80/CD11b-positive macrophages in sciatic nerves. Immunohistochemistry images of F4-80 (green), CD11b (red), DAPI (blue) and assembled images (left to right), as well as the phase contrast image (left) of proximal site of ipsilateral sciatic nerve surgery in (A) wild-type (WT) and (B) G2A-deficient (G2A^{-/-}) tissue. Bar scale 50 μm .

3.2.2. Distribution of immune cells at involved dorsal root ganglia

Since the sciatic nerve transmits the signal of the injury to its corresponding dorsal root ganglia (DRG), L4 to L6, it was also of interest to investigate the immune cell numbers at the site of L4-L6 DRGs. As the FACS measurements showed, one day after SNI, the number of all immune cell types were the same in ipsi- and contralateral site in wild-type and G2A-deficient animals (Fig. 12).

Results

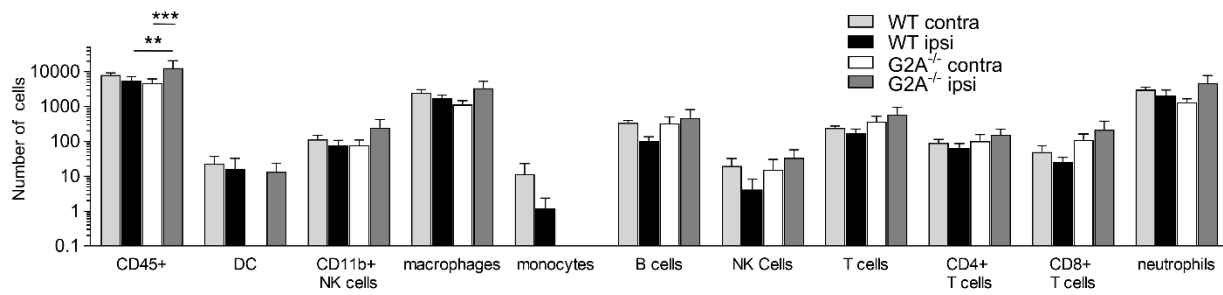


Figure 12. Number of immune cells in dorsal root ganglia (DRG) 1 d after SNI surgery. FACS measurements of immune cells at the ipsi- (ipsi) and contralateral site (contra) of L4-L6 DRG in wild-type (WT, black and light grey) and G2A-deficient ($G2A^{-/-}$, white and dark grey) mice. Data is presented as mean \pm SEM. $n=5$ animals per group, two-way ANOVA with Holm-Sidak method, * $p<0.05$, ** $p<0.01$, *** $p<0.005$, **** $p<0.001$. FACS sorting was performed by Praveen Mathoor and preanalysis was done by Andreas Weigert.

7 days after SNI surgery, in DRGs similar results were observed as in SN (Fig. 13). Thus, in wild-type mice CD45⁺ immune cells showed a significantly higher number at the ipsi- and contralateral site as in G2A-deficient (Fig. 13, black and dark grey). However, the overall number of the immune cell types did not differ as much as in SN at the ipsi- and contralateral site in both genotypes. Again, in G2A-deficient mice a general tendency of decreased numbers of DC, monocytes, NK cells, T cells and neutrophils was observed in both sites, compared to wild-type mice (Fig. 13). Moreover, the number of macrophages and neutrophils showed a significant decrease in ipsilateral L4-L6 DRGs of G2A-deficient animals (Fig. 13, dark grey), confirming reports of DRG macrophages being important in initiation and maintenance of neuropathic pain [161].

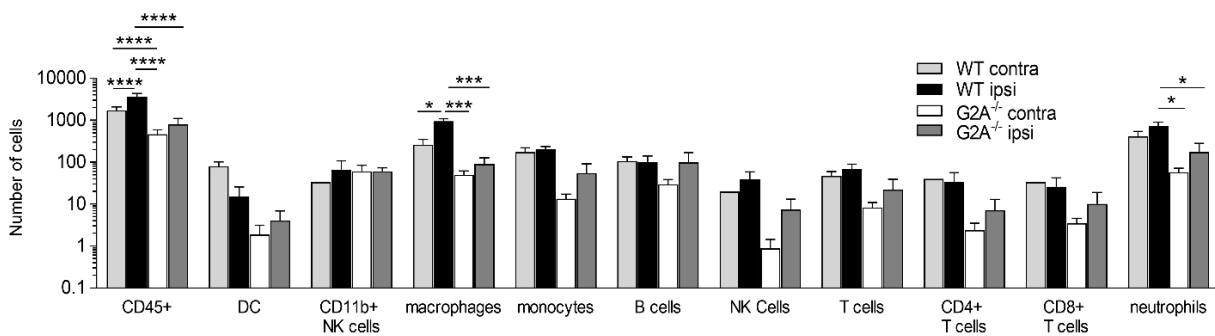


Figure 13. Number of immune cells in dorsal root ganglia (DRG) 7 d after SNI surgery. FACS measurements of immune cells at the ipsi- (ipsi) and contralateral site (contra) of L4-L6 DRG in wild-type (WT, black and light grey) and G2A-deficient ($G2A^{-/-}$, white and dark grey) mice. Data is presented as mean \pm SEM. $n=5$ animals per group, two-way ANOVA with Holm-Sidak method, * $p<0.05$, ** $p<0.01$, *** $p<0.005$, **** $p<0.001$. FACS sorting was performed by Béla Zimmer, Praveen Mathoor and preanalysis was done by Andreas Weigert.

3.2.3. Distribution of immune cells at spinal cord level

Following the path of nociceptive transmission, it was also of interest to investigate the immune cell composition in the spinal cord, comparing wild-type and G2A-deficient mice 1 d and 7 d after SNI surgery. Hu *et al.* reported in spinal cord an enhanced recruitment of lymphocytes after chronic constriction injury (CCI) [162]. However, at the contra- and ipsilateral site of spinal cord 1 d and 7 d after SNI surgery no difference in the number of all immune cell types were observed in (Fig. 14 and 15). Even in G2A-deficient mice the various immune cell types showed no difference between ipsi- and contralateral site. Although, 7 d after SNI surgery only the number of CD45⁺ immune cells was significantly decreased in G2A-deficient mice at both sites (Fig. 15). Regarding macrophages or neutrophils of the ipsilateral site, not such a strong difference was observed as in sciatic nerve (Fig. 10, 15).

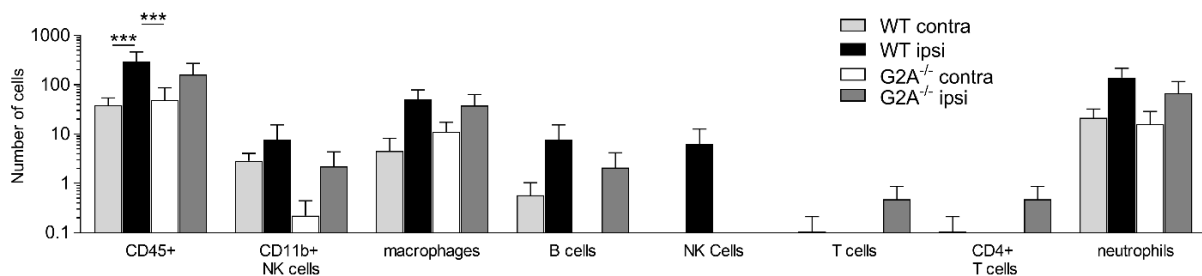


Figure 14. Number of immune cells in spinal cords 1 d after SNI surgery. FACS measurements of immune cells at the ipsi- (ipsi) and contralateral (contra) site of spinal cord in wild-type (WT, black and light grey) and G2A-deficient (G2A^{-/-}, white and dark grey) mice. Data is presented as mean ± SEM. n=5 animals per group, two-way ANOVA with Holm-Sidak method, *p<0.05, **p<0.01, ***p<0.005, ****p<0.001. FACS sorting was performed by Praveen Mathoor and preanalysis was done by Andreas Weigert.

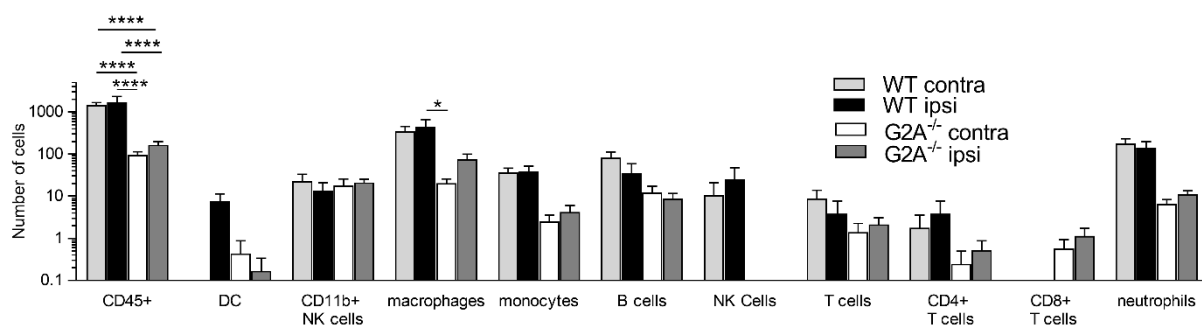


Figure 15. Number of immune cells in spinal cords 7 d after SNI surgery. FACS measurements of immune cells at the ipsi- (ipsi) and contralateral (contra) site of spinal cord in wild-type (WT, black and light grey) and G2A-deficient (G2A^{-/-}, white and dark grey) mice. Data is presented as mean ± SEM. n=5 animals per group, two-way ANOVA with Holm-Sidak method, *p<0.05, **p<0.01, ***p<0.005, ****p<0.001. FACS sorting was performed by Béla Zimmer, Praveen Mathoor and preanalysis was done by Andreas Weigert.

Results

However, an increased but time-dependent activation of astrocytes and microglia was reported in spinal cord [31, 163, 164]. These results could not be confirmed 7 d after SNI in spinal cord. As the immunohistochemistry staining with GFAP as prominent astrocyte marker [165, 166] showed, there was no difference in wild-type and G2A-deficient animals observed (Fig. 16).

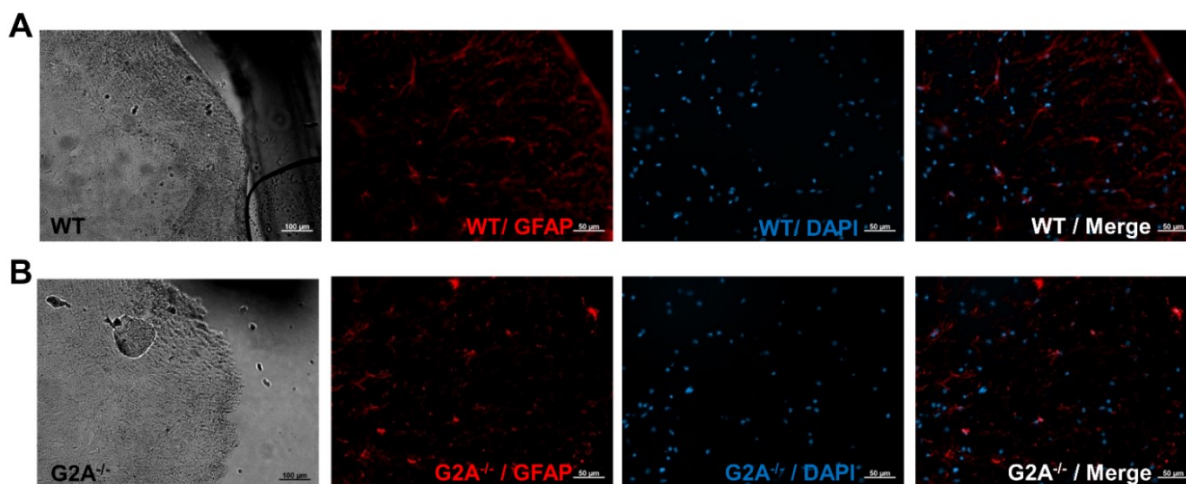


Figure 16. Activation of astrocytes in dorsal spinal cord. Immunohistochemistry images of GFAP (red), DAPI (blue) and assembled images (merge, from left to right), as well as the phase contrast image (left) of dorsal horn of ipsilateral site of (A) wild-type (WT) and (B) G2A-deficient (G2A^{-/-}) spinal cord tissue.

The herein presented numbers of immune cells correlate with the results of the behavioural measurements, since on day 7 the paw withdrawal response was increased in G2A-deficient mice (Fig. 8). Thus, a tentative conclusion at this point would be that G2A-deficiency results in a reduced number of immune cells 7 d after SNI surgery, especially regarding the number of CD45⁺ immune cells, the macrophages and neutrophils. All three showed remarkably reduced numbers in SN of G2A-deficient mice, but this reduction was less strong in DRGs and in spinal cord, where barely a reduction was observed. These results indicate that the difference in immune cell numbers between the two genotypes after nerve injury is more restricted to the peripheral site of the injured nerve than to the central nervous system (CNS).

3.2.4. Changes along the pain transmission pathway after SNI surgery: Cytokines, chemokines and growth factors

The reduced number of immune cells led to the hypothesis, that the concentrations of inflammatory mediators, such as cytokines, chemokines and growth factors, which are released by the immune cells, could also be altered in G2A-deficient mice. Therefore, the inflammatory mediators were examined by performing an ELISA or Luminex measurements with proteins extracted from SN, L4-L6 DRGs and L1-L6 spinal cord. As Figure 17 shows, the

Results

concentration of proinflammatory cytokines tumor necrosis factor α (TNF α) and interleukin 6 (IL-6) were significantly reduced in G2A-deficient mice at the ipsilateral site of SN 7 d after SNI (Fig. 17A and B). Regarding the vascular endothelial growth factor (VEGF), a significant reduced concentrations were observed in G2A-deficient mice in ipsilateral site of SN 7 d after SNI surgery (Fig. 17C). Interestingly growth factors, like transforming growth factor β (TGF β) or nerve growth factor (NGF), which are known to be increased during neuropathic pain, did not show any difference in their concentration between the genotypes (Fig. 17D and E) [6, 8, 53, 167–169]. Since NGF is the downstream target of the proinflammatory cytokine IL-1 β it is not surprising that there was no difference observed in the concentration of IL-1 β either [6, 53] (Fig. 17F).

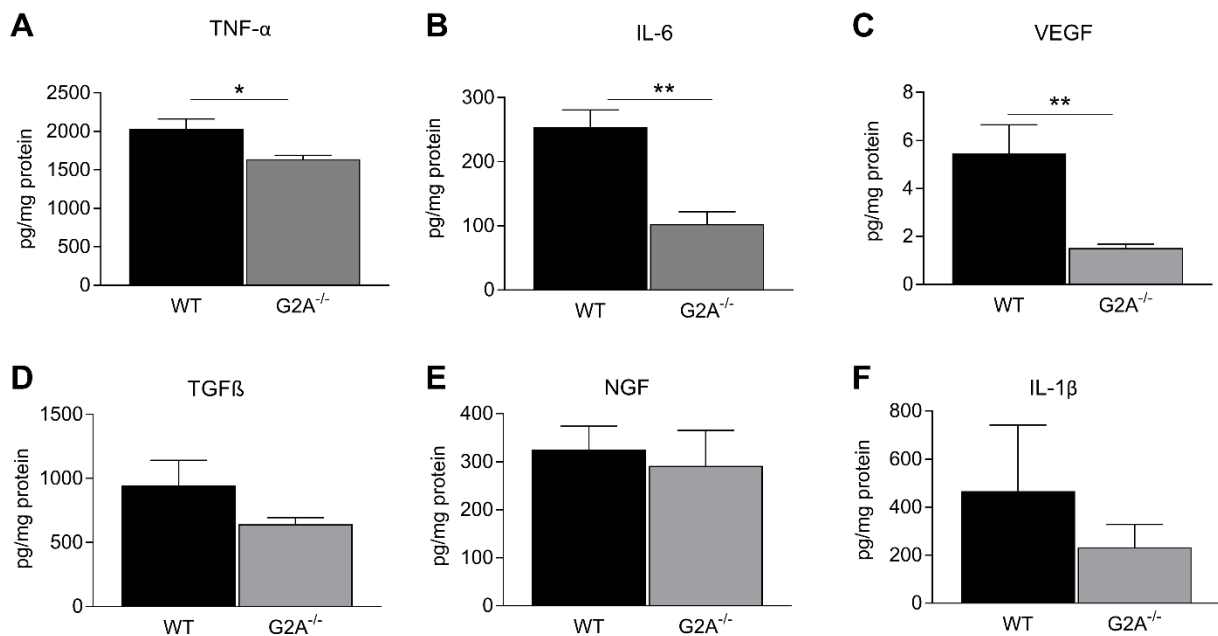


Figure 17. Cytokines and growth factors in injured sciatic nerves. ELISA of the amount of (A) TNF α , (B) IL6, (C) VEGF, (D) TGF β , (E) NGF and (F) IL-1 β at the ipsilateral site of sciatic nerve in wild-type (WT, black), G2A-deficient (G2A^{-/-}, grey) and sham-surgery (S, white) mice. n=4 animals per group, one-way ANOVA with Holm-Sidak method was used for A and B; two-sided t-test was used for C, D, E and F.

In a Luminex screen for further cytokines and chemokines, no difference in any of them was observed in wild-type and G2A-deficient animals in ipsilateral site of SN, either after 7 d (Fig. 18). However, basic fibroblast growth factor β (FGF β) showed a marked concentration decrease in G2A-deficient mice (Fig. 18A). Likewise, proinflammatory cytokines and chemokines keratinocytes-derived chemokine (KC), IL-17 and IL-5 showed a tendency of decreased concentrations in G2A-deficient animals 7 d after SNI surgery. However, this difference was not statistically significant (Fig. 18) [170–176].

Results

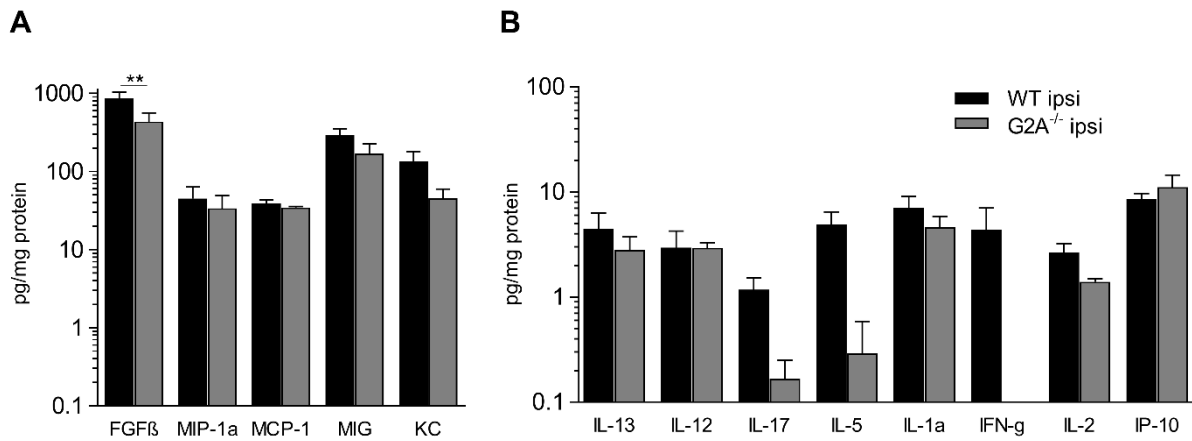


Figure 18. Concentrations of various cytokines and chemokines in ipsilateral sciatic nerves. Luminex measurement: Amount of FGF β , macrophage inflammatory protein 1a (MIP-1a), monocyte chemoattractant protein 1 (MCP-1), monokine induced by gamma (MIG) and KC (**A**) and various cytokines, chemokines and growth factors (**B**) 7d after SNI surgery in sciatic nerves. Shown are the ipsilateral site of sciatic nerves in wild-type (WT, black) and G2A-deficient (G2A^{-/-}, grey) mice. n=3-5 animals per group, two-way ANOVA with Holm-Sidak method was used. **p<0.01. 7d Luminex multiplex analysis was performed by Béla Zimmer.

The Luminex analysis was also performed with L4-L6 DRGs, where only IL-12 and interferon γ induced protein 10 (IP-10) revealed a significant decrease in G2A-deficient mice (Fig. 19A-C). Interestingly, when the relative mRNA expression of IL-12a and IL-12b was measured, no difference was found in both genotypes at the ipsilateral site of L4-L6 DRGs 7 d after SNI (Fig. 19D and E). However, a general tendency of decreased concentrations of all cyto- and chemokines was observed in L4-L6 DRGs 7d after SNI in G2A-deficient animals, especially of IL-1 α (Fig. 19B).

Since after chemotherapy-induced neuropathic pain, the G2A mRNA expression was increased in sensory neurons, the G2A expression was examined as well in L4-L6 DRGs [85]. However, the results showed no alteration in G2A mRNA expression in wild-type animals, sham-surgery animals or animals without any treatment 7 d after SNI surgery (Fig. 19F).

Results

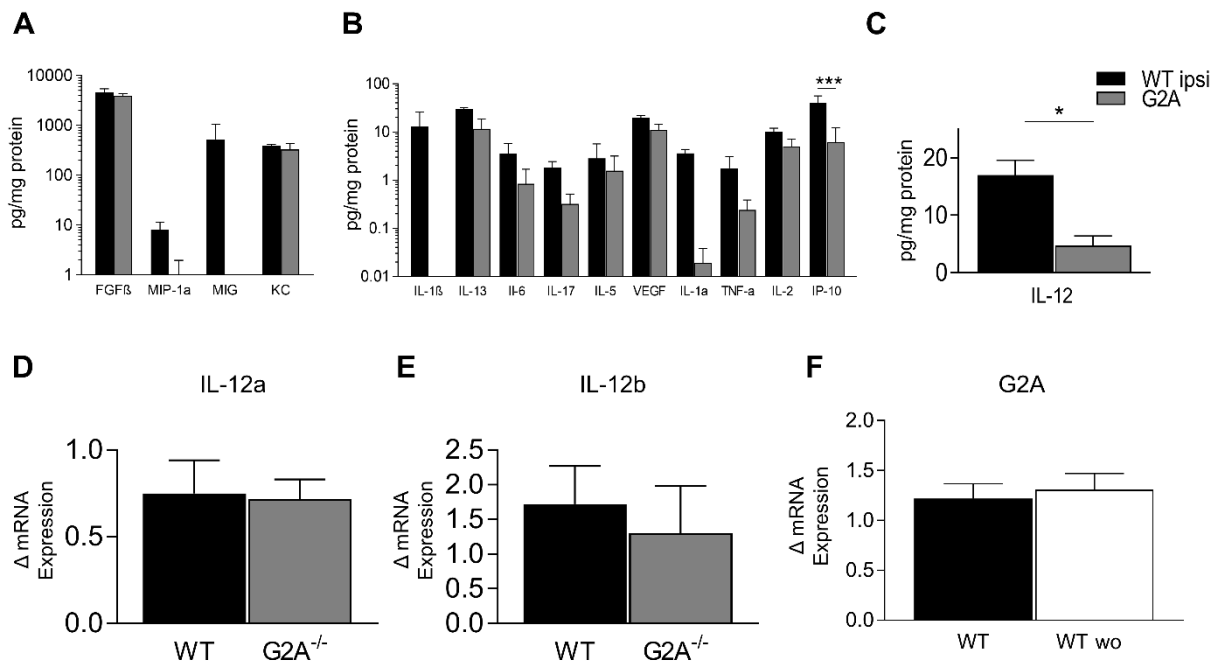


Figure 19. Concentrations of various cytokines and chemokines in ipsilateral L4-L6 DRGs. Luminex measurement: Amount of FGFβ, MIP-1a, MCP-1, MIG and KC (**A**) and (**B**) various further cytokines, chemokines and growth factors 7 d after SNI surgery in ipsilateral L4-L6 DRGs. (**C**) Concentration of IL-12 7 d after SNI surgery in ipsilateral DRGs. (**D** and **E**) Quantitative real-time PCR of IL-12a and IL-12b in L4-L6 DRGs 7 d after SNI surgery. Shown are the ipsilateral site of sciatic nerve in wild-type (WT, black) and G2A-deficient (G2A^{-/-}, grey) mice. (**F**) Quantitative real-time PCR of G2A in wild-type (WT, black) mice 7 d after SNI surgery and mice without any treatment (WT wo, white) in L4-L6 DRGs. n=3-5 animals per group, two-way ANOVA with Holm-Sidak method was used for A, B, and F, two-sided t-test was used for C, D and E. *p<0.05. Béla Zimmer performed Luminex measurements of A-C.

However, the expression of G2A itself in DRGs is unaffected by the spared-nerve injury. The injury is stress for the nerve fibers, therefore, the known stress markers activating transcription factor 3 (ATF3), transforming growth factor β (TGFβ), as well as the reactive oxygen species (ROS)-markers inducible isoform nitric oxide synthases (iNOS), NADPH oxidases (Nox) and matrix-metalloproteinase 9 (MMP9) were analyzed with qPCR in L4-L6 ipsilateral DRGs [169, 177–179] (Fig. 20). Interestingly, no differences were observed regarding the relative mRNA expression of the stress markers in both genotypes.

Results

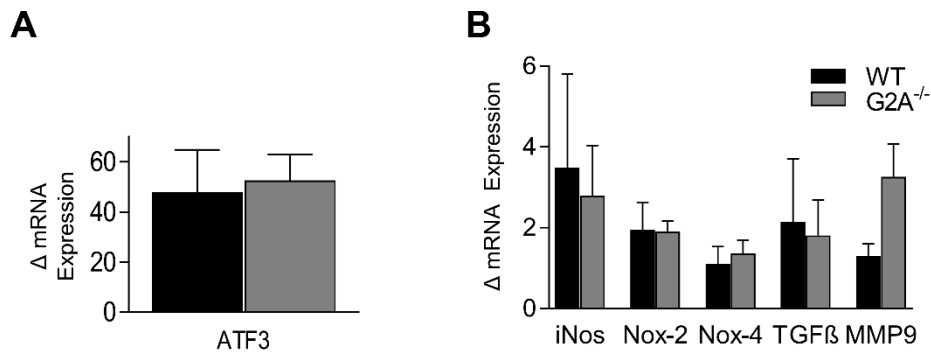


Figure 20. Stress and ROS-marker in L4-L6 ipsilateral DRGs. qPCR measurements of relative mRNA expression of (A) ATF3 and (B) iNOS, Nox, TGFβ and MMP9 in L4-L6 ipsilateral DRGs of wild-type (WT, black) and G2A-deficient mice (G2A^{-/-}, grey). n=4-8 animals per group. A two-sided t-test was performed for ATF3 and a two-way ANOVA for B.

Interestingly, in spinal cord there was also a general tendency in decreased concentrations of cytokines, chemokines and growth factors in G2A-deficient mice at the ipsilateral site 7 d after SNI surgery (Fig. 21). However, only the antiinflammatory cytokine IL-13 showed a significant 10-fold decrease in G2A-deficient mice 7 d at the ipsi- (Fig. 21B) and contralateral site after SNI surgery in spinal cord [170].

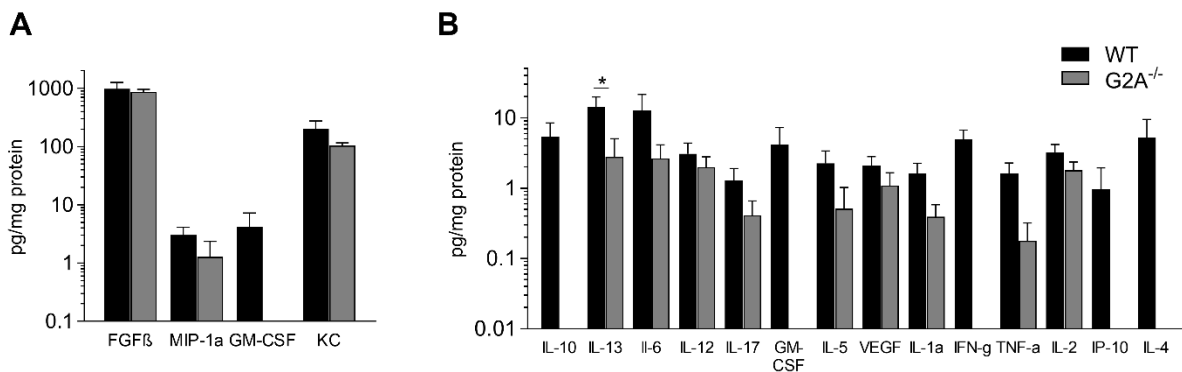


Figure 21. Concentrations of various cytokines and chemokines in ipsilateral spinal cords. Luminex measurement: Amount of FGFβ, MIP-1a, MCP-1, MIG and KC (A) and various cytokines, chemokines and growth factors (B) 7 d after SNI surgery in ipsilateral spinal cord in wild-type (WT, black) and G2A-deficient (G, grey) mice. n=3-5 animals per group, two-way ANOVA with Holm-Sidak method was used. *p<0.05, **p<0.01. 7 d Luminex multiplex analysis was performed by Béla Zimmer.

3.2.5. Changes along the pain transmission pathway after SNI surgery:

Lipid mediators

Besides by cytokines, chemokines and growth factors, TRP channels can also be modulated through endogenous lipid mediators acting mainly indirectly through, for example, GPCRs to modulate the activity of TRPV1 during inflammation [1, 8, 42]. In this regard, linoleic acid derived metabolites 9- and 13-hydroxyoctadecadienoic acid (9- and 13-HODE) are of particular importance during inflammation and inflammatory pain [85, 180, 181]. Therefore, the amount of linoleic acid derivatives was analyzed by liquid-chromatography tandem mass spectrometry (LC-MS/MS) in SN, DRGs and spinal cord, after dissecting the tissue 7 d after SNI surgery. 9- and 13-HODE disclosed in wild-type mice a strong and significant increase at the ipsilateral site of SN (Fig. 22A). In DRGs and spinal cord there was only a tendency of an increase observed for both metabolites (Fig. 22B and C). Since 9-HODE is an agonist of G2A, it was also of interest to see, whether loss of G2A has an effect on its ligand after SNI [84, 90]. However, in G2A-deficient animals no differences in the amount of 9- and 13-HODE could be detected in all three tissues (SN, DRGs and spinal cord) (Fig. 22D-F).

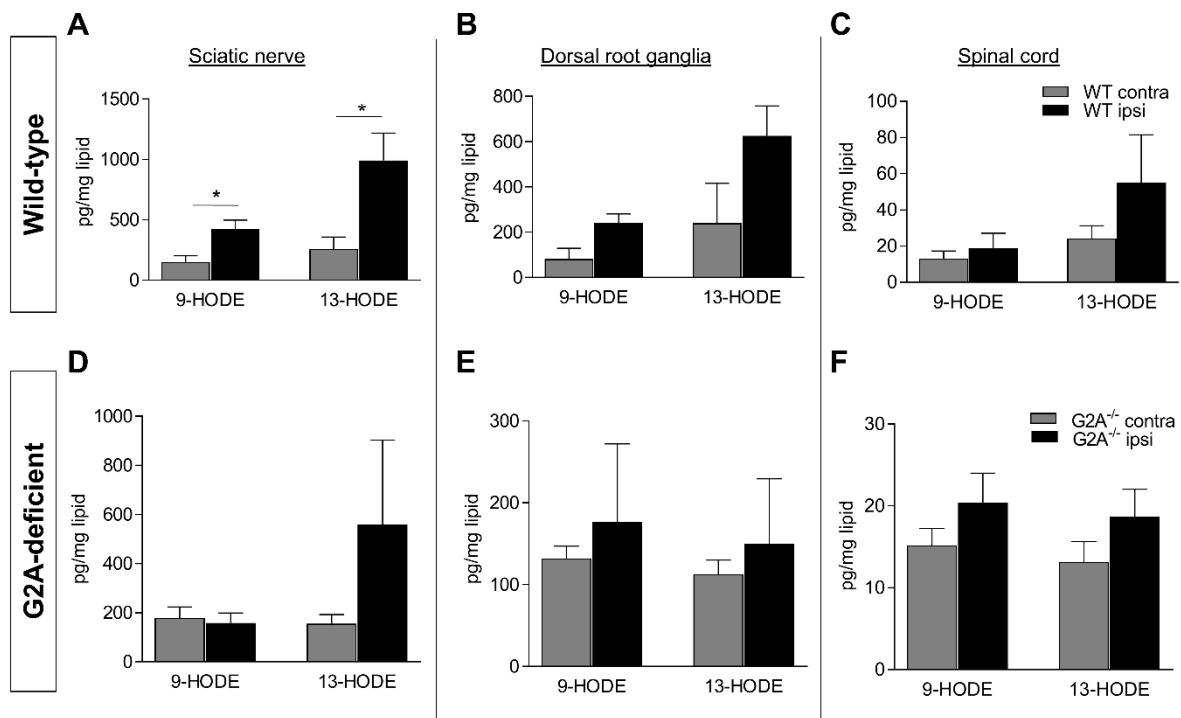


Figure 22. Concentrations of HODEs in sciatic nerves 7d after SNI surgery. LC-MS/MS analysis of amount of 9- and 13-HODE in (A-C) wild-type (WT) and (D-F) G2A-deficient (G2A^{-/-}) mice in contralateral (grey, contra) and ipsilateral (dark, ipsi) site of (A, D) sciatic nerve, (B, E) dorsal root ganglia and (C, F) spinal cord. Data represents mean \pm SEM. n=5 animals per group, multiple t-test. *p<0.05. LC-MS/MS measurements were performed by Carlo Angioni.

Results

The increased levels of 9-HODE in wild-type mice indicate a role for 9-HODE-G2A signaling in nerve-injury induced neuropathic pain, since 9-HODE is an agonist of G2A [85, 90]. As the above presented results indicate, 9-HODE is produced upon inflammation. Since it is not clear which enzyme is responsible for 9-HODE production, an assay was developed to investigate the enzymes involved in linoleic acid metabolism and their role in 9-HODE production upon inflammation [92]. Therefore, bone marrow derived macrophages (BMDMs) were stimulated with LPS and linoleic acid (LA) as precursor of 9-HODE. Additionally, the three major enzymes in LA metabolism, COX, LOX and CYP were inhibited with 50 μ M ketoconazole as CYP-inhibitor, 50 μ M Nordihydroguaiaretic acid (NDGA) as LOX inhibitor, 5 μ M Diclofenac as COX inhibitor, 5 μ M Zileuton as 5-LOX inhibitor or 5 μ M Baicalein as 12- and 15-LOX inhibitor [92, 132–135, 182].

Figure 23 shows that combination of LA and LPS leads to 9-HODE production in BMDMs (Fig. 23, black). When the different inhibitors were added before LA and LPS treatment, 9-HODE production was clearly reduced with baicalein (Bai) and diclofenac (Diclo), indicating that COX, 12- and 15-LOX might be responsible for the 9-HODE production during inflammation (Fig. 23). In contrast, 13-HODE production was unaffected by the inhibitors.

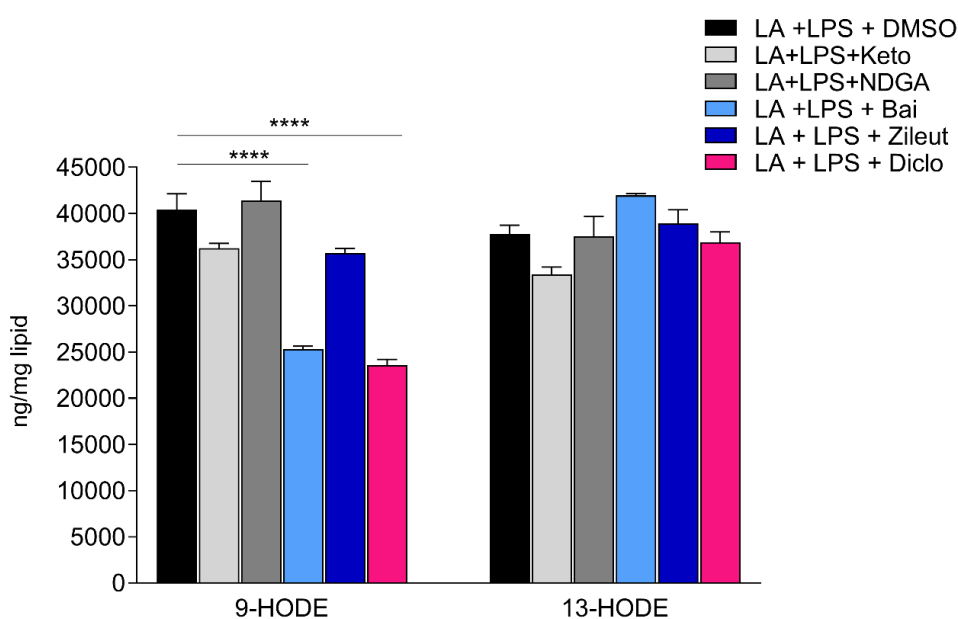


Figure 23. Inhibition of 9-HODE production in BMDMs after LPS stimulation. LC-MS/MS analysis of amount of 9- and 13-HODE in wild-type bone marrow derived macrophages, stimulated with linoleic acid (LA) and lipopolysaccharide (LPS), either alone or in combination with Cyp inhibitor ketoconazole (Keto), LOX inhibitor (NDGA), selective 5-LOX inhibitor Zileuton (Zileut), selective 12- and 15-LOX inhibitor (Bai) or COX inhibitor Diclofenac (Diclo) Data represents mean \pm SEM. Measurements were performed in triplicates, two-way ANOVA with Holm-Sidak method. LC-MS/MS measurements were performed by Carlo Angioni.

Results

Further lipid mediators, which were reported to play a role in neuropathic pain, are the epoxy-octadecenoic acids (EpOMEs) and the dihydroxy-octadecenoic acids (DiHOMEs) [121, 183]. In this work, the results of LC-MS/MS analysis showed significant elevated levels of 12,13-EpOME in ipsilateral site of SN, whereas the corresponding DiHOME, as well as 9,10-EpOME and -DiHOME showed no difference between contra- and ipsilateral site (Fig. 24A). Interestingly, both DiHOMEs were increased in ipsilateral site of DRGs 7 d after SNI. It was reported before, that 12,13-DiHOME is increased in DRGs 24 h after zymosan-injection and 7 d after CFA-induced inflammation [183]. For 9,10-DiHOME such an effect was only reported for spinal cord [183]. Thus, the herein presented data suggests a role of DiHOMEs in nerve-injury induced neuropathic pain. In ipsilateral SN of G2A-deficient mice a significant decrease of 12,13-DiHOME amount was observed 7 d after SNI surgery (Fig. 24D). Unfortunately, in DRGs only little or no amounts of EpOMEs and DiHOMEs were detectable in G2A-deficient mice (Fig. 24E and F).

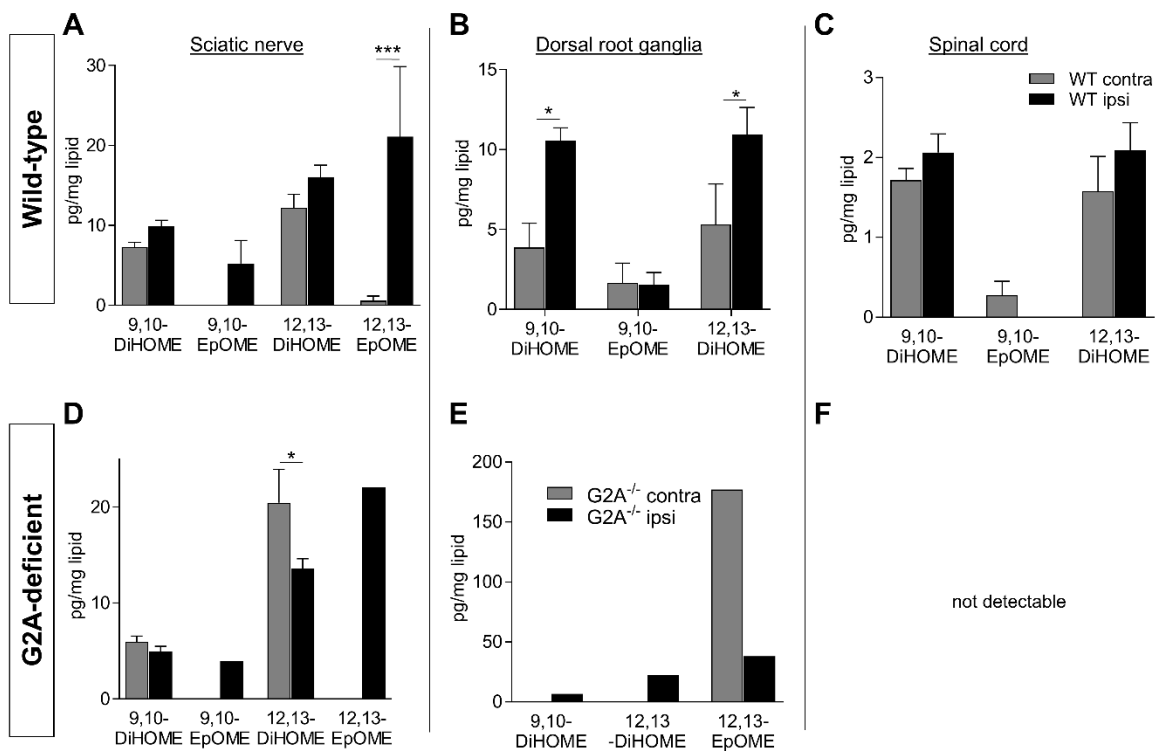


Figure 24. Concentrations of EpOMEs and DiHOMEs at sciatic nerves 7 d after SNI surgery. LC-MS/MS analysis of concentrations of 9,10- and 12,13-EpOME and -DiHOMEs in (A-C) wild-type (WT) and (D-F) G2A-deficient (G2A^{-/-}) mice in contralateral (grey, contra) and ipsilateral (dark, ipsi) site of (A, D) sciatic nerve, (B, E) dorsal root ganglia and (C, F) spinal cord. Data represents mean \pm SEM. n=1-5 animals per group. For statistical analysis a two-way ANOVA with Holm-Sidak method was used. *p<0.05, ***p<0.001. LC-MS/MS measurements were performed by Carlo Angioni.

In conclusion, in SN and DRGs the number of macrophages was strongly decreased at the ipsilateral site of G2A-deficient mice. Additionally, in SN the number of neutrophils was also significantly reduced in G2A-deficient animals. As the results further indicate the reduced number of immune cells resulted in less proinflammatory mediators such as TNF α , IL-6, IL-17, IL-5, IL-2, KC, VEGF, as well as 9- and 13-HODE at the ipsilateral site of SN in G2A-deficient mice. Thereby, the 9-HODE seems to be produced by COX and 12-LOX in BMDMs during inflammation. Next to this, in DRGs only the cytokine amount of IL-12 and IP-10 was reduced in G2A-deficient mice. It was reported earlier that inflammatory mediators such as TNF α , IL-1 β or IL-6 are able to sensitize TRPV1 by binding directly to TRPV1 or to GPCRs [27, 31, 184]. Thus, reduced immune cell numbers, TNF α and IL-6 concentrations may explain the reduced mechanical threshold of G2A-deficient mice presented earlier in this work (Fig. 8).

3.3. Signaling pathways in macrophages

So far, the results indicate a role of 9-HODE in nerve-injury induced inflammation and pain. An earlier study demonstrated that 9-HODE leads to migration of wild-type but not G2A-deficient BMDMs [100]. Therefore, the signaling pathways underlying the 9-HODE-G2A signaling were examined. Thus, BMDMs were isolated from wild-type and G2A-deficient mice, were stimulated with 9-HODE for 24 h, harvested and used for a global proteome analysis.

3.3.1. General comparison of wild-type and G2A-deficient macrophages

When untreated BMDMs of wild-type and G2A-deficient mouse were compared in the proteome analysis, less proteins were significantly regulated compared to wild-type mice after 24 h of 9-HODE stimulation (Fig. 25 and 26). In general, an equal amount of proteins were up- and downregulated in unstimulated macrophages. However, more proteins clustered in migration and immune system were up- than downregulated in unstimulated G2A-deficient macrophages (Fig. 25B and C). Furthermore, proteins concerning the hematopoiesis were downregulated in wild-type BMDMs (Fig. 25B) confirming earlier reports of G2A being involved in hematopoiesis [68]. A more detailed description of the groups and each regulated protein is shown in Table 11 in the annex.

Results

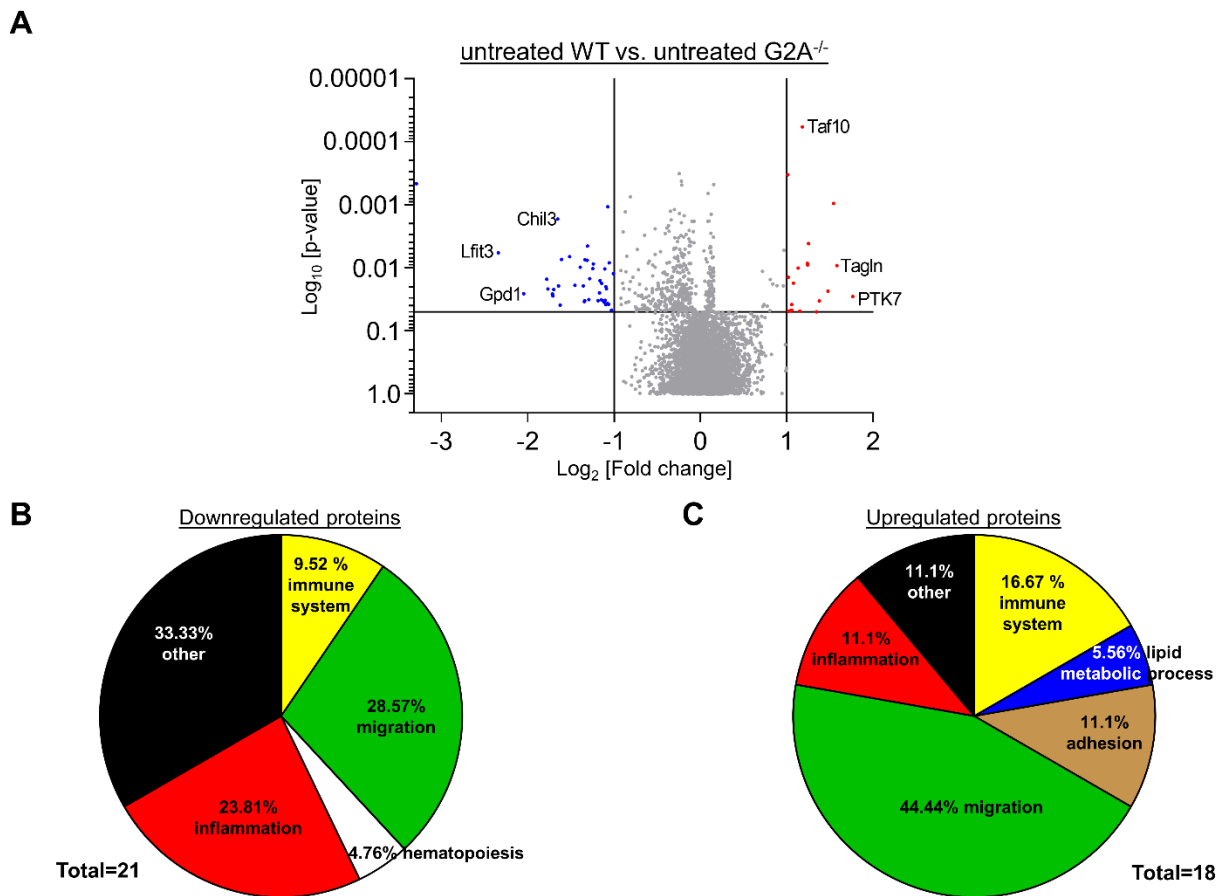


Figure 25. Global proteome analysis of bone marrow derived macrophages (BMDM) of wild-type and G2A-deficient mice without stimulation. (A) Identification of > 6.000 regulated proteins in unstimulated wild-type (WT) and G2A-deficient (G2A^{-/-}) BMDMs. Fold change (FC) [log₂] is plotted against *P* values [Log₁₀]. Significant downregulated proteins are depicted in blue, red represents upregulated proteins. Percentage of (B) downregulated and (C) upregulated proteins in unstimulated G2A-deficient BMDMs compared to untreated wild-type, clustered in migratory (green), adhesional (brown), apoptotic (grey), lysosomal (pink), hematopoietic (white), inflammatory (red), immune system (yellow), lipid metabolic (blue) and other (black) proteins. Samples were stimulated in duplicates. Proteomics were performed by Kevin Klann.

3.3.2. Signaling pathways after 9-HODE stimulation

The stimulation with 9-HODE evoked increased G2A expression in BMDMs (Fig. 26A). Wild-type BMDMs showed more down- than upregulated proteins after 24 h of 9-HODE stimulation (Fig. 26B). The up- and downregulated proteins were clustered in different groups to see the effect of each group more clearly (Fig. 26C and D). Thereby, it was observed that more proteins regarding the immune system (yellow) were down- than upregulated 24 h after 9-HODE stimulation, whereas migratory proteins (green) were twice as much up- than downregulated

Results

(Fig. 26C and D). A more detailed description of the groups and each regulated protein within its group is shown in Table 12 in the annex.

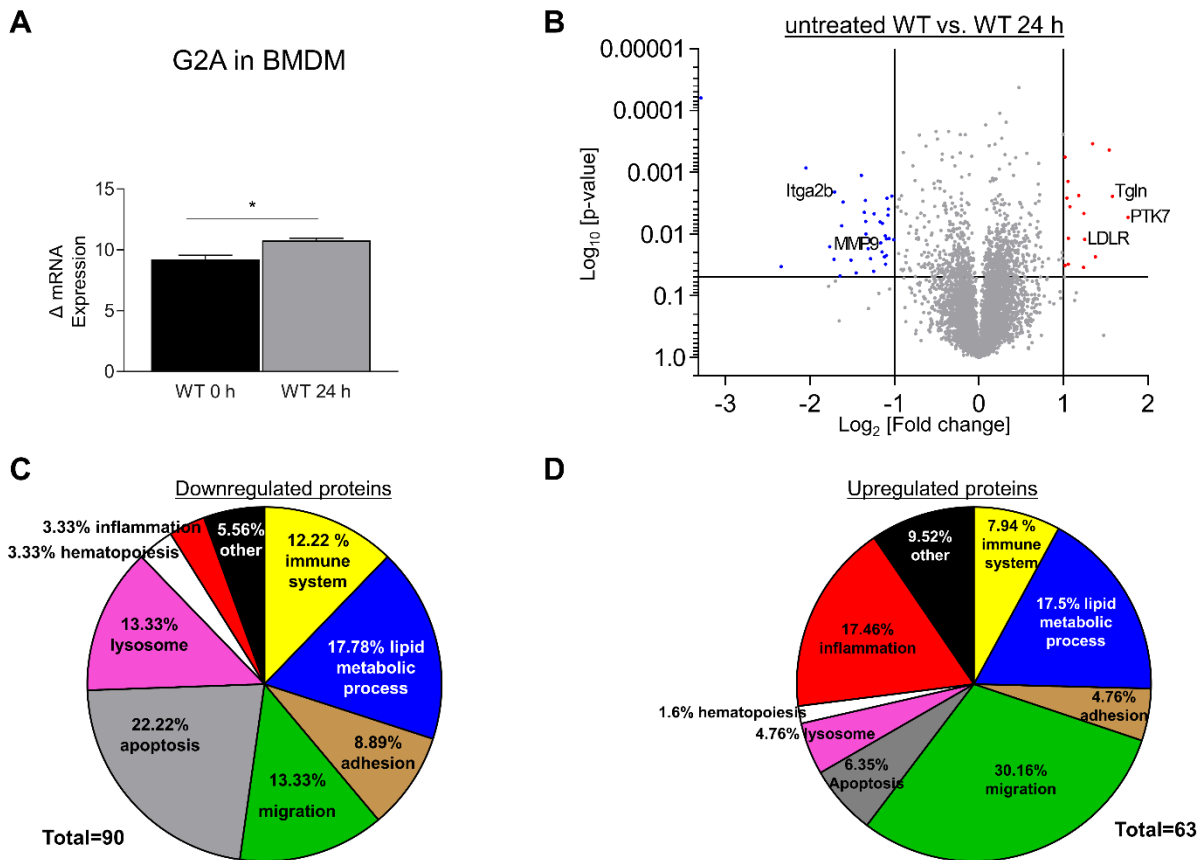


Figure 26. Global proteome analysis of wild-type BMDMs after stimulation with 9-HODE. (A) Relative mRNA expression of G2A in BMDMs 0 h and 24 h after 9-HODE stimulation. n=3, student's t-test with Welch correction. *p<0.05. (B) Identification of > 6.000 regulated proteins 24 h after stimulation with 1 μ M 9-HODE in wild-type (WT) BMDMs. Fold change (FC) [log₂] is plotted against P values [Log₁₀]. Significant downregulated proteins are depicted in blue, upregulated proteins in red. Percentage of (C) down- and (D) upregulated proteins in wild-type 24 h after 1 μ M 9-HODE stimulation compared to untreated wild-type, clustered in migratory (green), adhesional (brown), apoptotic (grey), lysosomal (pink), hematopoietic (white), inflammatory (red), immune system (yellow), lipid metabolic (blue) and other (black) proteins. Samples were stimulated in duplicates and triplicates. Proteomics were performed by Kevin Klann.

The clustered groups were further analysed by sorting the proteins in the most up- and downregulated proteins, regarding the migration cluster (Table 8 and 9). Protein tyrosine kinase 7 (PTK7, No. 5) and low-density lipoprotein receptor (LDLR, 6) as well as transgelin (Tgln, No. 3) were one of the most upregulated proteins (Table 8). Interestingly, in unstimulated G2A-deficient macrophages, Tgln and PTK7 showed already an upregulation (Fig. 25A and

Results

C). indicating that Tgln and PTK7 do not play a major role in migration of macrophages in wild-type after stimulation with 9-HODE.

Table 8. List of most upregulated migratory proteins in wild-type BMDMs 24 h after 1 μ M 9-HODE stimulation. Proteins are sorted by p-value.

	Name	Fold Change	p-value
1	Ctnna1	0.250	0.000
2	Myd88	0.309	0.001
3	Tgln	1.582	0.002
4	Cadm1	0.493	0.003
5	Ptk7	1.767	0.005
6	Ldlr	1.253	0.012
7	Pik3r5	0.231	0.012
8	Mylk	0.543	0.012
9	Col6a2	0.337	0.013
10	Actn1	0.282	0.016
90	ERK1	0.094	0.242
110	p38	0.122	0.394

Moreover, Tgln, as well as myeloid differentiation primary response protein 88 (MyD88) and phosphoinositide 3-kinase (PI3K) were strongly upregulated in wild-type BMDMs compared to G2A-deficient BMDMs (Fig. 27A). They are proteins downstream of the toll-like receptor 4 (TLR4) signaling pathway, which is known for its pro-migratory role [185–188]. Thus, 9-HODE-G2A signaling could lead into an activation of TLR4 (Fig. 27B).

Results

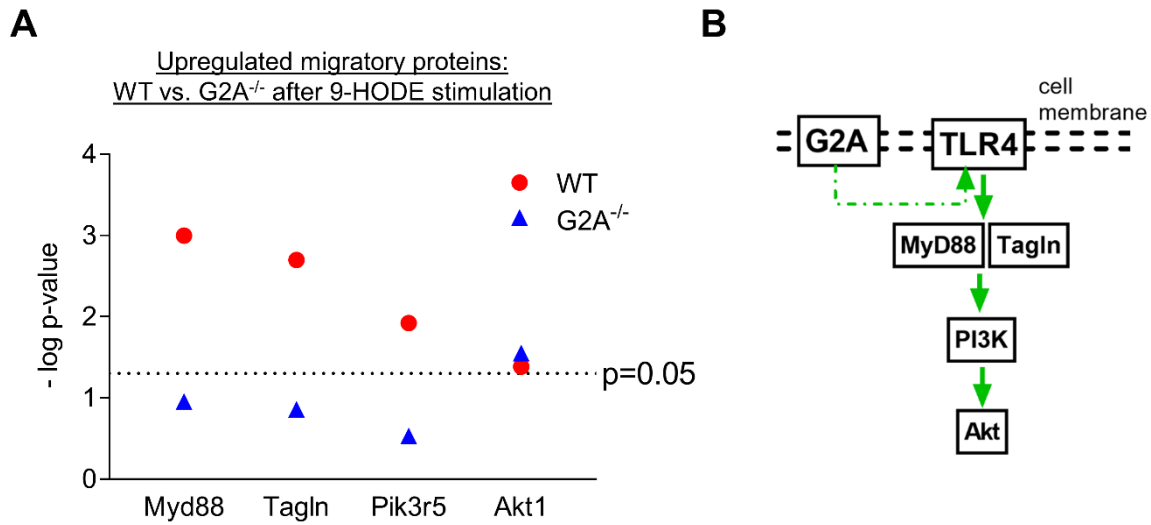


Figure 27. Upregulated migratory proteins and involved signaling pathways. (A) Strongest upregulated migratory proteins regarding the toll-like receptor 4 (TLR4) signaling pathway in wild-type (WT) and G2A-deficient (G) BMDMs after 9-HODE stimulation for 24 h, shown as $-\log p$ -value. (B) Suggestion of a possible G2A-TLR4 interaction and subsequent signaling in BMDMs. Published also in Osthues *et al.* 2020, Fig 5B and 5C [189].

MMP9 (Table 9, No. 9) and integrin alpha-IIb precursor (Itga2b, Table 9, No. 3) were one of the most downregulated proteins 24 h after 9-HODE stimulation.

Table 9. List of most downregulated migratory proteins in wild-type BMDMs 24 h after 1 μ M 9-HODE stimulation. Proteins are sorted by p-value.

	Name	Fold Change	p-value
1	Lgmn	-0.533	0.002
2	Cd5l	-0.463	0.002
3	Itga2b	-1.709	0.002
4	Itgb3	-0.917	0.002
5	Grb2	-0.281	0.004
6	Tmsb4x	-0.92	0.004
7	Il16	-0.339	0.007
8	Glg1	-0.12	0.007
9	MMP9	-1.165	0.014
10	CMKLR1	-1.105	0.031

In G2A-deficient BMDMs 24 h after 9-HODE stimulation more migratory and adhesion proteins were upregulated (Fig. 28A and C). However, it was half the amount of migratory proteins of the wild-type BMDMs treated with 9-HODE (Fig. 26 and 28C). Interestingly, more proteins

Results

regarding the immune system and apoptosis were down- than upregulated in G2A-deficient BMDMs after stimulation (Fig. 28), indicating a role of G2A in immune system processes and survival. A more detailed description of the groups and each regulated protein is shown in Table 13 in the annex.

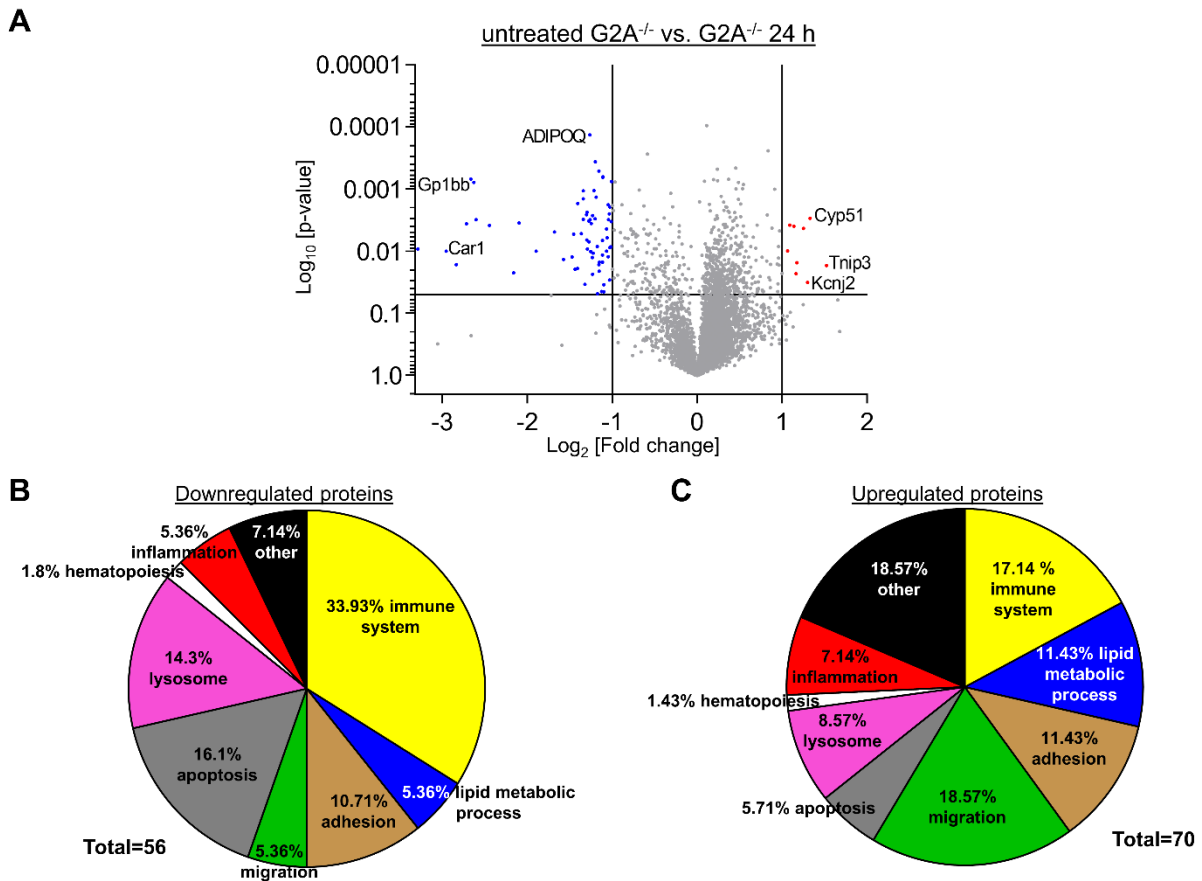


Figure 28. Global proteome analysis of BMDMs of G2A-deficient mice after 9-HODE stimulation. (A) Identification of > 6.000 regulated proteins 24 h after stimulation with 1 μ M 9-HODE in G2A-deficient (G2A^{-/-}) BMDMs. Fold change (FC) [log₂] is plotted against P values [Log₁₀]. Significant downregulated proteins are depicted in blue, red represents upregulated proteins. Percentage of (B) downregulated and (C) upregulated proteins in G2A-deficient BMDMs 24 h after 1 μ M 9-HODE stimulation compared to untreated G2A-deficient BMDMs, clustered in migratory (green), adhesional (brown), apoptotic (grey), lysosomal (pink), hematopoietic (white), inflammatory (red), immune system (yellow), lipid metabolic (blue) and other (black) proteins. Samples were stimulated in duplicates and triplicates. Proteomics were performed by Kevin Klann.

Comparing stimulated BMDMs of wild-type and G2A-deficient mice, the clustering showed that more migratory proteins were upregulated in G2A-deficient mice (Fig. 29). One of them is the known migratory protein CXCR4 [190, 191] (Fig. 29A and C). As figure 29 further depicts inflammatory proteins were more down- than upregulated in G2A-deficient BMDMs after stimulation with 9-HODE, indicating a rather proinflammatory role for the 9-HODE-G2A axis.

Results

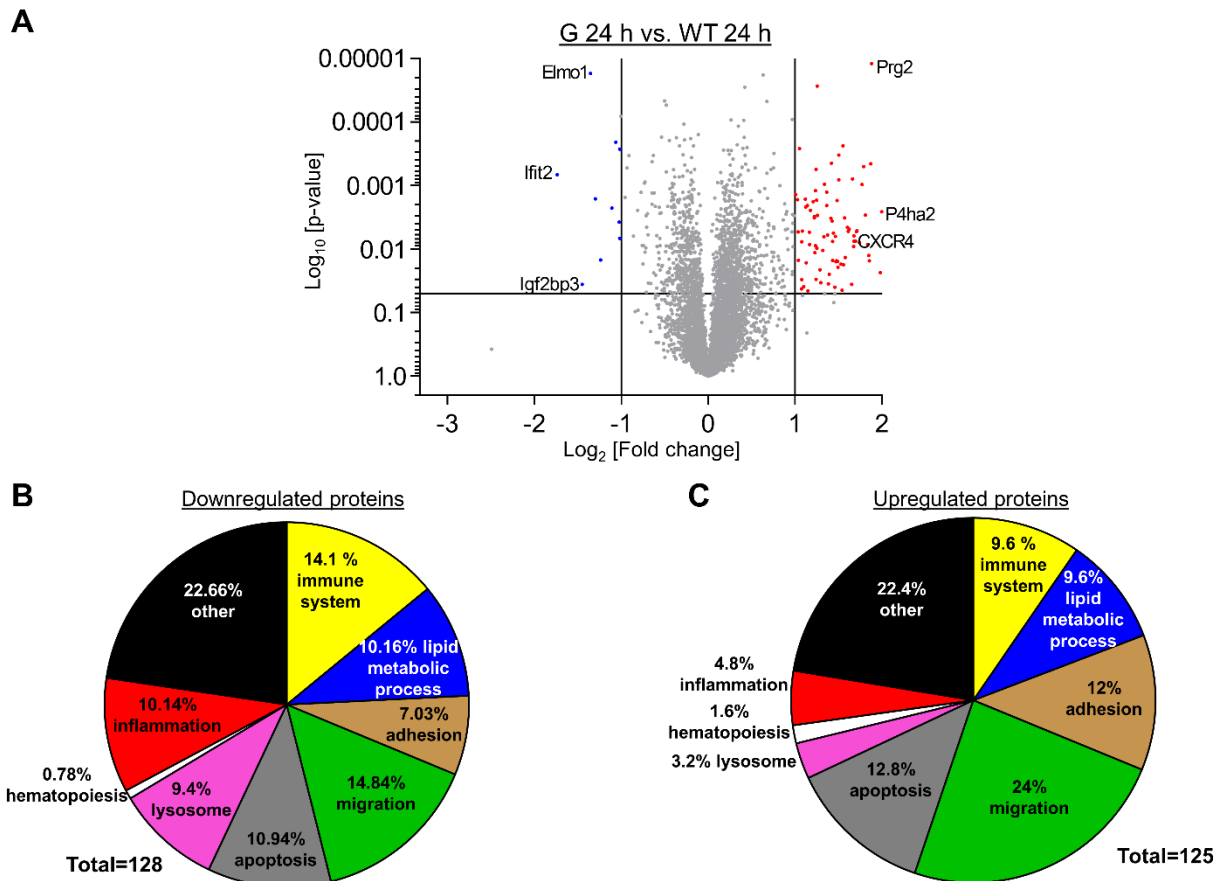


Figure 29. Global proteome analysis of BMDMs of wild-type and G2A-deficient mice after 9-HODE stimulation. (A) Identification of > 6.000 regulated proteins 24 h after stimulation with 1 μ M 9-HODE in wild-type and G2A-deficient BMDMs. Fold change (FC) [\log_2] is plotted against P values [\log_{10}]. Significant downregulated proteins are depicted in blue, red represents upregulated proteins. Percentage of (B) downregulated and (C) upregulated proteins in G2A-deficient BMDMs 24 h after 1 μ M 9-HODE stimulation compared to stimulated wild-type BMDMs, clustered in migratory (green), adhesional (brown), apoptotic (grey), lysosomal (pink), hematopoietic (white), inflammatory (red), immune system (yellow), lipid metabolic (blue) and other (black) proteins. Samples were stimulated in triplicates. Proteomics were performed by Kevin Klann.

3.3.3. MMP9 regulation after G2A activation in macrophages

For evaluation of the proteome analysis, some of the most up- and downregulated proteins were chosen for Western blot analysis. However, there were technical difficulties in obtaining a specific signal for some of the antibodies, like C-X-C chemokine receptor type 4 (CXCR4) showing only weak bands on the films (Fig. 30D). As figure 30 further shows the proteome data could not be confirmed for Itga2b, CXCR4, engulfment and cell motility protein 1 (Elmo1), chemokine like receptor 1 (CMKLR1) and LDLR. Regarding PTK7 and Tgln, the proteome screen already indicated a minor effect of them on migration, since they were also upregulated

Results

in unstimulated G2A-deficient macrophages (Fig. 25). Thus, it is not surprising that in Western Blots there was no difference observed after 24 h stimulation with 9-HODE in wild-type BMDMs (Fig. 30B and E). Interestingly, MMP9 showed a significant decrease 24 h after stimulation with 9-HODE in wild-type BMDMs (Fig. 30A).

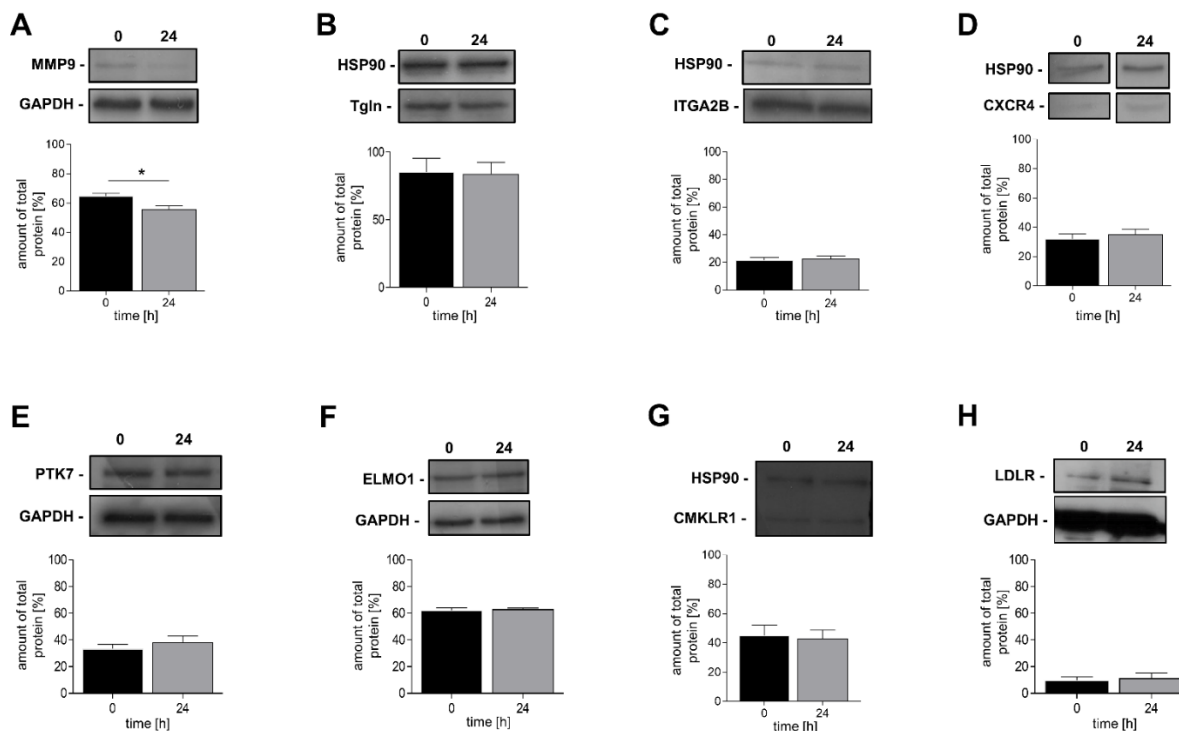


Figure 30. Western Blots of proteome analysis evaluation. Representative Western Blots of (A) MMP9, (B) Tgln, (C) Itga2b, (D) CXCR4, (E) PTK7, (F) Elmo1, (G) CMKLR1 and (H) LDLR expression in bone marrow derived macrophages of wild-type mice after stimulation with 1 μ M 9-HODE at 0 and 24 h. As loading control GAPDH or HSP90 was used. n=4-6. One-sided t-test was used for statistical analysis. *p<0.05

MMP9 was reported to be secreted and subsequent results in cell migration [192–197]. Therefore, the secretion of MMP9 of BMDMs after stimulation with 9-HODE was also examined in a time-dependent manner with ELISA (Fig. 31). As the data indicates, without stimulation the MMP9 secretion was relatively low at around 1 ng/ml, but already 1 h after stimulation with 9-HODE the secretion of MMP9 increased and reached a peak after 4 h at over 4 ng/ml (Fig. 31A). Afterwards, the secreted MMP9 amount decreased again to almost the same level as after 24 h (Fig. 31A). Since in the proteome screen and in the Western Blots a decrease of MMP9 was observed after 24 h in BMDMs, the pellets of the secretion experiments were also subjected to ELISA analyses. Interestingly, here was not such a strong effect observed as in the medium of the cells (Fig. 31B). In general, the amount of MMP9 was in the pellet higher than in the medium without stimulation. Its levels increased slightly after 1 h, but then dropped

to its starting point at 4 h (Fig. 31B). Interestingly, afterwards, the MMP9 amount in the cells even decreased further until it reached a minimum after 24 h (Fig. 31B).

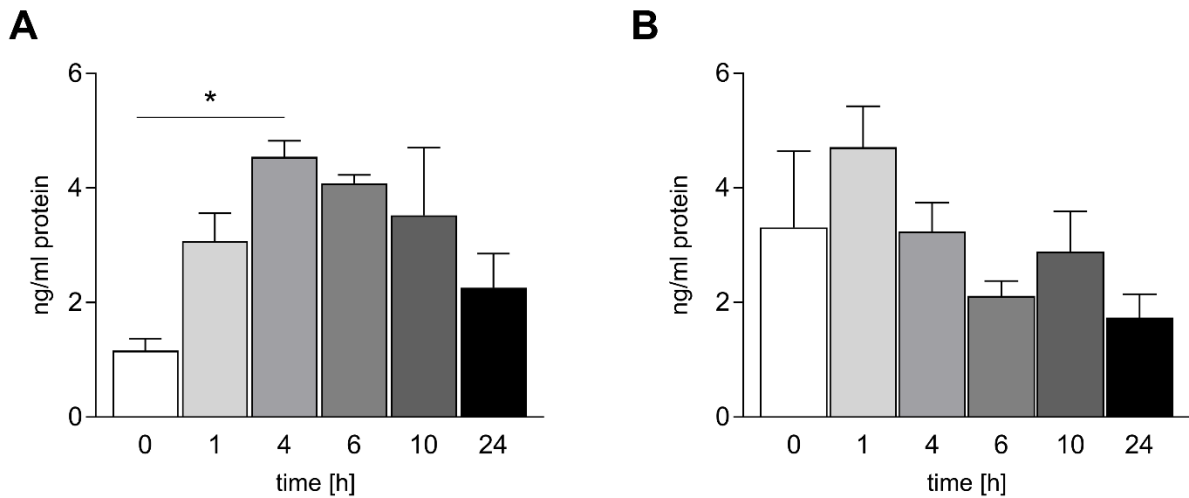


Figure 31. MMP9 concentrations in cell lysates of BMDMs. BMDMs were stimulated with 9-HODE for 1, 4, 6, 10 and 24 h. Medium of stimulated BMDMs and cells were harvested and analysed with ELISA. Time-dependent secretion of BMDMs (A) and production in BMDMs (B) of MMP9 after stimulation with 1 μ M 9-HODE. Samples were measured in duplicates with n=6-8. For statistics a one-way ANOVA with Holm-sidak method was chosen. *p<0.05.

3.3.4. Investigation of further signaling pathways involved in migration

Moreover, proteins known to be involved in migratory signaling pathways, like ERK and p38, were not upregulated in wild-type BMDMs 24 h after stimulation with 9-HODE (Table 8, No. 90 and 110) [198, 199]. As the proteome results indicate, these proteins were also not regulated in G2A-deficient macrophages, either with or without stimulation. These results could be confirmed with Western Blots, in wild-type and G2A-deficient mice (Fig. 32).

Results

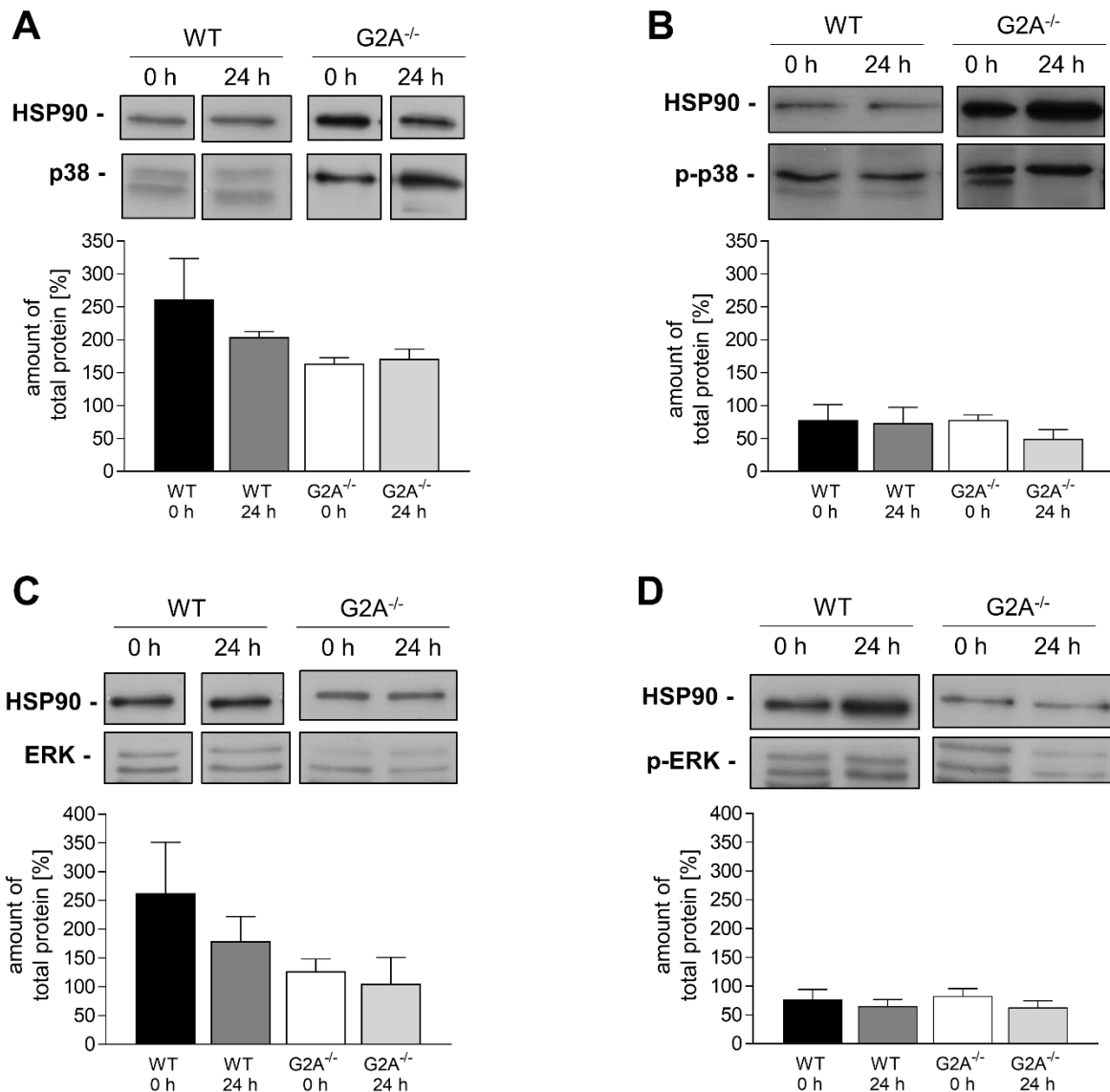


Figure 32. Western Blots of ERK, p38 and phosphorylated ERK (p-ERK) and p38 (p-p38). Representative Western Blots of (A) p38, (B) phosphorylated p38 (p-p38), (C) ERK and (D) phosphorylated ERK (p-ERK) in wild-type (WT) and G2A-deficient (G2A^{-/-}) BMDMs without stimulation (0 h) or with 24 h (24 h) stimulation with 9-HODE. As loading control HSP90 was used. n=5-12. For statistical significance a one-way ANOVA with Bonferroni post-hoc test was used.

Regarding the phosphorylation of p38 and ERK, there seems to be a slight increase of p-ERK in G2A-deficient BMDMs after 24 h stimulation with 9-HODE (Fig. 33B). Furthermore, in untreated G2A-deficient BMDMs the amount of p-38 seemed to be higher than in wild-type mice (Fig. 33B). Nevertheless, the differences were only small.

Overall, next to ERK and p-38 there are further proteins known to be involved in migration, such as PI3K. In the proteome screen it was strongly upregulated (Table 8) in wild-type

Results

BMDMs after stimulation with 9-HODE, but not in G2A-deficient macrophages. In Western blots there was no difference between treated and untreated BMDMs observed for wild-type or G2A-deficiency (Fig. 33A).

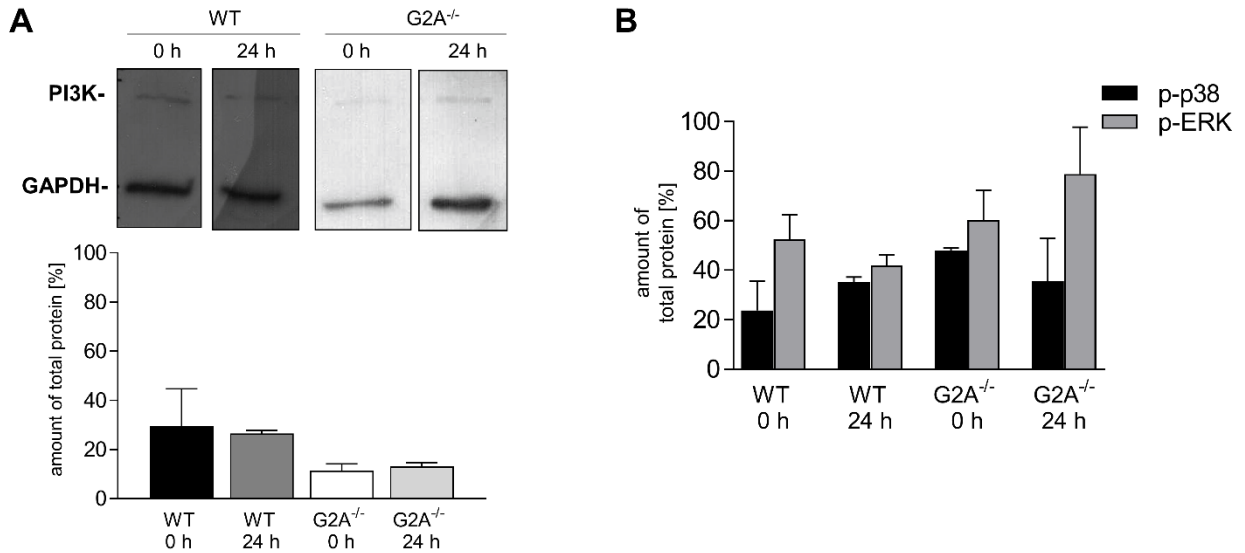


Figure 33. Western Blots of PI3K and phosphorylation amount of ERK and p38. Representative Western Blots of (A) PI3K in wild-type (WT) and G2A-deficient (G2A^{-/-}) BMDMs without stimulation (0 h) or with 24 h (24 h) stimulation with 9-HODE. As loading control GAPDH was used. (B) Amount of phosphorylated ERK (grey) and p38 (black) in wild-type and G2A-deficient BMDMs with (24 h) or without (0 h) stimulation. n=2-4. For statistical significance a one-way ANOVA with Bonferroni post-hoc test was used for A and a two-way ANOVA with Holm-Sidak method was used for B.

Next to this, ROCK1, ROCK2, Rac and Ras are known to be involved in migration of leukocytes [200–203]. Therefore, these proteins were also analyzed with Western blots. However, these signaling pathways seem to play only a minor role in macrophage migration, since there was no difference observed in Western blots in wild-type and G2A-deficient BMDMs (Fig. 34).

Results

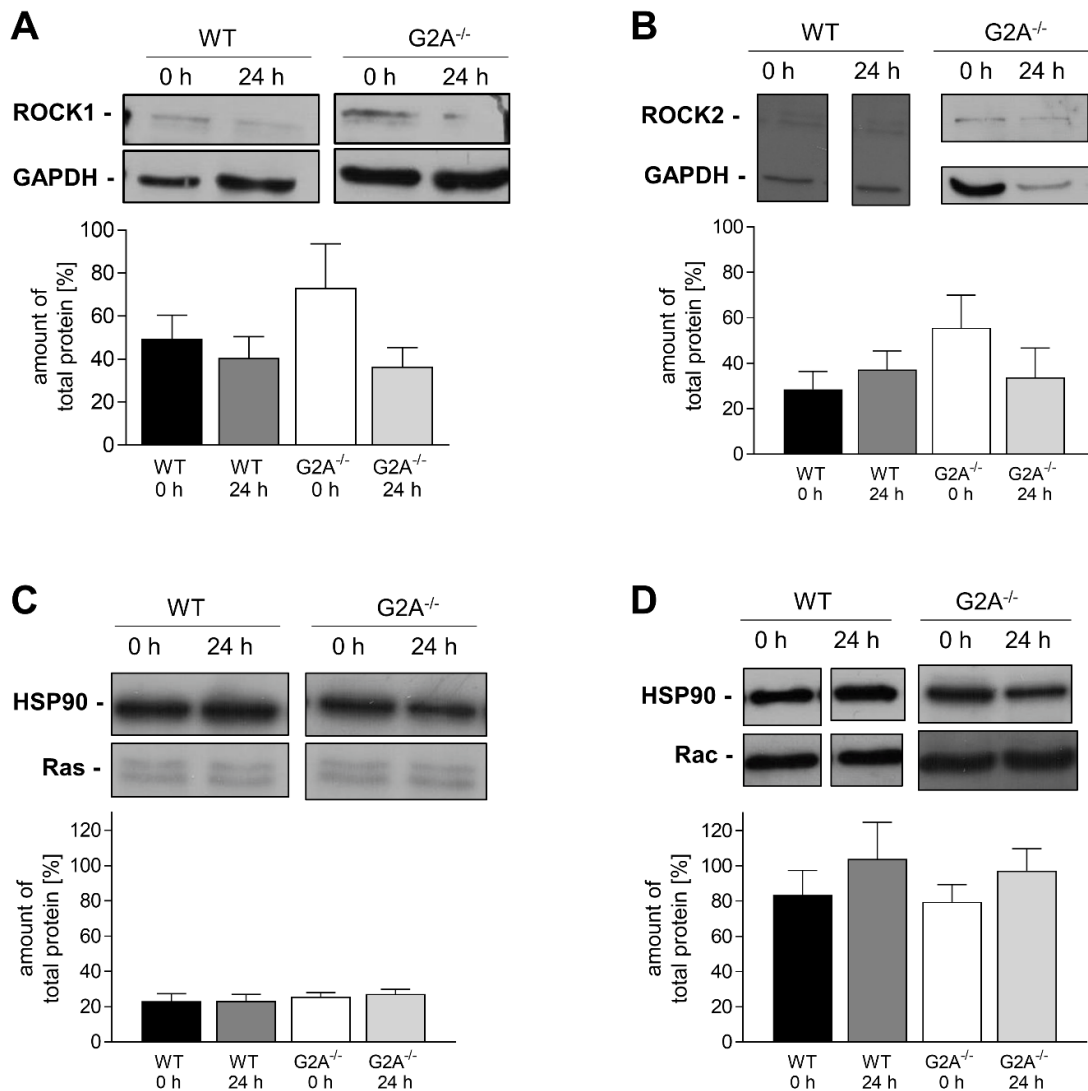


Figure 34. Western Blots of ROCK1 and -2, as well as Rac and Ras. Representative Western Blots of (A) ROCK1, (B) ROCK2, (C) Ras and (D) Rac in wild-type (WT) and G2A-deficient (G2A^{-/-}) BMDMs without stimulation (0 h) or with 24 h (24 h) stimulation with 9-HODE. As loading control HSP90 was used. n=5-11. For statistical significance a one-way ANOVA with Bonferroni post-hoc test was used.

In conclusion, neither Rac, Ras, ROCK or MAPK signaling pathways, that are known to be involved in migration, seem to be responsible for the migration of macrophages after 9-HODE stimulation [198, 200, 202, 203]. The only signaling pathway that is promigratory and is activated by 9-HODE in BMDMs is the TLR4 pathway (Fig. 27) [185, 188]. MMP9 is one of the most downregulated proteins in BMDMs when stimulated with 9-HODE for 24 h. But its secretion is increased after 4 h of stimulation with 9-HODE. Furthermore, G2A seems to play a role in immune system and inflammatory processes. Thus, the results suggest that 9-HODE-G2A signaling causes transient release of MMP9 and crosstalk with the TLR4-signaling pathway to initiate migration in BMDMs.

3.4. Inhibition of G2A receptor

3.4.1. Screen for G2A inhibitors

The results so far depict effects of G2A on the number of immune cells and proinflammatory mediators, as well as nociceptive behavior after nerve-injury. Moreover, as the 9-HODE stimulation experiments and the proteomics showed G2A seems to play a role in immune processes and migration of immune cells during inflammation. Therefore, G2A could be a promising target for treatment of neuropathic pain.

Since there is no known inhibitor of G2A so far, a global screen of about 20.000 substances was performed by Dr. Jan Heering at Fraunhofer ScreeningPort. Therefore, G2A and guanine nucleotide-binding subunit alpha-11 (GNA11) were cloned into vectors of the transposon-based system “sleeping beauty” in order to stably insert expression cassettes into the genome of Chinese hamster ovary K1 (CHO K1) cells [204, 205]. Single cell clones were identified to ensure genetic stability throughout the project. As a readout of G2A activity, the accumulation of IP1 was measured, which is a consequence of G_q-activation [206]. Clone #8 showed representative responsiveness to 9-HODE in the IP-One assay and was used during the screen, the hit evaluation and dose-response experiments.

Finally, 6 compounds showed antagonistic effects in CHO K1 cells expressing G2A. They were named G2A11, G2A12, G2A13, G2A19, G2A23 and G2A24 (Table 10). After selection, these compounds were subjected to toxicity tests, using “cell titer glo” (Promega, Madison, USA) on HeLa cells. Of those compounds G2A11, which had the lowest IC₅₀ showed one of the strongest toxic effects at a concentration of 100 μM. G2A12 and G2A19 showed at 100 μM higher live rates of the cells, but had higher IC₅₀ levels. However, they still showed some toxic effects (Table 10).

Results

Table 10. Results of G2A antagonist screening and subsequent cell toxicity assay of the screening hits.
The high throughput screen at Fraunhofer Screening port and the tox determination was performed by Jan Heering.

Compound	Agonism	Calculated IC ₅₀ [μ M] for G2A vs. 12.5 μ M 9-HODE	Cell toxicity determined with cell titer glo in HeLa cells	
			Live rate	concentration
G2A11	No	1.46	3 %	250 μ M
			30 %	100 μ M
			70 %	40 μ M
G2A12	No	5.49	80 %	250 μ M
			95 %	100 μ M
			100 %	40 μ M
G2A13	No	9.59	0 %	250 μ M
			80 %	100 μ M
			90 %	40 μ M
G2A19	Inactive below ~40 μ M	8.7	4 %	250 μ M
			80 %	100 μ M
			90 %	40 μ M
G2A23	No	9.33	0 %	250 μ M
			60 %	100 μ M
			100 %	40 μ M
G2A24	No	4.88	4 %	250 μ M
			50 %	100 μ M
			95 %	40 μ M

3.4.2. Inhibitory effect of G2A inhibitors on TRPV1-mediated Ca²⁺ influx

The effect of the inhibitors concerning G2A activation was only seen *in vitro* in CHO K1 cells overexpressing G2A. To see, whether the inhibitors have similar effects in a more physiological cell system, DRG neurons were used for Ca²⁺-Imaging experiments. Herein, the different

Results

inhibitors were used in different concentrations together with 9-HODE as G2A-stimulatory agent. After incubation of the DRG neurons with 9-HODE alone or together with the respective G2A inhibitor, the neurons were stimulated with the TRPV1-agonist capsaicin and their activation was determined. The ratio of the two determined wavelengths 340 and 380 nm increased after stimulation of the cells with capsaicin indicating a Ca^{2+} influx into the cells (Fig. 35A). However, after preincubation with 9-HODE (Fig. 35A, grey), the peak of the Ca^{2+} influx was more elevated than with its vehicle ethanol (Fig. 35A, black). In contrast, using the G2A inhibitor G2A11 at a concentration of 1 μM together with 9-HODE (Fig. 35A, red) the amplitude of the Ca^{2+} influx was at vehicle level. Figure 35A shows exemplary data. The different ratios of all used concentrations of G2A11 are shown in figure 35B. The TRPV1-mediated Ca^{2+} influx through G2A activation was decreased by G2A11 only at a concentration of 1, 10 and 50 μM (Fig. 35B).

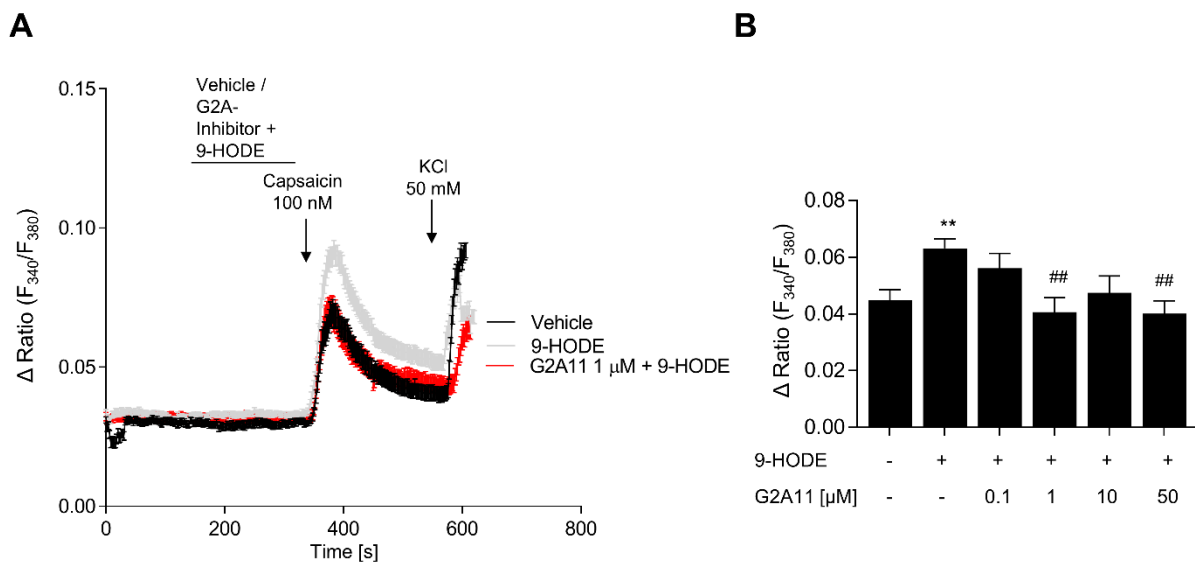


Figure 35. Inhibitory effects of G2A11 on 9-HODE dependent TRPV1-mediated calcium influx. Ca^{2+} -imaging: (A) Representative traces of amplitudes of capsaicin (100 nM, 30s) evoked by calcium influx in DRG neurons. Neurons were either first incubated with vehicle (black, 2 min), 9-HODE (grey, 1 μM , 2 min.) or 9-HODE together with 1 μM G2A11 (red, 2 min) before stimulation with capsaicin. Identification of neurons was conducted by KCl stimulation (50 mM, 45 s) at the end of measurement. (B) Δ ratio of F340/F380 of responding neurons after incubation with vehicle, 9-HODE, or 9-HODE together with different concentrations (0.1, 1, 10, 50 μM) of antagonist G2A11 followed by stimulation with capsaicin (100 nM, 30s). Data is calculated as delta ratio F340/F380 and is shown as mean \pm SEM from n=36-76 neurons per condition; #p<0.05 (compared with 9-HODE), **p<0.01 (compared with vehicle), One-Way ANOVA with Bonferroni Post-hoc test.

Results

Overall, G2A13 and G2A19 revealed the strongest inhibitory effects on TRPV1-mediated Ca^{2+} influx even at a concentration of 0.1 μM (Fig. 36, light grey and white). Interestingly, G2A12 (Fig. 36, dark grey) showed an opposite effect at 50 μM . Thus, at such a high concentration G2A12 caused a strong TRPV1-mediated Ca^{2+} influx into the neurons.

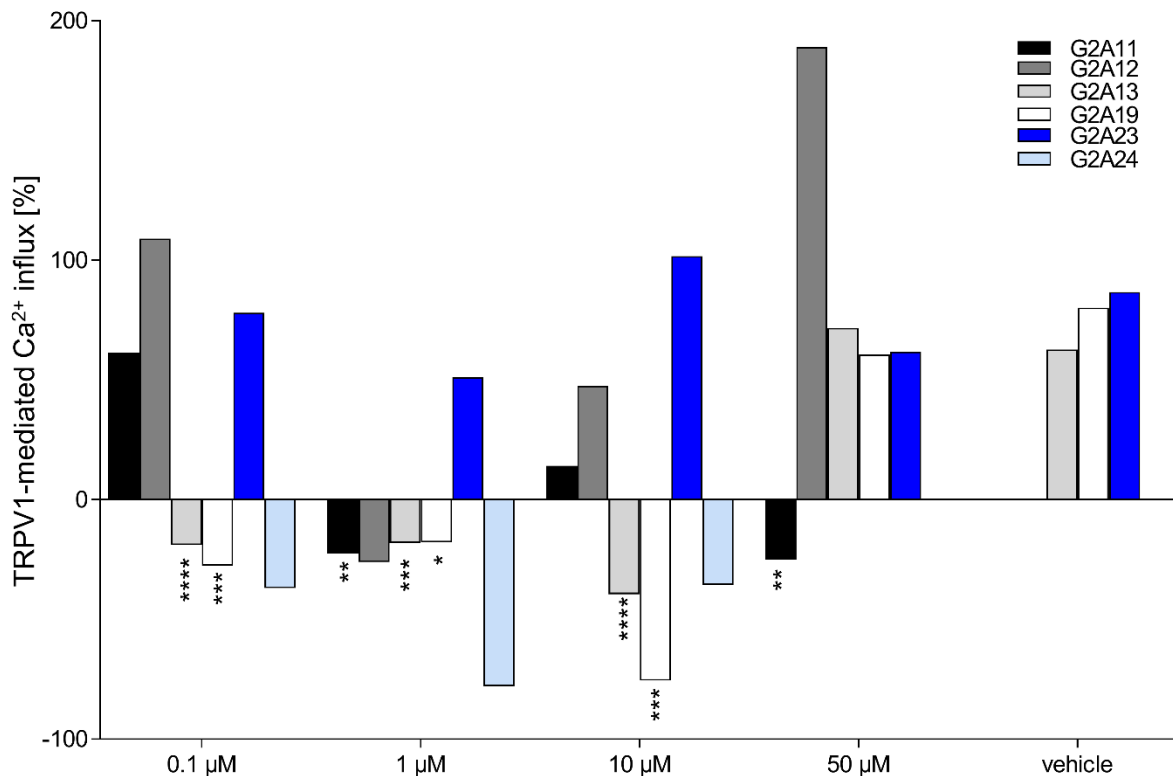


Figure 36. Inhibitory effects of 6 inhibitors on 9-HODE dependent TRPV1-mediated calcium influx. Ca^{2+} -Imaging: Percentage of sensitization of antagonists G2A11 (black), G2A12 (dark grey), G2A13 (light grey), G2A19 (white), G2A23 (light blue), G2A24 (dark blue) at different concentrations (0.1, 1, 10, 50 μM) and the vehicle of the antagonists. The percentage was calculated by normalizing the Δ ratio of F340/F380 to the sensitization of 9-HODE. One-way ANOVA with Turkey correction. * $p < 0.05$, ** $p < 0.01$, *** $p < 0.005$, **** $p < 0.001$. $n = 22-112$.

3.4.3. Effects of G2A11, G2A13 and G2A19 on the migratory behavior of macrophages

The inhibitors named G2A11, G2A13 and G2A19 showed the strongest inhibitory effects on TRPV1 sensitization on DRG neurons, indicating an antinociceptive effect. Next to this, in the presented thesis it was shown that loss of G2A resulted in reduced numbers of macrophages at the injured nerve (see 3.2.1 Distribution of immune cells at the site of injury). Therefore, the migratory behavior of macrophages was examined in presence of the three antagonists.

Results

For this, bone marrow derived macrophages (BMDMs) were cultivated and then 300 μ l of 7.44×10^5 cells/ml were seeded into an insert of a 24-well plate. In the well below the desired solutions were added. After 4 h the migrated cells were stained with DAPI and were determined by fluorescence microscopy. Exemplarily images of those images are shown in figure 37. Here obviously less macrophages migrated into medium without any migrating stimulus (Fig. 37A) (transwell medium, see 2.1.5 Cell culture medium). Whereas, using transwell – solution 1 (see 2.1.5 Cell culture medium) more macrophages migrated through the membrane to the medium with FCS as stimulating agent (Fig. 37B).

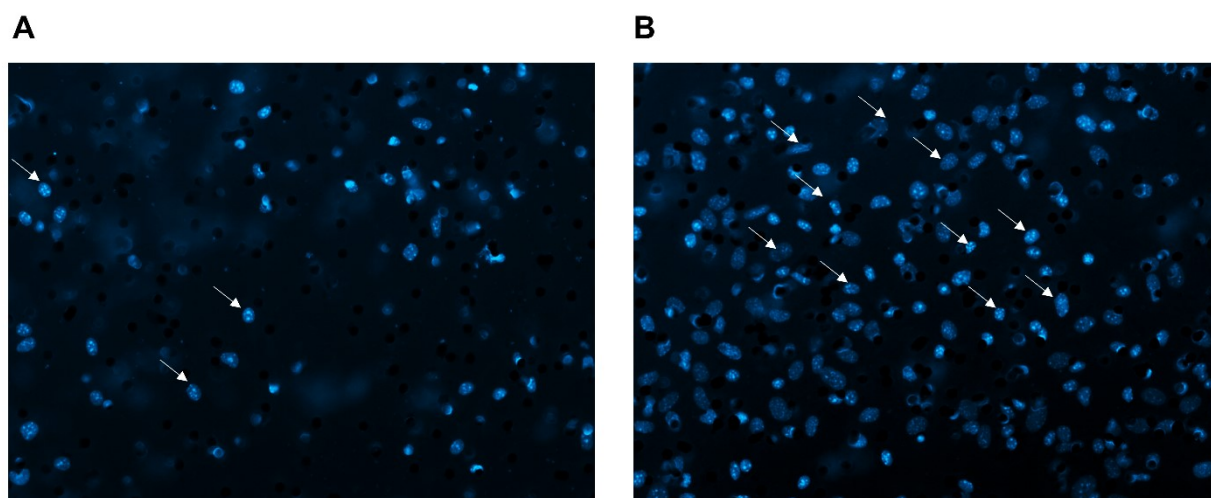


Figure 37. Exemplary images of BMDMs on membrane after migration. Migrated cells were stained with DAPI for visualization of the nucleus. BMDM migration through insert membrane (A) without and (B) with chemotactic stimulus (FCS). Arrows indicate migrated cells, characterized by dotted nucleus.

All single countings were averaged and are shown in figure 38. When the inhibitor G2A11 was used in different concentrations (0.1, 1 and 10 μ M), there was only a clear inhibition of migration at a concentration of 10 μ M (Fig. 38A). Unfortunately, 9-HODE had no effect on the migration of BMDMs as it was shown previously [100]. There was also no effect observed of 9-HODE on the migratory behavior of macrophages, when FCS was additionally in the medium (Fig. 38B). However, the formerly seen inhibition at 10 μ M of G2A11 was observed again, when FCS was added to the migrating medium (Fig. 38B).

Results

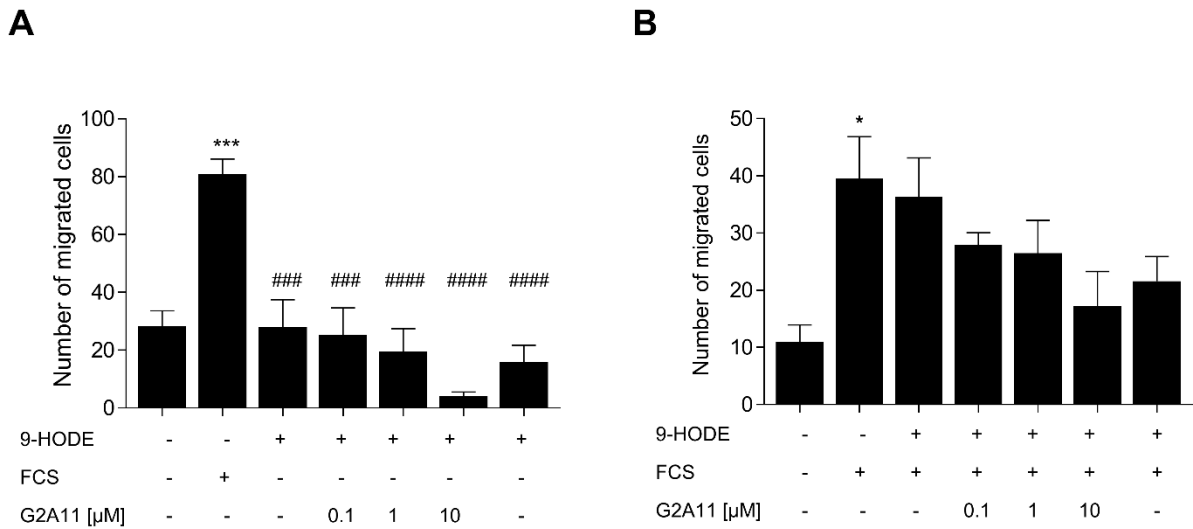


Figure 38. Inhibition of BMDMs migration through G2A11. Transwell BMDM migration through G2A11 in medium (A) without FCS and (B) with FCS in each solution used. Samples were measured in triplicates with n=4 independent measurements. For statistics a one-way ANOVA with Holm-sidak method was chosen. *p<0.05, ***p<0.001 (vs. without FCS), ###p<0.001, ####p<0.0001 (vs. FCS).

Regarding G2A13, there was also no effect seen on the migration of BMDMs when 9-HODE was added to transwell medium (Fig. 39). However, it revealed a tendency of a concentration dependent inhibition of migration, having the strongest effect at 10 μM.

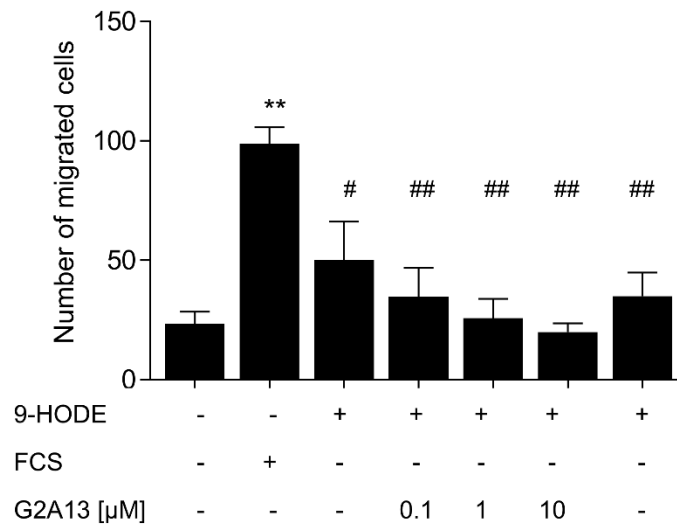


Figure 39. Inhibition of BMDMs migration through G2A13. Transwell BMDM migration through G2A13. For statistics a one-way ANOVA with Holm-sidak method was chosen. n=4 independent experiments, in each experiment triplicates were measured. **p<0.01 (vs. without FCS), #p<0.05, ##p<0.01 (vs. FCS).

Results

Again, the control of 9-HODE as migrating agent was not effective in the G2A19 transwell migration assay (Fig. 40A). However, a strong inhibition of the migration was observed at a concentration of 10 μM (Fig. 40A). When the experiments were repeated with FCS in each of the different solutions used for the migration assay, addition of 9-HODE showed a small migrating effect compared to the negative control without FCS in the medium (Fig. 40B). However, the strong inhibition of the migration of macrophages was not observed any more even at high concentrations of 10 μM of G2A19 (Fig. 40B), indicating no specific inhibition of G2A.

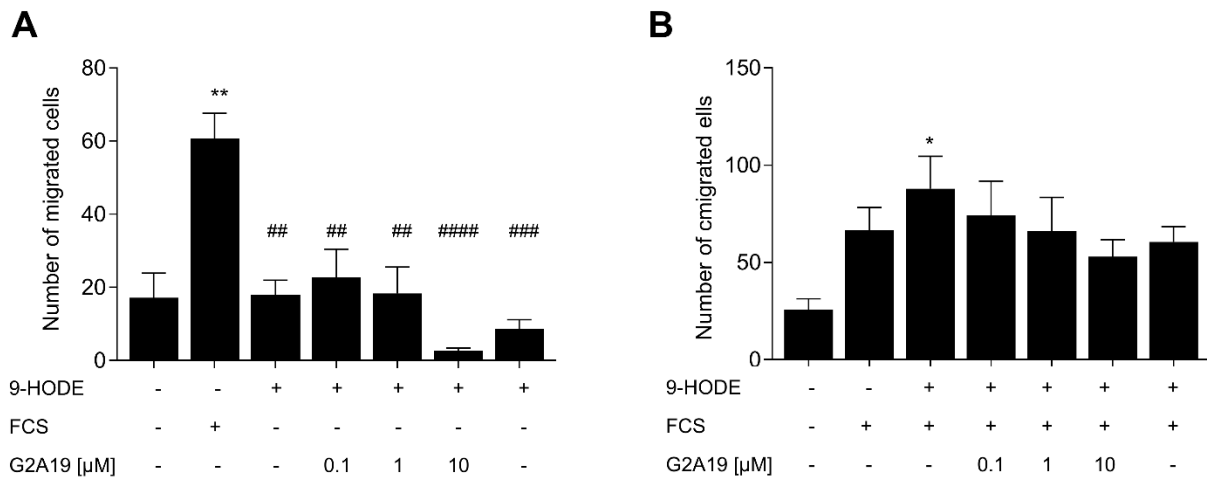


Figure 40. Inhibition of BMDMs migration through G2A19. Transwell BMDM migration through G2A19 in medium (A) without FCS and (B) with FCS in each solution used. Samples were measured in triplicates with n=4-5 independent measurements. For statistics a one-way ANOVA with Holm-sidak method was chosen. * $p < 0.05$, *** $p < 0.001$ (vs. without FCS), ## $p < 0.01$ ### $p < 0.001$, #### $p < 0.0001$ (vs. FCS).

In conclusion, G2A11 and G2A19 showed the most desensitizing effects on DRG neurons, but only weak effects on migratory behaviour of BMDMs. However, G2A11 showed the strongest inhibition on migration of macrophages even with FCS.

4. Discussion

4.1. Role of G2A in trauma induced neuropathies and subsequent neuroimmune interaction

So far, little effort has been devoted to clarifying the role of G2A in neuropathic pain conditions. There is only one report about G2A having a pronociceptive role in chemotherapy-induced neuropathic pain [85]. However, the inflammatory component does not play a major role in chemotherapy-induced neuropathic pain, but G2A is mainly expressed on immune cells [62]. Therefore, this work focused on the hypothesis of G2A modulating neurogenic inflammation and mechanical hypersensitivity in a neuropathic pain condition with a major inflammatory reaction, as for example after nerve injury.

Indeed, the results of this thesis indicate a reduction of the mechanical hypersensitivity after nerve injury in G2A-deficient mice. Similar results were observed in a previous study, where loss of G2A led to alleviated pain behavior in mice in oxaliplatin-induced neuropathic pain [85]. Thus, these results may be interpreted as an antinociceptive effect of loss of G2A in neuropathic pain, independent of the cause like nerve injury or chemotherapy. However, there is no research so far on G2A-deficiency in diabetes-induced neuropathic pain. Thus, additional research would be necessary to assess the question of G2A-deficiency in diabetes-induced neuropathic pain. Nevertheless, it is very doubtful whether a meaningful comparison can be made between oxaliplatin- and nerve injury induced neuropathic pain, since nerve injury induced neuropathic pain is characterized by a much stronger inflammatory component [48]. Drawing on earlier work of Su and colleagues, overexpression of G2A resulted in a slight antinociceptive effect during acute inflammatory pain, with increased G2A expression in DRGs for at least 90 min [107]. In contrast, in this thesis there was no increase in G2A expression in DRGs after nerve injury observed. This might be due to different time points. Thus, the peak of G2A expression might already have been at its highest and reached its baseline expression again, when it was analyzed in this work. In interpreting these findings, it has to be taken into account that Su and colleagues employed a chronic inflammatory mouse model with CFA and measured only mechanical hypersensitivity [107]. Nevertheless, in a zymosan-induced acute inflammatory model, loss of G2A seemed to reduce thermal hypersensitivity [100]. On this basis, it can be concluded that expression of G2A in DRGs and subsequent outcome of G2A-signaling depends on type of tissue and inflammation. Thus, in chronic inflammatory models G2A showed antinociceptive effects, whereas in acute inflammatory models G2A had pronociceptive effects, same as in the herein presented work after nerve injury [100, 107].

Therefore, considerably more work is necessary to fully understand the differences between acute, chronic and inflammatory models, with a strong neuronal component involved. Thus, a more detailed analysis would be needed concerning G2A loss and its effects on thermal hypersensitivity in a chronic inflammatory model with CFA, as well as after nerve injury induced neuropathic pain.

However, one has to keep in mind that chronic inflammations can be different according to the underlying causes [22, 207]. Neuroinflammation is a form of chronic inflammation and is accompanied by nerve injury. Thus, it is localized in particular in the peripheral but also in the central nervous system, mainly at the site of injury, where nociceptors and immune cells drive neuroinflammation through crosstalk of each other [7, 31, 34, 157, 208]. The findings of this thesis strongly support the central hypothesis of G2A modulating the neuroinflammation in nerve injury induced neuropathic pain. Following Cheng and Parks G2A is predominantly expressed in hematopoietic cells, especially macrophages [63, 65]. Upon nerve injury macrophages infiltrate the damaged tissue and T cells are getting activated, as several authors stated out [1, 9, 53, 209]. The infiltration of macrophages into damaged nerve tissue in wild-type was confirmed in this thesis. Although, loss of G2A reduced the number of immune cells, especially macrophages and neutrophils, which are known to be the first actors at an inflammatory site [95, 97]. However, in all examined tissues (SN, DRGs and spinal cord) less immune cells were found in G2A-deficient mice, indicating that G2A-deficient mice might exhibit a reduced number of immune cells in general. At this point, it is appropriate to raise the issue of the phenotype of G2A-deficiency. A previous report revealed no difference in the number of immune cells between wild-type and G2A-deficient mice unless the mice reached an age of 1 year. At this age G2A-deficient mice developed a lymphadenopathy and autoimmunity with lymphocytic infiltration and increased numbers of B- and T cells [67]. These observations suggest a pivotal role of G2A in immune cells and inflammatory processes. However, the researchers pointed out that G2A is not required for the development and immunological function of T and B lymphocytes. Nevertheless, only untreated wild-type and G2A-deficient mice were compared [67]. In contrast, in this thesis the number of immune cells after nerve injury was compared. On this basis, it seems as if G2A-deficiency affects the immune response in general after injury. However, reports on this issue are missing so far. Turning to a more recent report, a functional defect in competitive long-term engraftment with decreased numbers of functional long-term hematopoietic stem cells was observed [68]. Taken together, both studies and the herein presented data indicate a crucial role of G2A in regenerative processes during inflammation, regulation of lymphocyte growth factors and

homeostasis [67, 68]. Nonetheless, further experiments are required regarding the subject of immune cell numbers and regenerative processes in G2A-deficiency in various inflammatory models. The cause for the general reduced number of immune cells in SN, L4-L6 DRGs and spinal cord of G2A-deficient mice might be because of the tissue, since Le and colleagues examined the immune cell number in lymph nodes, spleens, bone marrow and thymus [67].

The reduced number of macrophages at the site of inflammation was reported in an earlier study, too, but only 24 h after zymosan injection into the paw, which is a common model for acute inflammation [100, 128, 210]. These findings could not be confirmed in this work 24 h after nerve injury. Interestingly, in a zymosan-induced peritoneal inflammatory model Parks and colleagues could observe an impaired clearance of apoptotic neutrophils through macrophages in G2A-deficient mice. But, they did not see any difference in the number of macrophages between wild-type and G2A-deficient mice, even in a bleomycin-induced lung inflammation [99]. These results differ considerably from the data Su and Frasch reported previously. Their findings implicate that knockdown or loss of G2A leads to an elevated number of macrophages or monocytes in chronic inflammatory mouse models [98, 107]. Furthermore, in a DSS-induced colitis model, the authors found a stronger inflammation in G2A-deficient mice. However, Frasch and colleagues did not differentiate between macrophages and monocytes, but observed less T cells [98]. These results are in good agreement with the presented data of this thesis regarding sciatic nerve after injury. In earlier studies researchers already reported the infiltration of T cells, which also express G2A, to the injured site contributing to long-lasting mechanical and thermal hypersensitivity [57, 90]. Together with the herein presented results, this contributes to the hypothesis that loss of G2A leads, next to a reduced number of macrophages, also to less T cells at the site of injury and subsequently reduced nociceptive behavior.

Nevertheless, the results of Frasch, Su and Parks may be interpreted as follows: G2A leads to an antiinflammatory effect, indicating that G2A deletion may lead to ongoing inflammation due to delayed resolution of inflammation, associated with chronic inflammatory disorders [98, 99, 107]. However, these results must be interpreted with caution, since Parks and colleagues only examined the bronchoalveolar lavage and not the tissue itself [99]. In contrast, in this thesis the number of immune cells in the tissue was examined, leading to the conclusion of G2A having proinflammatory effects. The proinflammatory effect might be not found in the study of Su and colleagues, because they silenced G2A only in DRGs, but not in macrophages or further immune or nonneuronal cells, expressing G2A [107]. Therefore, this thesis represents a more systematic approach for assessing the role of G2A during chronic

inflammation in macrophages and respective tissues. The results of this thesis suggest, that systemic loss of G2A leads to decreased numbers of macrophages and T cells at the site of injury, which might be the cause for the reduced mechanical hypersensitivity. The results further indicate a reduced number of macrophages in DRGs at the injured site of G2A-deficient mice. These results are in good agreement with a previous study, where the authors proposed a necessary expansion of macrophages in DRGs for the initiation of neuropathic pain [161]. Thus, a tentative conclusion at this point would be that G2A is an important player in macrophage and T cell recruitment in SN and DRGs leading to reduced mechanical hypersensitivity. However, G2A-signaling seems to depend on type of inflammation (chronic, acute, neuroinflammation) and the tissue of inflammation (lung, peritoneum, paw, nerve, DRGs, spinal cord). Moreover, the outcome of G2A-signaling also depends on whether G2A is silenced, indicating a residual activity of G2A, or whether there is a systemic loss of G2A [98, 107]. Nevertheless, considerably more work is necessary for complete understanding of the role of G2A during acute and chronic inflammation, as well as neuroinflammation. Interestingly, Frasch and colleagues reported after injection of an anti-CD45 antibody a strong reduction of monocyte numbers in wild-type mice with DSS-induced colitis, even in G2A-deficient mice [98]. Therefore, future research could examine the impact of an anti-CD45 antibody on the number of various immune cells after nerve injury.

This leads to the conclusion that loss of G2A seems to act on various levels, starting with its effects on mechanical hypersensitivity in different contexts and ending with a reduction of immune cell numbers at the site of injury, depending on the cause of inflammation (CFA, DSS, zymosan or nerve injury). Furthermore, the herein presented data indicate the strongest effect of inflammation at the site of injury, which decreases with distance, since at spinal cord nearly no effect was observed. Thereby, it seems as if the crosstalk between immune cells and primary sensory neurons are of importance after nerve injury. This will be discussed in more detail in the following section.

4.2. G2A in the crosstalk of immune cells and primary sensory neurons during acute phase of trauma induced neuropathies

One of the central hypotheses of this work was that G2A modulates the neuroinflammation due to its main expression on immune cells [62]. As the presented data here clearly show, G2A appears to influence the inflammation at the site of injury and by this affects the outcome of nociceptive behavior. This suggests a crosstalk between primary sensory neurons and immune cells at the site of nerve injury.

The reduced number of immune cells, especially at the site of injured nerve and to a lesser extent in DRGs resulted also in decreased amounts of inflammatory mediators such as TNF α , IL-6, VEGF and IL-12 in G2A-deficient mice. Further inflammatory mediators, such as 9- and 13-HODE, oxidized metabolites of linoleic acid, were increased only at the injured nerve in wild-type mice. Similar results were presented in earlier studies, where 9-HODE was increased in NGF- or *Propionibacterium acnes* induced inflammation and chemotherapy-induced neuropathic pain [85, 86, 116]. However, as Kern and colleagues discovered, 9-HODE was not increased at the site of inflammation 24 h after zymosan-injection [100]. Unfortunately, this data has its limitations, since it is not quite clear, where exactly 9-HODE is produced. There is a large amount of research showing that HODEs are produced by various cells and tissues [115, 211–213]. However, the herein presented data confirms, that neurons and macrophages are able to produce 9-HODE [211, 214]. Since 9-HODE is known to lead to macrophage migration, the data suggests that 9-HODE is mainly secreted by neural tissue upon injury or damage [100]. Nevertheless, future research should attempt to clarify what tissue or cells are responsible for 9-HODE production and by this contribute to the crosstalk between primary sensory neurons and immune cells in the context of nerve injury induced neuropathic pain. Next to this, 9-HODE production by enzymes is not fully understood, too. Thus, previous research suggested glutathione-peroxidase, lipoxygenases or non-enzymatically production of 9-HODE. These studies have been also declared a different synthesis of 13-HODE, which seems to be produced by 15-LOX [211, 215–218]. In this thesis, the data indicates that 9-HODE is produced differently as 13-HODE, in fact mainly by COX-2 and 12-LOX [133, 135]. This is in good agreement with earlier findings, hypothesizing a COX involvement and products of 12-LOX involved in TRPV1 sensitization [219, 220]. Thus, the elevated 9-HODE levels might be connected to mechanical hypersensitivity, since it binds to its receptor G2A and by this

sensitizes TRPV1 in primary sensory neurons, which is known to be responsible for pain perception [85, 180, 221].

In fact, the expression of G2A was found to be induced during cellular stress, like DNA damage or chemotherapy [62, 85, 115, 180]. Another kind of stress is nerve injury, leading to upregulation of enzymes and transcription factors like ATF3 in neurons [177, 222]. The observed amounts of ATF3 from previous reports were equally high to the herein presented data [161, 222]. However, the results of the mRNA expression analysis or the proteome screen indicate an altered expression of ATF3 expressed in G2A-deficient animals after SNI. Interestingly, there are no reports about the expression levels of ATF3 in G2A-deficient animals. Therefore, future research should address this topic. Further oxidative enzymes such as iNOS, Nox-2, Nox-4 and Xdh were demonstrated, by a number of authors, to play a role in initiation and maintenance of neuropathic pain [142, 223–226]. The data of this thesis did not show any difference on mRNA level between wild-type and G2A-deficient mice in DRGs. However, the protein activity might be different due to posttranslational modifications or the differences might occur at a different time point. For example, in Nox-4-deficient mice nociceptive behavior was attenuated after SNI or chronic constriction injury (CCI), but only at a later time point. In this report it was suggested, that H₂O₂-production through Nox-4 leads to SNI-induced demyelination [142]. Additionally, de Alba *et al.* reported that iNOS was only locally detected at the nerve after CCI [226]. Thus, future research should attempt to clarify the levels of iNOS and Nox-4 at later time points and the demyelination in wild-type and G2A-deficient mice at the site of nerve injury. The overall impression strongly supports the view of further mechanisms involved in pain initiation and maintenance after nerve injury in G2A-deficient animals, independent of ROS or ATF3 regulation.

As indicated above, 9-HODE leads to migration of macrophages through binding to G2A, which was upregulated in BMDMs after 9-HODE stimulation [100]. Thus, in G2A-deficient mice, less macrophages were found at the site of the injured nerve. Not surprisingly, the findings of this thesis support the view of reduced inflammation at the site of injury in G2A-deficient mice. Previous research has demonstrated that especially IL-1 β , IL-17, IL-6 and TNF α are increased during neuropathic pain, in animals and patients [59, 113, 161, 227–229]. As Yu and colleagues concluded, DRG macrophages are the main source of IL-1 β . However, the researchers only examined mRNA expression in DRGs and only 1 day after SNI surgery [161]. The data of this thesis reflects the protein amounts of IL-1 β at the site of nerve injury 7 days after SNI, which showed no difference between the genotypes. In recent studies it was demonstrated that IL-1 β amounts increased through actions of IL-17 and TNF α [230, 231]. In

G2A-deficient animals less IL-17 and less TNF α was found at the injured nerve indicating reduced IL-1 β levels, what could not be confirmed by this thesis. However, the experiments of the cited studies have their limitations, since only osteoblast and fibroblast cell lines were used and the experiments were conducted for 24 h [230, 231]. However, Park and colleagues observed similar results regarding IL-1 β secretion when G2A was silenced in THP-1 cells and after 9-HODE stimulation. On gene level they found also increased IL-1 β , either after inflammation or 9-HODE stimulation. Here, again the stimulation period was 24 h and only in the immortalized leukocyte cell line THP-1 [86]. Therefore, these reports have failed to address a physiological context regarding the effects of IL-17 and TNF α on IL-1 β levels, for example in nerve tissue after nerve injury. So far, few studies have investigated this issue of cytokine levels after SNI in mice. However, del Rey *et al.* reported increased IL-1 β levels in hippocampus, at day 10 and 24 after SNI in rats. Interestingly, the researchers observed an undeniably difference between the type of nerve injury, namely CCI or SNI, and the genotype of the rats. Thus, IL-1 receptor and IL-6 expression were highly diverse in Sprague Dawley and Wistar Kyoto rats [228]. Further studies have only examined different time points, like 24 h or 14 days [232, 233]. Only Ruohonen and colleagues reported IL-1 β levels to be increased at the injured site of nerve, but on day 14 and depending on the proximal or distal and epineurium and endoneurium part of the nerve. On day 7 after transection of the nerve no increase of IL-1 β levels were observed in wild-type rats [233]. Thus, IL-1 β levels seem to fluctuate during nerve injury induced neuropathic pain and may vary considerably depending on the investigated time point. Therefore, more work is required to understand the expression fluctuations of IL-1 β regarding the different tissues affected by nerve injury during the first 7 days in wild-type and G2A-deficient mice.

Interestingly, it was demonstrated that knockout of IL-17 reduces mechanical allodynia after nerve injury and that IL-17 induces COX-2 [231, 234]. These results indicate that the herein observed reduced IL-17 levels in G2A-deficient mice might lead to reduced COX-2 induction, which might result in reduced 9-HODE production and subsequently reduced inflammation. The reduced 9-HODE production was also observed in this thesis in G2A-deficient mice at the injured nerve.

More importantly, the proinflammatory cytokines IL-6 and TNF α play crucial roles during neuropathic pain [41, 55, 235–237]. The levels of these cytokines showed remarkably strong decreases in sciatic nerve after SNI in G2A-deficient animals in this thesis. Guerrero and colleagues identified TNF α as contributor to shift macrophages into proinflammatory M1 phenotype, suggesting that low amounts of TNF α prevent proinflammatory macrophage

phenotype [238]. This observation was recently confirmed, when a reduced amount of proinflammatory monocyte-derived macrophages were observed in acute inflammation in G2A-deficient mice [100]. This might explain the observations regarding the reduced amount of proinflammatory cytokines at the site of injury in G2A-deficient mice in this thesis. Another possible explanation could be that the herein observed TNF α amounts in wild-type mice potentiates the actions of IL-17 resulting in IL-6 secretion [227, 230, 231]. Thus, this leads to the conclusion that the herein observed reduced amounts of IL-17 and TNF α in injured nerve of G2A-deficient mice cause an undeniably stronger reduction in IL-6 in G2A-deficient mice than TNF α alone. These results are in good agreement with earlier findings, where silencing of G2A resulted in decreased IL-6, IL-12 and TNF α levels in monocytes stimulated with lysoPC [84, 96]. TNF α is also produced by Th₁ cells, which then activate macrophages. Thus, infiltration of T cells to the injured nerve leads to increased amounts of TNF α , and by this to increased macrophage activation and IL-6 production [57]. Additionally, several authors have reported that proinflammatory cytokines such as IL-6 and TNF α participate in the pathogenesis of neuropathic pain by direct nociceptive effects on sensory neurons [27, 31, 41, 55, 59, 184, 236]. However, increased amounts of TNF α , IL-6 and IL-12 were observed in G2A-deficient macrophages in an atherosclerosis model [73]. Despite that, the study was performed in double knockout mice of G2A and ApoE, indicating a compensatory effect of these two receptors [73]. As already pointed out, these different observations may be explained by pleiotropic effects of G2A depending on the cause of inflammation and tissue, the state of inflammation (acute versus chronic) and the related immune cell types and secreted mediators [96, 100].

Next to this, in DRGs the cytokine IL-12 was decreased in G2A-deficient mice. IL-12 promotes inflammation, the development of chronic inflammatory diseases like multiple sclerosis and induces iNOS expression [239–241]. Major producers are dendritic cells and macrophages, which secrete IL-12 leading to Th₁ differentiation [239]. Consequently, reduced IL-12 levels lead to reduced numbers of Th₁ cells, which produce less TNF α and subsequent minimize IL-6 secretion. Thus, the low amounts of cytokines result in reduced sensitization of primary sensory neurons and subsequent reduced mechanical hypersensitivity. This fits with the herein presented data: Less immune cells lead to less cytokine secretion and subsequent differentiation, activation or migration of further immune cells. The reduced concentrations of cytokines activate TPRV1 then to a lesser extent, resulting in reduced pain sensitization.

The reduced levels of TNF α in G2A-deficient mice may have further advantages: TNF α and IL-17 are potent regulators of MMP9 expression, resulting in reduced macrophage migration

[234, 242]. MMP9 belongs to the family of endopeptidases and is known for its critical role in neuropathic pain and inflammation [178, 243]. A number of studies have suggested that MMP9 signaling mechanisms lead to either macrophage migration or the opposite, macrophage migration inhibition [195–197]. In these studies the amount of MMP9 itself was not examined in macrophages. However, in this thesis the MMP9 amount in BMDMs was determined. There is a large amount of research that observed increased MMP9 amounts in DRG neurons, microglia, spinal cord and spinal nerve after nerve injury [243, 244]. Although, in this thesis in DRGs no difference was seen between G2A-deficient and wild-type mice in MMP9 mRNA expression. This does not exclude a high amount of MMP9 protein levels in DRGs after SNI.

Interestingly, MMP9 is able to cleave pro-IL-1 β leading to release of IL-1 β [178, 243]. Since the amount of IL-1 β was not altered in both genotypes in this thesis, the results indicate, that the MMP9-IL-1 β pathway might not be involved in migration of macrophages. However, the herein presented data showed a decrease of MMP9 amounts in BMDMs after G2A activation. A possible explanation for this might be that neurons secrete MMP9 to recruit macrophages and T cells to the site of injury, leading on the contrary to low amounts of MMP9 in BMDMs [178, 197, 243, 245]. A number of researchers have conducted MMP9 overexpression or knockout studies indicating an enhanced cell migration through MMP9 [192–194]. Nevertheless, the relationship between MMP9 and enhanced cell migration appears somehow misguided. The researchers worked with MMP9 overexpressing or MMP9 knockout cells and did not differentiate between MMP9 levels within the migrating cells, the extracellular matrix or non-migrating cells [192–194]. Meaning, the expression of MMP9 in for example neurons might lead to cell migration of immune cells, which do not express or secrete MMP9. Thus, further MMP9-independent mechanisms might be responsible for the migration of macrophages after treatment with 9-HODE. However, according to Cheng and colleagues already in untreated G2A-deficient bone marrow or spleen macrophages, MMP9 levels were decreased compared to wild-type mice [65]. Thus, stimulation with its agonist 9-HODE might result in G2A internalization and by this less G2A signaling leading to reduced MMP9 levels. Therefore, it is desirable to find the mechanisms behind the migration of macrophages due to 9-HODE stimulation. In fact, MMP9 expression seems to correlate with ERK downregulation [246]. Such a correlation was not observed in this thesis, either in Western Blots or in the proteome screen. However, in spinal dorsal horn there was reported to be an upregulation of p38 and ERK after peripheral nerve injury [61]. This indicates, that ERK and p38 signaling might be more crucial on CNS level than in macrophages after peripheral nerve injury.

Discussion

Despite all that, the proteome analysis revealed upregulation of several migratory and inflammatory proteins after 9-HODE stimulation like PTK7, Tgln and MyD88 [247, 248]. PTK7 was reported to be a co-receptor of Wnt and can activate non-canonical Wnt signaling. This leads to changed cell polarity and by this to cell migration, which might point towards an involvement of Wnt signaling upon G2A activation [249, 250]. Interestingly, it was also reported that Wnt signaling is involved in the pathogenesis of neuropathic pain after CCI and leads to increased TNF α levels. However, the study only examined DRG and spinal cord tissue, suggesting that same pathways could be activated in macrophages after nerve injury [164]. Thus, the herein presented data suggests an intensified Wnt signaling caused by PTK7 upregulation could enhance TNF α release, resulting in elevated inflammation at the site of injury in wild-type mice. Additionally, Tgln is also known to induce migration and results in increased IL-6 as well as TNF α expression [251–253]. The increased expression fits to the herein presented data, since reduced expression of IL-6 and TNF α were observed in G2A-deficient animals, as well as a reduced number of immune cells. Unfortunately, the proteome data could not be confirmed with western blots, what might be due to insufficient antibodies or due to regulations beyond western blot analysis like repression. Interestingly, Tgln and MyD88 were reported to act upstream of ERK and PI3K [253, 254]. In contrast, no difference was seen in ERK and PI3K 24 h after 9-HODE stimulation, indicating that future research should explore earlier or later time points to evaluate the levels of ERK and PI3K after 9-HODE stimulation.

Thus, migration of macrophages seems to be influenced by an increase of PTK7, MyD88, PI3K and Tgln on the one hand and a decrease of MMP9 on the other hand. A possible explanation might be an activation of TLR4 signaling through G2A activity, since PTK7, MyD88, PI3K, MMP9 and Tgln are all downstream effectors of TLR4 [185–187, 255]. This is in good agreement with the herein presented data regarding the MMP9 secretion of BMDMs after G2A activation during the first hours. Nevertheless, a more sophisticated approach is needed to fully understand and confirm the relationships among all components and their involvement in migration after SNI. Further proteins involved in migration, like Rho and Rac were reported to be activated upon G2A expression, leading to stress fiber formation [101, 256–259]. Those results could not be confirmed in this thesis. However, Frasch and colleagues used lyso-PS for their experiments, indicating that 9-HODE might lead to different downstream signaling of G2A than lyso-PS [259]. So, the data unambiguously indicate that classical known signaling pathways involved in migration such as ERK, p38, Rac and ROCK are not activated by the G2A-9-HODE signaling pathway 24 h after stimulation. In fact, pathways involving PTK7 and Wnt signaling, as well as TLR4 signaling pathways could have a stronger influence on

migration and inflammation through G2A activation by 9-HODE. Earlier reports already showed for Wnt signaling to be an important player in the pathogenesis of neuropathic and cancer pain [260, 261].

To recap the discussed points, the data of this thesis suggests the following crosstalk between primary sensory neurons and macrophages: Upon injury COX-2 and 12-/15-LOX produce 9-HODE. This factor then leads to macrophage migration through binding to its receptor G2A [101, 262] (Fig. 41). The activation of G2A seems to result in TLR4 signaling leading to upregulation of Tgln, MyD88, PTK7 and MMP9 (Fig. 41). Especially Tgln, MyD88 and PTK7 are known to be involved in migration through signaling pathways such as PI3K/Akt and Wnt [253, 254, 263]. Additionally, elevated levels of IL-17 lead to activation of COX resulting in additional 9-HODE production indicating a positive feedback loop of G2A activation [259]. Next to this, IL-17 and Wnt signaling increase TNF α release and TNF α together with IL-17 are responsible for increased IL-6 secretion. TNF α and IL-6 both are able to sensitize TRPV1 by binding directly to the channel or to GPCRs [27, 31, 184]. Furthermore, the injury leads to IL-12 production in DRGs, what induces T cells to differentiate into Th₁ cells, responsible for more TNF α release at the site of injury (Fig. 41).

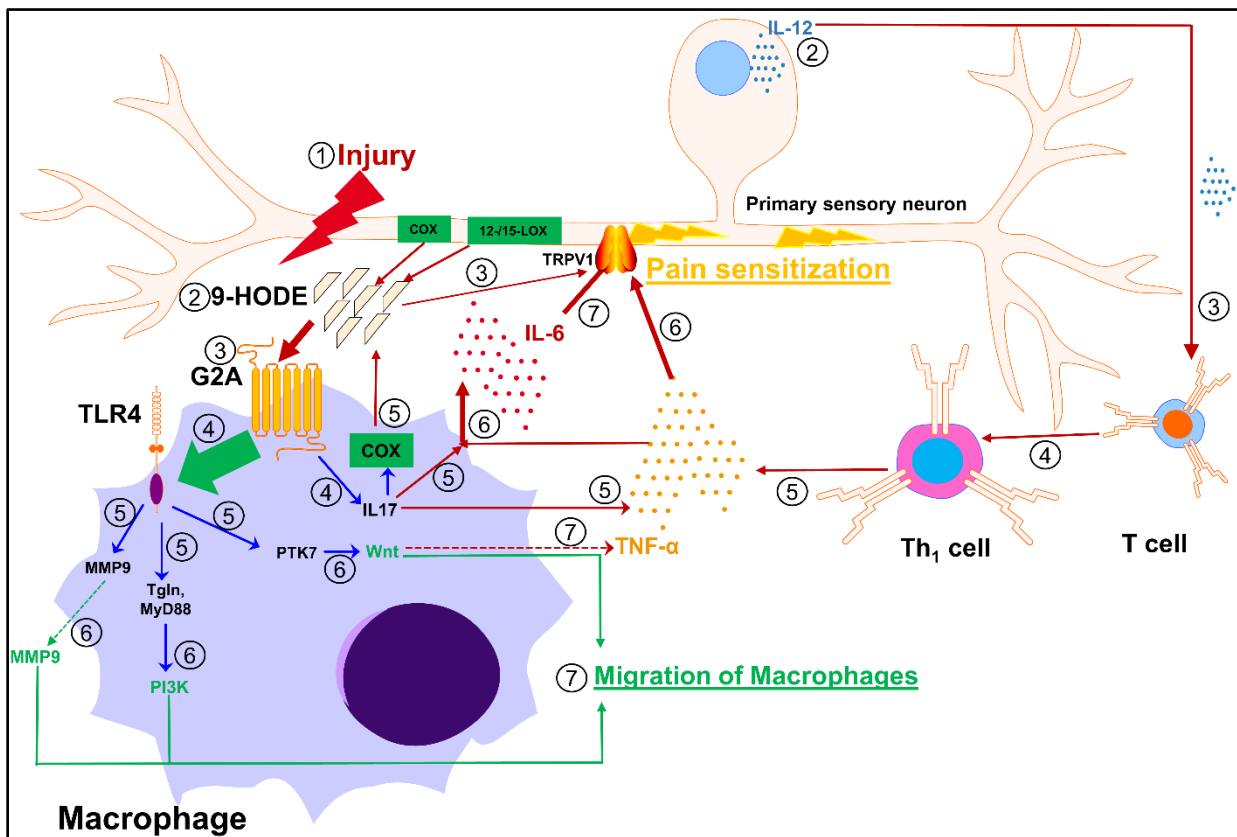


Figure 41. Overview of suggested crosstalk between injured sensory neuron and immune cells and the involvement of G2A. The scheme depicts the different signaling pathways activated through crosstalk between nerve and macrophages after nerve injury (1), leading to increased 9-HODE levels (2), which binds to G2A and sensitizes TRPV1 (3). Activation of G2A might lead to activation of TLR4 signaling (4) leading to MMP9, TgIn, MyD88 and PTK7 (5) expression and to macrophage migration (6, 7). Additionally, G2A activation leads to increase of IL17 (4) resulting in COX-2 producing 9-HODE (5). IL17 causes an increase of TNF α (5) and together with TNF α an increase of IL-6 (6) leading to TRPV1 sensitization (6, 7). The production of IL-12 in DRGs can stimulate (3) T cells to differentiate into Th₁ cells (4), which secrete TNF α (5).

4.3. G2A: A target for the treatment of neuropathic pain?

Neuropathic pain arises from a large amount of different mechanisms. Not surprisingly, it is very difficult to treat neuropathic pain, which is reflected by unsatisfactory pain relief, no response to drugs, a large amount of side effects or pharmacokinetic interactions [38, 40, 47, 58, 117]. Dealing with neuropathic pain results in a major health burden due to increased drug prescriptions and visits to health care providers [27, 38]. Therefore, novel approaches in the treatment of neuropathic pain are needed. Thus, one hypothesis of this thesis was that G2A, with its effects on TRPV1 sensitization and expression on immune cells, is a promising target for the treatment of neuropathic pain. At this point it is important to consider the role of TRPV1 during pain. TRP channels mainly respond to chemical mediators as well as to intense mechanical and thermal stimuli [9]. Thereby, TRPV1 is a main player in development of pain after thermal stimuli and its activation threshold is reduced by inflammatory mediators [4, 8, 36]. Therefore, in a first attempt TRPV1 was targeted in the context of neuropathic pain treatment. Inhibition or silencing of TRPV1 showed promising first results in mice, however, in humans and rats the inhibition resulted in hyperthermia [9, 35, 60]. Since TRPV1 plays a crucial role in detection of noxious heat stimuli, it is desired only to inhibit the TRPV1 sensitization and not its general function in noxious heat responsiveness and thermal regulation [34, 35, 60, 264]. IL-6 and TNF α are able to sensitize TRPV1 [27, 31, 184]. Thus, antibodies against the two cytokines were studied in clinical trials, where they showed unconvincing and contradictory effects [59, 227]. Further treatment approaches include cell therapy and gene therapy, which both have its limitations: Low efficacy, non approval, risk of tumor formation, immune reactions and the delivery way, which is either a brain surgery or a direct injection at the site of injury [265, 266]. Beyond any doubt, targeting TRPV1 is one of the best attempts concerning the treatment of neuropathic pain. However, direct inhibition is not possible, due to its physiological role as detector and regulator of human body temperature [60]. Therefore, indirect targeting of TRPV1 through GPCRs seem to be a promising approach. Already 30 % of drugs target GPCRs and there is a large amount of reports about GPCRs activation modifying the TRP channel signaling [7, 13, 14, 31, 48]. The GPCR G2A was shown to sensitize TRPV1 channel [85]. Thus, together with the herein presented data G2A seems to be a promising target in treatment of neuropathic pain. As figure 42 summarizes loss of G2A results in a reduced inflammatory reaction, including less immune cells and inflammatory mediators at the site of injury leading to attenuated mechanical hypersensitivity. Therefore, it was a declared aim of this thesis to test screened substances for their effects on TRPV1-mediated Ca²⁺ influx in neurons and migration of macrophages.

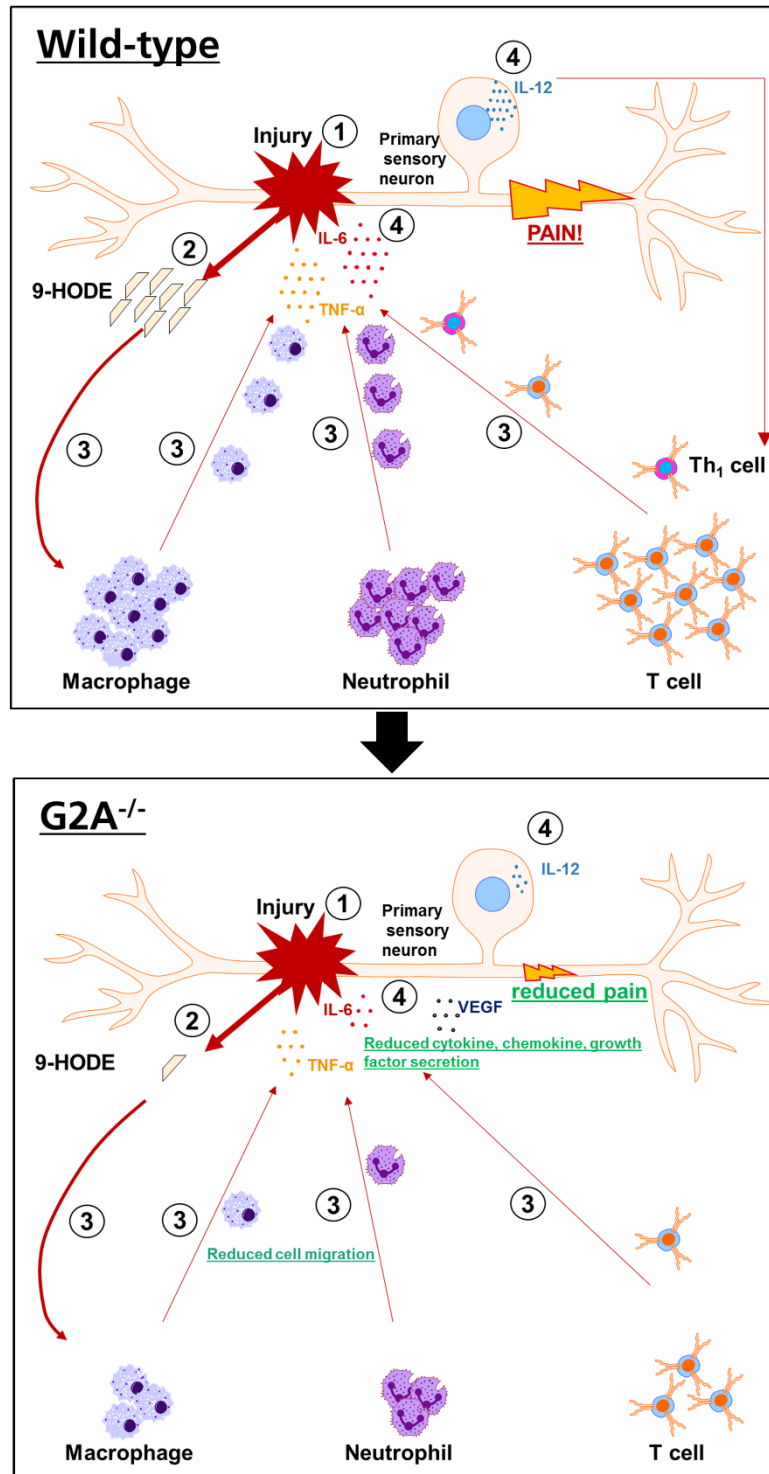


Figure 42. Overview of systemic actions through loss of G2A in neuropathic pain. After injury (1) of the nerve, 9-HODE is released (2) and immune cells (3) are recruited to the site of injury, where they secrete inflammatory cytokines (4) leading to pain sensitization in wild-type animals (upper image). In G2A-deficient animals (lower image), all the actions and the mechanical hypersensitivity are reduced.

Discussion

The results showed for three of the substances (G2A11, G2A13, G2A19) strong inhibiting effects on TRPV1-mediated Ca^{2+} influx. G2A11 and G2A19 showed a slight decrease on migration of macrophages, indicating a two-sided effect of them. On the one hand, they inhibited TRPV1-mediated Ca^{2+} influx into the neurons, on the other hand they inhibited migration of macrophages.

Drawing on earlier work, there was an antagonist of G2A already published, GSK1820795A, which is a telmisartan analogue [81]. Although, Foster and colleagues demonstrated the antagonizing effects only in a yeast expressing and β -arrestin coupled system [81]. The antagonist screening in this thesis was performed with CHO cells and with an IP-One accumulation assay. Thus, the reported antagonizing effects of GSK1820795A should be used also in the IP-One accumulation assay for comparability of the results of this thesis and the study of Foster *et al.* [81]. Furthermore, the results of Foster and colleagues should be used for future Ca-imaging experiments in neuronal cultures, to see whether it has the desired inhibiting effect on TRPV1-mediated Ca^{2+} influx in neurons as does the herein presented antagonists. Still, the herein presented data and the study of Fosters group on antagonists of G2A are preliminary, but promising [81]. Considerably more work is necessary to confirm this preliminary data *in vivo*. It would be of interest to see the possible effects of G2A inhibitors on chronic inflammations in the context of colitis or other inflammatory models, as well as cancer concerning the metastasis and outcome of breast cancer. In earlier studies on this issue, G2A seemed to have a contrary effect than in neuroinflammation [98, 107]. Drawing on these studies, it is also important to evaluate possible intestinal or cardiovascular side effects of G2A antagonism [98, 103]. Therefore, future research should concentrate, first of all, on modifying the substances to get stronger effects, especially regarding the migration of macrophages. Additionally, it is required to evaluate the substances after SNI *in vivo*, and to examine whether any side effects can already be observed in mice.

I. Zusammenfassung

Die vorliegende Arbeit hat sich mit der Fragestellung beschäftigt, welche Rolle der G-Protein gekoppelte Rezeptor G2A während neuropathischer Schmerzen nach peripheren Nervenverletzungen spielt. Auch sollten Signalwege, die durch Aktivierung des G2A-Rezeptors in Gang gesetzt werden, untersucht werden. Um diese Fragen zu beantworten, wurden in einem ersten Experiment G2A-defiziente Mäuse und Wildtyp-Mäuse auf ihre mechanische Hypersensitivität untersucht. Dazu wurden die Tiere einer sogenannten „spared-nerve injury“ (SNI) unterzogen, bei der nur auf der linken Pfote zwei der Äste des Ischiasnervs zunächst abgeschnürt und schließlich durchtrennt wurden. Anschließend wurde die mechanische Schmerzschwelle in einem dynamischen Aesthesiometer in einem Verlauf über sieben Tage gemessen. Die Ergebnisse zeigten, dass die G2A-defizienten Tiere bereits ab Tag 2 eine verringerte mechanische Hypersensitivität aufwiesen als die Wildtyp-Tiere. Es lässt sich daraus schließen, dass der Verlust des G2A-Rezeptors zu einer verringerten mechanischen Hypersensitivität nach einer Nervenverletzung führt.

Aufgrund dieser ersten Ergebnisse stellte sich die Frage, welche Ursache zu der geringeren mechanischen Hypersensitivität führen könnte. Ein charakteristisches Merkmal von neuropathischen Schmerzen nach einer Nervenverletzung ist eine starke Entzündungsreaktion und Immunzelleinwanderung am verletzten Nerv. Außerdem wird G2A vorwiegend in Immunzellen, insbesondere Makrophagen und T Zellen exprimiert. Das hat die Frage naheliegend gemacht, ob G2A einen Einfluss auf die Entzündungsreaktion hat. Daher wurden für die weitergehenden Analysen die Gewebe des Schmerzübertragungsweges, Ischiasnerv, lumbale Dorsalwurzelganglien L4-L6 und Rückenmark, sieben Tage nach SNI von der behandelten, als auch der unbehandelten Seite der Mäuse entnommen. Bei anschließenden FACS Messungen zeigte sich, dass grundsätzlich weniger Immunzellen sowohl in der behandelten als auch der unbehandelten Seite des Ischiasnervs in G2A-defizienten Mäusen zu finden waren. Bei genauerer Betrachtung der einzelnen Immunzelltypen war zu erkennen, dass vor allem die Zahl der Makrophagen und der neutrophilen Granulozyten eine starke Reduktion in dem behandelten Ischiasnerv von G2A-defizienten Mäusen zeigten. Die Ergebnisse zu der verringerten Zahl an Makrophagen im verletzten Nerv konnten durch immunhistologische Färbungen bestätigt werden. In den Dorsalwurzelganglien zeigte sich ein ähnliches Bild sieben Tage nach SNI. Die generelle Anzahl der Immunzellen war sowohl in der behandelten als auch der unbehandelten Seite stark verringert in G2A-defizienten Mäusen. Bei genauerer Betrachtung zeigte sich aber, dass

nur die Zahl der Makrophagen signifikant geringer auf der behandelten Seite von G2A-defizienten Mäusen war. Im Rückenmark war nur eine geringere Immunzellzahl in G2A-defizienten Mäusen zu beobachten sowohl auf der unbehandelten als auch der behandelten Seite. Die Reaktion von Astrozyten im Rückenmark auf die periphere Nervenverletzung wurde ebenfalls mit immunhistologischen Färbungen untersucht. Dabei zeigte sich keinerlei Unterschied der Astrozytenaktivierung zwischen G2A-defizienten und Wildtyp-Tieren.

Die geringere Zahl an neutrophilen Granulozyten und Makrophagen auf der behandelten Seite von G2A-defizienten Mäusen hat zu der Annahme geführt, dass dadurch auch die Konzentrationen an entzündlichen Mediatoren am verletzten Nerven beeinträchtigt sein könnten. Daher wurden die Konzentrationen von Entzündungsmediatoren, wie Zytokinen, Chemokinen und Wachstumsfaktoren in einem großen Ansatz mit Hilfe von ELISA und Luminex Multiplex-Messungen in neuronalen Geweben sieben Tage nach SNI-Behandlung untersucht. Die entzündlichen Zytokine Tumor Nekrose Faktor α (TNF α), Interleukin 6 (IL-6), sowie der vaskuläre endotheliale Wachstumsfaktor (VEGF) zeigten signifikant erniedrigte Konzentrationen am verletzten Nerven in G2A-defizienten Tieren sieben Tage nach SNI. In Dorsalwurzelganglien war nur für IL-12 eine starke Konzentrationsverringerung in G2A-defizienten Tieren zu beobachten. Interessanterweise war die G2A-Expression in Dorsalwurzelganglien unverändert in Wildtyp-Tieren im Vergleich zu unbehandelten Tieren. Ebenfalls interessant war, die mRNA Expression von bekannten Stressmarkern bei traumainduzierten neuropathischen Schmerzen zu untersuchen. Auch waren keine Veränderungen in der mRNA Expression der bekannten Stressmarker aktivierender Transkriptionsfaktor 3 (ATF3), induzierbare Isoform der Stickstoffmonoxidsynthase (iNos), NADPH Oxidase 2 (Nox-2), Nox-4, transformierender Wachstumsfaktor (TGF β) und Matrixmetalloproteinase 9 (MMP9) zu beobachten.

Da im Verhaltensversuch bereits einen Tag nach SNI eine erhöhte mechanische Hypersensitivität sowohl von G2A-defizienten als auch Wildtyp-Tieren zu beobachten war, wurde auch nach Tag 1 die Immunzellzahl analysiert. Hier zeigte sich kein Unterschied zwischen den Immunzellen insgesamt und den einzelnen Immunzelltypen im Nerven, den Dorsalwurzelganglien und im Rückenmark. Neben den typischen entzündlichen Mediatoren wie Zytokinen und Chemokinen, gehören auch Lipide und deren Metabolite zu entzündlichen Mediatoren. Aus diesem Grund wurden auch die Konzentrationen der Linolsäuremetabolite 9- und 13-Hydroxyoctadecadiensäure (9-/13-HODE) sowie 9,10-, 11,12-Epoxyoctadecaensäure (EpOME) und 9,10-, 11,12-Dihydroxyoctadecaensäure (DiHOME) mittels LC-MS/MS gemessen. Die Ergebnisse zeigten einen starken Konzentrationsanstieg von 9- und 13-HODE

im verletzten Ischiasnerv in Wildtyp-Mäusen, während in Dorsalwurzelganglien und im Rückenmark kein Unterschied zu sehen war. In G2A-defizienten Mäusen war in keinem der Gewebe ein Unterschied zwischen behandelter und unbehandelter Seite zu sehen. Auch hielten sich die Konzentrationen der Metabolite in G2A-defizienten Mäusen auf einem basalen Level von unbehandelten Wildtyp Tieren.

Da 9-HODE ein bekannter Agonist von G2A ist, wurde zunächst die Produktion von 9-HODE untersucht. Es ist zwar bisher nicht vollständig geklärt, ob die erhöhte Sekretion von 9-HODE am verletzten Nerv vom Nerv oder den Immunzellen kommt, allerdings konnte in dieser Arbeit die Produktion von 9-HODE in Makrophagen gezeigt und untersucht werden. Hierzu wurden die differenzierten Knochenmarksmakrophagen mit Inhibitoren spezifisch für 5-, 12- und 15-Lipoxygenase (LOX), Cyclooxygenase 1 (COX) und Cytochrom P450 (CYP) behandelt. Anschließend wurden die Zellen mit Linolsäure und Lipopolysaccharid stimuliert. Die Überstände der Zellen und die Zellpellets wurden mit LC-MS/MS auf die Menge an 9-HODE untersucht. Die Ergebnisse zeigen, dass 9-HODE vorwiegend durch 12-LOX und COX-1 produziert wird. Bei den weiteren Linolsäuremetaboliten war eine starke Erhöhung von 11,12-EpOME in der behandelten Seite des Ischiasnerv in Wildtyp Mäusen zu erkennen. In den Dorsalwurzelganglia waren 9,10- und 12,13-DiHOME in der behandelten Seite der Wildtyp Mäuse zu erkennen. In den G2A-defizienten Tieren zeigte sich nur 12,13-DiHOME mit einer geringeren Konzentration in der behandelten Nervseite verändert. Diese Ergebnisse lassen darauf schließen, dass der Verlust des G2A-Rezeptors zu einer verminderten Entzündungsreaktion, vor allem am verletzten Nerv führt. Das heißt, zum einen befinden sich weniger Immunzellen, insbesondere Makrophagen und neutrophile Granulozyten am verletzten Nerv in G2A-defizienten Mäusen. Zum anderen werden weniger entzündliche Mediatoren produziert, wie 9- und 13-HODE, TNF α , IL-6 und VEGF.

Aus diesen Ergebnissen geht allerdings noch nicht hervor, wie die G2A-Aktivierung mit der Zytokin- und Wachstumsfaktorauslösung zusammenhängt. Daher ging es im dritten Teil dieser Arbeit um die Analyse der Signalwege, die durch G2A in Makrophagen aktiviert werden. Daher wurden differenzierte Knochenmarksmakrophagen von Wildtyp und G2A-defizienten Mäusen 24 Stunden lang mit 1 μ M 9-HODE stimuliert. Nach Ernte der Makrophagen wurde ein Proteom-Screen in Kooperation mit der Arbeitsgruppe von Dr. Münch des Instituts für Biochemie II der Goethe Universität durchgeführt. Die Resultate zeigen, dass Proteine die das Immunsystem, die Apoptose und den Lipidstoffwechsel betreffen in Wildtyp-Makrophagen 24 Stunden nach Stimulation herunterreguliert sind. Besonders stark herunterreguliert sind dabei Integrin α -IIb Vorläufer (Itga2b), Matrixmetalloproteinase 9 (MMP9) und Chemokin-ähnlicher

Rezeptor 1 (CMKLR1), die allesamt an der Immunzellmigration beteiligt sind. Weitere Proteine betreffend die Migration und der Entzündung sind dagegen stark hochreguliert. Hierzu zählen das Protein der Primärreaktion der myeloischen Differenzierung 88 (Myd88), Transgelin (Tgln), Proteintyrosinkinase 7 (PTK7), B-Zelllymphom-ähnliche 1 (Bcl2l1), Proteinkinase C η (Prkch) und Vesikel assoziiertes Membranprotein 3 (Vamp3).

Wie durch ein weiteres Stimulationsexperiment gezeigt werden konnte, sekretieren Knochenmarksmakrophagen nach 9-HODE-Stimulation in den ersten 10 Stunden vermehrt Matrixmetalloproteinase 9 (MMP9), deren Menge in den Lysaten der Makrophagen nach 24 Stunden signifikant reduziert ist. Die in Wildtyp-Makrophagen durch G2A-Aktivierung stark hochregulierten Proteine Myd88, Tgln, PTK7, aber auch MMP9 werden allesamt durch den „Toll-like receptor 4“ (TLR4) reguliert. Interessanterweise zeigte sich im Proteomscreen, dass bereits ohne Stimulation in Wildtyp Makrophagen Proteine, die in die Migration involviert sind, stark hochreguliert sind. Die Migration wird dagegen weniger stark reguliert in G2A-defizienten Makrophagen nach 9-HODE Stimulation. Diese Ergebnisse lassen darauf schließen, dass G2A sowohl einen konstitutiven Einfluss auf die Migration von Makrophagen hat, aber auch durch Aktivierung die Migration von Makrophagen einleiten kann. Anhand der Ergebnisse dieser Arbeit geschieht dies über Aktivierung des TLR4 und den assoziierten Proteinen PTK7, Tgln, MyD88 und MMP9.

Da bisher keine zufriedenstellenden Antikörper oder Inhibitoren für den G2A Rezeptor bekannt oder gar in der Entwicklung sind, lag der Fokus im letzten Teil dieser Arbeit auf der Identifizierung und ersten Testungen von potenziellen Inhibitoren des G2A-Rezeptors. Aus diesem Grund wurde ein High-Throughput Screen am Fraunhofer ScreeningPort durchgeführt, bei dem über 20.000 Substanzen getestet wurden. Nach Dosis-Wirkungs-Analysen und Zelltoxizitätstests der potenziellen Kandidaten wurden sechs Substanzen ausgewählt, die eine starke Hemmung von G2A in „Chinese-Hamster-Ovary-Zellen“ (CHO-Zellen) zeigten. In weiteren Calcium-Imaging Experimenten konnte in dieser Arbeit gezeigt werden, dass drei der sechs Substanzen ebenfalls eine Wirkung auf Neuronen haben. Die hier benannten Inhibitoren G2A11, G2A13 und G2A19 zeigten bereits bei Konzentrationen von 100 nM – 1 μ M eine starke Hemmung des Calciumkanals „transient receptor potential channel vanilloid 1“ (TRPV1)-abhängigen Ca²⁺ Einstroms. Dieser Kanal ist bekannt für seine Rolle bei der Schmerzentstehung und seiner Beteiligung bei neuropathischen Schmerzen. Ebenso ist bekannt, dass G2A-Aktivierung den TRPV1 Kanal sensibilisiert [85].

Die drei Inhibitoren mit den stärksten hemmenden Effekten auf den TRPV1-abhängigen Ca^{2+} -Einstrom, G2A11, G2A13 und G2A19 wurden weiterhin auf ihre Fähigkeit untersucht, die Migration von Makrophagen zu beeinflussen. Für diese Experimente wurden 3-5 unabhängige Transwell-Migrationsassays durchgeführt mit jeweils 4 Stunden Migrationszeit. Als Migrationsstimulus wurde 9-HODE in serumfreiem oder serumhaltigem Medium verwendet. Wie die Ergebnisse zeigen, führt G2A11 zu einer starken konzentrationsabhängigen Hemmung der Migration. Das war sowohl in serumfreiem als auch in serumhaltigem Medium mit 9-HODE als Migrationsstimulus zu beobachten. Wobei der stärkste Unterschied zwischen 1 μM und 10 μM G2A11 zu erkennen war. G2A13 und G2A19 hingegen zeigten in serumfreiem Medium mit 9-HODE eine stetige konzentrationsabhängige Hemmung der Migration, die allerdings nicht so stark war wie bei G2A11. Bei G2A 19 zeigte sich vor allem bei einer Konzentration von 10 μM eine starke Hemmung der Migration, allerdings nur in serumfreiem Medium mit 9-HODE. In serumhaltigem Medium mit 9-HODE zeigte G2A19 kaum Hemmung, unabhängig von der Konzentration des Inhibitors. Die Ergebnisse lassen darauf schließen, dass vor allem G2A11 starke Effekte auf die G2A-Aktivierung hat. G2A11 führt sowohl zu einer starken Desensibilisierung als auch zu einer Hemmung der Makrophagenmigration. Daher ist die Substanz G2A11 ein vielversprechender Hemmstoff, dessen Eigenschaften durch chemische Modifikation verbessert werden könnten.

Zusammenfassend zeigen die Ergebnisse dieser Arbeit, dass G2A einen umfassenden Effekt im Verlauf von trauma-induzierten neuropathischen Schmerzen hat. Zum einen hat er einen direkten Einfluss auf die Schmerzwahrnehmung, zum anderen beeinflusst er die entstehende neuronale Entzündungsreaktion nach einer Nervenverletzung, indem er an der Initiation der Migration von Immunzellen zur verletzten Stelle beteiligt ist. Aus diesem Grund ist der G2A-Rezeptor ein vielversprechendes neues Zielprotein in der Therapie von trauma-induzierten neuropathischer Schmerzen. Durch Hemmung des G2A-Rezeptors könnten zwei wesentliche Mechanismen, die bei neuropathischen Schmerzen eine Rolle spielen, gezielt beeinflusst werden. Zum einen würde durch G2A-Hemmung die Schmerzwahrnehmung verringert, durch Reduktion des TRPV1-abhängigen Ca^{2+} -Einstroms in Neurone. Zum anderen würde die G2A Hemmung zu einer reduzierten neuronalen Entzündung am verletzten Nerv führen. Die weitere Entwicklung und Verbesserung von G2A-Hemmstoffen, sowie die Aufklärung der Rolle des G2A-Rezeptors bei weiteren entzündungsabhängigen Mechanismen und Erkrankungen sollten daher in den Fokus künftiger Forschung gerückt werden.

II. Abbreviations

μBCA	mikro Bicinochoninic acid
μg	microgram
μl	mikrolitre
μM	mikro molar
AA	arachidonic acid
ABC	ammonium-bicarbonate
ACN	acetonitrile
Actn1	alpha-actinin 1
AF	alexa Fluor
AM	acetoxymethylester
ANOVA	analysis of variance, statistical test
APC	allophycocyanin
APS	ammonium peroxydisulfate
ATF	activating transcription factor
Bai	baicalein
BDNF	brain derived neurotrophic factor
BHT	butylated hydroxytoluene
BMDM	bone marrow derived macrophages
BSA	bovine serum albumin

C	contralateral
Ca	calcium
CaCl ₂	calcium chloride
Cadm1	cell adhesion molecule 1
cAMP	cyclic Adenosinmonophosphate
CCI	chronic constriction injury
CD	cluster of differentiation
Cd5l	cluster of differentiation 5 molecule like
CF	cyanine fluorescent dye
CGRP	calcitonin gene related peptide
CHO K1	chinese hamster ovary K1 cells
CMKLR1	chemokine-like receptor 1
CNS	central nervous system
CO ₂	carbon dioxide
Col6a2	collagen alpha2 (VI) chain precursor
COX	cyclooxygenase
Ctnna1	catenin alpha1
CuSO ₄	copper sulfate
CXCL7	C-X-C chemokine ligand 7

CXCR4	C-X-C chemokine receptor type 4
Cy3	cyanine 3
Cyp	cytochrome enzyme
DAPI	4,6-Diamidin-2-Phenylindol
DC	dendritic cell
ddH ₂ O	double distilled water
Diclo	diclofenac
DiHDP A	dihydroxy-4Z,7Z,10Z,13Z,16Z-docosapentaenoic acid
DiHETE	dihydroxy-eicosa-5,8,11,17-Tetraenoic Acid
DiHOME	dihydrox -octadecenoic acid
DMEM	dulbecco's Modified Eagle's Medium
DMSO	dimehtyl sulfoxide
DPBS	dulbecco's phosphate-buffered saline
DRG	dorsal root ganglia
ECL	enhanced chemiluminescence
EDTA	ethylenediaminetetraacetic acid
EEQ	epoxyeicosatetraenoic acid
EET	epoxyeicosatrienoic acid
ELISA	enzyme-linked immunosorbent assay

Elmo-1	engulfment and cell motility protein 1
EpDPA	epoxydocosapentaenoic acid
EpOME	epoxy octadecenoic acid
EPSP	4-(2-Hydroxyethyl)-1-piperazinepropanesulfonic acid
ERK	extracellular signal regulated kinase
FA	formic acid
FACS	fluorescence-activated cell sorting
FCS	fetal calf serum
FITC	fluoresceinisothiocyanat
g	gravity
G / G2A-DEFICIENT	G2A-deficiency (in mouse/ tissue/ cell)
GAPDH	glyceraldehyde 3-phosphate dehydrogenase
GFAP	glial fibrillary acidic protein
GITR	glucocorticoid-induced tumor necrosis factor receptor
Glg1	golgi apparatus protein 1
GNA11	guanine nucleotide-binding subunit alpha 11
Gpr132	G-protein coupled receptor 132
Grb2	growth factor receptor-bound protein 2
h	hours

H ₃ PO ₄	phosphoric acid
HBSS	hank's Balanced Salt Solution
HCD	higher-energy collisional dissociation
HCl	hydrochloric acid
HCN	hyperpolarization-activated cyclic nucleotide-modulated channel
HEPES	4-(2-Hydroxyethyl)piperazine-1-ethanesulfonic acid
HODE	hydroxyoctadecadienoic acid
HPLC	high performance liquid chromatography
HRP	horse radish peroxidase
HSP	heat shock protein
HTRF	homogenous time resolved fluorescence
I	ipsilateral
Iba1	ionized calcium binding adapter molecule-1
Ig	immunoglobulin
IHC	immunohistochemistry
IL	interleukin
i-NOS	inducible nitric oxide synthase
IP	inositol monophosphate
IP-10	interferon γ induced protein 10

ISAP	international Association for the Study of Pain
Itga2b	integrin alpha-IIb precursor
Itgb3	integrin beta-3 precursor
JNK	c-Jun N-terminal kinase
KC	keratinocytes-derived chemokine
KCl	potassium chloride
kDa	kilo Dalton
Keto	ketokonazole
KI	potassium iodide
KNaC ₄ H ₄ O ₆	potassium sodium tartrate
KO	knockout
LA	linoleic acid
LC-MS	liquid-chromatography-tandem mass spectrometry
LDLR	low density lipoprotein receptor
Lgmn	legumain
LiCl ₂	lithium chloride
LOX	lipoxygenase
LPC	lysophosphatidylcholine
LPS	lipopolysaccharide <i>E.coli</i>

Ly6C	lymphocyte antigen 6 complex locus C
LysC	endoproteinase LysC
m	meter
mA	milliampere
MAPK	mitogen-activated protein kinase
M-CSF	macrophage - colony stimulating factor
MCP	monocyte chemoattractant protein
MgCl ₂	magnesium chloride
MHC	major histocompatibility complex
MIG	monokine induced by gamma
min	minutes
MIP-1a	macrophage inflammatory protein 1a
ml	milliliter
mm	millimeter
mM	millimolar
MMP9	matrix metalloproteinase 9
ms	milliseconds
MS	mass spectrometry
MW	molecular weight

MyD88	myeloid differentiation primary response protein 88
Mylk	myosin light chain kinase
N	nerve
Na ₂ HPO ₄	sodium phosphate dibasic
NADPH	nicotinamide adenine dinucleotide phosphate
NaCl	sodium chloride
NaH ₂ PO ₄	sodium phosphate monobasic monohydrate
NaOH	sodium hydroxide
NDGA	nordihydroguaiaretic acid
Neu-N	neuronal nuclei, neuronal cell marker
NF-κB	nuclear factor kappa-light-chain-enhancer
ng	nanogram
NGF	nerve growth factor
NK	natural killer
NK1.1	neurokinin receptor 1
nLC	nano-LC
nM	nanomolar
Nox	NADPH oxidase
P	cell pellet

P/S	penicillin / streptomycin
p38	p38 mitogen-activated protein kinase
PAGE	polyacrylamide gel electrophoresis
PBS	phosphate buffered saline
PBST	phosphate buffered saline with 0.1% triton-x
PCR	polymerase chain reaction
PDGF	platelet derived growth factor
PE	phycoerythrin
PFA	paraformaldehyde
PI3K	phosphoinositide 3-kinase
Pik3r5	phosphoinositide 3-kinase regulatory subunit 5
PKA	protein kinase A
PKC	protein kinase C
PLC	phospholipase C
PNS	peripheral nervous system
PPAR γ	peroxisome proliferator-activated receptor γ
PTK7	protein tyrosine kinase 7
qPCR	quantitative real-time PCR
QTRAP	quadrupole tandem mass spectrometer

Rac	ras-related C3 botulinum toxin substrate
Ras	rat sarcoma
ROCK	rho-associated protein kinase
RPMI	roswell Park Memorial Institute medium
RT	room temperature
S	supernatant
s	seconds
SC	spinal cord
SDS	sodium dodecyl sulfate
SEM	standard error of the mean
SNI	spared nerve injury
SPS-MS	synchronous precursor selection-based MS
TEMED	N,N,N',N'-Tetramethylethylene-1,2-diamine
TFA	trifluoroacetic acid
TGF- β	tumor growth factor- β
TgIn	transgelin
Tmsb4x	thymosin beta-4
TMT	trimethyltryptamine
TN	Tris-HCl, NaCl

TNF α	tumor necrosis factor α
TNT	Tris-HCl, NaCl + Tween
Tris	Tris(hydroxymethyl)aminomethane
Triton [®] X-100	O-[4-(1,1,3,3-tetramethylbutyl)phenoxy]polyethoxyethanol
TRP	transient receptor potential, family of ion channels
TRPC	transient receptor potential canonical
TRPM	transient receptor potential melastatin
TRPV	transient receptor potential vanilloid
Tween [®] -20	polyoxyethylen(20)-sorbitan-monolaurat
V	volt
v	volume
VEGF	vascular endothelial growth factor
w	weight
WT	wild-type
Xdh	xanthine dehydrogenase
Zileut	zileuton

III. Table of Figures

1. *Introduction*

Figure 1. Nociception.....	2
Figure 2. Peripheral sensitization.....	5
Figure 3. Induction of neuropathic pain.....	8
Figure 4. Alignment of G2A protein in different species.....	12
Figure 5. Binding of 9-HODE to G2A.....	14
Figure 6. G2A signaling through different G-protein coupled pathways.....	15
Figure 7. Scheme of open questions in nerve injury induced neuropathic pain.....	18

2. *Material and Methods*

Table 1. Conditions of the transwell migration assay for testing migratory behavior of bone-marrow derived macrophages regarding different substances.....	42
Table 2. Exemplary conditions of the 9-HODE production assay in order to see which enzyme is responsible for the 9-HODE production during inflammation.....	44
Table 3. Example of Dilution Series of one test compound in a 96-well plate.....	46
Table 4. Master mix composition for reverse transcription using First Strand cDNA Synthesis Kit.....	47
Table 5. Overview of the reverse transcription run.....	48
Table 6. Program for qPCR run conducted with QuantStudio™.....	48
Table 7. Overview running program of Ca-Imaging sensitization experiment.....	49

3. *Results*

Figure 8. Nociceptive behavior after spared-nerve injury with dynamic plantar.....	55
Figure 9. Number of immune cells in sciatic nerves 1 d after SNI surgery.....	56
Figure 10. Number of immune cells in sciatic nerves 7 d after SNI surgery.....	56
Figure 11. Amount of F4-80/CD11b-positive macrophages in sciatic nerve.....	57
Figure 12. Number of immune cells in dorsal root ganglia (DRG) 1 d after SNI surgery.....	58

Figure 13. Number of immune cells in dorsal root ganglia (DRG) 7 d after SNI surgery.....	58
Figure 14. Number of immune cells in spinal cords 1 d after SNI surgery.....	59
Figure 15. Number of immune cells in spinal cords 7 d after SNI surgery.....	59
Figure 16. Activation of astrocytes in dorsal spinal cord.....	60
Figure 17. Cytokines and growth factors in injured sciatic nerves.....	61
Figure 18. Concentrations of various cytokines and chemokines in ipsilateral sciatic nerves.....	62
Figure 19. Concentrations of various cytokines and chemokines in ipsilateral L4-L6 DRGs..	63
Figure 20. Stress and ROS-marker in L4-L6 ipsilateral DRGs.....	64
Figure 21. Concentrations of various cytokines and chemokines in ipsilateral spinal cords..	64
Figure 22. Concentrations of HODEs in sciatic nerves 7 d after SNI surgery.....	65
Figure 23. Inhibition of 9-HODE production in BMDMs after LPS stimulation.....	66
Figure 24. Concentrations of EpOMEs and DiHOMEs at sciatic nerves 7 d after SNI surgery.....	67
Figure 25. Global proteome analysis of bone marrow derived macrophages (BMDM) of wild-type and G2A-deficient mice without stimulation.....	69
Figure 26. Global proteome analysis of wild-type BMDMs after stimulation with 9-HODE....	70
Table 8. List of most upregulated migratory proteins in wild-type BMDMs 24 h after 1 μ M 9-HODE stimulation.....	71
Figure 27. Upregulated migratory proteins and involved signaling pathways.....	72
Table 9. List of most downregulated migratory proteins in wild-type BMDMs 24 h after 1 μ M 9-HODE stimulation	72
Figure 28. Global proteome analysis of BMDMs of G2A-deficient mice without after 9-HODE stimulation.....	73
Figure 29. Global proteome analysis of BMDMs of wild-type and G2A-deficient mice without after 9-HODE stimulation.....	74

Figure 30. Western Blots of proteome analysis evaluation.....	75
Figure 31. MMP9 concentrations in cell lysates of BMDMs.....	76
Figure 32. Western Blots of ERK, p38 and phosphorylated ERK (p-ERK) and p38 (p-p38)..	77
Figure 33. Western Blots of PI3K and phosphorylation amount of ERK and p38.....	78
Figure 34. Western Blots of ROCK1 and -2, as well as Rac and Ras.....	79
Table 10. Results of G2A antagonist screening and subsequent cell toxicity assay of the screening hits.....	81
Figure 35. Inhibitory effects of G2A11 on 9-HODE dependent TRPV1-mediated calcium influx.....	82
Figure 36. Inhibitory effects of 6 inhibitors on 9-HODE dependent TRPV1-mediated calcium influx.....	83
Figure 37. Exemplary images of BMDMs on membrane after migration.....	84
Figure 38. Inhibition of BMDMs migration through G2A11.....	85
Figure 39. Inhibition of BMDMs migration through G2A13.....	85
Figure 40. Inhibition of BMDMs migration through G2A19.....	86

4. Discussion

Figure 41. Overview of suggested crosstalk between injured sensory neurons and immune cells and the involvement of G2A.....	98
Figure 42. Overview of systemic actions through loss of G2A in neuropathic pain.....	100

Annex

Table 11. Overview of down- and upregulated proteins in untreated G2A-deficient compared to untreated wild-type BMDMs.....	151
Table 12. Overview of down- and upregulated proteins 24 h after 1 μ M 9-HODE stimulation in wild-type BMDMs.....	154
Table 13. Overview of down- and upregulated proteins in G2A-deficient BMDMs 24 h after 1 μ M 9-HODE stimulation.....	164

Table 14. Overview of down- and upregulated proteins in G2A-deficient compared to wild-type BMDMs 24 h after 1 μ M 9-HODE stimulation.....174

References

1. Basbaum A. I; Bautista, D. M; Scherrer, G; Julius, D. Cellular and molecular mechanisms of pain. *Cell*, **2009**, *139* 267–84. doi:10.1016/j.cell.2009.09.028
2. White F. A; Feldman, P; Miller, R. J. Chemokine signaling and the management of neuropathic pain. *Mol. Interv.*, **2009**, *9* 188–95. doi:10.1124/mi.9.4.7
3. Bennett D. L; Clark, A. J; Huang, J; Waxman, S. G; Dib-Hajj, S. D. The Role of Voltage-Gated Sodium Channels in Pain Signaling. *Physiological reviews*, **2019**, *99* 1079–151. doi:10.1152/physrev.00052.2017
4. Dubin A. E; Patapoutian, A. Nociceptors. *The Journal of clinical investigation*, **2010**, *120* 3760–72. doi:10.1172/jci42843
5. Grace P. M; Hutchinson, M. R; Maier, S. F; Watkins, L. R. Pathological pain and the neuroimmune interface. *Nature reviews. Immunology*, **2014**, *14* 217–31. doi:10.1038/nri3621
6. Ji R. R; Kohno, T; Moore, K. A; Woolf, C. J. Central sensitization and LTP. *Trends Neurosci.*, **2003**, *26* 696–705. doi:10.1016/j.tins.2003.09.017
7. Pinho-Ribeiro F. A; Verri, W. A., Jr; Chiu, I. M. Nociceptor Sensory Neuron-Immune Interactions in Pain and Inflammation. *Trends in immunology*, **2017**, *38* 5–19. doi:10.1016/j.it.2016.10.001
8. Julius D; Basbaum, A. I. Molecular mechanisms of nociception. *Nature*, **2001**, *413* 203–10. doi:10.1038/35093019
9. Costigan M; Scholz, J; Woolf, C. J. Neuropathic Pain. *Annu. Rev. Neurosci.*, **2009**, *32* 1–32. doi:10.1146/annurev.neuro.051508.135531
10. Kuner R; Flor, H. Structural plasticity and reorganisation in chronic pain. *Nature reviews. Neuroscience*, **2016**, *18* 20–30. doi:10.1038/nrn.2016.162
11. Peirs C; Seal, R. P. Neural circuits for pain. *Science (New York, N.Y.)*, **2016**, *354* 578–84. doi:10.1126/science.aaf8933
12. Woolf C. J; Walters, E. T. Common patterns of plasticity contributing to nociceptive sensitization in mammals and *Aplysia*. *Trends Neurosci.*, **1991**, *14* 74–8.
13. Kuner R. Central mechanisms of pathological pain. *Nature Medicine*, **2010**, *16* 1258. doi:10.1038/nm.2231

-
14. Talbot S; Foster, S. L; Woolf, C. J. Neuroimmune Physiology and Pathology. *Annu. Rev. Immunol.*, **2016** 16.1-16.27.
 15. Caterina M. J; Schumacher, M. A; Tominaga, M; Rosen, T. A; Levine, J. D; Julius, D. The capsaicin receptor: a heat-activated ion channel in the pain pathway. *Nature*, **1997**, 389 816–24. doi:10.1038/39807
 16. Ji R. R; Woolf, C. J. Neuronal plasticity and signal transduction in nociceptive neurons: implications for the initiation and maintenance of pathological pain. *Neurobiology of disease*, **2001**, 8 1–10. doi:10.1006/nbdi.2000.0360
 17. Ploner M; Gross, J; Timmermann, L; Schnitzler, A. Cortical representation of first and second pain sensation in humans. *PNAS*, **2002**, 99 12444–8. doi:10.1073/pnas.182272899
 18. Price D. D; Dubner, R. Mechanisms of first and second pain in the peripheral and central nervous systems. *The Journal of investigative dermatology*, **1977**, 69 167–71. doi:10.1111/1523-1747.ep12497942
 19. Staud R; Robinson, M. E; Price, D. D. Temporal Summation Of Second Pain And Its Maintenance Are Useful For Characterizing Widespread Central Sensitization Of Fibromyalgia Patients. *The journal of pain official journal of the American Pain Society*, **2007**, 8 893–901. doi:10.1016/j.jpain.2007.06.006
 20. Latremoliere A; Latini, A; Andrews, N; Cronin, S. J; Fujita, M; Gorska, K; Hovius, R; Romero, C; Chuaiphichai, S; Painter, M; et al. Reduction of Neuropathic and Inflammatory Pain through Inhibition of the Tetrahydrobiopterin Pathway. *Neuron*, **2015**, 86 1393–406. doi:10.1016/j.neuron.2015.05.033
 21. Ji R.-R; Chamesian, A; Zhang, Y.-Q. Pain regulation by non-neuronal cells and inflammation. *Science*, **2016**, 354 572–7. doi:10.1126/science.aaf8924
 22. Scholz J; Woolf, C. J. Can we conquer pain? *Nature neuroscience*, **2002**, 5 Suppl 1062–7. doi:10.1038/nn942
 23. Ji R. R; Xu, Z. Z; Gao, Y. J. Emerging targets in neuroinflammation-driven chronic pain. *Nat. Rev. Drug. Discov.*, **2014**, 13 533–48. doi:10.1038/nrd4334
 24. Liedgens H; Obradovic, M; Courcy, J. de; Holbrook, T; Jakubanis, R. A burden of illness study for neuropathic pain in Europe. *Clinicoecon Outcomes Res.*, **2016**, 8 113–26. doi:10.2147/ceor.s81396

-
25. Mills S. E.E; Nicolson, K. P; Smith, B. H. Chronic pain: a review of its epidemiology and associated factors in population-based studies. *BJA: British Journal of Anaesthesia*, **2019**, 123 e273-83. doi:10.1016/j.bja.2019.03.023
 26. Dahlhamer J; Lucas, J; Zelaya, C; Nahin, R; Mackey, S; DeBar, L; Kerns, R; Korff, M. von; Porter, L; Helmick, C. Prevalence of Chronic Pain and High-Impact Chronic Pain Among Adults - United States, 2016. *MMWR. Morbidity and mortality weekly report*, **2018**, 67 1001–6. doi:10.15585/mmwr.mm6736a2
 27. Hehn C. A. von; Baron, R; Woolf, C. J. Deconstructing the Neuropathic Pain Phenotype to Reveal Neural Mechanisms. *Neuron*, **2012**, 73 638–52. doi:10.1016/j.neuron.2012.02.008
 28. Leung L; Cahill, C. M. TNF-alpha and neuropathic pain--a review. *Journal of neuroinflammation*, **2010**, 7 27. doi:10.1186/1742-2094-7-27
 29. Grobe T. G; Steinmann, S; Szecsenyi, J. *Barmer GEK Arztreport 2016*, **2016**,
 30. Souza J. B; Grossmann, E; Perissinotti, D. M. N; Oliveira Junior, Jose Oswaldo de; Fonseca, Paulo Renato Barreiros da; Posso, I. d. P. Prevalence of Chronic Pain, Treatments, Perception, and Interference on Life Activities: Brazilian Population-Based Survey. *Pain Research and Management*, **2017**, 2017. doi:10.1155/2017/4643830
 31. Ji R. R; Nackley, A; Huh, Y; Terrando, N; Maixner, W. Neuroinflammation and Central Sensitization in Chronic and Widespread Pain. *Anesthesiology*, **2018**. doi:10.1097/aln.0000000000002130
 32. Tramullas M; Francés, R; La Fuente, R. de; Velategui, S; Carcelén, M; García, R; Llorca, J; Hurlé, M. A. MicroRNA-30c-5p modulates neuropathic pain in rodents. *Science translational medicine*, **2018**, 10. doi:10.1126/scitranslmed.aao6299
 33. Vallejo R; Tilley, D. M; Vogel, L; Benyamin, R. The role of glia and the immune system in the development and maintenance of neuropathic pain. *Pain Pract.*, **2010**, 10 167–84. doi:10.1111/j.1533-2500.2010.00367.x
 34. Calvo M; Dawes, J. M; Bennett, D. L. The role of the immune system in the generation of neuropathic pain. *The Lancet. Neurology*, **2012**, 11 629–42. doi:10.1016/s1474-4422(12)70134-5

-
35. Moran M. M; McAlexander, M. A; Biro, T; Szallasi, A. Transient receptor potential channels as therapeutic targets. *Nature reviews. Drug discovery*, **2011**, *10* 601–20. doi:10.1038/nrd3456
 36. Suter M. R; Wen, Y. R; Decosterd, I; Ji, R. R. Do glial cells control pain? *Neuron glia biology*, **2007**, *3* 255–68. doi:10.1017/s1740925x08000100
 37. Latremoliere A; Woolf, C. J. Central sensitization: a generator of pain hypersensitivity by central neural plasticity. *The journal of pain official journal of the American Pain Society*, **2009**, *10* 895–926. doi:10.1016/j.jpain.2009.06.012
 38. Colloca L; Ludman, T; Bouhassira, D; Baron, R; Dickenson, A. H; Yarnitsky, D; Freeman, R; Truini, A; Attal, N; Finnerup, N. B; et al. Neuropathic pain. *Nat. Rev. Dis. Primers*, **2017**, *3* 17002. doi:10.1038/nrdp.2017.2
 39. Bowsher D. Neurogenic pain syndromes and their management. *British medical bulletin*, **1991**, *47* 644–66.
 40. Inoue K. Purinergic signaling in microglia in the pathogenesis of neuropathic pain. *Proceedings of the Japan Academy. Series B, Physical and Biological Sciences*, **2017**, *93* 174–82. doi:10.2183/pjab.93.011
 41. Kiguchi N; Kobayashi, Y; Kishioka, S. Chemokines and cytokines in neuroinflammation leading to neuropathic pain. *Curr. Opin. Pharmacol.*, **2012**, *12* 55–61. doi:10.1016/j.coph.2011.10.007
 42. Nickel F. T; Seifert, F; Lanz, S; Maihofner, C. Mechanisms of neuropathic pain. *European neuropsychopharmacology the journal of the European College of Neuropsychopharmacology*, **2012**, *22* 81–91. doi:10.1016/j.euroneuro.2011.05.005
 43. Torrance N; Smith, B. H; Bennett, M. I; Lee, A. J. The Epidemiology of Chronic Pain of Predominantly Neuropathic Origin. Results From a General Population Survey. *The Journal of Pain*, **2006**, *7* 281–9. doi:10.1016/j.jpain.2005.11.008
 44. Bouhassira D; Lanteri-Minet, M; Attal, N; Laurent, B; Touboul, C. Prevalence of chronic pain with neuropathic characteristics in the general population. *Pain*, **2008**, *136* 380–7. doi:10.1016/j.pain.2007.08.013
 45. van Hecke O; Austin, S. K; Khan, R. A; Smith, B. H; Torrance, N. Neuropathic pain in the general population. *Pain*, **2014**, *155* 654–62. doi:10.1016/j.pain.2013.11.013

-
46. O'Connor A. B; Dworkin, R. H. Treatment of neuropathic pain. *Am. J. Med.*, **2009**, *122* S22-32. doi:10.1016/j.amjmed.2009.04.007
 47. Scholz J; Woolf, C. J. The neuropathic pain triad. *Nat. Neurosci.*, **2007**, *10* 1361–8. doi:10.1038/nn1992
 48. Lim E. Y; Kim, Y. T. Food-Derived Natural Compounds for Pain Relief in Neuropathic Pain. *BioMed Research International*, **2016**, *2016* 7917528. doi:10.1155/2016/7917528
 49. Kiguchi N; Kobayashi, D; Saika, F; Matsuzaki, S; Kishioka, S. Inhibition of peripheral macrophages by nicotinic acetylcholine receptor agonists suppresses spinal microglial activation and neuropathic pain in mice with peripheral nerve injury. *Journal of neuroinflammation*, **2018**, *15* 96. doi:10.1186/s12974-018-1133-5
 50. Park S. B; Goldstein, D; Krishnan, A. V; Lin, C. S.-Y; Friedlander, M. L; Cassidy, J; Koltzenburg, M; Kiernan, M. C. Chemotherapy-induced peripheral neurotoxicity: a critical analysis. *CA: a cancer journal for clinicians*, **2013**, *63* 419–37. doi:10.3322/caac.21204
 51. Areti A; Yerra, V. G; Naidu, V; Kumar, A. Oxidative stress and nerve damage: role in chemotherapy induced peripheral neuropathy. *Redox biology*, **2014**, *2* 289–95. doi:10.1016/j.redox.2014.01.006
 52. Cohen S. P; Mao, J. Neuropathic pain: mechanisms and their clinical implications. *BMJ (Clinical research ed.)*, **2014**, *348* f7656. doi:10.1136/bmj.f7656
 53. Campbell J. N; Meyer, R. A. Mechanisms of neuropathic pain. *Neuron*, **2006**, *52* 77–92. doi:10.1016/j.neuron.2006.09.021
 54. Sisignano M; Bennett, D. L; Geisslinger, G; Scholich, K. TRP-channels as key integrators of lipid pathways in nociceptive neurons. *Prog. Lipid Res.*, **2014**, *53* 93–107. doi:10.1016/j.plipres.2013.11.002
 55. Thacker M. A; Clark, A. K; Marchand, F; McMahon, S. B. Pathophysiology of peripheral neuropathic pain: immune cells and molecules. *Anesthesia and analgesia*, **2007**, *105* 838–47. doi:10.1213/01.ane.0000275190.42912.37
 56. Cobos E. J; Nickerson, C. A; Gao, F; Chandran, V; Bravo-Caparrós, I; González-Cano, R; Riva, P; Andrews, N. A; Latremoliere, A; Seehus, C. R; et al. Mechanistic Differences in Neuropathic Pain Modalities Revealed by Correlating Behavior with Global Expression Profiling. *Cell Rep.*, **2018**, *22* 1301–12. doi:10.1016/j.celrep.2018.01.006

-
57. Moalem G; Xu, K; Yu, L. T lymphocytes play a role in neuropathic pain following peripheral nerve injury in rats. *Neuroscience*, **2004**, *129* 767–77.
doi:10.1016/j.neuroscience.2004.08.035
58. Finnerup N. B; Attal, N; Haroutounian, S; McNicol, E; Baron, R; Dworkin, R. H; Gilron, I; Haanpää, M; Hansson, P; Jensen, T. S; et al. Pharmacotherapy for neuropathic pain in adults. *Lancet Neurol.*, **2015**, *14* 162–73. doi:10.1016/S1474-4422(14)70251-0
59. Hung A. L; Lim, M; Doshi, T. L. Targeting cytokines for treatment of neuropathic pain. *Scand. J. Pain*, **2017**, *17* 287–93. doi:10.1016/j.sjpain.2017.08.002
60. Gavva N. R; Treanor, J. J; Garami, A; Fang, L; Surapaneni, S; Akrami, A; Alvarez, F; Bak, A; Darling, M; Gore, A; et al. Pharmacological blockade of the vanilloid receptor TRPV1 elicits marked hyperthermia in humans. *Pain*, **2008**, *136* 202–10.
doi:10.1016/j.pain.2008.01.024
61. Costigan M; Moss, A; Latremoliere, A; Johnston, C; Verma-Gandhu, M; Herbert, T. A; Barrett, L; Brenner, G. J; Vardeh, D; Woolf, C. J; et al. T-cell infiltration and signaling in the adult dorsal spinal cord is a major contributor to neuropathic pain-like hypersensitivity. *J. Neurosci.*, **2009**, *29* 14415–22. doi:10.1523/JNEUROSCI.4569-09.2009
62. Weng Z; Fluckiger, A.-C; Nisitani, S; Wahl, M. I; Le, L. Q; Hunter, C. A; Fernal, A. A; Le Beau, M. M; Witte, O. N. A DNA damage and stress inducible G protein-coupled receptor blocks cells in G2/M. *Proc. Natl. Acad. Sci. U S A*, **1998**, *95* 12334–9.
63. Parks B. W; Gambill, G. P; Lusic, A. J; Kabarowski, J. H. S. Loss of G2A promotes macrophage accumulation in atherosclerotic lesions of low density lipoprotein receptor-deficient mice. *Journal of lipid research*, **2005**, *46* 1405–15. doi:10.1194/jlr.M500085-JLR200
64. Insel P. A; Sriram, K; Salmerón, C; Wiley, S. Z. Proton-sensing G protein-coupled receptors: detectors of tumor acidosis and candidate drug targets. *Future medicinal chemistry*, **2020**, *12* 523–32. doi:10.4155/fmc-2019-0357
65. Cheng W. Y; Huynh, H; Chen, P; Peña-Llopis, S; Wan, Y. Macrophage PPAR γ inhibits Gpr132 to mediate the anti-tumor effects of rosiglitazone. *eLife*, **2016**, *5*.
doi:10.7554/eLife.18501
66. Justus C. R; Dong, L; Yang, L. V. Acidic tumor microenvironment and pH-sensing G protein-coupled receptors. *Front. Physiol.*, **2013**, *4* 354. doi:10.3389/fphys.2013.00354

-
67. Le L. Q; Kabarowski, J. H; Weng, Z; Satterthwaite, A. B; Harvill, E. T; Jensen, E. R; Miller, J. F; Witte, O. N. Mice lacking the orphan G protein-coupled receptor G2A develop a late-onset autoimmune syndrome. *Immunity*, **2001**, *14* 561–71.
68. Lahvic J. L; Ammerman, M; Li, P; Blair, M. C; Stillman, E. R; Fast, E. M; Robertson, A. L; Christodoulou, C; Perlin, J. R; Yang, S; et al. Specific oxylipins enhance vertebrate hematopoiesis via the receptor GPR132. *Proc. Natl. Acad. Sci. U S A*, **2018**, *115* 9252–7. doi:10.1073/pnas.1806077115
69. Audet M; Stevens, R. C. Emerging structural biology of lipid G protein-coupled receptors. *Protein science a publication of the Protein Society*, **2019**, *28* 292–304. doi:10.1002/pro.3509
70. Gao H; Sun, Y; Wu, Y; Luan, B; Wang, Y; Qu, B; Pei, G. Identification of β -Arrestin2 as a G Protein-Coupled Receptor-Stimulated Regulator of NF- κ B Pathways. *Molecular Cell*, **2004**, *14* 303–17. doi:10.1016/S1097-2765(04)00216-3
71. Zeng Z; Mukherjee, A; Varghese, A. P; Yang, X.-L; Chen, S; Zhang, H. Roles of G protein-coupled receptors in inflammatory bowel disease. *WJG*, **2020**, *26* 1242–61. doi:10.3748/wjg.v26.i12.1242
72. Ogawa A; Obinata, H; Hattori, T; Kishi, M; Tatei, K; Ishikawa, O; Izumi, T. Identification and Analysis of Two Splice Variants of Human G2A Generated by Alternative Splicing. *Journal of Pharmacology and Experimental Therapeutics*, **2010**, *332* 469–78. doi:10.1124/jpet.109.158758
73. Bolick D. T; Skafien, M. d; Johnson, L. E; Kwon, S.-C; Howatt, D; Daugherty, A; Ravichandran, K. S; Hedrick, C. C. G2A Deficiency in Mice Promotes Macrophage Activation and Atherosclerosis. *Circ. Res.*, **2008**, *104* 318–27. doi:10.1161/CIRCRESAHA.108.181131
74. Alexander S. P; Christopoulos, A; Davenport, A. P; Kelly, E; Mathie, A; Peters, J. A; Veale, E. L; Armstrong, J. F; Faccenda, E; Harding, S. D; et al. THE CONCISE GUIDE TO PHARMACOLOGY 2019/20: G protein-coupled receptors. *British journal of pharmacology*, **2019**, *176 Suppl 1* S21-S141. doi:10.1111/bph.14748
75. Gurevich V. V; Gurevich, E. V. GPCR Signaling Regulation: The Role of GRKs and Arrestins. *Frontiers in pharmacology*, **2019**, *10* 125. doi:10.3389/fphar.2019.00125

-
76. Ishii S; Kihara, Y; Shimizu, T. Identification of T cell death-associated gene 8 (TDAG8) as a novel acid sensing G-protein-coupled receptor. *The Journal of biological chemistry*, **2005**, 280 9083–7. doi:10.1074/jbc.M407832200
77. Radu C. G; Nijagal, A; McLaughlin, J; Wang, L; Witte, O. N. Differential proton sensitivity of related G protein-coupled receptors T cell death-associated gene 8 and G2A expressed in immune cells. *Proc. Natl. Acad. Sci. U S A*, **2005**, 102 1632–7. doi:10.1073/pnas.0409415102
78. Chen P; Zuo, H; Xiong, H; Kolar, M. J; Chu, Q; Saghatelian, A; Siegwart, D. J; Wan, Y. Gpr132 sensing of lactate mediates tumor-macrophage interplay to promote breast cancer metastasis. *Proceedings of the National Academy of Sciences of the United States of America*, **2017**, 114 580–5. doi:10.1073/pnas.1614035114
79. Murakami N; Yokomizo, T; Okuno, T; Shimizu, T. G2A is a proton-sensing G-protein-coupled receptor antagonized by lysophosphatidylcholine. *J. Biol. Chem.*, **2004**, 279 42484–91. doi:10.1074/jbc.M406561200
80. Tan M; Yamaguchi, S; Yamahira, S; Nakamura, M; Nagamune, T. Quantitative image cytometry for analyzing intracellular trafficking of G protein-coupled receptors on a chemical-trapping single cell array. *Lab on a chip*, **2017**, 17 1933–8. doi:10.1039/c7lc00198c
81. Foster J. R; Ueno, S; Chen, M. X; Harvey, J; Dowell, S. J; Irving, A. J; Brown, A. J. N-Palmitoylglycine and other N-acylamides activate the lipid receptor G2A/GPR132. *Pharmacology Research & Perspectives*, **2019**, 7 e00542. doi:10.1002/prp2.542
82. Ludwig M.-G; Vanek, M; Guerini, D; Gasser, J. A; Jones, C. E; Junker, U; Hofstetter, H; Wolf, R. M; Seuwen, K. Proton-sensing G-protein-coupled receptors. *Nature*, **2003**, 425 93–8. doi:10.1038/nature01905
83. Obinata H; Izumi, T. G2A as a receptor for oxidized free fatty acids. *Prostaglandins & other lipid mediators*, **2009**, 89 66–72. doi:10.1016/j.prostaglandins.2008.11.002
84. Hattori T; Obinata, H; Ogawa, A; Kishi, M; Tatei, K; Ishikawa, O; Izumi, T. G2A plays proinflammatory roles in human keratinocytes under oxidative stress as a receptor for 9-hydroxyoctadecadienoic acid. *J. Invest. Dermatol.*, **2008**, 128 1123–33. doi:10.1038/sj.jid.5701172
85. Hohmann S. W; Angioni, C; Tunaru, S; Lee, S; Woolf, C. J; Offermanns, S; Geisslinger, G; Scholich, K; Sisignano, M. The G2A receptor (GPR132) contributes to oxaliplatin-

-
- induced mechanical pain hypersensitivity. *Sci. Rep.*, **2017**, 7 446. doi:10.1038/s41598-017-00591-0
86. Park A. J; Agak, G. W; Qin, M; Hisaw, L. D; Pirouz, A; Kao, S; Marinelli, L. J; Garban, H. J; Thiboutot, D; Liu, P. T; et al. G2A Attenuates Propionibacterium acnes Induction of Inflammatory Cytokines in Human Monocytes. *Annals of dermatology*, **2017**, 29 688–98. doi:10.5021/ad.2017.29.6.688
87. Murakami N; Hashidate, T; Harayama, T; Yokomizo, T; Shimizu, T; Nakamura, M. Transcriptional regulation of human G2A in monocytes/ macrophages: involvement of c/EBPs, Runx and Pu.1. *Genes to cells devoted to molecular & cellular mechanisms*, **2009**, 14 1441–55. doi:10.1111/j.1365-2443.2009.01360.x
88. Murakami M; Kudo, I. Phospholipase A2. *Journal of biochemistry*, **2002**, 131 285–92.
89. Bond J; Domaschenz, R; Roman-Trufero, M; Sabbattini, P; Ferreiros-Vidal, I; Gerrard, G; Asnafi, V; Macintyre, E; Merckenschlager, M; Dillon, N. Direct interaction of Ikaros and Foxp1 modulates expression of the G protein-coupled receptor G2A in B-lymphocytes and acute lymphoblastic leukemia. *Oncotarget*, **2016**, 7 65923–36. doi:10.18632/oncotarget.11688
90. Obinata H; Hattori, T; Nakane, S; Tatei, K; Izumi, T. Identification of 9-hydroxyoctadecadienoic acid and other oxidized free fatty acids as ligands of the G protein-coupled receptor G2A. *The Journal of biological chemistry*, **2005**, 280 40676–83. doi:10.1074/jbc.M507787200
91. Kabarowski J. H; Feramisco, J. D; Le, L. Q; Gu, J. L; Luoh, S. W; Simon, M. I; Witte, O. N. Direct genetic demonstration of G alpha 13 coupling to the orphan G protein-coupled receptor G2A leading to RhoA-dependent actin rearrangement. *Proceedings of the National Academy of Sciences of the United States of America*, **2000**, 97 12109–14. doi:10.1073/pnas.97.22.12109
92. Osthues T; Sisignano, M. Oxidized Lipids in Persistent Pain States. *Front. Pharmacol.*, **2019**, 10. doi:10.3389/fphar.2019.01147
93. Radu C. G; Yang, L. V; Riedinger, M; Au, M; Witte, O. N. T cell chemotaxis to lysophosphatidylcholine through the G2A receptor. *Proceedings of the National Academy of Sciences of the United States of America*, **2004**, 101 245–50. doi:10.1073/pnas.2536801100

-
94. Quan H; Bae, H.-B; Hur, Y.-H; Lee, K.-H; Lee, C.-H; Jang, E.-A; Jeong, S. Stearoyl lysophosphatidylcholine inhibits LPS-induced extracellular release of HMGB1 through the G2A/calcium/CaMKK β /AMPK pathway. *European journal of pharmacology*, **2019**, *852* 125–33. doi:10.1016/j.ejphar.2019.02.038
95. Peter C; Waibel, M; Radu, C. G; Yang, L. V; Witte, O. N; Schulze-Osthoff, K; Wesselborg, S; Lauber, K. Migration to apoptotic "find-me" signals is mediated via the phagocyte receptor G2A. *J. Biol. Chem.*, **2008**, *283* 5296–305. doi:10.1074/jbc.M706586200
96. Qin X; Qiu, C; Zhao, L. Lysophosphatidylcholine perpetuates macrophage polarization toward classically activated phenotype in inflammation. *Cellular immunology*, **2014**, *289* 185–90. doi:10.1016/j.cellimm.2014.04.010
97. Frasch S. C; Berry, K. Z; Fernandez-Boyanapalli, R; Jin, H.-S; Leslie, C; Henson, P. M; Murphy, R. C; Bratton, D. L. NADPH oxidase-dependent generation of lysophosphatidylserine enhances clearance of activated and dying neutrophils via G2A. *The Journal of biological chemistry*, **2008**, *283* 33736–49. doi:10.1074/jbc.M807047200
98. Frasch S. C; McNamee, E. N; Kominsky, D; Jedlicka, P; Jakubzick, C; Zemski Berry, K; Mack, M; Furuta, G. T; Lee, J. J; Henson, P. M; et al. G2A Signaling Dampens Colitic Inflammation via Production of IFN- γ . *J. Immunol.*, **2016**, *197* 1425–34. doi:10.4049/jimmunol.1600264
99. Parks B. W; Black, L. L; Zimmerman, K. A; Metz, A. E; Steele, C; Murphy-Ullrich, J. E; Kabarowski, J. H. CD36, but not G2A, modulates efferocytosis, inflammation, and fibrosis following bleomycin-induced lung injury. *J. Lipid Res.*, **2013**, *54* 1114–23. doi:10.1194/jlr.M035352
100. Kern K; Schäfer, S. M. G; Cohnen, J; Pierre, S; Osthues, T; Tarighi, N; Hohmann, S; Ferreiros, N; Brüne, B; Weigert, A; et al. The G2A Receptor Controls Polarization of Macrophage by Determining Their Localization Within the Inflamed Tissue. *Front. Immunol.*, **2018**, *9* 2261. doi:10.3389/fimmu.2018.02261
101. Zohn I. E; Klinger, M; Karp, X; Kirk, H; Symons, M; Chrzanowska-Wodnicka, M; Der, C. J; Kay, R. J. G2A is an oncogenic G protein-coupled receptor. *Oncogene*, **2000**, *19* 3866–77. doi:10.1038/sj.onc.1203731

-
102. Lin P; Ye, R. D. The Lysophospholipid Receptor G2A Activates a Specific Combination of G Proteins and Promotes Apoptosis. *J. Biol. Chem.*, **2003**, *278* 14379–86. doi:10.1074/jbc.M209101200
103. Bolick D. T; Whetzel, A. M; Skaffen, M; Deem, T. L; Lee, J; Hedrick, C. C. Absence of the G protein-coupled receptor G2A in mice promotes monocyte/endothelial interactions in aorta. *Circulation research*, **2007**, *100* 572–80. doi:10.1161/01.RES.0000258877.57836.d2
104. Huang Y.-H; Su, Y.-S; Chang, C.-J; Sun, W.-H. Heteromerization of G2A and OGR1 enhances proton sensitivity and proton-induced calcium signals. *Journal of Receptors and Signal Transduction*, **2016**, *36* 633–44. doi:10.3109/10799893.2016.1155064
105. Huang C. W; Tzeng, J. N; Chen, Y. J; Tsai, W. F; Chen, C. C; Sun, W. H. Nociceptors of dorsal root ganglion express proton-sensing G-protein-coupled receptors. *Molecular and cellular neurosciences*, **2007**, *36* 195–210. doi:10.1016/j.mcn.2007.06.010
106. Alles S. R; Garcia, E; Balasubramanyan, S; Jones, K; Tyson, J. R; Joy, T; Snutch, T. P; Smith, P. A. Peripheral nerve injury increases contribution of L-type calcium channels to synaptic transmission in spinal lamina II: Role of $\alpha 2\delta$ -1 subunits. *Molecular pain*, **2018**, *14*. doi:10.1177/1744806918765806
107. Su Y. S; Huang, Y. F; Wong, J; Lee, C. W; Hsieh, W. S; Sun, W. H. G2A as a Threshold Regulator of Inflammatory Hyperalgesia Modulates Chronic Hyperalgesia. *Journal of molecular neuroscience MN*, **2018**, *64* 39–50. doi:10.1007/s12031-017-1000-3
108. Salzer I; Ray, S; Schicker, K; Boehm, S. Nociceptor Signalling through ion Channel Regulation via GPCRs. *International journal of molecular sciences*, **2019**, *20*. doi:10.3390/ijms20102488
109. Hellstrom F; Gouveia-Figueira, S; Nording, M. L; Bjorklund, M; Fowler, C. J. Association between plasma concentrations of linoleic acid-derived oxylipins and the perceived pain scores in an exploratory study in women with chronic neck pain. *BMC musculoskeletal disorders*, **2016**, *17* 103. doi:10.1186/s12891-016-0951-9
110. Vangaveti V; Shashidhar, V; Collier, F; Hodge, J; Rush, C; Malabu, U; Baune, B; Kennedy, R. L. 9- and 13-HODE regulate fatty acid binding protein-4 in human macrophages, but does not involve HODE/GPR132 axis in PPAR-gamma regulation of FABP4. *Therapeutic advances in endocrinology and metabolism*, **2018**, *9* 137–50. doi:10.1177/2042018818759894

-
111. Vitali C; Dolcino, M; Del Papa, N; Minniti, A; Pignataro, F; Maglione, W; Lunardi, C; Puccetti, A. Gene Expression Profiles in Primary Sjögren's Syndrome With and Without Systemic Manifestations. *ACR open rheumatology*, **2019**, *1* 603–13.
doi:10.1002/acr2.11082
112. Osmers I; Smith, S. S; Parks, B. W; Yu, S; Srivastava, R; Wohler, J. E; Barnum, S. R; Kabarowski, J. H.S. Deletion of the G2A receptor fails to attenuate experimental autoimmune encephalomyelitis. *Journal of neuroimmunology*, **2009**, *207* 18–23.
doi:10.1016/j.jneuroim.2008.11.008
113. Brandolini L; d'Angelo, M; Antonosante, A; Allegretti, M; Cimini, A. Chemokine Signaling in Chemotherapy-Induced Neuropathic Pain. *International journal of molecular sciences*, **2019**, *20*. doi:10.3390/ijms20122904
114. Makker P. G; Duffy, S. S; Lees, J. G; Perera, C. J; Tonkin, R. S; Butovsky, O; Park, S. B; Goldstein, D; Moalem-Taylor, G. Characterisation of Immune and Neuroinflammatory Changes Associated with Chemotherapy-Induced Peripheral Neuropathy. *PloS one*, **2017**, *12* e0170814. doi:10.1371/journal.pone.0170814
115. Patwardhan A. M; Akopian, A. N; Ruparel, N. B; Diogenes, A; Weintraub, S. T; Uhlson, C; Murphy, R. C; Hargreaves, K. M. Heat generates oxidized linoleic acid metabolites that activate TRPV1 and produce pain in rodents. *The Journal of clinical investigation*, **2010**, *120* 1617–26. doi:10.1172/jci41678
116. Eskander M. A; Ruparel, S; Green, D. P; Chen, P. B; Por, E. D; Jeske, N. A; Gao, X; Flores, E. R; Hargreaves, K. M. Persistent Nociception Triggered by Nerve Growth Factor (NGF) Is Mediated by TRPV1 and Oxidative Mechanisms. *The Journal of neuroscience the official journal of the Society for Neuroscience*, **2015**, *35* 8593–603.
doi:10.1523/jneurosci.3993-14.2015
117. Attal N; Cruccu, G; Baron, R; Haanpää, M; Hansson, P; Jensen, T. S; Nurmikko, T. EFNS guidelines on the pharmacological treatment of neuropathic pain: 2010 revision. *European journal of neurology*, **2010**, *17* 1113–e88. doi:10.1111/j.1468-1331.2010.02999.x
118. Andrews N. A; Latremoliere, A; Basbaum, A. I; Mogil, J. S; Porreca, F; Rice, A. S; Woolf, C. J; Currie, G. L; Dworkin, R. H; Eisenach, J. C; et al. Ensuring transparency and minimization of methodologic bias in preclinical pain research. *Pain*, **2016**, *157* 901–9.
doi:10.1097/j.pain.0000000000000458

-
119. Decosterd I; Woolf, C. J. Spared nerve injury: an animal model of persistent peripheral neuropathic pain. *Pain*, **2000**, *87* 149–58. doi:10.1016/s0304-3959(00)00276-1
120. Pertin M; Gosselin, R.-D; Decosterd, I. The spared nerve injury model of neuropathic pain. *Methods in molecular biology (Clifton, N.J.)*, **2012**, *851* 205–12. doi:10.1007/978-1-61779-561-9_15
121. Sisignano M; Park, C. K; Angioni, C; Zhang, D. D; Hehn, C. von; Cobos, E. J; Ghasemlou, N; Xu, Z. Z; Kumaran, V; Lu, R; et al. 5,6-EET is released upon neuronal activity and induces mechanical pain hypersensitivity via TRPA1 on central afferent terminals. *J. Neurosci.*, **2012**, *32* 6364–72. doi:10.1523/jneurosci.5793-11.2012
122. Schuh C. D; Brenneis, C; Zhang, D. D; Angioni, C; Schreiber, Y; Ferreiros-Bouzas, N; Pierre, S; Henke, M; Linke, B; Nusing, R; et al. Prostacyclin regulates spinal nociceptive processing through cyclic adenosine monophosphate-induced translocation of glutamate receptors. *Anesthesiology*, **2014**, *120* 447–58. doi:10.1097/ALN.0b013e3182a76f74
123. Weigert A; Weichand, B; Sekar, D; Sha, W; Hahn, C; Mora, J; Ley, S; Essler, S; Dehne, N; Brüne, B. HIF-1 α is a negative regulator of plasmacytoid DC development in vitro and in vivo. *Blood*, **2012**, *120* 3001–6. doi:10.1182/blood-2012-03-417022
124. Weichand B; Popp, R; Dziumbila, S; Mora, J; Strack, E; Elwakeel, E; Frank, A.-C; Scholich, K; Pierre, S; Syed, S. N; et al. S1PR1 on tumor-associated macrophages promotes lymphangiogenesis and metastasis via NLRP3/IL-1 β . *The Journal of experimental medicine*, **2017**, *214* 2695–713. doi:10.1084/jem.20160392
125. Taylor S. C; Berkelman, T; Yadav, G; Hammond, M. A defined methodology for reliable quantification of Western blot data. *Mol. Biotechnol.*, **2013**, *55* 217–26. doi:10.1007/s12033-013-9672-6
126. Bradford M. M. A rapid and sensitive method for the quantitation of microgram quantities of protein utilizing the principle of protein-dye binding. *Anal. Biochem.*, **1976**, *72* 248–54.
127. Pierre S; Linke, B; Suo, J; Tarighi, N; Del Turco, D; Thomas, D; Ferreiros, N; Stegner, D; Frolich, S; Sisignano, M; et al. GPVI and Thromboxane Receptor on Platelets Promote Proinflammatory Macrophage Phenotypes during Cutaneous Inflammation. *The Journal of investigative dermatology*, **2017**, *137* 686–95. doi:10.1016/j.jid.2016.09.036

-
128. Linke B; Pierre, S; Coste, O; Angioni, C; Becker, W; Maier, T. J; Steinhilber, D; Wittpoth, C; Geisslinger, G; Scholich, K. Toponomics analysis of drug-induced changes in arachidonic acid-dependent signaling pathways during spinal nociceptive processing. *Journal of proteome research*, **2009**, 8 4851–9. doi:10.1021/pr900106v
129. Linke B; Schreiber, Y; Picard-Willems, B; Slattery, P; Nusing, R. M; Harder, S; Geisslinger, G; Scholich, K. Activated Platelets Induce an Anti-Inflammatory Response of Monocytes/Macrophages through Cross-Regulation of PGE2 and Cytokines. *Mediators of inflammation*, **2017**, 2017 1463216. doi:10.1155/2017/1463216
130. Justus C. R; Leffler, N; Ruiz-Echevarria, M; Yang, L. V. In vitro Cell Migration and Invasion Assays. *Journal of Visualized Experiments JoVE*, **2014**. doi:10.3791/51046
131. Ruparel S; Henry, M. A; Akopian, A; Patil, M; Zeldin, D. C; Roman, L; Hargreaves, K. M. Plasticity of cytochrome P450 isozyme expression in rat trigeminal ganglia neurons during inflammation. *Pain*, **2012**, 153 2031–9. doi:10.1016/j.pain.2012.04.027
132. Buczynski M. W; Svensson, C. I; Dumlao, D. S; Fitzsimmons, B. L; Shim, J.-H; Scherbart, T. J; Jacobsen, F. E; Hua, X.-Y; Yaksh, T. L; Dennis, E. A. Inflammatory hyperalgesia induces essential bioactive lipid production in the spinal cord. *Journal of neurochemistry*, **2010**, 114 981–93. doi:10.1111/j.1471-4159.2010.06815.x
133. Moore N. Coronary Risks Associated with Diclofenac and Other NSAIDs: An Update. *Drug safety*, **2020**. doi:10.1007/s40264-019-00900-8
134. Rubin P; Dubé, L; Braeckman, R; Swanson, L; Hansen, R; Albert, D; Carter, G. Pharmacokinetics, safety, and ability to diminish leukotriene synthesis by zileuton, an inhibitor of 5-lipoxygenase, **1991** 103–16.
135. Saul D; Weber, M; Zimmermann, M. H; Kosinsky, R. L; Hoffmann, D. B; Menger, B; Taudien, S; Lehmann, W; Komrakova, M; Sehmisch, S. Effect of the lipoxygenase inhibitor baicalein on bone tissue and bone healing in ovariectomized rats. *Nutrition & metabolism*, **2019**, 16 4. doi:10.1186/s12986-018-0327-2
136. Brenneis C; Sisignano, M; Coste, O; Altenrath, K; Fischer, M. J; Angioni, C; Fleming, I; Brandes, R. P; Reeh, P. W; Woolf, C. J; et al. Soluble epoxide hydrolase limits mechanical hyperalgesia during inflammation. *Molecular pain*, **2011**, 7 78. doi:10.1186/1744-8069-7-78
137. Zhang J. Y; Kowal, D. M; Nawoschik, S. P; Dunlop, J; Pausch, M. H; Peri, R. Development of an improved IP(1) assay for the characterization of 5-HT(2C) receptor

-
- ligands. *Assay and drug development technologies*, **2010**, *8* 106–13.
doi:10.1089/adt.2009.0205
138. Trinquet E; Fink, M; Bazin, H; Grillet, F; Maurin, F; Bourrier, E; Ansanay, H; Leroy, C; Michaud, A; Durroux, T; et al. D-myo-inositol 1-phosphate as a surrogate of D-myo-inositol 1,4,5-tris phosphate to monitor G protein-coupled receptor activation. *Analytical biochemistry*, **2006**, *358* 126–35. doi:10.1016/j.ab.2006.08.002
139. Bergsdorf C; Kropp-Goerkis, C; Kaehler, I; Ketscher, L; Boemer, U; Parczyk, K; Bader, B. A one-day, dispense-only IP-One HTRF assay for high-throughput screening of Galphaq protein-coupled receptors: towards cells as reagents. *Assay and drug development technologies*, **2008**, *6* 39–53. doi:10.1089/adt.2007.108
140. Degorce F; Card, A; Soh, S; Trinquet, E; Knapik, G. P; Xie, B. HTRF: A technology tailored for drug discovery - a review of theoretical aspects and recent applications. *Current chemical genomics*, **2009**, *3* 22–32. doi:10.2174/1875397300903010022
141. Treutlein E.-M; Kern, K; Weigert, A; Tarighi, N; Schuh, C.-D; Nüsing, R. M; Schreiber, Y; Ferreirós, N; Brüne, B; Geisslinger, G; et al. The prostaglandin E2 receptor EP3 controls CC-chemokine ligand 2-mediated neuropathic pain induced by mechanical nerve damage. *The Journal of biological chemistry*, **2018**, *293* 9685–95.
doi:10.1074/jbc.RA118.002492
142. Kallenborn-Gerhardt W; Hohmann, S. W; Syhr, K. M; Schroder, K; Sisignano, M; Weigert, A; Lorenz, J. E; Lu, R; Brune, B; Brandes, R. P; et al. Nox2-dependent signaling between macrophages and sensory neurons contributes to neuropathic pain hypersensitivity. *Pain*, **2014**, *155* 2161–70. doi:10.1016/j.pain.2014.08.013
143. Livak K. J; Schmittgen, T. D. Analysis of relative gene expression data using real-time quantitative PCR and the 2(-Delta Delta C(T)) Method. *Methods (San Diego, Calif.)*, **2001**, *25* 402–8. doi:10.1006/meth.2001.1262
144. Grienberger C; Konnerth, A. Imaging calcium in neurons. *Neuron*, **2012**, *73* 862–85.
doi:10.1016/j.neuron.2012.02.011
145. Schmitz K; Wilken-Schmitz, A; Vasic, V; Brunkhorst, R; Schmidt, M; Tegeder, I. Progranulin deficiency confers resistance to autoimmune encephalomyelitis in mice. *Cell Mol. Immunol.*, **2019**. doi:10.1038/s41423-019-0274-5
146. Scholz J; Abele, A; Marian, C; Häussler, A; Herbert, T. A; Woolf, C. J; Tegeder, I. Low-dose methotrexate reduces peripheral nerve injury-evoked spinal microglial

-
- activation and neuropathic pain behavior in rats. *Pain*, **2008**, *138* 130–42.
doi:10.1016/j.pain.2007.11.019
147. Münch C; Harper, J. W. Mitochondrial unfolded protein response controls matrix pre-RNA processing and translation. *Nature*, **2016**, *534* 710–3. doi:10.1038/nature18302
148. Klann K; Tascher, G; Münch, C. Functional Translatome Proteomics Reveal Converging and Dose-Dependent Regulation by mTORC1 and eIF2 α . *Molecular Cell*, **2019**. doi:10.1016/j.molcel.2019.11.010
149. Sisignano M; Angioni, C; Park, C. K; Meyer Dos Santos, S; Jordan, H; Kuzikov, M; Liu, D; Zinn, S; Hohman, S. W; Schreiber, Y; et al. Targeting CYP2J to reduce paclitaxel-induced peripheral neuropathic pain. *Proc. Natl. Acad. Sci. U S A*, **2016**, *113* 12544–9. doi:10.1073/pnas.1613246113
150. Guo S. H; Lin, J. P; Huang, L. E; Yang, Y; Chen, C. Q; Li, N. N; Su, M. Y; Zhao, X; Zhu, S. M; Yao, Y. X. Silencing of spinal Trpv1 attenuates neuropathic pain in rats by inhibiting CAMKII expression and ERK2 phosphorylation. *Scientific reports*, **2019**, *9* 2769. doi:10.1038/s41598-019-39184-4
151. Gavva N. R; Bannon, A. W; Surapaneni, S; Hovland, D. N., Jr; Lehto, S. G; Gore, A; Juan, T; Deng, H; Han, B; Klionsky, L; et al. The vanilloid receptor TRPV1 is tonically activated in vivo and involved in body temperature regulation. *The Journal of neuroscience the official journal of the Society for Neuroscience*, **2007**, *27* 3366–74. doi:10.1523/jneurosci.4833-06.2007
152. Gavva N. R; Bannon, A. W; Hovland, D. N., Jr; Lehto, S. G; Klionsky, L; Surapaneni, S; Immke, D. C; Henley, C; Arik, L; Bak, A; et al. Repeated administration of vanilloid receptor TRPV1 antagonists attenuates hyperthermia elicited by TRPV1 blockade. *The Journal of pharmacology and experimental therapeutics*, **2007**, *323* 128–37. doi:10.1124/jpet.107.125674
153. Zinn S; Sisignano, M; Kern, K; Pierre, S; Tunaru, S; Jordan, H; Suo, J; Treutlein, E.-M; Angioni, C; Ferreiros, N; et al. The leukotriene B4 receptors BLT1 and BLT2 form an antagonistic sensitizing system in peripheral sensory neurons. *The Journal of biological chemistry*, **2017**, *292* 6123–34. doi:10.1074/jbc.M116.769125
154. Chen Y.-J; Huang, C.-W; Lin, C.-S; Chang, W.-H; Sun, W.-H. Expression and function of proton-sensing G-protein-coupled receptors in inflammatory pain. *Molecular pain*, **2009**, *5* 39. doi:10.1186/1744-8069-5-39

-
155. Zheng F. Y; Xiao, W.-H; Bennett, G. J. The response of spinal microglia to chemotherapy-evoked painful peripheral neuropathies is distinct from that evoked by traumatic nerve injuries. *Neuroscience*, **2011**, *176* 447–54.
doi:10.1016/j.neuroscience.2010.12.052
156. Colleoni M; Sacerdote, P. Murine models of human neuropathic pain. *Biochimica et biophysica acta*, **2010**, *1802* 924–33. doi:10.1016/j.bbadis.2009.10.012
157. McMahon S. B; Bennett, D. L.H; Bevan, S. Inflammatory mediators and modulators of pain, **2006** 49–72. doi:10.1016/B0-443-07287-6/50008-4
158. Kiguchi N; Kobayashi, D; Saika, F; Matsuzaki, S; Kishioka, S. Pharmacological Regulation of Neuropathic Pain Driven by Inflammatory Macrophages. *International journal of molecular sciences*, **2017**, *18*. doi:10.3390/ijms18112296
159. Christensen J. E; Andreasen, S. O; Christensen, J. P; Thomsen, A. R. CD11b expression as a marker to distinguish between recently activated effector CD8(+) T cells and memory cells. *International immunology*, **2001**, *13* 593–600.
doi:10.1093/intimm/13.4.593
160. Waddell L. A; Lefevre, L; Bush, S. J; Raper, A; Young, R; Lisowski, Z. M; McCulloch, M. E. B; Muriuki, C; Sauter, K. A; Clark, E. L; et al. ADGRE1 (EMR1, F4/80) Is a Rapidly-Evolving Gene Expressed in Mammalian Monocyte-Macrophages. *Frontiers in immunology*, **2018**, *9* 2246. doi:10.3389/fimmu.2018.02246
161. Yu X; Liu, H; Hamel, K. A; Morvan, M. G; Yu, S; Leff, J; Guan, Z; Braz, J. M; Basbaum, A. I. Dorsal root ganglion macrophages contribute to both the initiation and persistence of neuropathic pain. *Nat Commun*, **2020**, *11* 1–12. doi:10.1038/s41467-019-13839-2
162. Hu P; Bembrick, A. L; Keay, K. A; McLachlan, E. M. Immune cell involvement in dorsal root ganglia and spinal cord after chronic constriction or transection of the rat sciatic nerve. *Brain, Behavior, and Immunity*, **2007**, *21* 599–616.
doi:10.1016/j.bbi.2006.10.013
163. Dubový P; Klusáková, I; Hradilová-Svíženská, I; Joukal, M; Boadas-Vaello, P. Activation of Astrocytes and Microglial Cells and CCL2/CCR2 Upregulation in the Dorsolateral and Ventrolateral Nuclei of Periaqueductal Gray and Rostral Ventromedial Medulla Following Different Types of Sciatic Nerve Injury. *Front. Cell Neurosci.*, **2018**, *12* 40. doi:10.3389/fncel.2018.00040

-
164. Zhao H; Alam, A; Chen, Q; A Eusman, M; Pal, A; Eguchi, S; Wu, L; Ma, D. The role of microglia in the pathobiology of neuropathic pain development: what do we know? *British journal of anaesthesia*, **2017**, *118* 504–16. doi:10.1093/bja/aex006
165. Bush T. G; Puvanachandra, N; Horner, C. H; Polito, A; Ostenfeld, T; Svendsen, C. N; Mucke, L; Johnson, M. H; Sofroniew, M. V. Leukocyte Infiltration, Neuronal Degeneration, and Neurite Outgrowth after Ablation of Scar-Forming, Reactive Astrocytes in Adult Transgenic Mice. *Neuron*, **1999**, *23* 297–308. doi:10.1016/S0896-6273(00)80781-3
166. Pekny M; Pekna, M. Astrocyte intermediate filaments in CNS pathologies and regeneration. *The Journal of pathology*, **2004**, *204* 428–37. doi:10.1002/path.1645
167. Huh Y; Ji, R.-R; Chen, G. Neuroinflammation, Bone Marrow Stem Cells, and Chronic Pain. *Front. Immunol.*, **2017**, *8* 1014. doi:10.3389/fimmu.2017.01014
168. Davidson E. B; van Caam, A. P; Vitters, E. L; Bennink, M. B; Thijssen, E; van den Berg, W. B; Koenders, M. I; van Lent, P. L; van de Loo, F. A; van der Kraan, P. M. TGF- β is a potent inducer of nerve growth factor in articular cartilage via the ALK5-Smad2/3 pathway. potential role in OA related pain? *Osteoarthritis and cartilage*, **2015**, *23* A62. doi:10.1016/j.joca.2015.02.129
169. Echeverry S; Shi, X. Q; Haw, A; Liu, H; Zhang, Z.-w; Zhang, J. Transforming growth factor-beta1 impairs neuropathic pain through pleiotropic effects. *Molecular pain*, **2009**, *5* 16. doi:10.1186/1744-8069-5-16
170. Wong C. K; Ho, C. Y; Ko, F. W; Chan, C. H; Ho, A. S; Hui, D. S; Lam, C. W. Proinflammatory cytokines (IL-17, IL-6, IL-18 and IL-12) and Th cytokines (IFN-gamma, IL-4, IL-10 and IL-13) in patients with allergic asthma. *Clinical and experimental immunology*, **2001**, *125* 177–83. doi:10.1046/j.1365-2249.2001.01602.x
171. Frink M; Hsieh, Y.-C; Hsieh, C.-H; Pape, H.-C; Choudhry, M. A; Schwacha, M. G; Chaudry, I. H. Keratinocyte-derived chemokine plays a critical role in the induction of systemic inflammation and tissue damage after trauma-hemorrhage. *Shock (Augusta, Ga.)*, **2007**, *28* 576–81. doi:10.1097/shk.0b013e31814b8e0d
172. Holmer S. M; Evans, K. S; Asfaw, Y. G; Saini, D; Schell, W. A; Ledford, J. G; Frothingham, R; Wright, J. R; Sempowski, G. D; Perfect, J. R. Impact of surfactant protein D, interleukin-5, and eosinophilia on Cryptococcosis. *Infection and immunity*, **2014**, *82* 683–93. doi:10.1128/IAI.00855-13

-
173. Rham C. de; Ferrari-Lacraz, S; Jendly, S; Schneiter, G; Dayer, J.-M; Villard, J. The proinflammatory cytokines IL-2, IL-15 and IL-21 modulate the repertoire of mature human natural killer cell receptors. *Arthritis research & therapy*, **2007**, 9 R125. doi:10.1186/ar2336
174. Kuwabara T; Ishikawa, F; Kondo, M; Kakiuchi, T. The Role of IL-17 and Related Cytokines in Inflammatory Autoimmune Diseases. *Mediators of inflammation*, **2017**, 2017 3908061. doi:10.1155/2017/3908061
175. Son D.-S; Parl, A. K; Rice, V. M; Khabele, D. Keratinocyte chemoattractant (KC)/human growth-regulated oncogene (GRO) chemokines and pro-inflammatory chemokine networks in mouse and human ovarian epithelial cancer cells. *Cancer biology & therapy*, **2007**, 6 1302–12. doi:10.4161/cbt.6.8.4506
176. Eik W; Marcon, S. S; Krupek, T; Previdelli, I. T. S; Pereira, O. C. N; Silva, M. A. R. C. P; Bazotte, R. B. Blood levels of pro-inflammatory and anti-inflammatory cytokines during an oral glucose tolerance test in patients with symptoms suggesting reactive hypoglycemia. *Brazilian journal of medical and biological research = Revista brasileira de pesquisas medicas e biologicas*, **2016**, 49. doi:10.1590/1414-431X20165195
177. Laedermann C. J; Pertin, M; Suter, M. R; Decosterd, I. Voltage-gated sodium channel expression in mouse DRG after SNI leads to re-evaluation of projections of injured fibers. *Mol. Pain*, **2014**, 10 19. doi:10.1186/1744-8069-10-19
178. Ji R. R; Xu, Z. Z; Wang, X; Lo, E. H. Matrix metalloprotease regulation of neuropathic pain. *Trends Pharmacol. Sci.*, **2009**, 30 336–40. doi:10.1016/j.tips.2009.04.002
179. Grace P. M; Gaudet, A. D; Staikopoulos, V; Maier, S. F; Hutchinson, M. R; Salvemini, D; Watkins, L. R. Nitroxidative Signaling Mechanisms in Pathological Pain. *Trends in neurosciences*, **2016**, 39 862–79. doi:10.1016/j.tins.2016.10.003
180. Patwardhan A. M; Scotland, P. E; Akopian, A. N; Hargreaves, K. M. Activation of TRPV1 in the spinal cord by oxidized linoleic acid metabolites contributes to inflammatory hyperalgesia. *Proc. Natl. Acad. Sci. U S A*, **2009**, 106 18820–4. doi:10.1073/pnas.0905415106
181. Green D. P; Ruparel, S; Roman, L; Henry, M. A; Hargreaves, K. M. Role of endogenous TRPV1 agonists in a postburn pain model of partial-thickness injury. *Pain*, **2013**, 154 2512–20. doi:10.1016/j.pain.2013.07.040

-
182. Ruparel S; Green, D; Chen, P; Hargreaves, K. M. The cytochrome P450 inhibitor, ketoconazole, inhibits oxidized linoleic acid metabolite-mediated peripheral inflammatory pain. *Molecular pain*, **2012**,
183. Zimmer B; Angioni, C; Osthues, T; Toewe, A; Thomas, D; Pierre, S. C; Geisslinger, G; Scholich, K; Sisignano, M. The oxidized linoleic acid metabolite 12,13-DiHOME mediates thermal hyperalgesia during inflammatory pain. *Biochim. Biophys. Acta Mol. Cell. Biol. Lipids*, **2018**, 1863 669–78. doi:10.1016/j.bbalip.2018.03.012
184. Basso L; Altier, C. Transient Receptor Potential Channels in neuropathic pain. *Current opinion in pharmacology*, **2017**, 32 9–15. doi:10.1016/j.coph.2016.10.002
185. Lu Y.-C; Yeh, W.-C; Ohashi, P. S. LPS/TLR4 signal transduction pathway. *Cytokine*, **2008**, 42 145–51. doi:10.1016/j.cyto.2008.01.006
186. Wu T.-T; Chen, T.-L; Chen, R.-M. Lipopolysaccharide triggers macrophage activation of inflammatory cytokine expression, chemotaxis, phagocytosis, and oxidative ability via a toll-like receptor 4-dependent pathway: validated by RNA interference. *Toxicol. Lett.*, **2009**, 191 195–202. doi:10.1016/j.toxlet.2009.08.025
187. Kim H.-R; Lee, H.-S; Lee, K.-S; Jung, I. D; Kwon, M.-S; Kim, C.-H; Kim, S.-M; Yoon, M.-H; Park, Y.-M; Lee, S.-M; et al. An Essential Role for TAGLN2 in Phagocytosis of Lipopolysaccharide-activated Macrophages. *Sci. Rep. (Scientific Reports)*, **2017**, 7 1–13. doi:10.1038/s41598-017-09144-x
188. Jackson L; Cady, C. T; Cambier, J. C. TLR4-mediated signaling induces MMP9-dependent cleavage of B cell surface CD23. *J. Immunol.*, **2009**, 183 2585–92. doi:10.4049/jimmunol.0803660
189. Osthues T; Zimmer, B; Rimola, V; Klann, K; Schilling, K; Mathoor, P; Angioni, C; Weigert, A; Geisslinger, G; Münch, C; et al. The Lipid Receptor G2A (GPR132) Mediates Macrophage Migration in Nerve Injury-Induced Neuropathic Pain. *Cells*, **2020**, 9. doi:10.3390/cells9071740
190. Petit I; Jin, D; Rafii, S. The SDF-1-CXCR4 signaling pathway: a molecular hub modulating neo-angiogenesis. *Trends in immunology*, **2007**, 28 299–307. doi:10.1016/j.it.2007.05.007
191. Sánchez-Martín L; Estecha, A; Samaniego, R; Sánchez-Ramón, S; Vega, M. Á; Sánchez-Mateos, P. The chemokine CXCL12 regulates monocyte-macrophage

-
- differentiation and RUNX3 expression. *Blood*, **2011**, *117* 88–97. doi:10.1182/blood-2009-12-258186
192. Dufour A; Zucker, S; Sampson, N. S; Kuscu, C; Cao, J. Role of Matrix Metalloproteinase-9 Dimers in Cell Migration DESIGN OF INHIBITORY PEPTIDES. *J. Biol. Chem.*, **2010**, *285* 35944–56. doi:10.1074/jbc.M109.091769
193. Mason D. P; Kenagy, R. D; Hasenstab, D; Bowen-Pope, D. F; Seifert, R. A; Coats, S; Hawkins, S. M; Clowes, A. W. Matrix metalloproteinase-9 overexpression enhances vascular smooth muscle cell migration and alters remodeling in the injured rat carotid artery. *Circulation research*, **1999**, *85* 1179–85. doi:10.1161/01.res.85.12.1179
194. Cho A; Reidy, M. A. Matrix metalloproteinase-9 is necessary for the regulation of smooth muscle cell replication and migration after arterial injury. *Circulation research*, **2002**, *91* 845–51. doi:10.1161/01.res.0000040420.17366.2e
195. Gong Y; Hart, E; Shchurin, A; Hoover-Plow, J. Inflammatory macrophage migration requires MMP-9 activation by plasminogen in mice. *The Journal of clinical investigation*, **2008**, *118* 3012–24. doi:10.1172/JCI32750
196. Shubayev V. I; Angert, M; Dolkas, J; Campana, W. M; Palenscar, K; Myers, R. R. TNFalpha-induced MMP-9 promotes macrophage recruitment into injured peripheral nerve. *Molecular and cellular neurosciences*, **2006**, *31* 407–15. doi:10.1016/j.mcn.2005.10.011
197. Lakhan S. E; Avramut, M. Matrix metalloproteinases in neuropathic pain and migraine. *Pain Res Treat*, **2012**, *2012* 952906. doi:10.1155/2012/952906
198. Tanimura S; Takeda, K. ERK signalling as a regulator of cell motility. *J Biochem*, **2017**, *162* 145–54. doi:10.1093/jb/mvx048
199. Saika S; Okada, Y; Miyamoto, T; Yamanaka, O; Ohnishi, Y; Ooshima, A; Liu, C.-Y; Weng, D; Kao, W. W.-Y. Role of p38 MAP kinase in regulation of cell migration and proliferation in healing corneal epithelium. *Investigative ophthalmology & visual science*, **2004**, *45* 100–9. doi:10.1167/iovs.03-0700
200. Travnickova J; Nhim, S; Abdellaoui, N; Djouad, F; Nguyen-Chi, M; Parmeggiani, A; Kissa, K. *Macrophage plasticity is Rac signalling and MMP9 dependant*, **2019**,
201. Hu C; Zhou, H; Liu, Y; Huang, J; Liu, W; Zhang, Q; Tang, Q; Sheng, F; Li, G; Zhang, R. ROCK1 promotes migration and invasion of non-small-cell lung cancer cells through

-
- the PTEN/PI3K/FAK pathway. *International journal of oncology*, **2019**, 55 833–44.
doi:10.3892/ijo.2019.4864
202. Takeda Y; Matoba, K; Kawanami, D; Nagai, Y; Akamine, T; Ishizawa, S; Kanazawa, Y; Yokota, T; Utsunomiya, K. ROCK2 Regulates Monocyte Migration and Cell to Cell Adhesion in Vascular Endothelial Cells. *International journal of molecular sciences*, **2019**, 20. doi:10.3390/ijms20061331
203. Castellano E; Molina-Arcas, M; Krygowska, A. A; East, P; Warne, P; Nicol, A; Downward, J. RAS signalling through PI3-Kinase controls cell migration via modulation of Reelin expression. *Nature communications*, **2016**, 7 11245.
doi:10.1038/ncomms11245
204. Ivics Z; Hackett, P. B; Plasterk, R. H; Izsvák, Z. Molecular Reconstruction of Sleeping Beauty, a Tc1-like Transposon from Fish, and Its Transposition in Human Cells, **1997**.
doi:10.1016/S0092-8674(00)80436-5
205. Izsvák Z; Ivics, Z. Sleeping beauty transposition: biology and applications for molecular therapy. *Molecular therapy the journal of the American Society of Gene Therapy*, **2004**, 9 147–56. doi:10.1016/j.ymthe.2003.11.009
206. Trinquet E; Bouhelal, R; Dietz, M. Monitoring Gq-coupled receptor response through inositol phosphate quantification with the IP-One assay. *Expert opinion on drug discovery*, **2011**, 6 981–94. doi:10.1517/17460441.2011.608658
207. Kirk S.L; Karlik, S.J. VEGF and vascular changes in chronic neuroinflammation. *Journal of Autoimmunity*, **2003**, 21 353–63. doi:10.1016/S0896-8411(03)00139-2
208. McMahon S. B; La Russa, F; Bennett, D. L. H. Crosstalk between the nociceptive and immune systems in host defence and disease. *Nat Rev Neurosci*, **2015**, 16 389–402.
doi:10.1038/nrn3946
209. Lindborg J. A; Niemi, J. P; Howarth, M. A; Liu, K. W; Moore, C. Z; Mahajan, D; Zigmund, R. E. Molecular and cellular identification of the immune response in peripheral ganglia following nerve injury. *J. Neuroinflammation (Journal of Neuroinflammation)*, **2018**, 15 1–17. doi:10.1186/s12974-018-1222-5
210. Suo J; Linke, B; Meyer dos Santos, S; Pierre, S; Stegner, D; Zhang, D. D; Denis, C. V; Geisslinger, G; Nieswandt, B; Scholich, K. Neutrophils mediate edema formation but not mechanical allodynia during zymosan-induced inflammation. *Journal of leukocyte biology*, **2014**, 96 133–42. doi:10.1189/jlb.3A1213-628R

-
211. Engels F; Willems, H; Nijkamp, F. P. Cyclooxygenase-catalyzed formation of 9-hydroxylinoleic acid by guinea pig alveolar macrophages under non-stimulated conditions. *FEBS letters*, **1986**, 209 249–53.
212. Fang X; Kaduce, T. L; Spector, A. A. 13-(S)-Hydroxyoctadecadienoic acid (13-HODE) incorporation and conversion to novel products by endothelial cells. *J. Lipid Res.*, **1999**, 40 699–707.
213. Ramsden C. E; Ringel, A; Feldstein, A. E; Taha, A. Y; MacIntosh, B. A; Hibbeln, J. R; Majchrzak-Hong, S. F; Faurot, K. R; Rapoport, S. I; Cheon, Y; et al. Lowering dietary linoleic acid reduces bioactive oxidized linoleic acid metabolites in humans. *Prostaglandins, leukotrienes, and essential fatty acids*, **2012**, 4-5 135–41.
214. Sisignano M; Angioni, C; Ferreiros, N; Schuh, C. D; Suo, J; Schreiber, Y; Dawes, J. M; Antunes-Martins, A; Bennett, D. L; McMahan, S. B; et al. Synthesis of lipid mediators during UVB-induced inflammatory hyperalgesia in rats and mice. *PloS one*, **2013**, 8 e81228. doi:10.1371/journal.pone.0081228
215. Oliw E. H. Oxygenation of polyunsaturated fatty acids by cytochrome P450 monooxygenases. *Progress in lipid research*, **1994**, 33 329–54.
216. Green F. A. Generation and metabolism of lipoxygenase products in normal and membrane-damaged cultured human keratinocytes. *The Journal of investigative dermatology*, **1989**, 93 486–91.
217. Meyer G. R. de; Bult, H; Verbeuren, T. J; Herman, A. G. The role of endothelial cells in the relaxations induced by 13-hydroxy- and 13-hydroperoxylinoleic acid in canine arteries. *British journal of pharmacology*, **1992**, 107 597–603.
218. Jisaka M; Kim, R. B; Boeglin, W. E; Nanney, L. B; Brash, A. R. Molecular cloning and functional expression of a phorbol ester-inducible 8S-lipoxygenase from mouse skin. *The Journal of biological chemistry*, **1997**, 272 24410–6.
219. Kaduce T. L; Figard, P. H; Leifur, R; Spector, A. A. Formation of 9-hydroxyoctadecadienoic acid from linoleic acid in endothelial cells. *The Journal of biological chemistry*, **1989**, 264 6823–30.
220. Gregus A. M; Dumlao, D. S; Wei, S. C; Norris, P. C; Catella, L. C; Meyerstein, F. G; Buczynski, M. W; Steinauer, J. J; Fitzsimmons, B. L; Yaksh, T. L; et al. Systematic analysis of rat 12/15-lipoxygenase enzymes reveals critical role for spinal eLOX3 hepoxilin synthase activity in inflammatory hyperalgesia. *FASEB journal official*

-
- publication of the Federation of American Societies for Experimental Biology*, **2013**, 27 1939–49. doi:10.1096/fj.12-217414
221. Yoshida Y; Niki, E. Bio-markers of lipid peroxidation in vivo. *BioFactors (Oxford, England)*, **2006**, 27 195–202.
222. Berta T; Perrin, F. E; Pertin, M; Tonello, R; Liu, Y.-C; Chamesian, A; Kato, A. C; Ji, R.-R; Decosterd, I. Gene Expression Profiling of Cutaneous Injured and Non-Injured Nociceptors in SNI Animal Model of Neuropathic Pain. *Scientific Reports*, **2017**, 7 9367. doi:10.1038/s41598-017-08865-3
223. Geis C; Geuss, E; Sommer, C; Schmidt, H. H. H. W; Kleinschnitz, C. NOX4 is an early initiator of neuropathic pain. *Experimental neurology*, **2017**, 288 94–103. doi:10.1016/j.expneurol.2016.11.008
224. Staunton C. A; Barrett-Jolley, R; Djouhri, L; Thippeswamy, T. Inducible nitric oxide synthase inhibition by 1400W limits pain hypersensitivity in a neuropathic pain rat model. *Experimental physiology*, **2018**, 103 535–44. doi:10.1113/EP086764
225. Topham L; Gregoire, S; Kang, H; Salmon-Divon, M; Lax, E; Millecamps, M; Szyf, M; Stone, L. The Transition from Acute to Chronic Pain: Dynamic Epigenetic Reprogramming of the Mouse Prefrontal Cortex up to One Year Following Nerve Injury. *bioRxiv*, **2020** 2020.02.22.956128. doi:10.1101/2020.02.22.956128
226. Alba J. de; Clayton, N. M; Collins, S. D; Colthup, P; Chessell, I; Knowles, R. G. GW274150, a novel and highly selective inhibitor of the inducible isoform of nitric oxide synthase (iNOS), shows analgesic effects in rat models of inflammatory and neuropathic pain. *Pain*, **2006**, 120 170–81. doi:10.1016/j.pain.2005.10.028
227. Lees J. G; Duffy, S. S; Moalem-Taylor, G. Immunotherapy targeting cytokines in neuropathic pain. *Frontiers in pharmacology*, **2013**, 4 142. doi:10.3389/fphar.2013.00142
228. del Rey A; Yau, H.-J; Randolph, A; Centeno, M. V; Wildmann, J; Martina, M; Besedovsky, H. O; Apkarian, A. V. Chronic neuropathic pain-like behavior correlates with IL-1 β expression and disrupts cytokine interactions in the hippocampus. *Pain*, **2011**, 152 2827–35. doi:10.1016/j.pain.2011.09.013
229. Clark A. K; Old, E. A; Malcangio, M. Neuropathic pain and cytokines: current perspectives. *Journal of Pain Research*, **2013**, 6 803–14. doi:10.2147/JPR.S53660

-
230. Katz Y; Nadiv, O; Beer, Y. Interleukin-17 enhances tumor necrosis factor α -induced synthesis of interleukins 1, 6, and 8 in skin and synovial fibroblasts: A possible role as a “fine-tuning cytokine” in inflammation processes. *Arthritis & Rheumatism*, **2001**, *44* 2176–84. doi:10.1002/1529-0131(200109)44:9<2176:AID-ART371>3.0.CO;2-4
231. Shen F; Ruddy, M. J; Plamondon, P; Gaffen, S. L. Cytokines link osteoblasts and inflammation: microarray analysis of interleukin-17- and TNF-alpha-induced genes in bone cells. *Journal of leukocyte biology*, **2005**, *77* 388–99. doi:10.1189/jlb.0904490
232. Üçeyler N; Rogausch, J. P; Toyka, K. V; Sommer, C. Differential expression of cytokines in painful and painless neuropathies. *Neurology*, **2007**, *69* 42–9. doi:10.1212/01.wnl.0000265062.92340.a5
233. Ruohonen S; Khademi, M; Jagodic, M; Taskinen, H.-S; Olsson, T; Røyttä, M. Cytokine responses during chronic denervation. *Journal of neuroinflammation*, **2005**, *2* 26. doi:10.1186/1742-2094-2-26
234. Kim C. F; Moalem-Taylor, G. Interleukin-17 Contributes to Neuroinflammation and Neuropathic Pain Following Peripheral Nerve Injury in Mice. *The Journal of Pain*, **2011**, *12* 370–83. doi:10.1016/j.jpain.2010.08.003
235. Zhou Y.-Q; Liu, Z; Liu, Z.-H; Chen, S.-P; Li, M; Shahveranov, A; Ye, D.-W; Tian, Y.-K. Interleukin-6: an emerging regulator of pathological pain. *J. Neuroinflammation*, **2016**, *13* 141. doi:10.1186/s12974-016-0607-6
236. Jin X; Gereau, R. W. Acute p38-mediated modulation of tetrodotoxin-resistant sodium channels in mouse sensory neurons by tumor necrosis factor-alpha. *J. Neurosci.*, **2006**, *26* 246–55. doi:10.1523/JNEUROSCI.3858-05.2006
237. Murphy P. G; Grondin, J; Altares, M; Richardson, P. M. Induction of interleukin-6 in axotomized sensory neurons. *The Journal of neuroscience the official journal of the Society for Neuroscience*, **1995**, *15* 5130–8. doi:10.1523/JNEUROSCI.15-07-05130.1995
238. Guerrero A. R; Uchida, K; Nakajima, H; Watanabe, S; Nakamura, M; Johnson, W. E. B; Baba, H. Blockade of interleukin-6 signaling inhibits the classic pathway and promotes an alternative pathway of macrophage activation after spinal cord injury in mice. *J Neuroinflammation*, **2012**, *9* 1–16. doi:10.1186/1742-2094-9-40

-
239. Sun L; He, C; Nair, L; Yeung, J; Egwuagu, C. E. Interleukin 12 (IL-12) family cytokines: Role in immune pathogenesis and treatment of CNS autoimmune disease. *Cytokine*, **2015**, 75 249–55. doi:10.1016/j.cyto.2015.01.030
240. Pahan K; Sheikh, F. G; Liu, X; Hilger, S; McKinney, M; Petro, T. M. Induction of nitric oxide synthase and activation of NF-kappaB by interleukin-12 p40 in microglial cells. *The Journal of biological chemistry*, **2001**, 276 7899–905. doi:10.1074/jbc.M008262200
241. Hikawa N; Ishikawa, Y; Takenaka, T. Interleukin-12 p40-homodimer production in sensory dorsal root ganglion neurons. *Neuroscience*, **2004**, 129 75–83. doi:10.1016/j.neuroscience.2004.07.035
242. Chattopadhyay S; Myers, R. R; Janes, J; Shubayev, V. Cytokine regulation of MMP-9 in peripheral glia: implications for pathological processes and pain in injured nerve. *Brain, behavior, and immunity*, **2007**, 21 561–8. doi:10.1016/j.bbi.2006.10.015
243. Kawasaki Y; Xu, Z.-Z; Wang, X; Park, J. Y; Zhuang, Z.-Y; Tan, P.-H; Gao, Y.-J; Roy, K; Corfas, G; Lo, E. H; et al. Distinct roles of matrix metalloproteases in the early- and late-phase development of neuropathic pain. *Nature Medicine*, **2008**, 14 331–6. doi:10.1038/nm1723
244. Kobayashi H; Chattopadhyay, S; Kato, K; Dolkas, J; Kikuchi, S.-I; Myers, R. R; Shubayev, V. I. MMPs initiate Schwann cell-mediated MBP degradation and mechanical nociception after nerve damage. *Molecular and cellular neurosciences*, **2008**, 39 619–27. doi:10.1016/j.mcn.2008.08.008
245. Tan T. K; Zheng, G; Hsu, T.-T; Lee, S. R; Zhang, J; Zhao, Y; Tian, X; Wang, Y; Wang, Y. M; Cao, Q; et al. Matrix metalloproteinase-9 of tubular and macrophage origin contributes to the pathogenesis of renal fibrosis via macrophage recruitment through osteopontin cleavage. *Laboratory investigation; a journal of technical methods and pathology*, **2013**, 93 434–49. doi:10.1038/labinvest.2013.3
246. Yu X; Lin, S.-G; Huang, X. R; Bacher, M; Leng, L; Bucala, R; Lan, H. Y. Macrophage migration inhibitory factor induces MMP-9 expression in macrophages via the MEK-ERK MAP kinase pathway. *Journal of interferon & cytokine research the official journal of the International Society for Interferon and Cytokine Research*, **2007**, 27 103–9. doi:10.1089/jir.2006.0054

-
247. Zhu G; Cheng, Z; Huang, Y; Zheng, W; Yang, S; Lin, C; Ye, J. MyD88 mediates colorectal cancer cell proliferation, migration and invasion via NF- κ B/AP-1 signaling pathway. *International journal of molecular medicine*, **2019**. doi:10.3892/ijmm.2019.4390
248. Lee J. Y; Ye, J; Gao, Z; Youn, H. S; Lee, W. H; Zhao, L; Sizemore, N; Hwang, D. H. Reciprocal modulation of Toll-like receptor-4 signaling pathways involving MyD88 and phosphatidylinositol 3-kinase/AKT by saturated and polyunsaturated fatty acids. *The Journal of biological chemistry*, **2003**, 278 37041–51. doi:10.1074/jbc.M305213200
249. Berger H; Breuer, M; Peradziryi, H; Podleschny, M; Jacob, R; Borchers, A. PTK7 localization and protein stability is affected by canonical Wnt ligands. *Journal of cell science*, **2017**, 130 1890–903. doi:10.1242/jcs.198580
250. Peradziryi H; Tolwinski, N. S; Borchers, A. The many roles of PTK7: A versatile regulator of cell–cell communication. *Archives of Biochemistry and Biophysics*, **2012**, 524 71–6. doi:10.1016/j.abb.2011.12.019
251. Huang L; Li, L; Yang, T; Li, W; Song, L; Meng, X; Gu, Q; Xiong, C; He, J. Transgelin as a potential target in the reversibility of pulmonary arterial hypertension secondary to congenital heart disease. *Journal of cellular and molecular medicine*, **2018**, 22 6249–61. doi:10.1111/jcmm.13912
252. Aldeiri B; Roostalu, U; Albertini, A; Wong, J; Morabito, A; Cossu, G. Transgelin-expressing myofibroblasts orchestrate ventral midline closure through TGF β signalling. *Development (Cambridge, England)*, **2017**, 144 3336–48. doi:10.1242/dev.152843
253. Jo S; Kim, H.-R; Mun, Y; Jun, C.-D. Transgelin-2 in immunity: Its implication in cell therapy. *Journal of leukocyte biology*, **2018**, 104 903–10. doi:10.1002/JLB.MR1117-470R
254. Zhou M; Xu, W; Wang, J; Yan, J; Shi, Y; Zhang, C; Ge, W; Wu, J; Du, P; Chen, Y. Boosting mTOR-dependent autophagy via upstream TLR4-MyD88-MAPK signalling and downstream NF- κ B pathway quenches intestinal inflammation and oxidative stress injury. *EBioMedicine*, **2018**, 35 345–60. doi:10.1016/j.ebiom.2018.08.035
255. Liu Z; Jiang, Y; Li, Y; Wang, J; Fan, L; Scott, M. J; Xiao, G; Li, S; Billiar, T. R; Wilson, M. A; et al. TLR4 Signaling Augments Monocyte Chemotaxis by Regulating G Protein–Coupled Receptor Kinase 2 Translocation. *The Journal of Immunology*, **2013**, 191 857–64. doi:10.4049/jimmunol.1300790
256. Arandjelovic S; Perry, J. S. A; Lucas, C. D; Penberthy, K. K; Kim, T.-H; Zhou, M; Rosen, D. A; Chuang, T.-Y; Bettina, A. M; Shankman, L. S; et al. A noncanonical role for

-
- the engulfment gene ELMO1 in neutrophils that promotes inflammatory arthritis. *Nature immunology*, **2019**, *20* 141–51. doi:10.1038/s41590-018-0293-x
257. Liu Z; Yu, J; Wu, R; Tang, S; Cai, X; Guo, G; Chen, S. Rho/ROCK Pathway Regulates Migration and Invasion of Esophageal Squamous Cell Carcinoma by Regulating Caveolin-1. *Medical science monitor international medical journal of experimental and clinical research*, **2017**, *23* 6174–85. doi:10.12659/msm.905820
258. Srinivasan S; Das, S; Surve, V; Srivastava, A; Kumar, S; Jain, N; Sawant, A; Nayak, C; Purwar, R. Blockade of ROCK inhibits migration of human primary keratinocytes and malignant epithelial skin cells by regulating actomyosin contractility. *Sci Rep*, **2019**, *9* 1–13. doi:10.1038/s41598-019-56447-2
259. Frasch S. C; Fernandez-Boyanapalli, R. F; Berry, K. Z; Leslie, C. C; Bonventre, J. V; Murphy, R. C; Henson, P. M; Bratton, D. L. Signaling via macrophage G2A enhances efferocytosis of dying neutrophils by augmentation of Rac activity. *The Journal of biological chemistry*, **2011**, *286* 12108–22. doi:10.1074/jbc.M110.181800
260. Zhang Y.-K; Huang, Z.-J; Liu, S; Liu, Y.-P; Song, A. A; Song, X.-J. WNT signaling underlies the pathogenesis of neuropathic pain in rodents. *The Journal of Clinical Investigation*, **2013**, *123* 2268–86. doi:10.1172/JCI65364
261. Yuan S; Shi, Y; Tang, S.-J. Wnt signaling in the pathogenesis of multiple sclerosis-associated chronic pain. *Journal of neuroimmune pharmacology the official journal of the Society on NeuroImmune Pharmacology*, **2012**, *7* 904–13. doi:10.1007/s11481-012-9370-3
262. Yang L. V; Radu, C. G; Wang, L; Riedinger, M; Witte, O. N. Gi-independent macrophage chemotaxis to lysophosphatidylcholine via the immunoregulatory GPCR G2A. *Blood*, **2005**, *105* 1127–34. doi:10.1182/blood-2004-05-1916
263. Sedgwick A. E; D'Souza-Schorey, C. Wnt Signaling in Cell Motility and Invasion: Drawing Parallels between Development and Cancer. *Cancers*, **2016**, *8*. doi:10.3390/cancers8090080
264. Petrocellis L. de; Schiano Moriello, A; Imperatore, R; Cristino, L; Starowicz, K; Di Marzo, V. A re-evaluation of 9-HODE activity at TRPV1 channels in comparison with anandamide. *British journal of pharmacology*, **2012**, *167* 1643–51. doi:10.1111/j.1476-5381.2012.02122.x

-
265. Jain K. K. Cell therapy for pain. *Expert opinion on biological therapy*, **2008**, 8 1847–53. doi:10.1517/14712590802496951
266. Ogawa N; Terashima, T; Oka, K; Chan, L; Kojima, H. Gene therapy for neuropathic pain using dorsal root ganglion-targeted helper-dependent adenoviral vectors with GAD67 expression. *Pain reports*, **2018**, 3 e695. doi:10.1097/pr9.0000000000000695

Annex

Table 11. Overview of down- and upregulated proteins in untreated G2A-deficient compared to untreated wild-type BMDMs. Proteom screen was performed in 02/2019.

Downregulated		Upregulated	
A) <u>Immune system processes</u>			
Sos1	Regulation of actin cytoskeleton; Focal adhesion; B cell receptor, T cell receptor, Chemokine, FC epsilon RI, Ras and PI3K-Akt signaling pathway; Natural killer cell mediated cytotoxicity	C1qa	Complement and coagulation cascades
Tradd	NF-κB and TNF signaling pathway	Plaur	
		Serpib2	
B) <u>Lipid metabolic processes</u>			
		Gpx7	Glutathione metabolism; Arachidonic acid metabolism
C) <u>Migration</u>			
Dock2	Chemokine signaling pathway; Fc gamma R-mediated phagocytosis	Col6a2	ECM-receptor interaction; Focal adhesion; PI3K-Akt signaling pathway
Elmo1	Chemokine signaling pathway; Rac protein signal transduction	Epb4.1	Tight junctions
Irak4	Toll-like receptor signaling pathway, cytokine signaling pathway	Flnb	MAPK signaling pathway; Focal adhesion

Map2k2	MAPK, Ras, B and T cell receptor signaling pathway; Natural killer cell mediated cytotoxicity; Long-term potentiation; Regulation of actin cytoskeleton	Hspb1	Amoebiasis; MAPK signaling pathway;
Pik3r1	Chemokine, B and T cell receptor, PI3K-Akt, Ras and TNF signaling pathway; Toll-like receptor signaling pathway; Fc gamma R-mediated phagocytosis; Inflammatory mediator regulation of TRP channels; Regulation of actin cytoskeleton; Leukocyte transendothelial migration; Axon guidance	Mylk	Calcium signaling pathway; Regulation of actin cytoskeleton; Focal adhesion
Was	Fc gamma R-mediated phagocytosis; Chemokine signaling pathway; Regulation of actin cytoskeleton; Adherens junction	Prkca	Leukocyte transendothelial migration; Ras and MAPK signaling pathway; Fc gamma R-mediated phagocytosis; Long-term potentiation; Inflammatory mediator regulation of TRP channels; Axon guidance; Calcium signaling pathway; Tight junction
		Serpine1	Complement and coagulation cascades
		Tgfbr1	Adherens junction; TGF β and MAPK signaling pathway; Cytokine-cytokine receptor interaction
D) <u>Cell adhesion</u>			
		H2-Aa	Antigen processing and presentation; Th1 and Th2 cell

			differentiation; Phagosome; Cell adhesion molecules (CAMs)
		Thbs1	Focal adhesion; ECM-receptor interaction; Phagosome; PI3K-Akt signaling pathway
E) <u>Apoptosis</u>			
Bcl2l1	Jak-STAT signaling pathway; Chronic myeloid leukemia; Ras signaling pathway; PI3K-Akt signaling pathway; NF-kappa B signaling pathway		
F) <u>Hematopoiesis</u>			
Cdk6	PI3K-Akt signaling pathway; Cell cycle; hematopoiesis		
G) <u>Inflammation</u>			
Casp1	NOD-like receptor signaling pathway; Cytosolic DNA-sensing pathway; Pertussis	Ltbp1	TGFβ signaling pathway
Nfkb1	Ras, MAPK, TNF, PI3K-Akt, NF-κB, B and T cell receptor signaling pathway; Chemokine signaling pathway; Th1 and Th2 cell differentiation	Ube2i	NF-κB signaling pathway
Prkch	Tight junction; Inflammatory mediator regulation of TRP channels		
Rps6ka5	TNF signaling pathway; MAPK signaling pathway		

H) <u>Other</u>			
Atp6v1 (a, b2, e1)	Oxidative phosphorylation; Metabolic pathways; Synaptic vesicle cycle; Phagosome	Ndufab1	Oxidative phosphorylation
Map4k1	MAPK signaling pathway	Rps6-ps4; Rps6	HIF-1 signaling pathway; PI3K-Akt signaling pathway
Ndufa11	Oxidative phosphorylation		
Prkacb	MAPK signaling pathway		
Sdhb	Oxidative phosphorylation		

Table 12. Overview of down- and upregulated proteins 24 h after 1 μ M 9-HODE stimulation in wild-type BMDMs. Proteom screen was performed in 02/2019.

Downregulated		Upregulated	
A) <u>Immune system processes</u>			
B2m	Antigen processing and presentation	Alcam	Cell adhesion molecule, hematopoiesis, adaptive immune response
Blnk	B cell receptor signaling pathway; Primary immunodeficiency; NF- κ B signaling pathway; Osteoclast differentiation	Cd72	B cell receptor signaling pathway
C3	Complement and coagulation cascades; Viral carcinogenesis; Chagas disease (American trypanosomiasis); Systemic lupus erythematosus; Phagosome	Lilrb4	Osteoclast differentiation, B cell receptor signaling pathway

Ccl9	Cytokine-cytokine receptor interaction; Chemokine signaling pathway	Lyn	B cell receptor signaling pathway
Fcgr	Phagocytosis-promoting receptors, B cell receptor signaling, Natural killer cell mediated cytotoxicity	Pik3ap1	B cell receptor signaling pathway, PI3K-Akt signaling pathway
Lgmn	Lysosome; Antigen processing and presentation		
Ly96	NF-κB signaling pathway; Toxoplasmosis; Toll-like receptor signaling pathway; Pertussis		
Notch2	Notch signaling pathway; Th1 and Th2 cell differentiation		
Plau	NF-κB signaling pathway; Complement and coagulation cascades		
Plin2	PPAR signaling pathway		
Tlr8	Toll-like receptor signaling pathway		
B) <u>Lipid metabolic processes</u>			
Abca1	ABC transporters; Fat digestion and absorption	Acadvl	Fatty acid degradation; Fatty acid metabolism
Acaa2	Fatty acid elongation; Fatty acid metabolism; Fatty acid degradation	Cept1	Ether lipid metabolism; Glycerophospholipid metabolism
Acadsb	Fatty acid degradation; Fatty acid metabolism	Chkb	Metabolic pathways; Glycerophospholipid metabolism

Acat1	Fatty acid metabolism; Fatty acid degradation	Dgkh, Dgkz	Glycerophospholipid metabolism
Acox1	α -Linolenic acid metabolism; Biosynthesis of unsaturated fatty acids; PPAR signaling pathway; Fatty acid degradation; Fatty acid metabolism	Fads1	Biosynthesis of unsaturated fatty acids; Fatty acid metabolism
Akr1a1	Glycerolipid metabolism	Fasn	Fatty acid biosynthesis; Metabolic pathways; Fatty acid metabolism
Aldh1b1	Lysine degradation; Glycerolipid metabolism; Fatty acid degradation	Gnpat	Peroxisome; Glycerophospholipid metabolism
Echs1	Fatty acid metabolism; Fatty acid elongation; Fatty acid degradation	Lpl	Glycerolipid metabolism; PPAR signaling pathway
Gpcpd1	Glycerophospholipid metabolism	Hacd3	Fatty acid metabolism; Biosynthesis of unsaturated fatty acids; Fatty acid elongation
GPx1	Arachidonic acid metabolism; Glutathione metabolism	Smpd2	Sphingolipid metabolism; Sphingolipid signaling pathway
Hadh	Fatty acid metabolism; Fatty acid elongation; Fatty acid degradation		
Neu1	Lysosome; Sphingolipid metabolism		
Pcyt1a	Glycerophospholipid metabolism		
Pld3	Glycerophospholipid metabolism; Ether lipid metabolism		

Sdha	Oxidative phosphorylation; Non-alcoholic fatty liver disease (NAFLD); Metabolic pathways		
Smpd1	Sphingolipid signaling pathway; Sphingolipid metabolism		
C) <u>Migration</u>			
CCl6	Chemokine signaling pathway; Cytokine-cytokine receptor interaction	Actn1	Tight junction; Regulation of actin cytoskeleton; Focal adhesion; Adherens junction; Leukocyte transendothelial migration; Amoebiasis
Cd5l	inflammatory response, migration	Akt1	Fc gamma R-mediated phagocytosis; B cell receptor signaling pathway; Chemokine signaling pathway; Toll-like receptor signaling pathway; Focal adhesion; Tight junction; T cell receptor signaling pathway; Ras signaling pathway; mTOR signaling pathway; Jak-STAT signaling pathway
Cxcr4	Axon guidance; Cytokine-cytokine receptor interaction; Chemokine signaling pathway; Leukocyte transendothelial migration	Cadm1	Neural system cell adhesion
Ig1	Cell adhesion molecules (CAMs)	Col6a2	ECM-receptor interaction; Focal adhesion; PI3K-Akt signaling pathway
Grb2	Ras signaling pathway; Focal adhesion; Gap junction; Chemokine signaling pathway; PI3K-Akt	Ctnna1	Tight junction; Leukocyte transendothelial migration; Adherens junction

	signaling pathway; MAPK signaling pathway		
Il16	cytokine signaling pathway, unclassified to CD4	Ctnnb1	Leukocyte transendothelial migration; Focal adhesion; Tight junction; Adherens junction
Itga2b	Platelet activation; Hematopoietic cell lineage; Rap1 signaling pathway; Focal adhesion; PI3K-Akt signaling pathway; Regulation of actin cytoskeleton	Elmo1	Chemokine signaling pathway; Rac protein signal transduction
Itgb3	Focal adhesion; Rap1 signaling pathway; Hematopoietic cell lineage; Platelet activation; Regulation of actin cytoskeleton; PI3K-Akt signaling pathway	Epb4.1	Tight junction
Tmsb4x	Regulation of actin cytoskeleton	Itga5	Regulation of actin cytoskeleton; PI3K-Akt signaling pathway; Phagosome; Focal adhesion; ECM-receptor interaction;
Pik3r1	Chemokine signaling pathway; Natural killer cell mediated cytotoxicity; Fc gamma R-mediated phagocytosis; B cell receptor and PI3K-Akt signaling pathway; Regulation of actin cytoskeleton; Leukocyte transendothelial migration; Axon guidance; T cell receptor and Ras signaling pathway	MyD88	Toll-like receptor signaling pathway; NF-κB signaling pathway; MAPK signaling pathway
Cmklr1	chemotaxis, complement receptor mediated signaling pathway, immune response, inflammatory response	Mylk	Calcium signaling pathway; Regulation of actin cytoskeleton; Focal adhesion
		Ncf2	Leukocyte transendothelial migration; Phagosome

		Parvb	Focal adhesion
		Pik3r5	Ras signaling pathway; Regulation of actin cytoskeleton; Chemokine signaling pathway; Leukocyte transendothelial migration; Inflammatory mediator regulation of TRP channels; Focal adhesion
		Plcg2	Natural killer cell mediated cytotoxicity; Ras, B cell receptor and NF- κ B signaling pathway; Inflammatory mediator regulation of TRP channels; Axon guidance; Leukocyte transendothelial migration
		Ppp1cc	Focal adhesion; Inflammatory mediator regulation of TRP channels; Long-term potentiation; Regulation of actin cytoskeleton
		Prkcb	gap junctions
		Pten	Tight junction; Focal adhesion; regulation of ERK1 and 2 cascade
		Ptk2b	chemokine signaling pathway, positive regulation of ERK1 and 2 cascade
		Rasa1	Axon guidance; MAPK signaling pathway; Ras signaling pathway
		Tgfb1	Adherens junction; TGF β and MAPK signaling pathway; Cytokine-cytokine receptor interaction

		Was	Fc gamma R-mediated phagocytosis; Chemokine signaling pathway; Regulation of actin cytoskeleton; Adherens junction
D) <u>Cell adhesion</u>			
CD22	Cell adhesion molecules (CAMs); Hematopoietic cell lineage; B cell receptor signaling pathway	Arpc1b	actin polymerization, regulation of actin cytoskeleton
H2-Aa	Antigen processing and presentation; Th1 and Th2 cell differentiation; Phagosome; Cell adhesion molecules (CAMs), MHCII; hematopoiesis	Braf	Regulation of actin cytoskeleton; Chemokine signaling pathway; Focal adhesion; Natural killer cell mediated cytotoxicity; Long-term potentiation and depression
H2-Ab1	Cell adhesion molecules (CAMs); Antigen processing and presentation; MHCII	MyI6	regulation of actin cytoskeleton
Icam1	Cell adhesion molecules (CAMs); NF-κB signaling pathway; Natural killer cell mediated cytotoxicity; Leukocyte transendothelial migration; macrophages T-cell adhesion		
Parvg	focal adhesion		
Shc1	Natural killer cell mediated cytotoxicity; Chemokine signaling pathway; Focal adhesion; Ras and chemokine signaling pathway		
Stmn1	MAPK signaling pathway		
Thbs1	Focal adhesion; PI3K-Akt signaling pathway; Phagosome		

E) <u>Apoptosis</u>			
Casp8	apoptosis	Aifm2	necroptosis
Ct(bs,sa, sb, sc, sd, sf, sg, sl, ss, sz)	Cathepsine, Lysosomal, Apoptosis	Capn1	Apoptosis
Fadd	Apoptosis; TNF signaling pathway; Toll-like receptor signaling pathway	Traf2	apoptosis, necroptosis
Gadd45	Apoptosis		
Glul	necroptosis		
Mcl1	Jak-STAT signaling pathway; Apoptosis; PI3K-Akt signaling pathway		
Ppid	necroptosis		
Rbck1	NOD-like receptor signaling pathway, necroptosis		
Spna2	apoptosis		
Vdac1	Calcium signaling pathway; necroptosis		
F) <u>Hematopoiesis</u>			
Cd38	Hematopoietic cell lineage	Cdk6	PI3K-Akt signaling pathway; Cell cycle; hematopoiesis

Csf1	Hematopoietic cell lineage; TNF, Ras and PI3K-Akt signaling pathway; Cytokine-cytokine receptor interaction		
Gp1bb	hematopoiesis		
G) <u>Inflammation</u>			
Adcy3	Rap1 signaling pathway; Chemokine signaling pathway; Inflammatory mediator regulation of TRP channels;	Acs15	Peroxisome; PPAR signaling pathway
Hgs	Endocytosis; Phagosome	Bcl2l1	Jak-STAT, PI3K-Akt, NF-κB and Ras signaling pathway; Chronic myeloid leukemia
Mpo	Transcriptional misregulation in cancer; Phagosome	Bmp2k	cytokine signaling pathway
		Chuk	MAPK signaling pathway, inflammation (IKK), survival factor, apoptosis
		Coro2a	Phagosome
		Pla2g4a	MAPK and Ras signaling pathway; Fc gamma R-mediated phagocytosis; Long-term depression; Inflammatory mediator regulation of TRP channels
		Prkch	Tight junction; Inflammatory mediator regulation of TRP channels
		Ptpn7	MAPK signaling pathway

		Rab5a	Amoebiasis; Ras signaling pathway; Phagosome;
		Trpv2	Inflammatory mediator regulation of TRP channels; NOD-like receptor signaling pathway
		Vamp3	SNARE interactions in vesicular transport; Phagosome
H) <u>Lysosome</u>			
Aga	Lysosome; Other glycan degradation	Ctns	Lysosome
Dnase2a	Lysosome	Hgsnat	Glycosaminoglycan degradation; Lysosome
Gaa	Lysosome	Scarb1	Lysosome; phagosome
Galns	Glycosaminoglycan degradation; Lysosome		
Gba	Lysosome; Other glycan degradation		
Gga1	Lysosome		
Gm2a	Lysosome		
Gns	Metabolic pathways; Lysosome		
Idua	Lysosome		
Napsa	Lysosome		
Npc2	Lysosome		

Pla2g15	Lysosome; Glycerophospholipid metabolism		
l) <u>Other</u>			
Cox7a2	Oxidative phosphorylation	Dapk3	Autophagy, ER stress
Map4k1	MAPK signaling pathway	Pik3c3	Autophagy; Phagosome; Metabolic pathways
Ndufa2	Oxidative phosphorylation	Prkcd	Autophagy
Ndufv	Oxidative phosphorylation	Rps6ka1	Thermogenesis
Uqcrcf1	Metabolic pathways; Oxidative phosphorylation	Rptor	Thermogenesis
		Stx5a	Autophagy

Table 13. Overview of down- and upregulated proteins in G2A-deficient BMDMs 24h after 1 μ M 9-HODE stimulation. Proteom screen was performed in 02/2019.

Downregulated		Upregulated	
A) <u>Immune system processes</u>			
C1qa-c	Complement and coagulation cascades	Alcam	Cell adhesion molecule, hematopoiesis, adaptive immune response
C7	Complement and coagulation cascades	Arrb2	MAPK signaling pathway
CFH		Btk	B cell receptor signaling pathway; Fc epsilon RI signaling pathway; Platelet activation; NF- κ B signaling pathway; Primary immunodeficiency

CFI	Complement and coagulation cascades	Cd72	B cell receptor signaling pathway
CLU		Inpp1	Fc gamma R-mediated phagocytosis; Phosphatidylinositol signaling system; B cell receptor signaling pathway
		Nfatc2	Wnt, B and T cell receptor signaling pathway; Th1 and Th2 cell differentiation; VEGF signaling pathway; Natural killer cell mediated cytotoxicity
F2	Neuroactive ligand-receptor interaction; Complement and coagulation cascades	Pik3ap1	B cell receptor signaling pathway; PI3K-Akt signaling pathway
Fcgr4	Natural killer cell mediated cytotoxicity; Phagosome	Pik3cb	Leukocyte transendothelial migration; TNF, Ras, mTOR, Jak-STAT, Rap1, VEGF, PI3K-Akt, T and B cell receptor signaling pathway; Axon guidance; Amoebiasis; Inflammatory mediator regulation of TRP channels;; Fc gamma R-mediated phagocytosis; Chemokine signaling pathway; Toll-like receptor signaling pathway; Platelet activation; Fc epsilon Focal adhesion; Regulation of actin cytoskeleton; Natural killer cell mediated cytotoxicity;

H2-D1	Phagosome; Antigen processing and presentation; Natural killer cell mediated cytotoxicity	Ppp3cb	MAPK, Wnt, VEGF, B and T cell receptor signaling pathway; Long-term potentiation; Th1 and Th2 cell differentiation; Natural killer cell mediated cytotoxicity; Axon guidance
H2-Eb1	Inflammatory bowel disease (IBD); Antigen processing and presentation; Th1 and Th2 cell differentiation; Phagosome; Intestinal immune network for IgA production; Cell adhesion molecules (CAMs)	Ptpn6	B and T cell receptor signaling pathway
KNG1	Complement and coagulation cascades	Tap2	Primary immunodeficiency; Phagosome; Antigen processing and presentation
Lgmn	Lysosome; Antigen processing and presentation	Tbk1	Epstein-Barr virus infection; Herpes simplex infection; Measles; Influenza A; RIG-I-like receptor signaling pathway; Ras signaling pathway; Cytosolic DNA-sensing pathway; Toll-like receptor signaling pathway; Hepatitis C; Hepatitis B; NOD-like receptor signaling pathway
Plaur	Complement and coagulation cascades		
PLG	Complement and coagulation cascades; Neuroactive ligand-receptor interaction		
Serpina5			

SerpinC1			
SerpinF2			
SerpinG1	Complement and coagulation cascades		
B) <u>Lipid metabolic processes</u>			
Phospho1	Glycerophospholipid metabolism	Agpat4	Glycerophospholipid metabolism; Phospholipase D signaling pathway; Glycerolipid metabolism
Pld3	Glycerophospholipid metabolism; Ether lipid metabolism	Akr1b10	Glycerolipid metabolism
Pld4	Glycerophospholipid metabolism	Dgat1	Fat digestion and absorption; Glycerolipid metabolism
		Dgkq	Glycerophospholipid metabolism; Phospholipase D signaling pathway; Phosphatidylinositol signaling system; Glycerolipid metabolism
		Dgkz	Glycerophospholipid metabolism
		Lpl	Glycerolipid metabolism; PPAR signaling pathway
		Pnpla7	Glycerophospholipid metabolism
		Ppp2r5d	sphingolipid signaling pathway
C) Migration			

Cxcl12	cytokine-cytokine receptor interaction	Abcc1	Cell chemotaxis, Sphingolipid signaling pathway; Vitamin digestion and absorption
Itgb3	Focal adhesion; Rap1 and PI3K-Akt signaling pathway; ECM-receptor interaction; Regulation of actin cytoskeleton	Actn1	Tight junction; Regulation of actin cytoskeleton; Focal adhesion; Adherens junction; Leukocyte transendothelial migration; Amoebiasis
Itgb4	PI3K-Akt signaling pathway	Akt1	Fc gamma R-mediated phagocytosis; Ras, mTOR, Jak-STAT, B and T cell receptor signaling pathway; Chemokine signaling pathway; Toll-like receptor signaling pathway; Focal adhesion; Tight junction
		Git1	Regulation of actin cytoskeleton; Endocytosis
		Itga5	Regulation of actin cytoskeleton; PI3K-Akt signaling pathway; Phagosome; Focal adhesion; ECM-receptor interaction;
		Itga6	Pi3k-Akt signaling pathway
		Itgav	PI3K-Akt signaling pathway; Phagosome; Focal adhesion; Regulation of actin cytoskeleton; Cell adhesion molecules (CAMs)
		Itgb1	PI3K-Akt and Rap1 signaling pathway; Focal adhesion; Phagosome; Platelet activation; Regulation of actin cytoskeleton; Axon guidance; Leukocyte transendothelial migration; ECM-

			receptor interaction; Cell adhesion molecules (CAMs)
		Map2k2	MAPK, mTOR, PI3K-Akt, HIF-1, Rap 1, VEGF, Ras, B and T cell receptor signaling pathway; Natural killer cell mediated cytotoxicity; Long-term potentiation and depression; Regulation of actin cytoskeleton; Fc epsilon RI signaling pathway; Gap junction
		Msn	Leukocyte transendothelial migration; Regulation of actin cytoskeleton
		Ncf4	Leukocyte transendothelial migration; Phagosome
		Pten	Tight junction; Focal adhesion; regulation of ERK1 and 2 cascade
		Was	Fc gamma R-mediated phagocytosis; Chemokine signaling pathway; Regulation of actin cytoskeleton; Adherens junction; Endocytosis
D) <u>Cell adhesion</u>			
Cd22	Cell adhesion molecules (CAMs); Hematopoietic cell lineage; B cell receptor signaling pathway	Csda	Tight junction
Cntnap2	Cell adhesion molecules (CAMs)	Col12a1	Protein digestion and absorption
H2-Aa	Antigen processing and presentation; Th1 and Th2 cell	Myh9	Tight junction; Regulation of actin cytoskeleton

	differentiation; Phagosome; Cell adhesion molecules (CAMs), MHCII; hematopoiesis		
H2-Ab1	Phagosome; Th1 and Th2 cell differentiation; Cell adhesion molecules (CAMs); Antigen processing and presentation; MHCII	Ptpn1	Adherens junction
Spnb2	Tight junction	Ptprj	
Thbs1	Focal adhesion; ECM-receptor interaction; Phagosome; PI3K-Akt signaling pathway; Phagosome	Pvr	Cell adhesion molecules (CAMs)
		Rapgef1	Rap1 signaling pathway; Focal adhesion
		Sympk	Tight junction
E) <u>Apoptosis</u>			
Bcl2l11	FoxO signaling pathway; EGFR tyrosine kinase inhibitor resistance; Apoptosis - multiple species; Apoptosis; Non-alcoholic fatty liver disease (NAFLD); PI3K-Akt signaling pathway; MicroRNAs in cancer	Capn2	Apoptosis; Natural killer cell mediated cytotoxicity; Amoebiasis; MAPK and TNF signaling pathway
Ct (sb, sc, sh, sl, ss, sz)	Antigen processing and presentation; Lysosome; Apoptosis, Phagosome	Casp6	
Cycs		Casp3	

Spna1	Apoptosis	Diablo	
F) <u>Hematopoiesis</u>			
Csf1	Hematopoietic cell lineage; TNF signaling pathway; Ras signaling pathway; Cytokine-cytokine receptor interaction; PI3K-Akt signaling pathway	Cdk6	PI3K-Akt signaling pathway; Cell cycle; hematopoiesis
G) <u>Inflammation</u>			
Mik1	TNF signaling pathway	Csf2ra	Cytokine-cytokine receptor interaction; Jak-STAT signaling pathway
Mpo	Phagosome	Dync1li1	Phagosome
Rasgrp2	Ras, Rap1, MAPK and Chemokine signaling pathway; Platelet activation	Gnb4	PI3K-Akt, Ras and Chemokine signaling pathway
		Nfkb1	Ras, MAPK, TNF, NF-κB, PI3K-Akt, B and T cell receptor signaling pathway; Amoebiasis; Toll-like receptor signaling pathway; Longevity regulating pathway; Inflammatory bowel disease (IBD); Chemokine signaling pathway; Th1 and Th2 cell differentiation
		Ptpn7	MAPK signaling pathway

H) <u>Lysosome</u>			
Arsb	Lysosome; Glycosaminoglycan degradation	Ap3m2	Lysosome
Arsg	Lysosome	Hgsnat	Glycosaminoglycan degradation; Lysosome
Galns	Glycosaminoglycan degradation; Lysosome	Igf2r	Endocytosis; Lysosome
Gga3	Lysosome	Lipa	Steroid biosynthesis; Lysosome
Gm2a	Lysosome	Nagpa	Lysosome
Gns	Glycosaminoglycan degradation; Lysosome	Rps6ka5	Adrenergic signaling in cardiomyocytes; Neurotrophin signaling pathway; Circadian entrainment; TNF and MAPK signaling pathway
Lamp2	Phagosome; Lysosome; Tuberculosis	Scarb1	Fat digestion and absorption; Aldosterone synthesis and secretion; Phagosome; Vitamin digestion and absorption
Man2b1	Lysosome; Other glycan degradation		
I) <u>Other</u>			
Col4a1	Protein digestion and absorption; ECM-receptor interaction; Focal adhesion; PI3K-Akt signaling pathway	Atg1611	Autophagy
Hprt	Purine metabolism; Drug metabolism - other enzymes; Metabolic pathways	Eif4e	RNA transport; HIF-1, mTOR and PI3K-Akt signaling pathway; EGFR tyrosine kinase inhibitor

			resistance; Longevity regulating pathway;
Ltbp1	TGF β signaling pathway	Gabarapl2	FoxO signaling pathway; Autophagy; NOD-like receptor signaling pathway
Rab33b	Autophagy	Impdh2	Drug metabolism - other enzymes; Purine metabolism
		Inpp1	Phosphatidylinositol signaling system; Metabolic pathways
		Pck2	FoxO signaling pathway; PI3K-Akt signaling pathway; PPAR signaling pathway; Proximal tubule bicarbonate reclamation; Insulin signaling pathway; AMPK signaling pathway; Pyruvate metabolism
		Pip4k2a	Regulation of actin cytoskeleton; Phosphatidylinositol signaling system
		Ppp2r5d	PI3K-Akt signaling pathway
		Prkacb	MAPK signaling pathway
		Rrm2	p53 signaling pathway; Pyrimidine metabolism; Metabolic pathways; Glutathione metabolism; Purine metabolism
		Stk11	FoxO, mTOR and PI3K-Akt signaling pathway; Longevity regulating pathway; AMPK signaling pathway
		Taok3	MAPK signaling pathway

--	--	--	--

Table 14. Overview of down- and upregulated proteins in G2A-deficient compared to wild-type BMDMs 24h after 1 μ M 9-HODE stimulation. Proteom screen was performed in 02/2019.

Downregulated		Upregulated	
A) <u>Immune system processes</u>			
Alcam	Cell adhesion molecule, hematopoiesis, adaptive immune response	C1qa-c	Complement and coagulation cascades
Araf	FoxO and ErbB signaling pathway; Vascular smooth muscle contraction; Long-term potentiation and depression; EGFR tyrosine kinase inhibitor resistance; Regulation of actin cytoskeleton; Natural killer cell mediated cytotoxicity	Dlg1	Tight junction, T cell receptor signaling pathway
Blnk	B cell receptor signaling pathway; Primary immunodeficiency; NF- κ B signaling pathway	Ecsit	MAPK signaling pathway
Btk	B cell receptor signaling pathway; Fc epsilon RI signaling pathway; Platelet activation; NF- κ B signaling pathway; Primary immunodeficiency	F13a1	Complement and coagulation cascades
Ccl9	Cytokine-cytokine receptor interaction; Chemokine signaling pathway	Fgr	Chemokine signaling pathway
Fcgr4	Natural killer cell mediated cytotoxicity; Phagosome	Lgmn	Lysosome; Antigen processing and presentation

F8a	complement and coagulation cascade	Nfatc1	MAPK signaling pathway, B cell receptor signaling pathway
H2-D1	Phagosome; Antigen processing and presentation; Natural killer cell mediated cytotoxicity	Ppp3cb	MAPK, Wnt, VEGF, B and T cell receptor signaling pathway; Long-term potentiation; Th1 and Th2 cell differentiation; Natural killer cell mediated cytotoxicity; Axon guidance
H2-T23	Antigen processing and presentation; Phagosome; Endocytosis; Natural killer cell mediated cytotoxicity	Serpinb2	Complement and coagulation cascades
Inpp1	Fc gamma R-mediated phagocytosis; Phosphatidylinositol signaling system; B cell receptor signaling pathway	Traf6	MAPK, NF-κB signaling pathway; Toll-like receptor signaling pathway; RIG-I-like receptor signaling pathway; Endocytosis
Lfi47	TNF signaling pathway		
Lyn	NF-κB and B cell receptor signaling pathway		
Malt1	NF-κB, B and T cell receptor signaling pathway		
Rnf31	NOD-like receptor signaling pathway		
SerpinA5	Complement and coagulation cascades		
SerpinG1	Complement and coagulation cascades; Pertussis		

Stat6	Inflammatory bowel disease (IBD); Jak-STAT signaling pathway; Th1 and Th2 cell differentiation		
Tec	T cell receptor signaling pathway		
B) <u>Lipid metabolic processes</u>			
Agpat3	Phospholipase D signaling pathway; Glycerophospholipid metabolism; Glycerolipid metabolism	Acad5b	Fatty acid degradation; Fatty acid metabolism
Cbr4	Fatty acid metabolism	Acadvl	Fatty acid degradation; Fatty acid metabolism
Cdipt	Phosphatidylinositol signaling system; Glycerophospholipid metabolism	Acat1	Fatty acid metabolism; Fatty acid degradation
Cept1	Ether lipid metabolism; Glycerophospholipid metabolism	Cpt2	Fatty acid metabolism; Fatty acid degradation
Cers6	Sphingolipid metabolism	Echs1	Fatty acid metabolism; Fatty acid elongation; Fatty acid degradation
Dgkz	Glycerophospholipid metabolism	Fads1	Biosynthesis of unsaturated fatty acids; Fatty acid metabolism
Galc	Sphingolipid metabolism; Metabolic pathways	Gpd2	Glycerophospholipid metabolism
Glb1	Sphingolipid metabolism; Glycosphingolipid biosynthesis - ganglio series	Gpx7	Glutathione metabolism; Arachidonic acid metabolism
Gnpat	Glycerophospholipid metabolism	Hadh	Fatty acid metabolism; Fatty acid elongation; Fatty acid degradation
Gpd1	Glycerophospholipid metabolism	Lpcat2	Glycerophospholipid metabolism; Ether lipid metabolism

Hpgds	Arachidonic acid metabolism	Ppt1	Fatty acid elongation; Fatty acid metabolism
Pld1	Ether lipid metabolism, glycerolipid metabolism	Ptplb	Fatty acid elongation; Biosynthesis of unsaturated fatty acids; Fatty acid metabolism
Ppp2r5e	Sphingolipid signaling pathway		
C) <u>Migration</u>			
Actn4	Leukocyte transendothelial migration; Amoebiasis; Adherens junction; Regulation of actin cytoskeleton; Focal adhesion; Tight junction	Col6a1	PI3K-Akt signaling pathway; ECM-receptor interaction; Focal adhesion
Arpc2	Regulation of actin cytoskeleton; Bacterial invasion of epithelial cells; Salmonella infection; Endocytosis; Fc gamma R-mediated phagocytosis	Col6a2	
Arpc5	Regulation of actin cytoskeleton; Bacterial invasion of epithelial cells; Salmonella infection; Endocytosis; Fc gamma R-mediated phagocytosis	Ctnna1	Tight junction; Leukocyte transendothelial migration; Adherens junction
Ccr5	Chemokine signaling pathway; Endocytosis; Cytokine-cytokine receptor interaction	Ctnnb1	Leukocyte transendothelial migration; Focal adhesion; Tight junction; Adherens junction
Cdc42	Axon guidance; Fc gamma R-mediated phagocytosis; Ras, Rap1, MAPK, VEGF and T cell receptor signaling pathway; Adherens junction; Endocytosis; Focal adhesion; Tight junction; Regulation	Ctnn	Tight junction; Bacterial invasion of epithelial cells

	of actin cytoskeleton; Chemokine signaling pathway; Leukocyte transendothelial migration		
Cfl1	Regulation of actin cytoskeleton; Axon guidance; Fc gamma R-mediated phagocytosis;	Cxcr4	Axon guidance; Cytokine-cytokine receptor interaction; Endocytosis; Intestinal immune network for IgA production; Chemokine signaling pathway; Leukocyte transendothelial migration
Ddx58	RIG-I-like receptor signaling pathway; NF-κB signaling pathway	Ezr	Regulation of actin cytoskeleton; Leukocyte transendothelial migration
Diaph1	Regulation of actin cytoskeleton	Flnb	MAPK signaling pathway; Focal adhesion
Dock2	Chemokine signaling pathway; Fc gamma R-mediated phagocytosis	Fn1	focal adhesion
Elmo1	Bacterial invasion of epithelial cells; Chemokine signaling pathway	Hspb1	Amoebiasis; MAPK signaling pathway; Epstein-Barr virus infection; VEGF signaling pathway
Epb4.1	Tight junction	Il16	Cytokine-cytokine receptor interaction
Itgam	Amoebiasis; Cell adhesion molecules (CAMs); Complement and coagulation cascades; Rap1 signaling pathway; Leukocyte transendothelial migration; Phagosome; Regulation of actin cytoskeleton	Itga2b	Platelet activation; Hematopoietic cell lineage; Rap1 signaling pathway; Focal adhesion; PI3K-Akt signaling pathway; Regulation of actin cytoskeleton
Itgax	Complement and coagulation cascades; Regulation of actin cytoskeleton	Itga5	Regulation of actin cytoskeleton; PI3K-Akt signaling pathway; Phagosome; Focal adhesion; ECM-receptor interaction;

Pkn1	PI3K signaling pathway	Itgav	PI3K-Akt signaling pathway; Phagosome; Focal adhesion; Regulation of actin cytoskeleton; Cell adhesion molecules (CAMs)
Prkcb	gap junctions	Itgb3	Focal adhesion; Rap1 signaling pathway; Hematopoietic cell lineage; Platelet activation; Regulation of actin cytoskeleton; PI3K-Akt signaling pathway
Ptk2	Chemokine signaling pathway; Leukocyte transendothelial migration; PI3K-Akt and VEGF signaling pathway; Regulation of actin cytoskeleton; Axon guidance; Amoebiasis; Focal adhesion	Lama5	PI3K-Akt signaling pathway; Toxoplasmosis; Pathways in cancer; Metabolic pathways; Focal adhesion; Amoebiasis; ECM-receptor interaction; Small cell lung cancer
Rac2	Fc gamma R-mediated phagocytosis; Axon guidance; MAPK, Wnt, Rap1, Ras, VEGF and B cell receptor signaling pathway; Focal adhesion; Regulation of actin cytoskeleton; Natural killer cell mediated cytotoxicity; Adherens junction; Leukocyte transendothelial migration; Chemokine signaling pathway	Lamb1	Amoebiasis; ECM-receptor interaction; Focal adhesion; PI3K-Akt signaling pathway
Rasa1	Axon guidance; MAPK signaling pathway; Ras signaling pathway	Lamc1	PI3K-Akt signaling pathway; Focal adhesion; Amoebiasis; ECM-receptor interaction
Vav3	B and T cell receptor signaling pathway; Natural killer cell mediated cytotoxicity; Focal adhesion; Fc gamma R-mediated phagocytosis; Chemokine signaling pathway; Regulation of actin	Mmp14	GnRH and TNF signaling pathway

	cytoskeleton; Leukocyte transendothelial migration		
		Mmp9	TNF signaling pathway; Leukocyte transendothelial migration; Estrogen signaling pathway
		MyI9	Tight junction; Focal adhesion; Leukocyte transendothelial migration; Regulation of actin cytoskeleton
		Nckap1	Regulation of actin cytoskeleton
		Prex1	Chemokine signaling pathway
		Prkca	Leukocyte transendothelial migration; Ras and MAPK signaling pathway; Fc gamma R-mediated phagocytosis; Long-term potentiation; Inflammatory mediator regulation of TRP channels; Axon guidance; Calcium signaling pathway; Tight junction
		Pten	Tight junction; Focal adhesion; regulation of ERK1 and 2 cascade
		Scin	Regulation of actin cytoskeleton; Fc gamma R-mediated phagocytosis
		Sdc4	Cell adhesion molecules (CAMs); ECM-receptor interaction
		Stat3	Chemokine signaling pathway; HIF-1, Jak-STAT signaling pathway

		Vasp	Focal adhesion; Leukocyte transendothelial migration; Rap1 signaling pathway; Fc gamma R-mediated phagocytosis
		Vcan	Cell adhesion molecules (CAMs)
		Vcl	Adherens junction; Regulation of actin cytoskeleton; Amoebiasis; Focal adhesion; Leukocyte transendothelial migration
D) <u>Cell adhesion</u>			
Arpc1a	Regulation of actin cytoskeleton; Fc gamma R-mediated phagocytosis	Cd276	Cell adhesion molecules (CAMs)
Arpc1b	Regulation of actin cytoskeleton	Cntnap2	Cell adhesion molecules (CAMs)
Arpc4	Regulation of actin cytoskeleton; Fc gamma R-mediated phagocytosis; Endocytosis	Cyfip2	Regulation of actin cytoskeleton
Braf	Regulation of actin cytoskeleton; Chemokine signaling pathway; Focal adhesion; Natural killer cell mediated cytotoxicity; Long-term potentiation and depression	Enah	
Cd274	Cell adhesion molecules (CAMs)	Fgd3	
Ppp2cb	Tight junction; Long-term depression; PI3K-Akt, TGF β and Hippo signaling pathway	Finc	MAPK signaling pathway; Focal adhesion
Rab8b	Tight junction	H2-Aa	Antigen processing and presentation; Cell adhesion molecules (CAMs), MHCII; hematopoiesis

Siglec1	Cell adhesion molecules (CAMs)	Itga11	PI3K-Akt signaling pathway; ECM-receptor interaction; Focal adhesion; Regulation of actin cytoskeleton
Tln1	Platelet activation; Focal adhesion; Rap1 signaling pathway	Myh9	Tight junction; Regulation of actin cytoskeleton
		Ncam1	Cell adhesion molecules (CAMs)
		Ppp1r12a, b	Focal adhesion; Regulation of actin cytoskeleton, cAMP and cGMP-PKG signaling pathway; Focal adhesion; Platelet activation
		Shc1	Natural killer cell mediated cytotoxicity; Chemokine signaling pathway; Focal adhesion; Ras and chemokine signaling pathway
		Sympk	Tight junction
		Thbs1	Focal adhesion; PI3K-Akt signaling pathway; Phagosome
E) <u>Apoptosis</u>			
Apaf1	Apoptosis; p53 signaling pathway	Atf2	PI3K-Akt, TNF and MAPK signaling pathway
Bcl2l11	FoxO signaling pathway; EGFR tyrosine kinase inhibitor resistance; Apoptosis - multiple species; Apoptosis; Non-alcoholic fatty liver disease (NAFLD); PI3K-Akt signaling pathway; MicroRNAs in cancer	Casp6	Apoptosis
Bax	p53 signaling pathway; Apoptosis; Neurotrophin signaling pathway;	Csda	Tight junction

Camk2d	necroptosis	Csnk2a1	Wnt signaling pathway; Adherens junction; Tight junction; NF-κB signaling pathway
Capn2	Apoptosis; Focal adhesion	Ct (se, sf, sk)	Lysosome, Apoptosis
Casp1	Apoptosis	Dapk1	Apoptosis
Casp8	Necroptosis, TNF signaling pathway	Diablo	
Ct (sa, sb, sl, ss, sz)	Apoptosis, phagosome, lysosome,	Faf1	Necroptosis
Traf2	NF-κB signaling pathway, Apoptosis	Hmgb1	
		Hsp90b1	PI3K-Akt signaling pathway
		Lmnb1	Apoptosis
		Ppid	Necroptosis
		Spna2	Apoptosis
F) <u>Hematopoiesis</u>			
Csf2ra	Cytokine-cytokine receptor interaction; Hematopoietic cell lineage; Jak-STAT signaling pathway	Csf1	Hematopoietic cell lineage; TNF, Ras and PI3K-Akt signaling pathway; Cytokine-cytokine receptor interaction
		Sp1	Endocrine resistance; Transcriptional misregulation in cancer; TGF-beta signaling pathway; Choline metabolism in

			cancer; Breast cancer; Estrogen signaling pathway; Huntington's disease
G) <u>Inflammation</u>			
Acs15	Peroxisome; Fatty acid degradation; PPAR signaling pathway	Colec12	Phagosome
Adcy7	Rap1, Chemokine signaling pathway; Endocrine resistance; Gap junction; Inflammatory mediator regulation of TRP channels; Platelet activation	Mrc2	Phagosome
Chuk	MAPK signaling pathway, inflammation (IKK), survival factor, apoptosis	Parp1	NF-κB signaling pathway
Clecl7a	Phagosome	Ppp1cb	Regulation of actin cytoskeleton; Inflammatory mediator regulation of TRP channels; Platelet activation; Hippo signaling pathway; Long-term potentiation; Focal adhesion
Eif2ak2	Influenza A; Viral carcinogenesis; Herpes simplex infection; Hepatitis C; Epstein-Barr virus infection; Measles; Protein processing in endoplasmic reticulum	Rasgrp2	Ras, Rap1, MAPK and Chemokine signaling pathway; Platelet activation
Gng2	PI3K-Akt, Chemokine and Ras signaling pathway;	Rps6ka4	MAPK signaling pathway; TNF signaling pathway
Mik1	TNF signaling pathway		

Prkch	Tight junction; Inflammatory mediator regulation of TRP channels		
Rab5a	Amoebiasis; Ras signaling pathway; Phagosome		
Rab5c	Amoebiasis; Ras signaling pathway; Phagosome		
Stat1	Chemokine signaling pathway; Jak-STAT signaling pathway; Toll-like receptor signaling pathway; Th1 and Th2 cell differentiation		
Tfrc	HIF-1 signaling pathway; Phagosome; Endocytosis		
Trim25	NF-κB signaling pathway; RIG-I-like receptor signaling pathway		
H) <u>Lysosome</u>			
Ap1g2	Lysosome	Acp5	Lysosome
Ap3s1		Arsb	
Ap4m1		Nagpa	
Fuca1		Sort1	
Gm2a			
Gusb			
Idua			

Lamp1	Phagosome; Lysosome		
Lipa	Lysosome		
Litaf			
Man2b1			
Manba			
l) <u>Other</u>			
Aldh3b1	Drug metabolism - cytochrome P450; Metabolism of xenobiotics by cytochrome P450;	Actl6a	Thermogenesis
Atp6 (ap1, v0d2, v1a, v1b2, v1c1, v1d, v1e1, v1f, v1g1, v1h)	Oxidative phosphorylation; Metabolic pathways; Synaptic vesicle cycle; Phagosome	Atp5e	Oxidative phosphorylation
Atp1a1	Thyroid hormone signaling pathway; Gastric acid secretion; Endocrine and other factor-regulated calcium reabsorption; Adrenergic signaling in cardiomyocytes; Proximal tubule bicarbonate reclamation Protein digestion and absorption	Cdk2	PI3K-Akt, p53 and FoxO signaling pathway; Oocyte meiosis; Cell cycle
Atpv60a1	Rheumatoid arthritis; Collecting duct acid secretion; Oxidative	Eif4b	mTOR signaling pathway; PI3K-Akt signaling pathway

	phosphorylation; Synaptic vesicle cycle; Phagosome		
Chmp6	Endocytosis	Eif4e	HIF-1, mTOR and PI3K-Akt signaling pathway; EGFR tyrosine kinase inhibitor resistance; Longevity regulating pathway
Cmpk1	Pyrimidine metabolism	Ephx1	Metabolism of xenobiotics by cytochrome P450; Bile secretion; Chemical carcinogenesis
Cox11	Oxidative phosphorylation; Metabolic pathways	Fbn1	TGF β signaling pathway
Cytb	Cardiac muscle contraction; Oxidative phosphorylation	Gmps	Purine metabolism; Drug metabolism - other enzymes
Gabarapl1	NOD-like receptor and FoxO signaling pathway; Autophagy; GABAergic synapse	Gnaz	Long-term depression
Gstm1	Drug metabolism - other enzymes	Gstp1	Metabolism of xenobiotics by cytochrome P450; Drug metabolism - cytochrome P450
Ndufa11	Oxidative phosphorylation;	Gstt1	Drug metabolism - cytochrome P450; Metabolism of xenobiotics by cytochrome P450; Glutathione metabolism; Chemical carcinogenesis; Platinum drug resistance
Ndufa12		Gys1	Glucagon signaling pathway; PI3K-Akt and AMPK signaling pathway; Starch and sucrose metabolism
Pygb	Glucagon signaling pathway; Starch and sucrose metabolism	Hspa2	Endocytosis; Antigen processing and presentation; MAPK signaling pathway; Protein processing in endoplasmic reticulum; Spliceosome

Rasa4	Ras signaling pathway	Kdm1a	Thermogenesis
Rb1cc1	Longevity regulating pathway	Ltbp1	TGF β signaling pathway
Rps6ka3	Neurotrophin signaling pathway; Progesterone-mediated oocyte maturation; mTOR and MAPK signaling pathway; Long-term potentiation	Maoa	Phenylalanine metabolism; Drug metabolism - cytochrome P450; Histidine metabolism; Serotonergic synapse; Dopaminergic synapse
Smcr8	Autophagy	Mtmr3	Autophagy
Taok3	MAPK signaling pathway	Ndufs3	Oxidative phosphorylation
Tcirg1	Oxidative phosphorylation; Collecting duct acid secretion; Synaptic vesicle cycle; Phagosome	Nedd4	Endocytosis; Ubiquitin mediated proteolysis
Xdh	Metabolic pathways; Drug metabolism - other enzymes; Peroxisome	Pck2	FoxO, PPAR and PI3K-Akt signaling pathway; Citrate cycle (TCA cycle); Pyruvate metabolism; Adipocytokine signaling pathway
		Ppa1	Oxidative phosphorylation
		Rasa3	Ras signaling pathway
		Rps6ka1	Thermogenesis
		Rrm2	p53 signaling pathway; Glutathione metabolism; Purine metabolism
		Sqstm1	Osteoclast differentiation, autophagy
		Umps	Pyrimidine metabolism; Drug metabolism - other enzymes

		Vdac3	cGMP-PKG signaling pathway; Calcium signaling pathway; NOD-like receptor signaling pathway
		Wipi1	Autophagy

Publikationen

Osthues T, Sisignano M. Oxidized lipids in persistent pain states. *Front Pharmacol* (2019).

Kern K, Schäfer SMG, Cohnen J, Pierre S, **Osthues T**, Tarighi N, Hohmann S, Ferreiros N, Brüne B, Weigert A, Geisslinger G, Sisignano M, Scholich K. The G2A receptor controls polarization of macrophage by determining their localization within the inflamed tissue. *Front Immunol* (2018)

Winter SJ, Kunze-Schumacher H, Imelmann E, Grewers Z, **Osthues T**, Krueger A. MicroRNA miR-181a/b-1 controls MAIT cell development. *Immunol Cell Biol* (2018).

Zimmer B, Angioni C, **Osthues T**, Toewe A, Thomas D, Pierre SC, Geisslinger G, Scholich K, Sisignano M. The oxidized linoleic acid metabolite 12,13-DiHOME mediates thermal hyperalgesia during inflammatory pain. *Biochim Biophys Acta Mol Cell Biol Lipids* (2018).

Osthues, T.; Kusch, M.; Keitel, S.; Grundmann, C. et al. (2016): Inhibition of FXIa and FXIIa by recombinant *Curcubita maxima* trypsin inhibitor-V (CMTI-V), 60th Annual Meeting of the Society of Thrombosis and Haemostasis Research, 17.-20. Februar 2016, Münster.

Danksagung

Ich bedanke mich bei Herrn Prof. Dr. Dr. Geißlinger als Institutsleiter für die Möglichkeit, die vorliegende Arbeit im Fraunhofer Institut für Molekularbiologie und Angewandte Ökologie – Zweig Translationale Medizin und Pharmakologie (IME-TMP) anfertigen zu können.

Bei Herrn Prof. Dr. Dr. Achim Schmidtke möchte ich mich für seine Bereitschaft bedanken, die Betreuung der Arbeit von Seiten des Fachbereichs Pharmazie zu übernehmen, sowie die stets ideenreichen Gespräche zu meiner Arbeit, die mir immer wieder neue Einsichten und Richtungen gezeigt haben.

Bei Herrn Prof. Dr. Klaus Scholich möchte ich mich bedanken für die Erstellung des Gutachtens von Seiten des Fachbereichs Medizin der Johann Goethe Universität Frankfurt. Auch war er eine wichtige Anlaufstelle, wenn es um Ratschläge oder konstruktive Kritik ging.

Besonderer Dank gilt meinem direkten Betreuer PD Dr. Marco Sisignano, der mit seiner Geduld und Ausdauer mir stets mit wertvollen Tipps und herausfordernden Diskussionen zur Seite stand. Ohne seine Idee zu dem Projekt und seiner Weitsicht, wäre der Erfolg dieses Projekts nicht möglich gewesen.

Weiterhin möchte ich mich auch bei meinen Kollegen und Mitarbeitern der Arbeitsgruppe Sisignano und Scholich bedanken, die mir mit Rat und Tat zur Seite gestanden haben und immer für eine konstruktive und positive Arbeitsatmosphäre gesorgt haben.

Vielen Dank an Herrn Carlo Angioni, der die Analytik-Messungen gemacht hat. Ebenso möchte ich mich bei der AG Münch des Instituts für Biochemie I und hier besonders Kevin Klann bedanken, die sich für eine Zusammenarbeit ausgesprochen haben und die Proteomanalyse übernommen haben.

Auch möchte ich mich bei meinem Partner Rolf Egert bedanken, der mich die komplette lange Zeit der Doktorarbeit begleitet und ebenfalls mit hilfreichen Ratschlägen unterstützt hat.

Für das Korrekturlesen möchte ich mich bei Vanessa Königs, Vittoria Rimola, Maksim Sendetski, Paula Reichelt und Hanna Raus bedanken.

Lebenslauf

Tabea Osthues

Persönliche Daten

Geboren am 12. Januar 1989 in Starnberg

Berufliche Erfahrung

Seit 10/2017

Wissenschaftliche Mitarbeiterin

Fraunhofer IME-TMP, Frankfurt

- SNI-Modell, ELISA, Western Blot, Ca-Imaging
- Projektmanagement
- Labororganisation

10/2014 – 04/2017

Wissenschaftliche Mitarbeiterin

Fuchs Patentanwälte, Frankfurt

- Recherche zu Gesetzen, Urteilen, Patent- und Markenangelegenheiten
- Verfassen von Fachartikeln, Mitteilungen an Mandanten und Ämter

08/2013 – 10/2014

Werkstudentin

PR-Agentur newswerk, Frankfurt

- Verfassen und Redigieren von Pressemitteilungen und Berichten
- Organisation von Pressekonferenzen und Fachkongressen

Ausbildung

10/2017 – heute

Promotion Pharmazie

AG Sisignano, Klinische Pharmakologie

Goethe Universität, Frankfurt am Main

- Schwerpunkte: FELASA B, SNI-Modell, Ca-Imaging, biochemische Analysen, Inhibitorscreen
- Thesis: Rolle des G2A und beteiligte Signalwege bei neuropathischen Schmerzen nach Nervenverletzungen

10/2015 – 10/2017

Masterstudium Molekulare Medizin

Goethe Universität, Frankfurt am Main

- Studienschwerpunkte: Molekulare Tumorimmunologie und Onkologie, Molekulare Arzneimittelforschung, Herz-Kreislaufforschung
- Master-Thesis: Mutual regulation of the activity of blood clotting factors and membrane curvature

Abschlussnote: 1,8

10/2012 – 08/2015

Bachelorstudium Biowissenschaften

Goethe Universität, Frankfurt am Main

- Bachelor-Thesis: Recombinant expression, purification and functional characterization of corn and pumpkin inhibitors of coagulation factor XIIa

Abschlussnote: 1,4

10/2009 – 07/2012

Bachelorstudium Wissenschaftsjournalismus

Hochschule Darmstadt, Darmstadt

- Bachelor-Thesis: Produktion eines Podcast für das Deutsche Museum

Abschlussnote: 1,4

Auslandsaufenthalte und Praktika

01 – 2/2012	Praktikantin AG Krueger Forschungspraktikum (6 Wo.) im Rahmen des Studiums, Prof. Dr. Andreas Krueger, Institut für Molekulare Medizin, Goethe Universität Frankfurt <ul style="list-style-type: none">➤ Thema: Characterisation of MAIT cell populations in various organs of miR-181 a/b-1^{-/-} mice➤ Isolation von Lymphozyten aus verschiedenen Organen, MACS, FACS
11 – 12/2016	Praktikantin AG Brieger Forschungspraktikum (6 Wo.) im Rahmen des Studiums, PD Dr. Angela Brieger, Medizinische Klinik 1, Biomedizinisches Forschungslabor, Goethe Universität Frankfurt <ul style="list-style-type: none">➤ Thema: Analysis of the cellular localization of phosphorylated DNA mismatch repair protein MLH1➤ Transfektion, Proteinisolation, Kern-Zytoplasma-Extraktion, Immunopräzipitation, Western Blot
09 – 10/2016	Praktikantin AG Scholich Forschungspraktikum (6 Wo.) im Rahmen des Studiums, Prof. Dr. Klaus Scholich, Institut für Klinische Pharmakologie, Goethe Universität <ul style="list-style-type: none">➤ Thema: Effect of G2A on macrophages at inflammation sites➤ MELC, Makrophagen-Primärkultur, Migrations-Assay, FACS
08/2012 – 10/2012	Praktikantin Administration College of East London, London <ul style="list-style-type: none">➤ Bearbeitung von Telefon-, Studenten- und Dozentenanfragen➤ Einarbeitung neuer Mitarbeiter

Qualifikationen

Sprachkenntnisse	Englisch: fließend in Wort und Schrift Französisch: Grundkenntnisse Spanisch: Grundkenntnisse
EDV-Kenntnisse	Hervorragende Kenntnisse in MS Office, Grundkenntnisse in Adobe

Fortbildungen

2020	GxP Zertifikat Pharmaakademie
2019 -2020	Mentee Mentoring Hessen, Mentorin Dr. Beatrix Wiesler (Merck KGaA)
2017- heute	Fortbildungsprogramm GRADE, Goethe Universität, Frankfurt Projekt- und Qualitätsmanagement, Kommunikationstechniken, BWL

Sonstiges

09/2008 – 04/2009	Freiwilliges Engagement im Rahmen eines Freiwilligen Ökologischen Jahres Pro Regenwald, München
-------------------	---